Universitat Autònoma de Barcelona

Inkjet-Printed Devices for Chemical and Biosensing Applications

Carme Martínez Domingo

Universitat Autònoma de Barcelona

Tesi doctoral

Inkjet-Printed Devices for Chemical and Biosensing Applications

Carme Martínez Domingo

Directors:

Dr. Eloi Ramon Garcia

ICREA Prof. Arben Merkoçi

Tutor:

Dr. Lluís Terés Terés

Universitat Autònoma de Barcelona

Departament d'Enginyeria Electrònica

Programa de Doctorat en Enginyeria Electrònica i de Telecomunicació

Bellaterra (Barcelona), Setembre 2018

I certify that I have read the dissertation "*Inkjet-Printed Devices for Chemical and Biosensing Applications*" and that, in my opinion, it is fully adequate in scope and quality as a dissertation for the degree of Doctor of Philosophy.

Dr. Eloi Ramon Garcia, ICREA Prof. Arben Merkoçi and Dr. Lluís Terés Terés

Universitat Autònoma de Barcelona
Departament d'Enginyeria Electrònica
Programa de Doctorat en Enginyeria Electrònica i de Telecomunicació

This work was carried out at Institut de Microelectrònica de Barcelona- Centre Nacional de Microelectrònica (CSIC) and Institut Català de Nanociència i Nanotecnologia (ICN2).

The science of today is the technology of tomorrow

Edward Teller

Abstract

Inkjet printing is a nascent technology that is evolving from text and graphic printing into a major topic of scientific research and R&D, where it can be used as a highly reproducible non-contact patterning technique to deposit liquid functional materials at high speed on either small or large areas of flexible and non-flexile substrates. It is a low-cost technique because minimizes the waste products and reduces the process steps. Moreover, the development of organic materials such as polymers with electrical features has boosted the fabrication of new organic printed electrical devices.

In this framework, this thesis is devoted to a development of novel organic devices for chemical and biosensing applications for a low-cost cost devices using inkjet printing technology. A Metal-Insulator-Semiconductor (MIS) diode was developed as a NO_2 gas sensor and a Biological Field-Effect Transistor (BioFET) was fabricated and optimized to operate correctly under aqueous media and to detect biomolecules.

This thesis presents the fabrication and characterization of a novel inkjet-printed MIS diode on flexible plastic substrates. The structure consists of a polymeric insulator/semiconductor interface sandwiched between two silver electrodes. It is proposed that the rectification properties are due to a voltage controlled leakage current across the insulator/semiconductor interface. The current across the insulator is caused by the formation of a semiconductor brush-like morphology into the underneath porous insulator layer. The carrier injection into the insulator follows a thermionic emission model. Temperature dependent measurements reveal an interfacial barrier height between 0.97 eV and 0.36 eV depending on the morphology and type of insulator layer used. MIS based diodes show rectification ratios up to 150 at |10V| and a current density up to approximately 1 μAcm^{-2}. The simple fabrication process of the diodes also makes it advantageous for scaling up to roll-to-roll production. Moreover, it has been shown that the MIS diode shows a good selectivity to detect NO_2.

Moreover, in this thesis biosensors based on Organic Field-Effect Transistors (OFETs) have developed due to the possibility of rapid, label-free, and inexpensive detection. However, top-gate BioFETs using a polymer as insulator and an amorphous polymer as organic semiconductor have been seldom reported. Therefore in this thesis, a systematic investigation in terms of topographical and electrical characterization has been carried out in order to find the optimal fabrication process for obtaining a reliable polymer insulator. Moreover, a simple immobilization protocol was used to ensure the proper attachment of a model biomolecule onto the Cytop's hydrophobic surface whilst keeping its remarkable insulating properties with gate current in the range of dozens of pico Ampers. The top-gate BioFETs fabricated using conventional techniques operated at voltages in the range of few volts and showed durability even when they were

exposed to oxygen plasma, wet amine functionalization treatment, and aqueous media. As the final phase, the BioFET was fabricated using inkjet printing technology. Drain/Source electrodes and the organic semiconductor were inkjet-printed achieving very thin films which are primordial for the correct electrical performance. Furthermore, the electrical characteristics were studied showing a good performance. Finally, as a preliminary result, the both top-gate BioFETs developed in the first and second phase demonstrated the capability of detecting the presence of biomolecules through changes in the drain current, which opens the way for further use in the immunosensing field.

Resum

En els darrers anys ha anat creixent l'interès per la tecnologia d'impressió electrónica (*Printed Electronics*, en anglès). La impressió d'injecció de tinta és una tecnologia que ha evolucionat des de la impressió gràfica fins a la investigació científica R&D, on es pot utilitzar com una tècnica de fabricació sense contacte molt reproduïble per dipositar materials funcionals a gran velocitat, ja sigui a superfícies petites o grans flexibles i/o rígides. És una tècnica de baix cost perquè minimitza els residus i redueix el número de processos de fabricació respecte a la tecnologia convencional. A més, el desenvolupament de materials orgànics, com polímers amb característiques elèctriques, ha impulsat la fabricació de nous dispositius elèctrics impresos orgànics.

En aquest marc, aquesta tesi està dedicada al desenvolupament de nous dispositius orgànics per a aplicacions químiques i de *biosensing* per a l'obtenció d'un sensor de baix cost utilitzant tecnologies d'impressió. D'aquest manera, en aquest treball s'ha desenvolupat: i) un díode basat en metall-dielèctric-semiconductor (*MIS*, en anglès) com un sensor de gas NO_2 i, ii) s'ha fabricat i optimitzat un transistor biològic de efecte de camp (*BioFET*, en anglès) el qual funciona correctament en condicions aquoses i també es capaç de detectar biomolècules.

Aquesta tesi presenta la fabricació i caracterització d'un nou díode MIS imprès sobre substrats plàstics flexibles. L'estructura consisteix en una interfície aïllant polimèrica/ semiconductor intercalada entre dos elèctrodes de plata. Les propietats de rectificació es deuen a un corrent de fuga controlada per la tensió aplicada a través de la interfície aïllant /semiconductor. La injecció de portadors a l'aïllant segueix un model d'emissió tèrmica. Les mesures en funció de la temperatura revelen una alçada de barrera interfacial entre 0.97 eV i 0.36 eV, depenent de la morfologia i el tipus de capa aïllant utilitzada. Els díodes basats en MIS mostren índexs de rectificació de fins a 150 a |10V| i una densitat de corrent fins a aproximadament 1 μAcm^{-2}. El procés simple de fabricació dels díodes fa que també sigui avantatjós per a la producció a gran escala. A més, s'ha demostrat que el díode MIS tenen una bona selectivitat per detectar NO_2.

A més, en aquesta tesi s'han desenvolupat biosensors basats en transistors orgànics d'efecte de camp (*OFET*, en anglès). Aquests dispositius presenten molts avantatges com la detecció ràpida, lliure de marcadores i de baix cost. Tanmateix, el BioFETs fabricats amb un polímer com a aïllant de porta i un polímer amorf com a semiconductor orgànic han sigut molt poc reportats a la literatura. Per tant, en aquesta tesi s'ha realitzat una estudi sistemàtic en termes de caracterització morfològica i elèctrica per tal de trobar el procés de fabricació òptim per obtenir un aïllant fiable. D'altra banda, es va utilitzar un simple protocol d'immobilització per garantir l'adequada fixació d'una biomolècula model a la superfície hidrofòbica del aïllant de porta Cytop, mantenint a la mateixa vegada les seves propietats aïllants. Els BioFET desenvolupat

funciona a voltatges baixos i mostrem durabilitat fins i tot quan estaven exposats a tractaments químics. Com a etapa final, el BioFET es va fabricar utilitzant la tecnologia d'impressió. Els elèctrodes de drenador/font i el semiconductor orgànic es van imprimir amb aquesta tecnologia aconseguint capes molt primes, les quals que són primordials per al correcte funcionament elèctric. A més, es van estudiar les característiques elèctriques del BioFET imprès, mostrant un bon comportament. Finalment, i com a resultat preliminar, els dos BioFETs desenvolupats han demostrat la capacitat de detectar la presència de biomolècules a través de canvis en el corrent de drenador. Aquests resultats obren un nou camí als BioFETs impresos i orgànics per ser utilitzats en el camp d'*inmunosensing*.

Acknowledgments

M’agradaria començar agraint al Dr. Eloi Ramon, Dr. Lluís Terés i al ICREA Prof. Arben Merkoçi per donar-me la oportunitat de fer el doctorat. Gràcies pel suport, guia i, per deixar-me flexibilitat en aquesta tesi. Poder-me expressar a través d’aquesta tesi ha sigut un plaer. També agrair al Dr. Alfredo de la Escosura per tot el temps dedicat a la meva tesi i per la seva gran disposició. També aprecio molt l’oportunitat que m’ha donat la Dra. Annalisa Bonfiglio per fer una estada a Cagliari. Gràcies a tot el seu fantàstic equip, per fer-me sentir com a casa.

També m’agradaria expressar la meva gratitud al professor Dr. Jordi Suñé, qui em va introduir en el món de la investigació. Més endavant, la passió per la investigació l’he pogut desenvolupar gràcies als meus companys del CAIAC-UAB. Gràcies a tots ells per tota l’experiència rebuda durant aquells anys.

Gràcies a tota la gent que ha estat en moments puntuals però importants, a tots els companys del projecte TDK4PE, i especialment al professor Henrique Leonel Gomes per ajudar-me a distància.

També estic molt agraïda a tota la gent que he conegut al ICN2, ha estat un luxe poder conèixer gent de tot el món. Gràcies a tots ells pels moments viscuts, per totes les alegries i hores de feina.

Agraeixo a tothom de la meva “casa”, el CNM. Lloc on he fet la tesi, lloc on he conegut gent molt maca, lloc on he après i lloc d’esforços. Gràcies a tots ells, per cada xerrada al passadís, per fer agradable aquesta etapa. Especialment, m’emporto molt bons moments viscuts al despatx, gràcies a tots ells: Miquel, August, Roger i Alba. Voldria donar les gràcies especialment a la Silvia per ajudar-me a l’última etapa de la tesi.

No em deixaré d’agrair a totes les meves amigues de Calella, juntes des de la guarderia.

I acabaré els agraïments dedicant-los a la meva família: als meus pares, a la meva germana, als meus avis, tiets i cosins, a tots vosaltres que esteu on estic sempre.

Carme Martínez Domingo

Table of Contents

1

Dissertation overview

Bioelectronics, combination of bioprocess with electronics, is quite important for the development of biomedical instrumentations. This field is with interest for the development of electronic sensor devices for the detection, quantification and monitoring of specific chemical and biological species. However, the main limitation in developing new applications for this technology is the use of conventional rigid and inorganic materials.[1] One aspect that cannot be neglected is the need to lower the cost of silicon-based electronics due to the emergence of single-use systems designed, for instance, for Point-of-Care (PoC) sensing. In addition, recent reports decoupling fabrication of high quality, single-crystal Si semiconductors from lower-temperature processing steps present potential alternative approaches toward the realization of low cost electronics.[2] Since all approaches face similar challenges and address similar markets, organic electronics (OE) solutions must show unique advantages such as mechanical flexibility, low-cost fabrication, and the use of delicate and biodegradable substrates.

The interest in organic electronic materials dates back to fundamental studies of their electronic structure conducted in the '60s. The development of conducting polymers in the '70s and the application of organic semiconductors (OSCs) in electrophotography in the '80s contributed to the creation of basic electronic structures. The research community started using OSCs in the '90s, and launched a variety of organic-based devices including light emitting diodes, transistors, and solar cells among others.[3] The application of OE at the interface with life sciences creates many opportunities because of some unique features of these materials.

Organic and Printed Electronics (PE) is based on the combination of new materials and cost-effective large area production processes that open up new fields of application. Being thin, light-weight, flexible and environmentally friendly, it also enables a wide range of electronic devices that can be produced and directly integrated in low cost reel-to-reel processes. By using different printing technologies, the process becomes all-additive bottom-up method without the need of expensive lithography or vacuum processes, resulting in a significant reduction of production costs and material waste. Therefore, printing electronics techniques can also promote the production of small batches. The use of functional materials converted disruptively the PE into an established cost-effective technology for flexible electronics.

Among the current digital printing technologies, drop-on-demand inkjet printing stands out as a cost-effective, fast prototyping and, maskless technique suitable for research.

1.1 | MOTIVATION AND OBJECTIVES

Since the last decade, the interest in the development of organic electronic-based sensors which can be integrated in circuits has grown. For a broad range of sensing applications (e.g., medical diagnostics, food monitoring, detection of chemical, etc.), there is a demand for portable, small and inexpensive sensors. A wide variety of printed organic sensors can be found in the literature, mostly electrochemical electrodes.[4]

However, organic semiconductor-based electronic devices offer a great deal of promise for applications in chemical and biological sensing.[5] These kinds of devices have many other advantages over electrochemical electrodes. OSCs can be deposited using low-temperature processes on a variety of substrates. Moreover, they present very interesting features since they can be easily processed from solution, and through precise synthesis, their chemical and physical properties can be tuned. Miniaturization of these devices is straightforward, so portability, small samples volumes, and arrays with many elements are achievable. In addition, they provide a response (current change) without the need to use a label making them is easy to measure with simple electronic instrumentation.

The electronic devices based on OSCs and, proposed as sensors in the literature are: Organic Thin-Film Transistors (OTFTs), Organic Light-Emitting Diodes (OLED), and diodes.[5][6] However, they are currently less represented in the literature compared with the electrochemical electrodes. These new opportunities present challenges in terms of fabrication processes since they are based on functional layer stacks. Up to date, very few examples of inkjet-printed diodes and OTFTs operating as chemical or biological sensors have been reported, limiting the potential of OE in this field.

The main objective of this thesis is the development of flexible inkjet-printed sensors using functional inks with electronic properties. In particular, the effort is being

focused on their fabrication processes and on the characterization of their electrical performances. Furthermore, different sensor architectures will be developed such as chemosensors and biosensors for detection in gas and liquid media. Aiming at obtaining low-cost devices, they will be realized using organic semiconductor technology and low-cost printing techniques.

Different kinds of active devices suitable for detection of chemical and biological species will be investigated with a focus on the **development and optimization of the fabrication processes and device performances** in order to obtain:

i) Metal-Insulator-Semiconductor (MIS) diode devices as gas sensors.

ii) OTFTs devices as biomolecule sensors, called Biological Field-Effect Transistor (BioFET)

In this thesis, inkjet printing technology will be used as a versatile fabrication technique for the manufacturing of the electronic devices and as a complement and alternative to conventional fabrication process for depositing organic materials on polymeric substrates.

To achieve these goals, some sub-objectives need to be addressed first:

- **Material characterization**. In order to achieve functional devices, different materials have been evaluated and deeply characterized. The main organic material studied was the insulator ink. Various insulators inks were characterized in order to achieve the electrical requirements for each device. In fact, this material is present both in MIS and BioFET structures but its electrical performance differs strongly with each one. Therefore, a deep study in terms of morphology and electrical performance was carried out. In this context, a great effort along the thesis was done in order to optimize the insulator ink in terms of technology.

- **Development of novel devices**. The goal of this thesis is to provide novel inkjet-printed organic sensors for sensing applications. This represents a challenge in terms of fabrication processes, material selection, and device's architecture. The goal is to achieve devices that can be called new from several angles. The proposed MIS structure is based on a novel working principle not yet explored in the literature. Moreover, the development of the BioFET will present innovation in terms of the achievement of a functional organic polymeric device based on field-effect operating in aqueous media.

- **Biofuncionalitzation strategy.** Regarding the BioFET, a suitable functionalization of the gate dielectric surface while keeping its insulating properties is an important goal of this thesis. In the literature, a big amount of functionalization recipe has been studied. In fact, a tailored functionalization recipes needs to be carried out for the BioFET since their particular novel organic material and architecture used. Therefore, a deep study of different

functionalization recipes to attach biomolecules was carried on. This task required a great deal of efforts devoted to thesis to ensure proper device's operability.

- **Static and dynamic electrical characterization over time**. Static electrical measurements such as current-voltage, capacitance-voltage, and current-voltage as a function of temperature are used widely in this thesis. Since the high technological dominance of this thesis, the quality and the processing of materials (semiconductors, conductors and, dielectrics) have been studied using electrical characterization techniques. These techniques have several advantages since they are fast, non-destructive and, accurate so that important parameters such as mobility of carriers, interface quality, threshold voltage and, energy barrier can be determined. OSCs and dielectrics can be used in a big set of device applications, starting from the conventional solid state devices up to some innovative and multifunctional applications in which the operation can be widely sustained by exploiting the peculiar structural and mechanical properties of organics, as happens in the case of sensoristics. In fact, aging phenomena, electrical stresses, but also environmental and chemical agents may concur at the same time, each one with a certain weight, to the worsening of device performances. In this respect, the short device lifetime limits the employment of organics to those applications in which it is not required a long time operation. In this respect, this thesis also will pay attention to the dynamic techniques of electrical characterization for the comprehension of organic devices.

- **Printability of organic materials.** In this work, additive manufacturing such as inkjet printing technology was used to fabricate both the MIS and the BioFET devices. In order to successfully print the devices, appropriate printing parameters must be selected for the metallic and the OSC inks. A good printability of the materials in terms of thickness and, surface roughness will affect the final electrical performances. For these reasons, an optimization of each ink is essential for each printing process in order to fulfil the requirements of the different devices.

- **Validatation of developed sensors.** MIS and BioFET devices are presented as novel electronic devices. Moreover, proof-of-concepts of their sensing capabilities will be reported. MIS devices will be assessed as gas sensor and the BioFET will be tested as an immunosensor. In this context, preliminary results will be reported. Further studies including, for example, complex biological matrix, are beyond the goal of this thesis.

1.2 | MAIN CONTRIBUTION OF THIS THESIS

This thesis has been focused on the **technological development of organic electronic devices for the field of bioelectronics**. Therefore, the principal effort was dedicated to the development of novel electronic devices. Sensor applications were developed as proof-of-concepts to demonstrate the capability of the presented structures as transducers.

The first device developed in this thesis has been a MIS diode. The device structure has novel aspects which make it unique with respect to all the other organic diodes reported in the literature. MIS diode devices were previously realized to obtain a rectifying behaviour using: i) standard fabrication techniques for the deposition of the electrodes and, ii) inorganic materials. Compared to the previously published diodes, the MIS diode realized in this thesis relies on the use of only polymeric materials as far as the rectifying interface is concerned. Inkjet-printed MIS structures have been developed as novel devices that allow to overcome the use of metal electrodes with different work functions, which is currently difficult in the field of PE due to the reduced availability of printable metals.

The implementation of gas sensing devices was demonstrated by using the MIS diode as gas sensor for the detection of NO_2 at room temperature thanks to the OSC electrical properties.

In the second part of this thesis, an OTFT-based biosensor, called Biological Field-Effect Transistor (BioFET), was developed. Its architecture allows to overcome several typical drawbacks of the commonly reported biosensors fabricated with organic polymers for the detection of charged biomolecules in liquid media.

The inkjet-printed BioFETs developed and optimized as sensors for biomolecules present a new transistor architecture that can be used as immunosensors. This choice is related to the increase demand for low-cost, portable and label-free recognition systems in many medical fields. In particular, the fabrication of the BioFET device has been carried out in two phases:

i) First-phase: the BioFETs were fabricated using organic materials and conventional micro-fabrication techniques such as evaporation and spin-coating onto flexible substrates in order to study and optimize their electrical characteristics using mature fabrication techniques.

ii) Second-phase: once the organic materials used in the first-phase were fully characterized, the BioFETs were fabricated using inkjet printing technologies onto flexible substrates to obtain low-cost devices.

As a summary, the focus of this thesis deals with the development of low-cost, flexible sensors based on novel architectures and working principles not already reported in the literature. Great efforts were focused on the technology challenges related to the inkjet

printing fabrication of organic devices that can detect gases or biomolecules and can operate correctly under aqueous media.

1.3 | THESIS OUTLINE

The thesis is organized as follows:

Chapter 2, entitled *Introduction to Printed Electronics*, is devoted to introduce the technologies used in this thesis for the fabrication of MIS and BioFETs devices. Among the wide range of micro-technologies, the attention is focused on the use of Printing Techniques. In the first part, an overview on PE is reported. In the second section, the general characteristics of the principal printing techniques are described. A particular attention is given to inkjet printing technology.

Chapter 3, entitled *Introduction to Organic and Printed Sensors*, gives an introduction to the printed and organic sensors currently present on the market. This chapter also describes the background of organic diodes. A deep insight is given to the Metal-Insulator-Semiconductor (MIS) diodes state-of-the art. An overview of the most relevant works about organic diodes employed as gas sensors is reported.

Moreover, an introduction on Biosensors is reported. In order to explain the reasons and the specific choices behind the development of the presented structure, a brief introduction to several OTFT structures as sensors and an overview of the most relevant works about OTFTs as biosensor are reported.

Chapter 4 is entitled *Inkjet-printed MIS diode-based sensors*. The first part is devoted to the working principle of the MIS diodes. In the second part, a new MIS diode fabricated using polymeric materials is presented. A deep study in terms of: i) morphology of the inkjet-printed layers and ii) electrical performances has been carried out. It has been demonstrated that the electrical performances of these devices are correlated with the properties of the dielectric layer. Finally, these devices have been used as NO_2 sensors due to the capability of the OSC to detect gases.

Chapter 5 is entitled *Organic Inkjet-Printed BioFETs*. The first part is devoted to the description of the working principle of the BioFET-based sensors. Afterwards, the attention is specifically focused on the development of reliable BioFETs using organic materials and microfabrication techniques. A deep study to achieve functional BioFETs that can operate in aqueous media was conducted. Moreover, a simple functionalization procedure of the insulator surface in order to attach biomolecules without losing its performance as a transistor is developed. Finally, as a proof-of-concept, the capability of these devices as immunosensors was demonstrated. The last part of the chapter is focused on the development of functional inkjet-printed BioFET for low-cost devices. The first part describes a morphological characterization of the inkjet-printed layers of the BioFET. In the second part, the experimental results about the functionalized BioFETs as proof-of-concept immunosensors are reported.

Finally, Chapter 6 gives a brief overview of the topics and summarizes the conclusions of the presented PhD dissertation. It is also discussed the future possibilities related to the developed devices.

1.4 | THESIS FRAMEWORK

The main part of this thesis has been carried out in the facilities at the Institut de Microelectrònica de Barcelona (IMB-CNM) del Consejo Superior de Investigaciones Científicas (CSIC) in the group of Integrated Circuits and System leaded by Dr. Lluís Terés; and at the Institut Català de Nanociencia i Nanotecnologia (ICN2) in the group of Biosensors and Bioelectronics leaded by ICREA Prof. Arben Merkoçi.

Carme Martínez-Domingo has been working in the following Projects during her PhD activity:

- "*Nuevas Soluciones basadas en PRINTED ELECTRONICS para la detección de variables físicas y la liberación de compuestos orgánicos", Ministerio de Industria, Energía y Turismo* (TSI-100101-2013-94), Technology transfer contract with CARINSA, S.A. 1/1/2013-31/12/2015. Funding: 62.125 €.

-SMART PRINTED PAPER: "*Printed Electronics para nuevas funcionalidades en papel", Ministerio de Economía y Competitividad* (RTC-2014-2619-7), 1/2/2014-31/12/2016. Funding: 155.284 €. Partners: Jusmer SL, ICN, IMB-CNM

- NANOCARDIOFLEX – "Desarrollo de biosensores sobre tecnología flexible y rígida para la detección de marcadores cardíacos", Ministerio de Economía y Competitividad (RTC-2015-4184-1), 25/2/2015-31/12/2017. Funding: 175.584 € Partners: BRIP Apps AlphaSIP SL, Universidad Complutense de Madrid, IDIBAPS, IMB-CNM.

Moreover, Carme Martínez spent 3 months (May-July 2016) for a practical-stage at the Electrical Department of Università degli Studi di Cagliari, Sardegna, Italy. She carried out part of her thesis in the group of DEALAB leaded by the Prof. Annalisa Bonfiglio.

1.5 | REFERENCES

[1] Malliaras GG. Organic bioelectronics: A new era for organic electronics. *Biochim Biophys Acta BBA - Gen Subj* 2013; 1830: 4286–4287.

[2] Kelley TW, Baude PF, Gerlach C, et al. Recent Progress in Organic Electronics: Materials, Devices, and Processes. *Chem Mater* 2004; 16: 4413–4422.

[3] Malliaras G, Friend R. An Organic Electronics Primer. *Phys Today* 2007; 58: 53.

[4] Li J, Rossignol F, Macdonald J. Inkjet printing for biosensor fabrication: combining chemistry and technology for advanced manufacturing. *Lab Chip* 2015; 15: 2538–2558.

[5] Mabeck JT, Malliaras GG. Chemical and biological sensors based on organic thin-film transistors. *Anal Bioanal Chem* 2006; 384: 343–353.

[6] Shinar J, Shinar R. Organic light-emitting devices (OLEDs) and OLED-based chemical and biological sensors: an overview. *J Phys Appl Phys* 2008; 41: 133001.

[7] Martínez-Domingo C, Conti S, Terés L, et al. Novel flexible inkjet-printed Metal-Insulator-Semiconductor organic diode employing silver electrodes. *Org Electron* 2018; 62: 335–341.

[8] Gomes HL, Medeiros MCR, Villani F, et al. All-inkjet printed organic transistors: Dielectric surface passivation techniques for improved operational stability and lifetime. *Microelectron Reliab* 2015; 55: 1192–1195.

[9] Sowade E, Ramon E, Mitra KY, et al. All-inkjet-printed thin-film transistors: manufacturing process reliability by root cause analysis. *Sci Rep* 2016; 6: 33490.

[10] Sowade E, Mitra KY, Ramon E, et al. Up-scaling of the manufacturing of all-inkjet-printed organic thin-film transistors: Device performance and manufacturing yield of transistor arrays. *Org Electron* 2016; 30: 237–246.

[11] Mitra KY, Polomoshnov M, Martínez- Domingo C, et al. Fully Inkjet-Printed Thin-Film Transistor Array Manufactured on Paper Substrate for Cheap Electronic Applications. *Adv Electron Mater* 2017; 3: 1700275.

[12] Mitra KY, Sternkiker C, Martínez-Domingo C, et al. Inkjet printed metal insulator semiconductor (MIS) diodes for organic and flexible electronic application. *Flex Print Electron* 2017; 2: 015003.

[13] Ramon E, Martinez-Domingo C, Alcalde-Aragones A, et al. Development of a Simple Manufacturing Process for All-Inkjet Printed Organic Thin Film Transistors and Circuits. *IEEE J Emerg Sel Top Circuits Syst* 2017; 7: 161–170.

2

Introduction to Printed Electronics

This chapter is an introduction to the novel manufacturing technologies used in this thesis work. Firstly, an overview on printed electronics and its applications in sensors and biosensors are reported. Then, the general characteristics of the principal printing techniques are described. Moreover, the inkjet printing technology will be explained in detail since it is used in this thesis.

Nowadays the high demand in our lives of printed materials such as newspapers, food packaging, magazine, and advertising among others has revolutionized the printing technologies coming from the graphic arts (GA), over the past decades. The fast growing of these technologies has led the emergence of the concept of Printed Electronics (PE) which is one of the fastest growing technologies to manufacture electronic and optoelectronic circuits. This technology has enabled a new paradigm of electronic manufacturing using new materials and new devices with different functionalities announcing a revolution in the microelectronics industry that currently is focused in silicon and conventional manufacturing techniques. Conventional fabrication of integrated circuits involves various fabrication steps such as vacuum deposition along with lithography processes among others to transfer a desired pattern onto the substrate. These patterning methods require masks and subtraction of material already deposited, which increase the cost of fabrication. In contrast, printing techniques results in a much simpler and cost-effective way to fabricate devices. Printing techniques is an additive manufacturing technique used to deposit and pattern functional materials such as conducting, insulating and semiconducting among others in order to create a wide variety of devices, such as transistors, resistors, capacitors, diodes, memories, sensors etc...

2.1 | OVERVIEW OF PRINTED ELECTRONICS

PE utilizes printing techniques such as flexography, screen, gravure and inkjet printing technologies because their viability to manufacture low-cost, high volume and high throughput production of electronic components. The essential requirement for printed materials is their processability in liquid form (as solution, dispersions or suspensions) to be constituted as an ink. Thanks to the efforts in the field of Organic Electronics (OE) to substitute inorganic semiconductors (silicon, gallium arsenide, etc.) and oxides (silicon dioxide), a range of functional inks materials that can be printed has increased greatly during the last decades. Therefore, organic materials offer the possibility to process at low thermal budget and a high degree of mechanical flexibility opening new opportunities to produce flexible, rollable, lightweight and environmentally friendly thin films for electronic applications over a small (sheet-to-sheet manufacturing) or large areas (roll-to-roll manufacturing).

Organic-based inks can be printed directly to an unmodified or pre-treated substrate in order to achieve a better deposition in terms of adhesion, wettability, etc. After the deposition of the functional material in form of ink, generally one post-processing step is required related to the sintering or curing of the ink. Although PE is not a substitute for conventional silicon based electronics, which requires a high density integration and high switching speed performances, it take advantages from the organic materials to fabricate stacks of functional layers in much simpler and more cost-effective way. Figure 2-1 shows a thorough comparison between PE and photolithography processes.

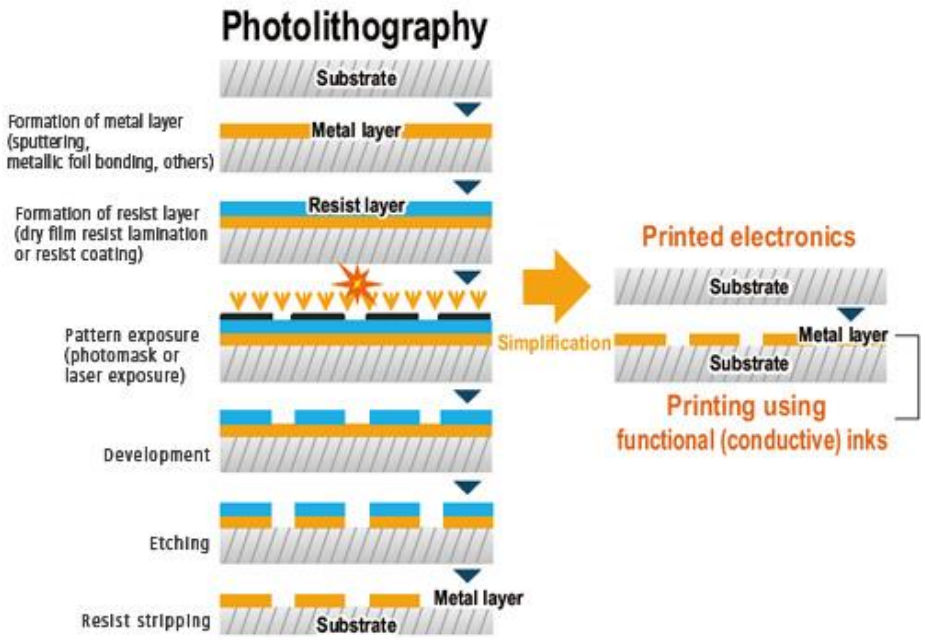

Figure 2-1 Schematic diagram showing the fabrication steps for the deposition of a metallic layer electrode using photolithography and PE.[1]

2.2 | APPLICATIONS OF PRINTED ELECTRONICS

New devices and applications have been developed in to the fields of Organic Photovoltaics (OPVs), Flexible Displays (OLED), Lighting (including both OLED and electroluminescent products), Electronics and Components (including radio frequency identification (RFID), memories, batteries and others) and Integrated Smart Systems (including smart objects, sensors and smart textiles). Figure 2-2 shows the roadmap for organic and printed electronic applications published by the Organic Electronics Association (OE-A)[1].

[1] Organic Electronics Association (OE-A), http://www.oe-a.org/

Figure 2-2 Roadmap for Organic and Printed Electronics Applications.[2]

Some of the solutions are already commercial on significant scale, while others are still proof-of-concept prototypes. Some of the most important ones include:

- **RFID tags and smart objects**

  The widespread demand of wireless communication is increasing the development of wearable antennas that can transmit and receive high-frequency signals, such as RFID tags. A RFID tag is essentially a well-designed conductive pattern that acts as an antenna capable of receiving and transmitting data (Figure 2-3). The RFID systems are expected to replace the UPC barcode to improve automation of inventory control. Furthermore, item-level RFID tags can potentially be integrated with a sensor and a display to provide product information such as expiration date. Most economic analysis suggests that the cost of each tag needs to be less than one cent USD to be used massively and become economically viable, since the individual tagged product typically has a price in the range of few cents to few tens of cents USD. This goal is extremely challenging.[3]

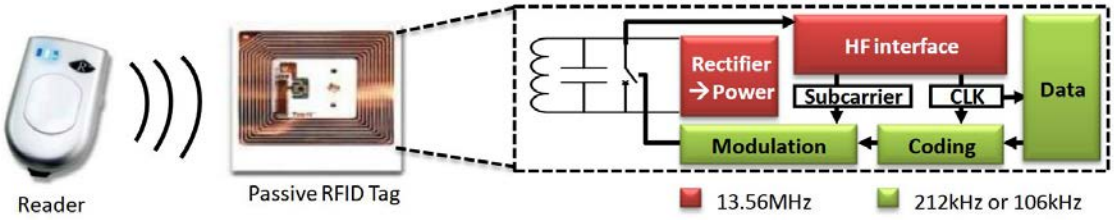

Figure 2-3 A basic RFID system comprises a reader and a passive tag.[4]

- **OLED lighting**

  It is moving from an expensive design option into more mainstream architectural lighting as prices are beginning to decrease. Non-planar and bendable lighting has appeared in initial products, such as automotive taillights and bendable OLED lighting panels. Complete flexible and transparent OLEDs are intended to be commercial products in medium-term.

- **Organic Photovoltaics (OPV)**

  OPV have been significant breakthroughs in efficiency and in semi-transparent modules, detailed environmental impact studies are available, and lifetimes up to 20 years have been reported. Since the production capacity has increased, flexible OPV modules can be bought online for a low price, and more building integration installations have been built, however their complete integration is expected to be in medium-term.

- **Electronics and components**

  Electronic devices and components are generally divided into two main families: passive or active elements. Passive elements are commonly two-terminal structures, formed by a single functional conductive material.[5] For instance, passive components are conducting pad-stripes, resistors, capacitors, inductors which do not introduce any energy into the electronics system. On the contrary, active devices are typically more complex structures than passive elements. Transistors, diodes, batteries, solar cells rely on a source of power and inject net energy into the electronics systems.[6] Active PE devices are not established in the market yet, even though organic semiconductors (OSCs) are already compatible with inorganic materials.

- **Integrated Smart Systems**

  Smart systems refer to products that integrate multiple functionalities and technologies to create added value. The hybrid system integration of PE, e.g. for sensing, antennas and energy harvesting/storage, with the computing power of small silicon chips is becoming recognized as an area where PE can be a true

enabler. Wearable health and wellbeing applications are also emerging. In the sensing area, with the emergence of the need for Point-Of-Care (POC) devices, the use of PE, in particular, screen-printing and inkjet printing techniques have become widely used.[7]

2.3 | BENEFITS OF THE TECHNOLOGY

As already mentioned, although PE will not achieve high electrical performance as silicon-based electronics, it presents large advantages which conventional electronics cannot compete and these are listed below:

- **Flexible substrates**

  Silicon-based electronics use pure, monocrystalline silicon wafers as bulk substrates for the fabrication of electronic devices: therefore, they are rigid and cannot be conformed to every surface's shape. PE uses a totally different approach: paper and plastic substrates are employed as bulk structures over which organic layers are deposited. This allows the use low-weight and, flexible substrates directly related to their portability and their conformability almost to every surface. Clear examples are the flexible displays for mobile devices and smart textiles.

- **Large area electronics**

  It allows printing on large surfaces not constrained by wafer size. PE can employ flexible plastic rolls as substrates and therefore easily extend deposition processes to large areas.

- **Mass production**

  Printing can be much faster than traditional microelectronics fabrication and it is a direct consequence of the processability over large areas and the simple fabrication methods employed. Since PE does not require photolithography and other post-processing chemical treatments, but carries out all the fabrication in a single step, it is suitable for mass production. This is the key to low cost production and is the facilitator of disposable electronics.

- **Low fabrication costs**

  Thanks to the possibility of having an additive process, overall tool costs are reduced, both because the cost of individual tools is expected to drop somewhat and also because the number of required tools is reduced. The precise cost advantages relative to silicon depend on process throughput and material costs, although cost advantages on the range of 1–3 orders of magnitude per unit area are expected. Moreover, since materials are deposited in liquid form, they can be processed at room temperature and then annealed at medium temperature, usually not exceeding 150-200 ºC. On the contrary, other techniques, among all thermal

evaporation, require high temperatures and high-vacuum conditions, which dramatically increase the fabrication costs especially at industrial level. Moreover, printing has a low capital investment cost than other fabrication techniques. It is estimated that a PE plant will cost 25 million €, just a fraction of a 2.5 billion €, of a conventional silicon fabrication plant.[2]

- **Integration**

  It allows complete system integration since printing could be capable of the assembly of devices using multiple technologies (logic, memory, battery, displays, etc.).

- **Environmentally friendly**

  Organic materials use more efficient printing processes in terms of low power consumption and selective deposition processes improving the environmental impact of electronic industry.

- **Bio-compatibility**

  Using organic materials in biomedicine can improve acceptance of these systems in contact with human body.

2.4 | PRINTING TECHNIQUES

PE technologies are basically divided in two major classes: contact printing, which deposits inks by direct contact between the printing plate and the bulk substrate, and non-contact printing, by which ink is deposited on the substrate without any contact with the printing plate (Figure 2-4).

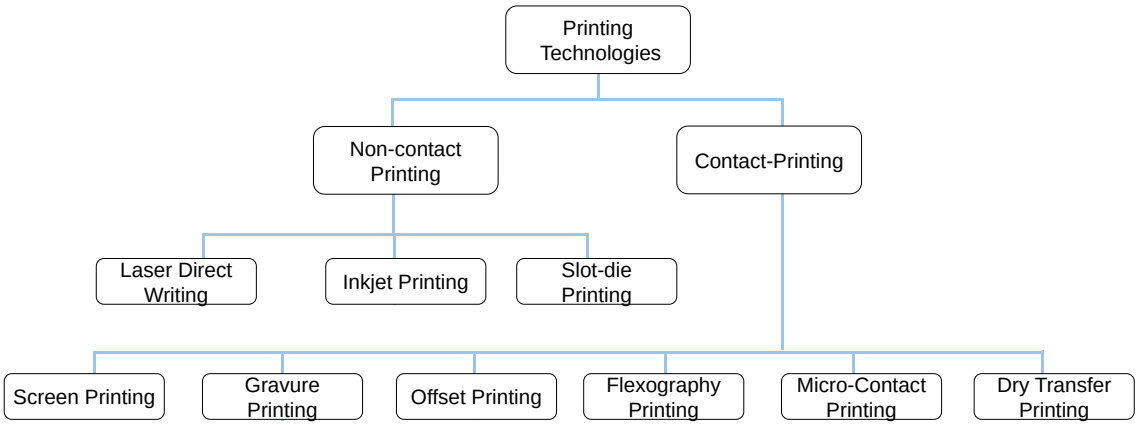

Figure 2-4. Scheme of the classification of Printing techniques.

The contact-based printing technologies comprise: gravure printing, gravure-offset printing and, flexographic printing among others. The prominent non-contact printing

techniques include laser direct writing, slot-die coating and, inkjet printing. The non-contact printing techniques have received greater attention due to their capabilities such as affordability, simplicity, adaptability to the fabrication process, reduced material wastage, and high resolution of patterns. Moreover, it allows printing onto very fragile substrates. Typical contact-printing methods such as gravure and flexography are commonly employed as roll-to-roll methods, while other methods such as inkjet and screen printing are mostly used as sheet-fed methods.[8] Moreover, the inkjet printing technique is also classified as digital printing. Digital printing refers to methods of printing from a digital-based image and its great advantage is the non-use of masks, meaning that it can quickly switch from one design to another without the need for a new set of expensive masks, which enables a more flexible processing flow.

A general description of all the printing techniques goes beyond the aim of this thesis dissertation. In particular, as inkjet printing is the technique employed in this work, it is described more in detail with respect to the other technologies. A wide literature has been published which compares in detail the different printing techniques: for more specific information, a careful reading of these articles is warmly advisable.[9][10][11]

2.4.1 | Contact printing techniques

- **Screen Printing**

  Screen-printing is the most popular and matured technology for printed electronics as it has been practiced in electronics industry for printing metallic interconnects, and others on printed circuit boards. It is faster and more versatile in comparison to other printing tools, as it adds simplicity, affordability, speed and adaptability to the fabrication process. It is a contact printing technology where ink is transferred through, and not from, a patterned surface (Figure 2-5). It is composed of a screen mesh stretched over a screen frame. In a pre-printing process, an emulsion, whose properties depend on the chemical and physical properties of the ink to be printed, is poured onto the back side of the mesh.

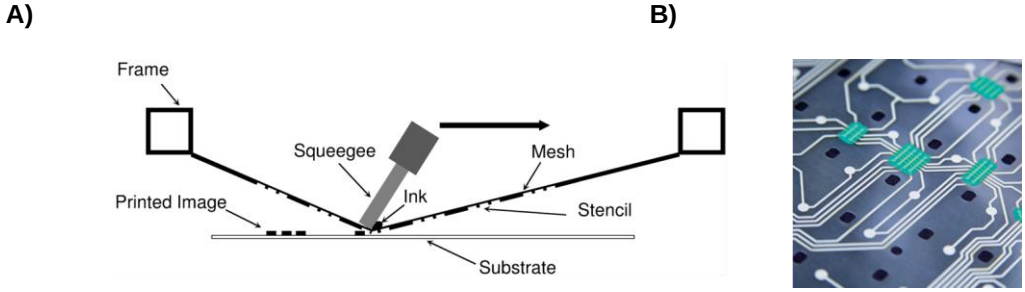

Figure 2-5 A) Scheme of the screen printing technology. B) Picture of a circuit fabricated using screen printing technology.

An exposure unit removes the unnecessary emulsion, leaving a pattern which presents the negative image of the desired final pattern. Then the screen is placed on top of the substrate and the ink is poured on the front side of then mesh; a flood bar is used to push the ink through the mesh holes. The actual printing process starts when a rubber blade, named squeegee, is slid at a fixed speed along the screen, moving the mesh down in contact with the substrate. The ink which fills the mesh holes is therefore pumped through the openings, i.e. the emulsion vacancies, directly to the substrate. Although it is a very simple process, the print quality and characteristics are affected by various factors such as the solution viscosity, printing speed, angle and geometry of the squeegee, snap off between screen and substrate, mesh size and material. The paste viscosity and surface tension of the substrate are important to complete dispensing of the paste trough the screen mask.

Screen printing technique is usually compatible with the high-viscosity inks as the lower viscosity ones will simply run through the mesh rather than dispensing out of the mesh.[12] Without giving any consideration to proper tuning of the ink properties and mesh count, the nominal values of 50-100 microns are common print resolutions and wet thicknesses of a few microns. A compromise between surface energies of substrates and surface energies of the inks is important for high-resolution line widths. Material, strength and number of meshes in screen also play a major role in high-resolution patterning, as screen is developed by using different sizes of mesh openings and several materials ranging from polyester to stainless steel. The technological developments in the screen mesh are mainly focused in the modification of the silk strength by using materials such as nylon, polyester and stainless steel. By an opportune tuning of the printing parameters, only the desired amount of ink in the desired position creates the final pattern. This technique is most employed for the fabrication of organic photovoltaic cells, RFID antennas, electrodes, etc.

- **Flexography**

  It is a roll-to-roll contact printing technique used for high speed runs of printed electronics (schematized in Figure 2-6A) employing a set of cylinders. The transfer of ink is done through direct contact of a soft printing plate cylinder, typically made of rubber or a photopolymer, that reproduces the positive image of the final pattern (like on a traditional stamp). The inking of the printing plate cylinder is provided via a ceramic anilox roller characterized by engraving, i.e. small cavities separated by small walls, where the ink is deposited by an ink supplier.

  The anilox cylinder is continuously supplied with ink by contact with a fountain roller that is partly immersed in an ink bath. The excess ink on the anilox is removed by a doctor blade ensuring good control of the wet layer thickness,

which is defined by the volume of the cavities in the anilox cylinder (anilox volume) and the transfer rates from the printing plate cylinder to the substrate. From the anilox, the ink is transferred in a precise controlled way to the molded printing plane, in a raised position. The printing substrate is pressured between the rolling plate cylinder and a third hard cylinder, called impression cylinder. The ink is thus impressed from the raised position of the soft mold to the sliding substrate and the final pattern is the exact positive reproduction of the patterned soft mold. This process will result in uniform thin layers and offers improved pattern reliability and sharp edges. A wide range of inks can be printed with such technology (solvent-based, water-based, electron-beam curing inks, UV curing inks etc.) and no strict physical requirements are necessary for the ink formulation. Being dependent on the picked-up ink by the printing cylinder with engraved trenches, flexography is an inconvenient way of getting continuous printing patterns in the case of cells being blocked or eroded by continuous operations. Moreover, due to the inclusion of flexible plate for transferring ink onto substrate, the major drawback of this technique is represented by the halo effect. The actual pattern lines tend to diverge from the targeted resolutions as the ink tends to spread outside the image areas due to the compression applied, thus limiting the resolution of the process. The current technology limits the highly desirable features such as high switching speed and reduced supply voltage that are needed for many applications. These limitations result in degraded device parameters like charge carrier mobility, parasitic capacitances and overlay precision registration accuracy when printing e.g. Organic Thin-Film Transistors (OTFTs).

- **Gravure printing**

  It is an intaglio printing technique in which ink is carried from an ink fountain to a printing surface using an engraved cylinder (gravure cylinder), which is electroplated with chrome to protect it from wear and tear during the ink transfer and contact with the substrate (Figure 2-6B). The cylinder comprises periodic cells filled with ink, and the excess is scraped off the surface using a doctor blade. Therefore, the ink is kept only in the cavities of the mold in a recessed position and, when the printing cylinder presses the sliding flexible substrate, the printed pattern is the negative pattern of the molded form. Smoothness, compressibility, porosity, ink receptivity, wettability, viscosity, solvent evaporation rate, drying, doctor blade angle and pressure, impression pressure, printing speed and uniformity of the gravure cylinder diameter are some of the parameters defining the printed results on flexible substrates. The printing plate/ink/substrate temperature can be controlled to optimize the printed features. The width and thickness of the printed features depend on the width and depth of the engravings in the mold, the printing speed, the ink viscosity, and the ink/substrate surface energies. This technique is generally characterized by the same advantages

(versatility, speed) and disadvantages (non-high resolution) as flexography. Standard molds are made of small separated points which allow the fabrication of electronic device components. The use of gravure in Organic Field-Effect Transistors (OFET) printing is attractive because it is high throughput, permits control over the feature size, and is flexible in terms of substrate selection. Where continuous conductive elements are required, such as RFID tags, the mold is engraved with linear structures: in this case the technique is called intaglio.

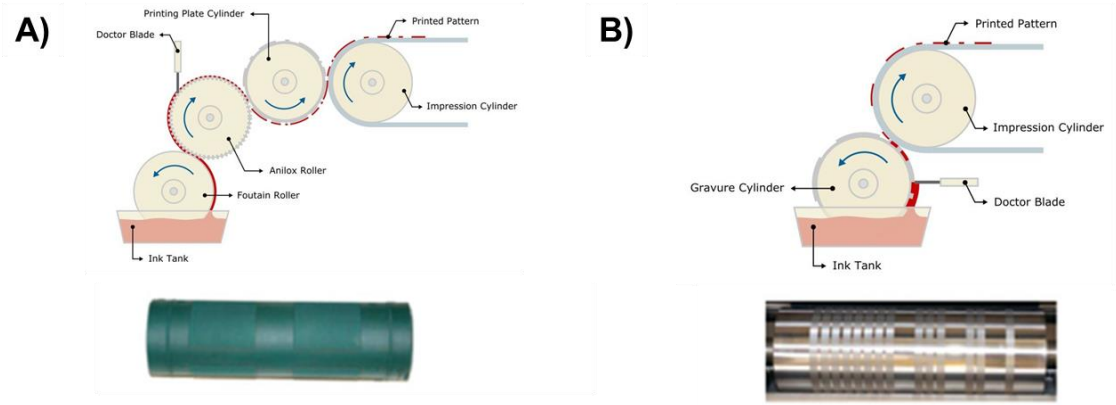

Figure 2-6. Schematic diagram of A) Flexography and B) Gravure.[13]

2.4.2 | Non-contact printing techniques

As already mentioned, in non-contact printing techniques the substrate is in contact only with materials which make up the device thus lowering the risks of damage and contamination. The non-contact patterning method also permits to obtain accurate alignment with patterns already on the substrate, which is an indispensable functionality to pattern multilayered devices. Furthermore, the absence of direct contact between the printhead and the support together with the low processing temperature required by this kind of technologies, makes them compatible with various kinds of surfaces such as glass, silicon, paper, metals, rubber, plastics (e.g. flexible polyester films, which can be irreversibly damaged and deformed if subjected to thermal stresses and high temperature processes) and, generally with contact-sensitive substrates. Also, non-contact techniques are typically digitally implemented i.e. a physical master of the to-be-printed pattern is not needed. Instead, the pattern is only represented as information in a digital form and every print can be different without additional tooling cost.[14]

This class includes a wide range of printing technologies; roughly, they can be divided into four main sub-classes, depending on the physical principle they work by: Xerography, Laser-based techniques, Inkjet printing and Slot-Die Coating. In the following, an example of the laser group, namely the Laser Direct Writing and Slot-Die

Coating will be briefly described. More attention will be given to Inkjet printing technology, which has been used during this thesis.

- **Slot Die Coating**

  Slot die coating is a direct way of developing Roll-to-Roll (R2R) processes whereby solution is coated on the substrate by dispensing, as shown in Figure 2-7A. In slot-die coating, the ink is poured from top through a via-opening and it is placed very close to the substrate, but without touching it. The substrate is mounted on the rotating cylinder. The constant supply of ink forms a standing meniscus between the moving substrate and the coating head. This creates a continuous coat of quite even thickness over a large area. Because of the use of a pump it is possible to regulate the wet layer thickness with very high precision as it is defined by the pumping speed, the width of the meniscus, and the web speed. Slot-die coating can be used for inks with large variations in viscosity and solvents. Compared to many other coating and printing techniques they are also relatively forgiving with respect to wetting of the substrate as the ink is ‘‘poured’’ into the substrate compared to printing techniques where surface tension and surface energy play a more significant role in the transfer of the ink. De-wetting of the formed film will occur if the surface tension of the ink is larger than the surface energy of the substrate.

  This type of coating is favorable for large areas, but pattering of high resolution structures is difficult to obtain. That is why this technique is usually practiced for large area devices i.e. light emitting diodes and solar cells. The operation is affected by various coating defects such as dripping, air entrainment, ribbing, start-up and shut-down periods of coating cycle. Inefficient control of the printing process results in wastage of the coating solution and also affects the shape of the patterns on the substrate by introducing the edge effects.[15][16]

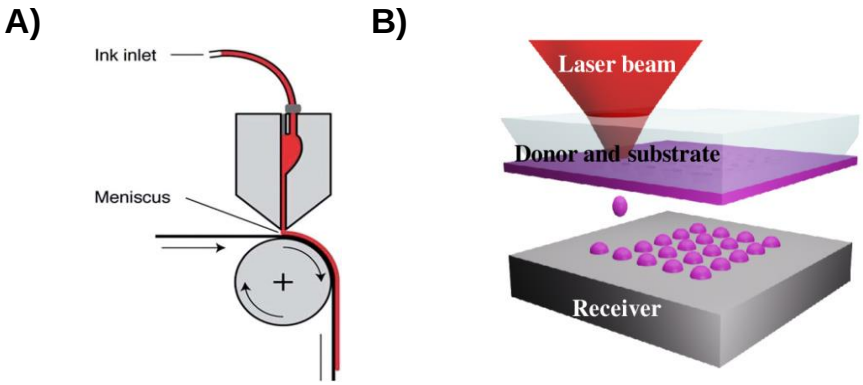

Figure 2-7 Schematic diagram of A) Slot Die Coating and B) Laser-Induced Forward Transfer.

- **Laser Direct Writing**

  This technique is a set of non-contact printing techniques used both for the deposition of inorganic and organic materials. A detailed overview of the process is given by Park et al. [17] while an example of specific application in the organic field is reported by Ribierre et al. [16]. A wide range of materials can be printed by means of these technologies, from metals to polymers and ceramics, and they can be deposited from a vapor, liquid or solid precursors. The techniques involve either laser-induced chemical/electrochemical or physical reaction that lead to the deposition of a material onto the substrates.

- **Laser Chemical Vapour Deposition** (LCVD)

  This technique employs an argon ion laser focused by means of an optical microscope lens to a spot of less than 2 microns onto a substrate target. The process takes place in a reaction chamber filled with a gas precursor containing the element to be deposited. When the laser beam scans over the substrate, this is heated up causing the dissociation of gas precursor and, consequently, the deposition of a thin solid layer onto the surface. The repetition of scans permits the deposition of multilayered structures. This technique involves higher costs than other printing methods due to the employment of sophisticated equipment, such as, for example, the vacuum pump. Also, it is limited by the gas phase because it allows the deposition only of volatile metal-organic and inorganic materials. A detailed review was presented by Duty et al.[18]

- **Laser-Enhanced Electroless Plating** (LEEP),

  Instead, the substrate is submerged in a chemical solution which contains the metallic ions required for the deposition. As for LCVD, the laser beam, focused on a spot, causes a rapid heating that leads to the liquid decomposition and to the printing of a metallic plate on the substrate. A subsequent electroplating o electroless plating process can be used to increase the thickness of the layer deposited; however, this process, described in many reviews [19], does not allow a precise control of the layer thickness and the creation of 3D structures.

- **Laser-Induced Forward Transfer** (LIFT)

  This technique is based on a solid transparent support containing the material to be deposited. The target substrate is placed in parallel at a distance of about 100 microns below or above. In this case, the laser beam vaporizes the solid precursor which rapidly condenses on the substrate (Figure 2-7B). The versatility of this technique allows the deposition of a wide range of materials, since it does not have strict physical requirements, while the main limitation is that target surfaces

must be very flat due to the proximity with the solid support containing the material precursor.[20]

Nevertheless, the most used non-contact printing technique in PE, inkjet printing, will be introduced in detail in the following section.

2.5 | INKJET PRINTING TECHNIQUE

Inkjet printing is one of the most important printing techniques for maskless PE nowadays for its characteristics such as non-contact patterning, high reproducibility, high speed and high quality deposition on both small and large areas. This technique is a cost-effective and flexible method for the deposition of functional fluids, in the form of polymer solution and pure solvents or solvent mixtures, onto various surfaces and substrates. Some examples of functional materials include metal inks, conductive and semiconducting polymers, surface coating, proteins and nanoparticles.

The versatility of the inkjet printing is highlighted in several research areas such as chemical, mechanical, optical and life sciences and in a wide range of applications like electronics, opto-electronics and, displays.

Inkjet printing represents an accurate and reproducible film preparation technique, which relies on the formation of individual droplets that are ejected from a nozzle. This approach is attracting a lot of interest because it allows simplifying the patterning process, controlling the amount of material that can be deposited on the substrate and avoiding direct contact between the printhead and the substrate. It also cuts down the material and energy consumption through the reduction of the number of processing steps and, as a consequence, of time, space, and waste production within the fabrication process; thus, allowing the scaling-up from lab prototype device to industrial production. Furthermore, inkjet typically allows the use of lower viscosity inks than any other printing technology. This allows the realization of higher quality inkjet-printed patterns. Finally, being a digital fabrication technique, it allows for on-the-fly correction as well as easy pattern changes.

Unfortunately, inkjet printing has also several drawbacks. First, the process stability of inkjet is generally a concern, although this issue is being addressed through the production of advanced printheads specifically designed for PE applications. Second, since inkjet uses a drop-by-drop approach, it typically requires several passes to produce relatively thick films for applications that require thicker film buildup. This, in turn, reduces process throughput. Third, since it tends to be a relatively slow technique, it is necessary to use large arrays of printheads to produce high-throughput jetting systems; the manufacturability and process stability of such large arrays of printheads is still uncertain for electronics applications, although page-wide heads are already in use in the graphic arts industry.[36][37][38][39]

The drop ejection can be caused by various transducers and in different ways: the most common, described in the followings, include Continuous Inkjet Printing and Drop-on-Demand Inkjet Printing. The differences between the two drop generation mechanisms have been reviewed in detail elsewhere[40], however it is appropriate to distinguish between them here. Figure 2-8 gives a summary of all the possible Inkjet Printing technologies.[41]

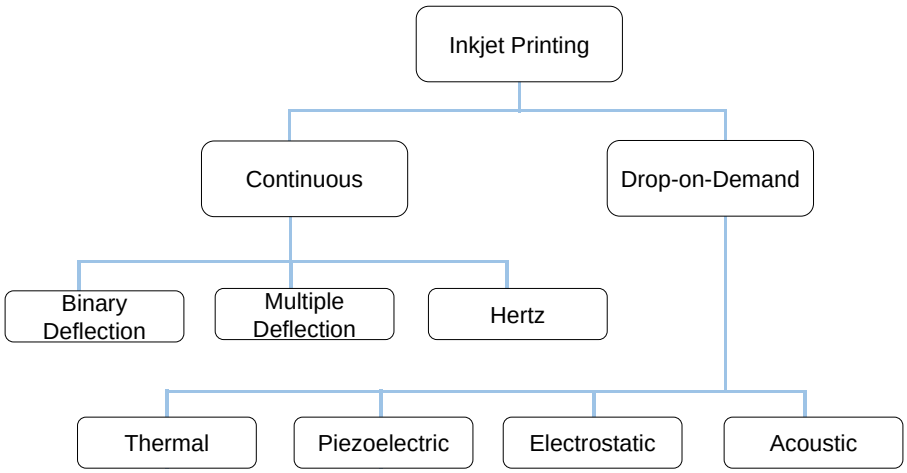

Figure 2-8 Classification of the different Inkjet Printing mechanisms.[41]

2.5.1 | Continuous inkjet printing

Continuous inkjet is mainly used in industrial techniques for large-scale production that needs of high-speed printing. Mostly used for marking and coding of products and packages. Figure 2-9 shows a schematic of Continuous Inkjet Printing mode.

The operating principle of a continuous inkjet system is based on the continuous stream of droplets during the printing. Next, the droplets are exposed to an electric field by means of a charging electrode. So, the droplets become charged. Afterwards, they move towards the substrate, passing through a second electric field and their path is bended due to the field. By varying the charge applied to the drops, the deflection of each drop can be controlled.

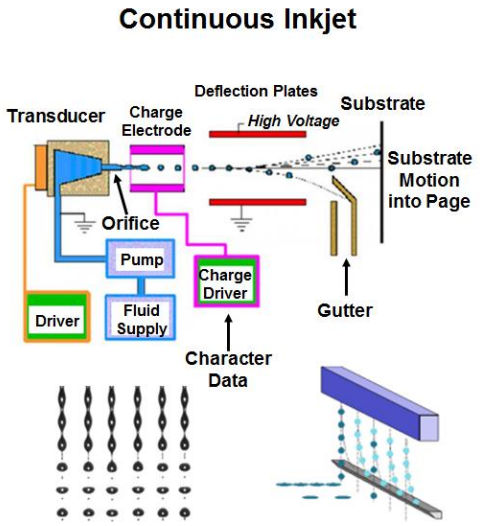

Figure 2-9 Schematic of the Continuous Inkjet Printing working principle.[42]

Only a little amount of the droplets are used to print, the rest are directed into a gutter for recirculation and the ink is reused. The droplets generated are usually twice the size in diameter than the printing orifice, 150 microns is the typical drop size, but it can be as small as 20 microns. With the continuous approach, high printing frequencies (up to 80 kHz) and jet velocity (20 $m \cdot s^{-1}$) can be reached. The fact that there is a continuous flow of ink through the nozzles minimizes the risk of clogging. There are three main categories related to the different levels of charge and so, levels of droplet deflection: Binary Deflection, Multi-Deflection and Hertz.

However, the resolution can be reduced due to the high-speed of printing (a resolution not better than 100 microns can be achieved). Other disadvantages of the continuous inkjet printer are that the inks are restricted to those that can be charged and the printer is relatively expensive because of the requirements for drop selection, a recycling system, and a high maintenance cost. Moreover, due to the recirculation process, a high contamination probability can degrade the ink. This technique finds its best application in high-speed textile printing or product expiration date marking.

2.5.2 | Drop-on-Demand inkjet printing technique

Drop-on-Demand (DoD) is a technology which only ejects drops required for printing (Figure 2-10). Mainly it is used in the majority of printers. The DoD eliminates the complex droplet charging, deflection and recycling system required for the continuous inkjet printer. Therefore, all the droplets ejected are directly deposited to the target substrate and form the patterned layer. Moreover, no recirculation system is needed, leading to a reduced contamination risk. With respect to continuous inkjet printing, it allows smaller drop size generation and higher placement accuracy. But, DoD generation faces some ink instabilities due to the specific ejection of each droplet.

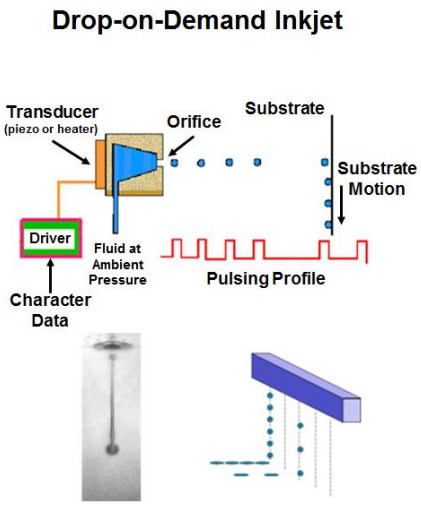

Figure 2-10 Schematic of the Drop-on-Demand (DoD) Inkjet Printing working principle.[42]

The ejected drop size approximates the diameter of the orifice, and less than 20 microns droplets can be achieved. Four techniques exist to eject droplets from a printhead. These are thermal, piezoelectric, electrostatic and acoustic. However, the most common inkjet printers are based on either drop-on-demand thermal and piezoelectric printheads. Figure 2-11 shows a comparison between Thermal and Piezoelectric printheads.

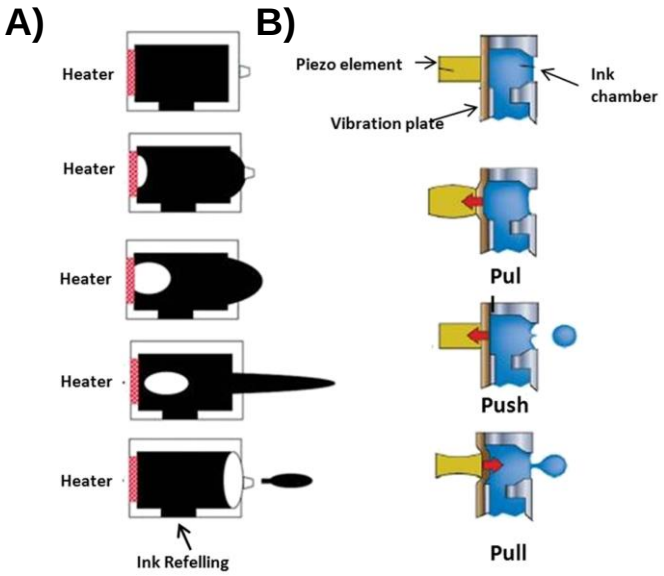

Figure 2-11 Detailed schematic structure of A) thermal printheads and B) piezoelectric printheads.[43]

The working principle of a Thermal DoD inkjet printer is based on the Joule effect (Figure 2-12). The transducer of the drop chamber is a simple heating resistor. When it is subjected to a considerable current flow, its temperature increases rapidly (Joule effect) as well as that of the surrounding ink, which reaches the threshold temperature, T_T, and a vapor bubble is formed. Usually, bubble formation occurs in just 2 ms, at a temperature of approximately 300 ºC. As the bubble grows, the pressure inside the nozzle increases until a droplet of ink is ejected through the orifice, almost simultaneously with the collapse of the bubble. The pressure then decreases within the system and the nozzle becomes refilled with ink. The entire procedure is fast, taking less than 10 microseconds. Owing to the relative simplicity of printheads using such designs, highly scaled printheads have been realized using thermal bubble processes. However, the drawback of printheads that use thermal ink-jetting is that the requisite heating step poses compatibility concerns for thin-film electronic materials, where the inks are usually temperature sensitive.[44]

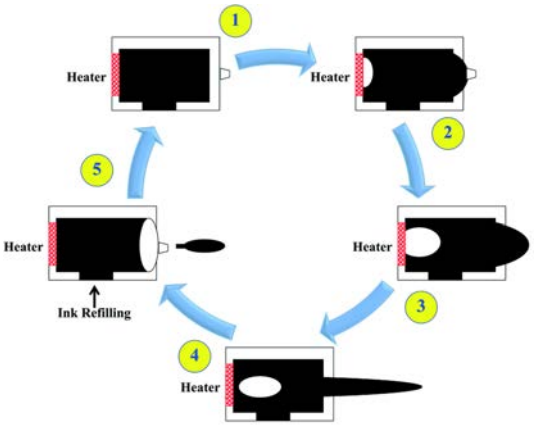

Figure 2-12 Thermal DoD mechanism. Ink is rapidly heated to a high temperature to vaporize which creates a bubble at the surface of the heater causing a pressure pulse that exudes ink droplets trough the nozzle. The vapor bubble collapses, as the ink droplets are ejected. Thereby generating a force to refill the ink.[44]

Thereby, this technique can cause the degradation of the material properties of functional inks. Since this problem, in this thesis, thermal technique is ruled out and we will focus on the use of piezoelectric printheads.

The piezoelectric inkjet technology is based on piezoelectric crystals confined in each printhead nozzle. Piezoelectric materials deform the shape and size when a voltage is applied onto them. In an inkjet printhead, this deformation is used to displace volume in a fluid chamber for droplet ejection. Thus a drop of ink is released through the small orifice of the nozzle as shown in Figure 2-13. The process is purely mechanical and therefore does not present degradation problem of the inks, e.g. no evaporation of solvents thus the piezoelectric inkjet printer accepts a wide range of inks; moreover, the printhead has a long life since it is not subjected to heat damage.[45][46] The

piezoelectric inkjet printer can be classified into squeeze, bend, push, and shear mode based on the distortion of the piezo-ceramic plate.

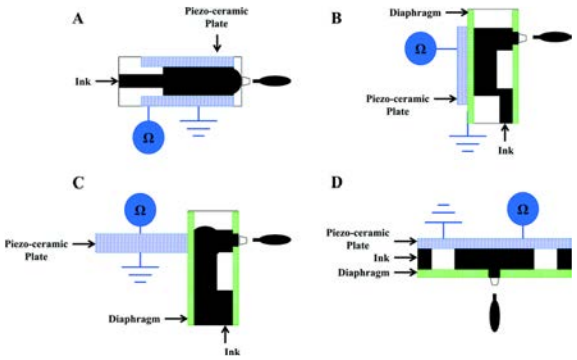

Figure 2-13 Drop-on-demand (DoD) piezoelectric inkjet printer. The piezoelectric inkjet printer applies a piezo-ceramic plate to create ink droplets. A: Squeeze mode; B: bend mode; C: push mode; D: shear mode.[44]

The thermal inkjet mechanism is simpler in operation than piezoelectric. In addition, more environmentally friendly solvents are permitted and fewer ink additive modifiers are required as thermal technology does not require as much control of ink viscosity and surface tension compared to piezoelectric technology. In fact, thermal inkjet printing requires viscosities of 1–1.5 cPs whereas piezoelectric inkjet printing requires 5–10 cPs viscosity values and surface tension higher than 30 dyn cm^{-1}. However, even if the resolutions achievable by thermal and piezoelectric devices are similar and large improvements have been made with regard to the thermal stability of inks, most of the inkjet printers on the PE market for research and development are based on piezoelectric technology. This is primarily driven by the fact that it is a more cost-effective and easy-to-use deposition technology as well as remaining concerns as to the effect of high temperatures on ink constituents.

2.5.3 | Inkjet printer parameters

As a tool for depositing materials, inkjet printing must generate repeatability droplets, obtain a required drop volume, deliver material accurately and achieve a desired delivery rate. Moreover, the basic premise of digital printing is the accurate positioning of a liquid droplet particle of a microscopically small volume directly correlated with the presence of information at each binary unit of the bitmap file to be reproduced. Unfortunately all these requirements for an optimal printing are not always achieved but, by tuning several parameters of the inkjet printer, one can optimize the printing. Following are detailed all these parameters.

A piezo inkjet system, as its name indicates, consists of a piezoelectric transducer that is actuated by a voltage pulse. In commercial printing systems, the frequency of the

voltage pulse usually ranges from 1 kHz to 20 kHz. Figure 2-14 illustrates a commonly used waveform with a brief description of the significance of each segment of the waveform. This is just an example, as many different types of waveforms can usually be applied to an inkjet printhead to create droplets. Thus, the waveform applied is one of the most important parameters to ensure reliable and reproducible drop ejection. Through a fiducial camera, the operator can determine the optimized piezo-voltage, pulse-duration and frequency parameters of the waveform to provide a reliable droplet ejection.

The typical basic waveform is divided into segments. Each segment has three properties: duration, level and slew rate. The applied voltage relates directly to the volume of the pumping chamber, and the slew rate how fast is that operation.

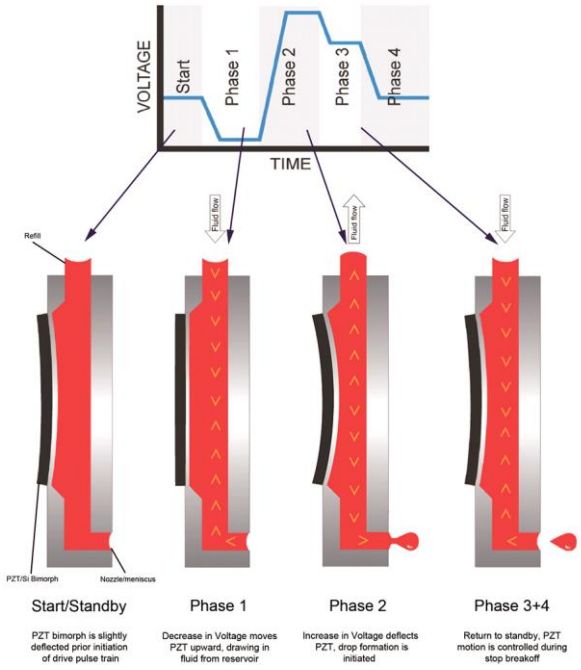

Figure 2-14 Four-phases voltage wave of the piezoelectric crystal: standby (a), voltage decrease (b), rapid voltage increase (c), and gradual return to standby waveform used in piezo inkjet systems.

Changing duration, slew rate or level values has a strong influence on drop formation. The voltage applied to the piezoelectric mechanism modifies the velocity and size of the drop. Figure 2-15Ai and Figure 2-15Bi shows a good ejection of a droplet and a picture of optimum jetting printed lines. However, if the applied voltage is not enough, the drop is not created, but if the applied voltage is higher than the suited one, then the formation of the drop is accompanied by satellite drops (Figure 2-15Aii). Satellite drops are undesired drops generated besides the main drop and are usually generated when the kinetic energy of the drop is too high, so the ejected liquid column breaks up into more than one drop. In some cases, satellite drops have the same trajectory as the main drop and may collapse with it if their velocity is higher than the

speed of the main drop. On the contrary, the trajectory of satellites is not well controlled. Figure 2-15Bii shows a picture of printed lines in presence of satellite drops. If the voltage continues being increased the ejection is a random fluid spray (Figure 2-15Aiii).

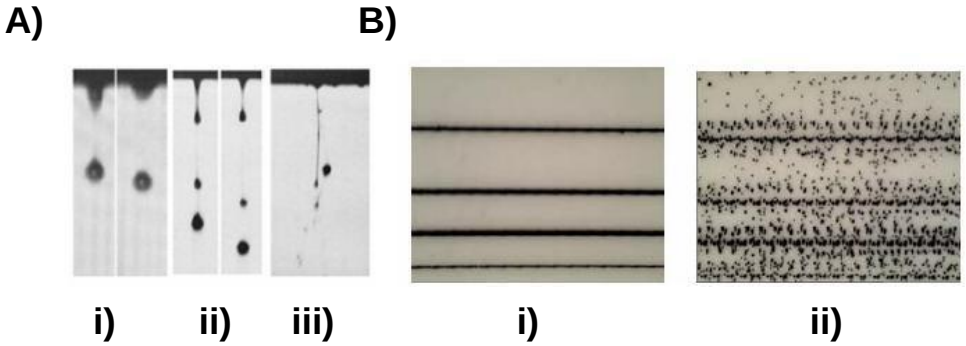

Figure 2-15 Pictures of A) i) Good jetting drops, ii) drops with satellites and, iii) random spray jetting; B) i) optimum jetting printed line and, ii) satellites effects on a printed line.[Source: Fujifilm Dimatix]

In inkjet process, it is possible to control the distance between ejected drops that creates an overlapped discrete spots of deposited fluid. The resolution of printed patterns basically depends on spot size and drop overlapping. Drop overlap is determined by spot size and spot spacing. Spot spacing is controlled, in first term, by printhead Drop Spacing (DS) parameter. Drop overlap depends also on spot size, and spot size is subjected to ejected drop volume and substrate-ink interaction.

A few principal behaviors emerge when examining printed patterns across a variety of DS, delay periods, and temperatures. We label these as individual drops, a scalloped line, an uniform line, a bulging line and, stacked coins.[47] Figure 2-16 shows these four basic morphologies.

If the DS is too high, the drops are too far apart to interact, more than twice a drop's radius, and then isolated drops land and dry as shown in Figure 2-16B. Individual drops occur at DS independent of temperature or delay in our system.

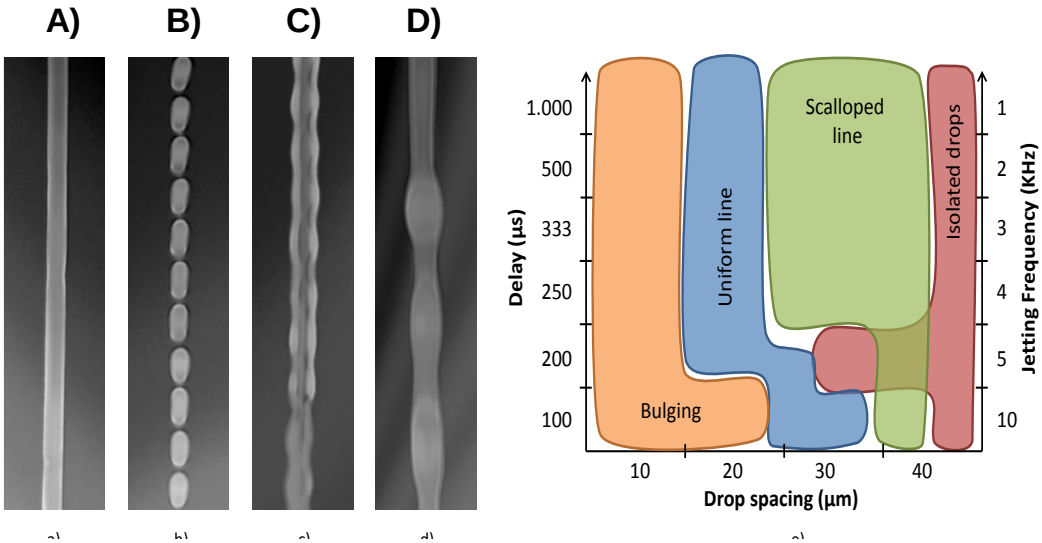

Figure 2-16 Examples of principal printed-line behaviors: A) uniform line; B) individual drops; C) scalloped; and D) bulging. Drop spacing (DS) increases from left to right.

At lower temperatures, as DS decreases, isolated drops overlap and merge but retain individual rounded contact lines, and a scalloped pattern emerges as shown in Figure 2-16C. These scalloped lines are narrower than an isolated drop as fluid expansion is partially arrested. Further decreasing the DS will eliminate the scalloping and lead to a smooth, straight line (Figure 2-16C). These lines have a uniform smooth edge and top. They are the narrowest lines printed. Printing drops even closer together leads to discreet bulging along the line length, separated by regions of uniform narrow lines. These bulges tend to form periodically and also at the beginning of the line, Figure 2-16D.

The task of achieving the best accuracy is time consuming for the printer operator due to dynamic errors caused by variation of some physical mechanism of the printer. During printing, many sources of random errors will be introduced such as nozzle placement, jet trajectory (drop landing), drop placement and machine wear over time as is shown in Figure 2-17. The importance of these errors is the impact on drop placement accuracy and, consequently the need of a design review process to refine and improve system stability and precision.

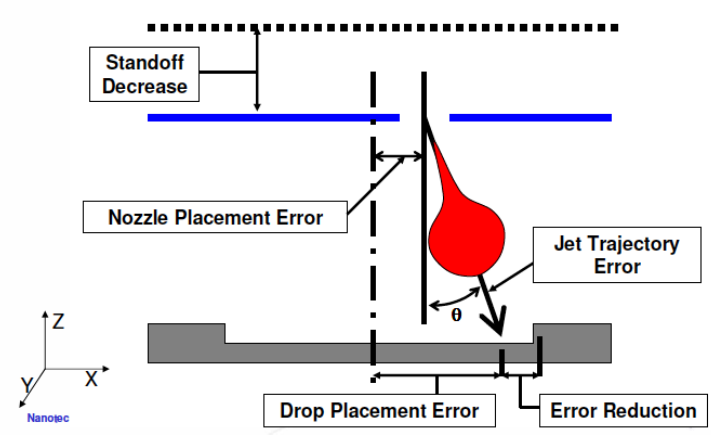

Figure 2-17 Some dynamic errors that can appear during the printing process.(Source:PixDro)

- **Misdirected nozzles**

  It refers to drops that are traveling off axis from left to right, or front to back. The primary causes of misdirected nozzles are contamination on the nozzle plate (air inside the nozzle orifice that is forcing the drop to eject at an angle) or the nozzle placement error.

- **Non-jetting nozzles**

  It refers to the nozzles that do not eject a drop under any condition and are adjacent to nozzles that are jetting properly. The reason can be for air entrapment in the pumping chamber or nozzle is dried.

- **Non-Matched Velocities**

  When a new printhead is installed it is absolutely essential to adjust the drop velocities for all the nozzles.[4] This has a direct impact on image quality and overall line fidelity but not is a guarantee of volume uniformity. When the drop velocities are mismatched the result are drops that arrives with a small delay and are not aligned with the rest of ejected drops shown in Figure 2-18.

  For example, the Dimatix printhead, the ideal fluid viscosity should be between 10-12 cPs ($1.0 \cdot 10^{-2}$ - $1.2 \cdot 10^{-2}$ Pa·s) at room temperature. The viscosity is a measure of a fluid´s internal flow resistance. If the fluid viscosity exceeds these values, the fluid could not be ejected by the piezo actuation. On the other hand, if the fluid viscosity is too low, the fluid can be idle in the nozzle resulting poor jetting quality with the presence of filaments or satellites. The ink viscosity is usually adjustable by modifying the solvent or the material concentration in the fluid.

Although low viscous fluids are desirable for jetting purposes, the high viscosity guarantee the reduced droplet spreading when the fluid lands on the substrate. The control of this parameter is critical since the droplet condition strongly influences the film uniformity.

Therefore, a good ejecting quality is usually characterized by:

- small ejecting drop volume variation among the generated droplets
- no wetting of nozzle plate during ejection
- uniform droplet velocity from droplet to droplet
- absence of satellite droplets
- straight droplet trajectory along the nozzle/substrate direction
- long term ejecting stability, including during the on/off cycles

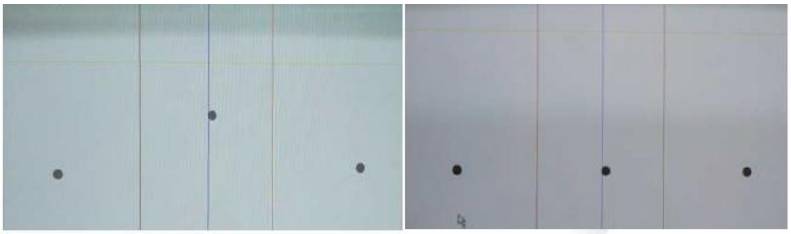

Figure 2-18 Left: non-matched velocities of droplets; right: matched velocities of droplets.

2.5.4 | Ink-substrate interactions

Initial activity for PE was oriented towards using glass and a narrow range of plastic substrates. Substrates for PE will probably continue to be dominated by plastics, in particular polyethylene terephthalate (PET) because of its low-cost and polyethylene naphthalate (PEN) because of low surface roughness. For smart packaging and other applications, paper is seen as potentially useful. Printing on paper is very logical and seem to be essential to the emergence of a significant smart packaging sector.

The non-contact nature of inkjet deposition makes it a very versatile process being applicable to a wide range of substrates. The interaction between the deposited fluid and the substrate surface is a crucial factor to optimize the deposition process. Another critical aspect of the inkjet printing technique for the quality of the printed material is related to drop drying process. In the following, these issues are addressed.

- **Wetting of the substrate**

  In the printing processes, the main ruling factor in the spreading of the fluid droplet on the substrate is the surface tension of the components. This property is revealed, for example, in floating of some objects on the surface of water, although they are denser than water. Surface tension is caused by cohesion of

molecules and is responsible of many behaviors of liquids. Because of surface tension, the surface of a liquid can support light objects. The surface tension is defined as the energy to increase the surface area of a unit. Therefore, its unit of measurement is energy for unit of area.

In general, the molecules in a fluid are subjected to the attraction of the surrounding molecules. Inside the fluid, the resultant of all the attraction forces is zero, while on the surface these forces are directed toward inside. This effect of "compression" represents the tendency of every system to reach the minimum energy state.

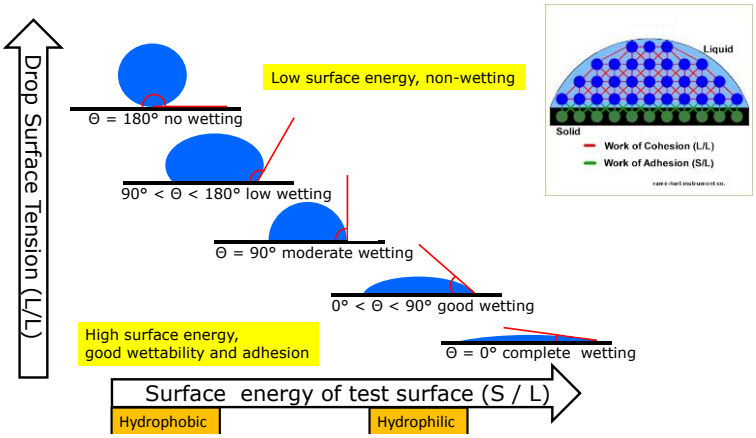

Figure 2-19 Relation between Drop Surface Tension and Surface energy of test. Generally, adhesion increases with decreasing surface energy and increasing hydrophobicity. Low surface tension is undesirable.

The increased surface of a liquid corresponds to an increased energy and, in this case, the equilibrium is reached when the liquid assume the minimum possible size (spherical shape). Thus, surface tension is responsible for the spherical shape of drops of liquid; spheres minimize the surface area of the drop and thus minimize surface tension. The wetting, which is the ability of a liquid to maintain contact with a solid surface, is determined not only by the liquid surface tension, but even by the surface energy of the solid surface and by the balance between adhesive (between molecules in the liquid and solid) and cohesive forces (between the molecules in the liquid) at the interface (interfacial tension).

Surface energy derives from the unsatisfied bonding potential of molecules at a surface. The term surface energy is also closely linked with surface hydrophobicity. Whereas surface energy describes interactions with a range of materials, surface hydrophobicity describes these interactions with water only. Therefore, hydrophobicity generally decreases as surface energy increases as shown in Figure 2-19. Hydrophilic surfaces such as glass therefore have higher surface energies. Generally, adhesion increases with decreasing surface energy

and increasing hydrophobicity. From the wetting perspective, it is undesirable to have very low surface tension because of the wider spreading on the target substrate that makes difficult the realization of a well-defined structure. In order to modify the wetting, different surface treatments are applied. Typically, oxygen plasma, corona and silane treatments are the commonly used processes to modify the surface energy of the substrate.

- **Coffee-ring effect**

  One of the crucial features of the printing process is correlated to the droplet drying process that basically induces a final printed droplet that is characterized by the presence of high ridges at drop edge. This effect, called "coffee-ring effect", was first explained by Deegan et al. in 1997.[48] This phenomenon, shown in Figure 2-20, describes the propensity of the solute to flow out towards the droplet edge through a capillary flow during drying. This occurs owing to the maximum of the evaporation rate. The coffee ring effect appears both in droplets and shapes.

  During the process of solvent evaporation, a capillary flow takes place inside the sessile drop from its center towards the edges, where the evaporation rate is higher, replenishing the evaporation losses. As consequence, at the end of the drying process the material results largely localized at the edge of the printed droplet. The coffee ring stain is detrimental for a homogeneous film formation, as relatively thicker walls can appear at the outer edges.

  As a result of this effect, the solvent at the edges has a lower surface tension than in the center, resulting in a surface tension gradient, and then a surface-tension driven Marangoni flow occurs to carry the solute inward to the center. This Marangoni flow can thus compensate the outward convective flow, balancing or even eliminating the coffee ring effect.

  So, the coffee ring can be reduced using several methods: e.g. changing the substrate temperature has been demonstrated to eliminate the coffee ring. In such case, the difference of temperature in the substrate can delay the evaporation in the outer edges much more than in the center of the deposited drop, resulting in a reduced outward flow and hence reduction of coffee ring formation.

  Another method is based in the incorporation of a co-solvent system with a higher boiling point and a lower surface tension. Due to higher evaporation at the outer edges, the solvent composition at the outer edges becomes mainly the solvent with high boiling point with slower evaporation rates. Thus, the mixture of solvents is a key in order to obtain uniform thin layers.

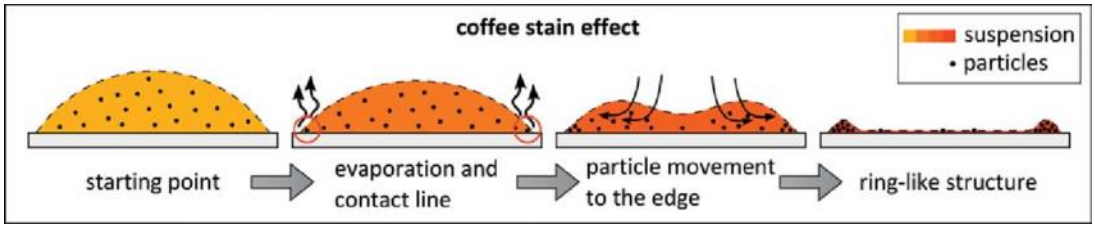

Figure 2-20. A schematic representation of coffee ring effect.[49]

2.5.5 | Functional inks and substrates for PE

Functional materials employed for printing electronics could be classified into conductive, semiconducting and insulating inks according to the most elemental electrical characteristics. Moreover, another important classification is its division between organic and inorganic ink materials. Inorganic materials demonstrated the best electrical performances, but often require high temperature processing. Organic materials present higher flexibility, low-cost formulation and low-temperature sintering, suitable for flexible substrates. However, their electrical performances hamper their development spreading. For this reason, a device structure based on organic and inorganic materials take advantages of both categories. On the following lines, the three main basic types of functional inks will be described.

- **Conductive inks**

  The conductive inks have been used in many applications, such as interconnections for a circuity on printed circuits boards, disposable displays, RFID tags, Organic Thin Film Transistors (OTFTs), electrochromic and electrochemical devices, etc. Several conducting materials are adaptable and compatible with current printing technologies. Up to date, inks based on metals, conducting polymers and other conducting carbon-based materials have been developed to fulfill the high demand for fully –printed flexible electronics.

  Metal inks, based on nanoparticles, are commonly employed as conductive elements due to their conductivity (~10^7 $S \cdot cm^{-1}$). There has been progress in lowering the sintering temperature of nanoparticle inks, and this fact has made the inks more compatible with fast roll-to-roll processing and delicate substrates. Currently, the most used ink in inkjet printing technology is the silver.[21] However, in many applications, the use of gold material is preferable over silver because of the chemical inertness of this metal, especially for bio-applications.

  Typical organic conductive materials are polymer composites, such as poly(3,4-ethylenedioxythiophene) polystyrene sulfonate (PEDOT:PSS)[22], polypyrrole (PPy)[23] and polyaniline (PANI)[24], which are appealing since they are semi-transparent, flexible, light-weight, biocompatible and at the same time they ensure low-cost synthesis. Nevertheless, organic polymers reach low conductivity values

($\sim 10^3$-10^4 $S \cdot cm^{-1}$), which currently is a drawback in several electronic application areas. Finally, other conducting organic materials, including carbon-based graphene [25] and carbon nanotubes (CNT)[26] have been demonstrated as suitable conductive materials for flexible transparent printed devices.

- **Semiconducting inks**

  Semiconducting materials represents the key element for multipurpose OTFTs in PE. Inorganic semiconductors show better electrical performance and stability, OSCs generally ensure cheaper and easier synthesis producing (low-temperature processing), and higher mechanical flexibility.

  Common inorganic semiconductor materials are metal-oxide (ZnO, In_2O_3,)[27] and chalcogenide chemical compounds (MoS_2,etc…).[28] Although their higher electrical performances, the high-temperature post-processing makes inorganic semiconducting materials incompatible for many flexible applications.

  OSCs materials are carbon-rich compounds generally classified into two categories: *small molecules* and *polymers*. Small molecules have a well-defined molecular weight, while polymers are macromolecules consisting of repeating structural units, which are usually connected by covalent chemical bonds forming a chain. The electronic properties of the organic molecules depend on the specific characteristics of the individual molecules, such as bonding, chain length and nature of substituents, but also on the processing conditions that determine the structural order of the molecules in the film. Small molecule OSCs typically exhibit random crystal orientation and the charge-carrier mobilities are around 1-2 $cm^2 \cdot V^{-1}s^{-1}$. There are several advantages in using polymeric versus small molecules semiconductors. Thin films of polymeric materials are generally very smooth and uniform, enabling a great control over a large range of the film structural and morphological characteristics. But, the charge-carrier mobilities for OSC based on polymer are lower than the small molecules. Printing requires great control of the solution rheological properties, which can be tuned efficiently for polymeric materials. Polymer crystalline domains are typically much smaller than the length scale of several optoelectronic devices, resulting in isotropic transport characteristics. This results in low device-to-device performance variability, which is particularly important for Thin Film Transistors (TFTs) integration into circuits.

  OSCs can be prepared from either polymeric organic composites such poly(3-hexylthiophene) (P3HT) and, benzothieneo-[3,2-b]benzothiphene (BTBT) among others.[29] Although, CNTs have been previously presented as metal conductor, they can furthermore perform as a semiconductor with promising high-mobilities. Lately, considerable attention and resources has been dedicated to the category of 2D semiconducting nanomaterials (Graphene, transition metal dichalcogenide

monolayers – TMDs) due to their theoretical and experimental outstanding electronic properties provided by their single-atomic layer structure.

Additionally, semiconducting hybrid materials are also being investigated in order to combine the advantages of each material while compensating their drawback, such as organic semiconductor merging a carbon-based semiconductor or an in inorganic semiconductor combining with an organic semiconductor.

- **Dielectric inks**

Insulators have diverse useful purposes, spanning from avoiding possible short-circuits into multilayered conductive structures to enhance the capacitance in electronic devices such as capacitors or transistors. Printable dielectric materials can be classified in organic materials, polymers and organic/inorganic hybrid materials.

Existing inorganic dielectric inks are fused (SiO_2)[30] and alumina (Al_2O_3)[31], which require a high-temperature processing. Moreover, several dielectrics gained increasing interest due to their appealing high dielectric constant (ε_r), such as the high-k hafnium oxide (HfO_2) and $BaTiO_3$.[31][32]

Currently, the most frequently employed insulating polymers in flexible electronic applications are the poly(4-vinylphenol) (PVP), poly(methyl methacrylate) (PMMA), polymide (PI), polypropylene (PP) and polystyrene (PS). In addition, thin 2D nanomaterials with wide band gap energy can be used as dielectric layers for capacitors and gate dielectrics, such as boron nitride (h-BN) and oxides such as graphene oxide (GO).[33]

- **Substrates**

Inkjet printing technology is exceptionally encouraging because of its compatibility with different substrates. The polymers are the best candidates used in PE, and also in inkjet printing technology, mainly due to their low-cost and flexibility. They are widely used for disposable devices in clinical applications. Thermosets polymers, such as poly(ethylene 2,6-naphthalate (PEN), poly(ethylene terephthalate (PET) and Kapton^{TM} are the most common used in PE.[34]

Currently, the emergence of the Point-of-Care (PoC) systems and other disposable applications is demanding the use of paper as a substrate.[35] Using paper substrate has enhanced the advantage of inkjet printing technologies because paper is eco-friendly and a low-cost material.

Surface energy of the substrate, together with the surface tension of the ink, are the most important parameters which defines the wettability and adhesion between ink and substrate. To improve this, different treatments can be applied to

the substrate before its use. As an example, plasma treatment is widely used in plastic substrates in order to improve the wettability and adhesion of the ink.

2.6 | DIMATIX MATERIALS PRINTER DMP2831

The inkjet printer employed during this thesis has been the Dimatix Materials Printer DMP2831, a piezoelectric Drop-on-Demand printer fabricated by FUJIFILM Dimatix and shown in Figure 2-21.

All the description below is a summary of the DMP2831 main functionalities. This printer is a low-cost commercial research inkjet printer. The main features that contains are: an A4-size substrate platen, a cartridge holder module, a drop watcher system and, a fiducial camera for alignment.

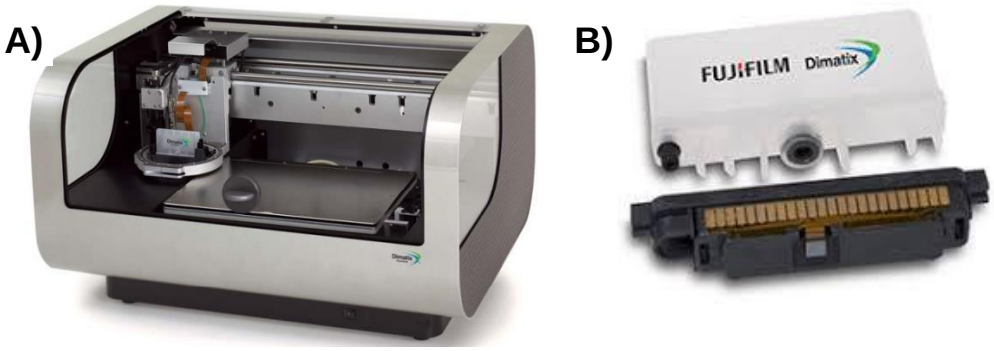

Figure 2-21. Picture of A) FujiFilm 2831 Dimatix printer and B) printhead and cartridge.

The printer is composed of four main parts:

- **Drop Watcher**

  It consists of a video-camera which is used to characterize and examine the drop formation and its progression from each of the printhead's nozzles. This is a primordial preliminary step, since every type of ink requires a fine calibration of all the possible printing parameters.

- **Platen**

  It is a movable metallic plane where the substrate is placed during the printing process. It can be heated up to 60ºC in order to enhance the drop drying and to improve the film formation. It also includes a vacuum system with many holes that should keep the substrate fixed during the printing.

- **Print Carriage**

  It is the carriage where the cartridge, i.e. the printhead, is placed. Its controlled movement over the substrate is an essential parameter to obtain a good printing. It includes a video-camera, called fiducial camera that allows the pattern alignment and the screening, at micro-scale, of the printed patterns. This cartridge is compatible with most solvents: aliphatic hydrocarbons (such as hexane and dodecane), aliphatic alcohols (high boiling points better than low in all cases), aliphatic and aromatic ketones, aromatic hydrocarbons (such as anisole and trimethylbenzene), cellosolves, glycols (polyethylene glycols and polypropylene glycols), and lactate esters among others.

- **Printheads**

  The printer is equipped with printheads with nozzles that can deliver a drop volume of 10 pL. Additionally, printheads with 1pL nozzles can be used but this kind of cartridges suffers from clogging thus making difficult the printing operation of e.g, nanoparticle-based inks.

  The desired pattern can be generated importing a bitmap pattern file. However, the pattern can only be printed in a raster manner, i.e one horizontal row at a time, even when printing a vertical line. This fact, for example restricts the printing of single pixel lines of interdigitated printed devices such as OTFTs.

Other specifications of the Dimatix DMP2831 are sum up in the following points:

- Resolution: ± 25μm
- Accuracy: ± 10μm
- 4 mL maximum cartridge volume
- Maximum cartridge temperature: 70°C
- Maximum substrate dimensions: 210mm x 315mm
- Minimum substrate dimensions: 50mm x 50mm

2.7 | REFERENCES

[1] Materials for Printed Electronics | Sustainability | DIC, http://www.dic-global.com/en/csr/special/archive/2014/special05.html (accessed 6 August 2018).

[2] Roadmap - my_OEA, http://www.oe-a.org/roadmap (accessed 9 August 2018).

[3] Subramanian V, Frechet JMJ, Chang PC, et al. Progress Toward Development of All-Printed RFID Tags: Materials, Processes, and Devices. *Proc IEEE* 2005; 93: 1330–1338.

[4] Tseng H-Y. Scaling of Inkjet-Printed Transistors using Novel Printing Techniques. 121.

[5] Ostfeld AE, Deckman I, Gaikwad AM, et al. Screen printed passive components for flexible power electronics. *Sci Rep*; 5. Epub ahead of print December 2015. DOI: 10.1038/srep15959.

[6] Gelinck GH, Huitema HEA, van Veenendaal E, et al. Flexible active-matrix displays and shift registers based on solution-processed organic transistors. *Nat Mater* 2004; 3: 106–110.

[7] Komuro N, Takaki S, Suzuki K, et al. Inkjet printed (bio)chemical sensing devices. *Anal Bioanal Chem* 2013; 405: 5785–5805.

[8] Caironi M, Noh Y-Y. Front Matter. In: *Large Area and Flexible Electronics*. Wiley-Blackwell, pp. I–XXVIII.

[9] Søndergaard RR, Hösel M, Krebs FC. Roll-to-Roll fabrication of large area functional organic materials. *J Polym Sci Part B Polym Phys* 2013; 51: 16–34.

[10] Kang B, Lee WH, Cho K. Recent Advances in Organic Transistor Printing Processes. *ACS Appl Mater Interfaces* 2013; 5: 2302–2315.

[11] Khan S, Lorenzelli L, Dahiya RS. Technologies for Printing Sensors and Electronics Over Large Flexible Substrates: A Review. *IEEE Sens J* 2015; 15: 3164–3185.

[12] Liang T-, Sun WZ, Wang L-, et al. Effect of surface energies on screen printing resolution. *IEEE Trans Compon Packag Manuf Technol Part B* 1996; 19: 423–426.

[13] Mandal S, Noh Y-Y. Printed organic thin-film transistor-based integrated circuits. *Semicond Sci Technol* 2015; 30: 064003.

[14] f7db0e98b8e58920b90636658a62eac4cc17.pdf, https://pdfs.semanticscholar.org/13e8/f7db0e98b8e58920b90636658a62eac4cc17.pdf (accessed 7 August 2018).

[15] Hon KKB, Li L, Hutchings IM. Direct writing technology—Advances and developments. *CIRP Ann* 2008; 57: 601–620.

[16] Ribierre JC, Fujihara T, Watanabe S, et al. Direct Laser Writing of Complementary Logic Gates and Lateral p–n Diodes in a Solution-Processible Monolithic Organic Semiconductor. *Adv Mater* 2010; 22: 1722–1726.

[17] Park JB, Xiong W, Gao Y, et al. Fast growth of graphene patterns by laser direct writing. *Appl Phys Lett* 2011; 98: 123109.

[18] Duty C, Jean D, Lackey WJ. Laser chemical vapour deposition: materials, modelling, and process control. *Int Mater Rev* 2001; 46: 271–287.

[19] von Gutfeld RJ, Hodgson RT. Laser enhanced etching in KOH. *Appl Phys Lett* 1982; 40: 352–354.

[20] Kang CL, Xu Y, Yung KL, et al. Laser Induced Forward Transfer. *Advanced Materials Research*. Epub ahead of print 2012. DOI: 10.4028/www.scientific.net/AMR.591-593.1135.

[21] Titkov AI, Bukhanets OG, Gadirov RM, et al. Conductive inks for inkjet printing based on composition of nanoparticles and organic silver salt. *Inorg Mater Appl Res* 2015; 6: 375–381.

[22] Eom SH, Senthilarasu S, Uthirakumar P, et al. Polymer solar cells based on inkjet-printed PEDOT:PSS layer. *Org Electron* 2009; 10: 536–542.

[23] Weng B, Morrin A, Shepherd R, et al. Wholly printed polypyrrole nanoparticle-based biosensors on flexible substrate. *J Mater Chem B* 2014; 2: 793–799.

[24] Synthesis and characterization thin films of conductive polymer (PANI) for optoelectronic device application: AIP Conference Proceedings: Vol 1733, No 1, https://aip.scitation.org/doi/pdf/10.1063/1.4948838 (accessed 27 August 2018).

[25] Ciesielski A, Samorì P. Supramolecular Approaches to Graphene: From Self-Assembly to Molecule-Assisted Liquid-Phase Exfoliation. *Adv Mater* 2016; 28: 6030–6051.

[26] Coleman JN. Liquid-Phase Exfoliation of Nanotubes and Graphene. *Adv Funct Mater* 2009; 19: 3680–3695.

[27] Sun Y, Maemoto T, Sasa S. Fully transparent ZnO thin-film transistors using conducting AZO films fabricated at room temperature. In: *2014 IEEE International Meeting for Future of Electron Devices, Kansai (IMFEDK)*. 2014, pp. 1–2.

[28] Radisavljevic B, Radenovic A, Brivio J, et al. Single-layer MoS_2 transistors. *Nat Nanotechnol* 2011; 6: 147–150.

[29] Liao C, Yan F. Organic Semiconductors in Organic Thin-Film Transistor-Based Chemical and Biological Sensors. *Polym Rev* 2013; 53: 352–406.

[30] Arias AC, MacKenzie JD, McCulloch I, et al. Materials and Applications for Large Area Electronics: Solution-Based Approaches. *Chem Rev* 2010; 110: 3–24.

[31] Hourdakis E, Nassiopoulou AG. High performance MIM capacitor using anodic alumina dielectric. *Microelectron Eng* 2012; 90: 12–14.

[32] Yoon D-H, Zhang J, Lee BI. Dielectric constant and mixing model of BaTiO3 composite thick films. *Mater Res Bull* 2003; 38: 765–772.

[33] Porro S, Ricciardi C. Memristive behaviour in inkjet printed graphene oxide thin layers. *RSC Adv* 2015; 5: 68565–68570.

[34] Nie X, Wang H, Zou J. Inkjet printing of silver citrate conductive ink on PET substrate. *Appl Surf Sci* 2012; 261: 554–560.

[35] Yamada K, Henares TG, Suzuki K, et al. Paper-Based Inkjet-Printed Microfluidic Analytical Devices. *Angew Chem Int Ed* 2015; 54: 5294–5310.

[36] de Gans B-J, Duineveld PC, Schubert US. Inkjet Printing of Polymers: State of the Art and Future Developments. *Adv Mater* 2004; 16: 203–213.

[37] Singh M, Haverinen HM, Dhagat P, et al. Inkjet printing-process and its applications. *Adv Mater Deerfield Beach Fla* 2010; 22: 673–685.

[38] Inkjet printing of conductive materials: a review | Circuit World | Vol 38, No 4, https://www.emeraldinsight.com/doi/full/10.1108/03056121211280413 (accessed 8 August 2018).

[39] Organic Electronics II: More Materials and Applications. *Wiley.com*, https://www.wiley.com/en-es/Organic+Electronics+II%3A+More+Materials+and+Applications-p-9783527326471 (accessed 8 August 2018).

[40] Martin GD, Hoath SD, Hutchings IM. Inkjet printing - the physics of manipulating liquid jets and drops. *J Phys Conf Ser* 2008; 105: 012001.

[41] Progress and Trends in Ink-jet Printing Technology, http://www.imaging.org/site/IST/Resources/Imaging_Tutorials/Progress_and_Trends_in_Ink-Jet_Printing_Technology/IST/Resources/Tutorials/Inkjet.aspx?hkey=4af47800-9584-4480-be8d-45fc3ee53e86 (accessed 8 August 2018).

[42] Inkjet Analysis, https://engineering.buffalo.edu/chemical-biological/research/areas.host.html/content/shared/engineering/chemical-biological/Research/research-projects/ed-furlani/Inkjet-Analysis-systems.detail.html (accessed 8 August 2018).

[43] Olivieri F, Todino M, Coppola S, et al. Fabrication of polymer lenses and microlens array for lab-on-a-chip devices. *Opt Eng* 2016; 55: 081319.

[44] Li J, Rossignol F, Macdonald J. Inkjet printing for biosensor fabrication: combining chemistry and technology for advanced manufacturing. *Lab Chip* 2015; 15: 2538–2558.

[45] Wijshoff H. The dynamics of the piezo inkjet printhead operation☆. *Phys Rep* 2010; 491: 77–177.

[46] Chen Y-S, Huang Y-L, Kuo C-H, et al. Investigation of design parameters for droplet generators driven by piezoelectric actuators. *Int J Mech Sci* 2007; 49: 733–740.

[47] Soltman D, Subramanian V. Inkjet-Printed Line Morphologies and Temperature Control of the Coffee Ring Effect. *Langmuir* 2008; 24: 2224–2231.

[48] Deegan RD, Bakajin O, Dupont TF, et al. Capillary flow as the cause of ring stains from dried liquid drops. *undefined*, /paper/Capillary-flow-as-the-cause-of-ring-stains-from-Deegan-Bakajin/58a3d6931999d59bd35dbea5b288601ea0557e60 (1997, accessed 6 August 2018).

[49] Lim JA, Lee WH, Lee HS, et al. Self-Organization of Ink-jet-Printed Triisopropylsilylethynyl Pentacene via Evaporation-Induced Flows in a Drying Droplet. *Adv Funct Mater* 2008; 18: 229–234.

3

Introduction to Organic and Printed Sensors

This chapter describes first the theory and the state-of-the-art of organic and printed sensors. Moreover, it is reported an introduction to the organic Metal-Insulator-Semiconductor (MIS) diodes and the Biological Field-Effect Transistors (BioFET), which are the two devices developed in this thesis work. Finally, it will be presented the state-of-the-art of organic MIS diodes as gas sensors and Organic Thin Film Transistor-based (OTFT) sensors, particularly those that detect biomolecules such as DNA hybridization and proteins.

3.1 | OVERVIEW OF PRINTED AND ORGANIC SENSORS

Sensor development continues to expand and is largely driven by the advances in the field of micro-technologies.[1] Currently, silicon planar technology is widely used in the fabrication of many of today's sensors.[2] But, the major drawback of silicon sensors concerns their ability to provide a cost-effective solution to a particular problem. If the demand is sufficiently high (of the order of several million sensors per year), this technology is suitable for the market. For low-to-medium volume requirements (few tens of thousands of sensors per year), they can be justified under special circumstances.

Printing technologies are aiding and revolutionizing the field of flexible/bendable organic sensors and electronics by providing cost-effective routes for processing diverse electronic materials at temperatures compatible with polymeric and paper substrates. Printed Electronics (PE) has allowed researchers to explore new avenues for materials processing and to develop sensors and systems on even non-planar surfaces, which otherwise are difficult to realize with the conventional wafer-base fabrication techniques.[3][4]

Sensors that are printed on flexible substrates represent a growing market. The next generation of printed sensors will enable several applications, from human-machine interfaces to environmental sensing. These sensors benefit from the latest materials and technologies in the PE industry. While some consist of a very simple structure with only a few electrodes, others are much more complex and require the deposition of multiple layers. Nevertheless, they have in common the capability to be manufactured on both paper and plastic substrates, which offer advantages in terms of mechanical flexibility, thinness and weight reduction among other features.

Sensor RFID tags, pressure sensor arrays, and human-machine interfaces are all examples of smart sensors and objects; Figure 3-1 shows some examples of printed sensors.

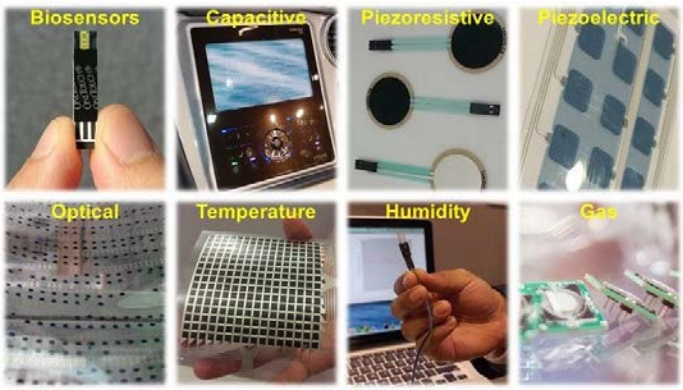

Figure 3-1 Pictures of different categories of printed sensors: biosensors, capacitive, piezoresistive, piezoelectric, optical, temperature, humidity, and gas sensors.[5]

Printed disposable glucose sensors currently generate the majority of industrial revenues. These sensors are used by diabetics as a self-diagnosis tool. This technology is essential for those patients but the market is currently commoditized and there is pressure on price. This explains why the industry is developing new biosensors, where the innovation lies in recognizing various biomarkers. This transition from R&D to commercialization will drive growth in emerging applications.

One significant developing sensor market is in the area of photosensitive devices. Organic and printed electronic versions of photo-optical devices are beginning to emerge as products. Some companies are developing photodetectors to detect the presence or proximity of stock items, for use in inventory control and supply chain management.

Regarding gas detection, air quality monitoring has been an important application for sensing technology for many years. Conventional metal oxide and electrochemical sensors based on electronic production methods are also now being replaced with printed sensors. These sensors are already on the market and integrated into several gas measurement products.

Finally, diagnostics is already a well-established marked for printed sensors, particularly blood test strips for analytes such as glucose and cholesterol. Some companies are developing systems for the measurement of ammonia in breath based on organic printed sensors. The sensitivity of the devices is part per billion and has a range of diagnostic applications.

In the following sections, taking into account the goal of this thesis already explained in the Chapter 1, we will focus in particular on the introduction of concepts of the sensors based on organic materials fabricated using printing techniques. Particularly, the sensors based on diodes and transistors will be detailed.

3.2 | ORGANIC SENSORS FOR CHEMICAL AND BIOSENSING APPLICATIONS

The ideal chemical sensor is an inexpensive and, portable device that responds with perfect and instantaneous selectivity to a particular target chemical substance (analyte) present in any desired medium. The scientific committee defined chemical sensors as devices or instruments that determine the presence, concentration, or quantity of a given analyte. The complexity of a chemical sensor is related to the technical difficulties associated with the specific nature (i.e. elemental or molecular) of the chemical substance to be analysed. Given the high number of known molecular substances, molecular sensing typically relies on recognition of molecular structure or associated reactivity; this recognition aspect is called selectivity. The analyte can be present in a gas, liquid, or solid phase on various dimensional scales ranging from bulk volumes of liters to picoliters, or surface layers from nanoscopic to monomolecular scale. The

design of chemical sensors also requires appreciation of the needed degree of quantitative reliability. Finally, economic resources and constraints can affect the design and strategy of any sensing task in many different ways. The capability of chemical sensing technology is substantial and has grown steadily over the past several decades, but it has been outpaced by the needs and diversity of chemical measurements. Materials limitations are prominent among the existing constraints of chemical sensors. The following discussion outlines the various chemical sensor types.

The word ‘‘Bioelectronics’’ is referred to the electronic combined with biology and biotechnology and attracts worldwide research efforts mainly because of the potential practical applications of these systems.[6] In fact, Bioelectronics is an interdisciplinary research field where electronics, physics, materials science and biology combine.[7] The electrical communication between the biomaterials and the respective transducers is the essence of the bioelectronic devices. The biomaterials (enzymes, antigens, antibodies, DNA...) constitute a wide platform of functional units for their integration with electronic elements, such as electrodes, field-effect transistors (FET) or piezoelectric crystals.[8] Biosensing is one of the fastest growing fields motivated by its impact on health, well-being, food, energy, and society fields. Thanks to the high sensitivity, low-cost and easy miniaturization of the electronic detection, bioelectronic devices can become a good option for analytical tools in different fields, such as diagnosis of genetic diseases, detection of infectious agents, study of genetic predisposition and, development of personalized medicine, among others. There is a worldwide increase in funding opportunities for research and innovation in bio-based technologies, as is clearly evident in the EU Horizon 2020[2] calls as well as the US NIH programs.[9] Available literature provides a tangible market of this collective effort. In this respect, the trend in published items per year in the field of bioelectronics indicates that, during the last year, the number of publications has doubled with respect to the previous 5 years.[10]

3.2.1 | Sensor basics

According to the International Union of Pure and Applied Chemistry[3] (IUPAC) (1991), a “*sensor is a device that transforms chemical/physical/biological information, ranging from the concentration of a specific sample component to the total composition analysis, into an analytically useful signal*”.[11] Typically, in a sensor, chemical/biological/physical information is converted into electrical information. The device core consists of two basic components connected in series: a recognition system, the receptor, and a physico-chemical transducer. As a general rule, the receptor is directly in contact with the target-analyte to be tested and transforms the chemical/biological information into a form of energy which may be measured by the transducer. The interaction with the target affects a receptor’s general property, this

[2] https://ec.europa.eu/programmes/horizon2020/en/area/biotechnology

[3] https://iupac.org/

change is translated by the transducer in an output signal, most usually electrical. In chemosensors, receptors are generally thin layers that can interact with the analyte by mechanisms such as surface adsorption, ion exchange and chemical reactions. Biosensors are a special class of chemical sensor: a "*biosensor is a device that uses specific biochemical reactions mediated by isolated enzymes, immunosystems, tissues, organelles or whole cells to detect chemical compounds usually by electrical, thermal or optical signals*".[11] As a result of the presence and biochemical action of the analyte, a physicochemical change is produced within the receptor layer and measured by the physicochemical transducer; a signal, proportionated to the concentration of the analyte, is generated, acquired, elaborated and, finally, displayed (Figure 3-2).[12][13]

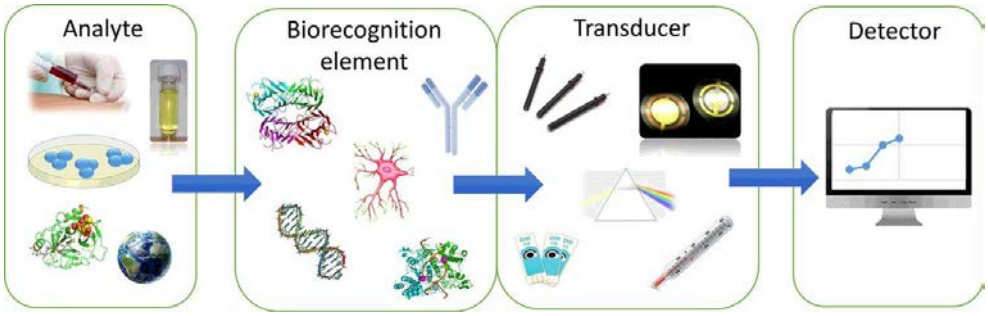

Figure 3-2 Generic components of a biosensor: the samples contain the analyte, the component to be detected.The biorecognition element represents the receptor (biocompound or synthetic) and is usually immobilized (in close contact) with the transducer, responsible for the signal transduction once the recognition occurs. Finally, the results are presented thanks to a user-friendly interface to visualize the data.[12]

There are three so-called “generations” of sensors: in the first generation, the normal product of the reaction diffuses to the transducer and causes the electrical response; the second generation involves specific “mediators” between the reaction and the transducer in order to generate improved response; finally, in the third generation, the reaction itself is a part of the sensor and causes the response; thus, no product or mediator diffusion is directly involved. The electrical signal from the transducer may be output directly but it is usually converted to a digital signal read by a microprocessor where the data is processed, converted to concentration units and output to a display device or data stored.

Regarding the chemical sensors, they respond to various chemicals reactions. They have the ability to identify and quantify liquid or gaseous chemical species. This class of sensors is currently used in many chemical analysis techniques, such as mass spectroscopy, chromatography, infrared technology and others, due to the miniaturization of sensors. There is a variety of chemical sensors with various methods of transduction. The transduction methods of chemical sensors can be organized into three classes based on their modes of measurement: (i) electrical and electrochemical properties, (ii) changes in the physical properties, and (iii) optical absorption of the chemical analytes to be measured.[14]

Electrochemical sensors are the most common approach, and operate by reacting with the chemical solutions thus producing an electrical signal that is proportional to the analyte concentration.[15] These types of sensors can be classified into three categories according to their operation mode [16]:

- **Potentiometric**, which relies on the measurement of voltage. To measure the concentration of chemicals it is necessary for a combination of electric and ionic current to flow in a closed circuit.
- **Amperometric**, which relies on the measurement of current. These sensors have been shown to be effective in a broad range of applications, such as volatile organic compounds (VOCs) detection in soils and groundwater, detection of mines and analytes detection in blood.[17]
- **Conductometric** relies on the measurement of either conductivity or resistivity. This type of chemical sensor comprises a capacitor that changes its capacitance when exposed to the desired analyte. The capacitance of the sensor changes due to a selectively absorbing material such as polymers or other insulators. These absorbing materials serve as the dielectric layer of the capacitor and their permittivity changes with exposure to the analyte. These sensors are commonly used to detect humidity as well as carbon dioxide and volatile organic compounds.[18] In the humidity sensor case, the dielectric layer comprises a water-sensitive polymer.[19]

A fundamental requirement of any bioelectronic system is the existence of electronic coupling and communication between the biomolecules and the electronic supports. However, most of the proteins lack direct electron transfer communication with electrodes/transducer, and therefore the lack of electrical communication between the biomaterials and the electronic elements present one of the fundamental difficulties of bioelectronic systems. The miniaturization of the bioelectronic systems is a requisite for implantable devices, and these types of applications will certainly introduce the need for biocompatibility. In most cases, actually, sensing requires that biocompatible and/or active materials (e.g., tissue, cell receptors, enzymes, antibodies, aptamers, and peptides) as well as artificial biomimetic structures (e.g., synthetic receptors, imprinted polymers, and biomolecules) are used to obtain a surface both sensitive and selective to the target components.[9] The need of methods to guarantee the electrical contact between biomaterials and electronic features and the preservation of the bioactive structure leads to the choice of a fabrication technology that respects these necessities.

So, a successful biosensor must possess at least some of the following beneficial features:

• The bioreceptor must be specific for the purpose of the analyses;

• If the biosensor is to be used for invasive monitoring in clinical situations, the probe must be tiny and biocompatible, having no toxic or antigenic effects;

Biosensors are typically classified according to the employed receptors or to the transduction mechanism. The bioreceptors are responsible in defining the specificity and the selectivity of the device. Common types of bioreceptors are:

- **antibodies**: as an antibody specifically binds its correspondent antigen, immunologic reactions can be detected; several detection mechanisms can be implemented, by labelling the molecules with fluorescent or radioactive elements (indirect detection) or by exploiting the modification in the electrical features of the antibody due to the immunologic response (direct detection);
- **enzymes**: enzymatic reactions are strongly specific, and several detection mechanisms can be implemented: for example, the products of the enzymatic reaction can be detected, as well as the activation/deactivation of the enzymes due to the interaction with the analytes;
- **cells**: whole cells are more stable than organelles, and their environmental sensitivity make them suitable for detecting global parameters as stress conditions, toxicity and organic compounds; moreover, treatment effects of drugs can be studied on the base of the variation in the cell metabolism;
- **nucleic acids**: the specificity of the interaction between nucleic acids is determined by complementary base pairing: for instance, DNA strands are the repetition of four kind of nucleotides, namely adenine, cytosine, thymine and guanine, and only adenine-thymine and cytosine-guanine bonds are possible; consequently, only one (complementary) nucleic acid is admitted for every sequence; the detection of the reactions that bring to the bond (hybridization) or separation (denaturation) of two complementary oligonucleotides can be performed in different ways, both direct and indirect.

As shown in Figure 3-3, according to the type of the transducer, biosensors are [13][20]:

- **electrochemical**: bioreceptors are anchored onto the surface of an electrode, namely working electrode, whose electrical properties are modified by the chemical interaction between bioreceptors and analytes; according to the considered electrical quantity, they can be distinguished into:
  - *amperometric*: variation of the current flowing between a counter electrode and the working electrode immersed in an electrochemical cell;
  - *potentiometric*: variation in the interface potential of the working electrode measured with respect to that of a reference electrode;
  - *impedencemetric*: the variation of the conductivity of the working electrode in electrolytes is represented by the variation of its electrochemical impedance, which can be measured by standard electrochemical procedures as Electrochemical Impedance Spectroscopy (EIS);

- *conductometric*: as several biological reactions determine a variation in the ion concentration and distribution inside a liquid media, conductivity measurements on electrolytes can be performed to detect them.

- **electronic**: the investigated biological reaction is detected on the basis of its effect on the electrical characteristics of semiconductor-based devices, including diodes, metal-insulator-semiconductor capacitors and transistors;
- **optical**: the investigated reaction results in an emission or absorption of photons which can be collected by means of appropriate photodetectors; several biological reactions can be optically detected, typically by modifying the bioreceptor or the analytes with light-emitting labels as fluorescent dyes or fluorochromes;
- **gravimetric**: the detection is made by evaluating the change of mass induced by the investigated reaction; commonly used transducers are Quartz Crystal Microbalance (QCM) and Surface Acoustic Wave (SAW) devices;
- **pyroelectric**: as pyroelectric elements generate a current as response to temperature variations, they can be employed to detect biological reactions which determine a variation in the temperature of the measurement environment;
- **piezoelectric**: piezoelectric elements are able to generate a potential in response to applied mechanical stress; if the bioreceptors modify the mechanical properties of a piezoelectric element in consequence of a biological reaction, this may be detected in terms of variation of the piezoelectric effect.

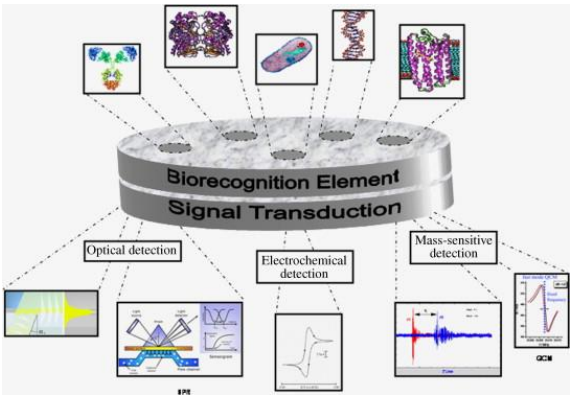

Figure 3-3 Generic function of a biosensor is to convert binding events between biological receptors and target agents into a signal that can be read by different transducers.[20]

3.2.2 | Organic sensors

Organic Electronics (OE) is a branch of materials science; it gives thin and flexible devices being an environmental friendly technology. OE differs from the conventional electronics due to the use of organic materials instead of inorganic conductors and semiconductors. OE allows the production of a wide range of thin-film and low-cost electrical components. It is a rapidly expanding area because of their wide range of

applications, including intelligent textiles, antennas, electronics, and sensors. One of the most important structures made by this technology is the organic field effect transistor (OFET), which is a powerful single element in semiconductor manufacture and the base for a great number of electronic devices: memories[21], photovoltaic[22], logic gates[23], sensors[24], etc.; however some new challenges, such as the high operating voltage requirement, material stability and lifetime are appearing. OFETs based on solution processable semiconducting material have obtained impressive improvements in their performances during recent years.

In general, the most interesting properties of the organic materials, based on π-conjugated organic small molecules or polymers, are related to their high processability, tunability of physical properties, stimuli-responsiveness and high conformability. These features allow a suite of fabrication techniques to be employed to develop appropriate architectures that can effectively interface with biological systems at the nano- and micro-dimensions.[25] Furthermore, with respect to the inorganic materials, many organic compounds have interesting properties such as good mechanical flexibility and biocompatibility. Flexibility makes them naturally compatible with low-cost substrates such as plastic, paper or metal foils. Their low elastic modulus allows bending, while biocompatibility makes them adaptable to biological systems. They can be easily processed over large areas with low-cost fabrication techniques at low processing temperatures, making them attractive materials for conformable devices. Deposition processes, such as, for example, solution processing, spin coating, or roll-to-roll technology, are very simple and cost-effective techniques, which have paved the way to printable production schemes that are well suited to large-area and flexible applications.

The realization of flexible electronics is one of the most exciting challenges in the research community and is expected to significantly broaden the application scope of electronics. As already underlined, flexible electronics offer the possibility for the easy spreading of electronics over arbitrarily curved surfaces and movable parts. Bendable and rollable organic electronics have been extensively investigated and used in the applications of pressure sensing and e-skins.[26] Moreover, bioelectronic devices can be easily integrated with the textiles to fabricate wearable smart devices.[27],[28]

In the following sections will be introduced the two devices developed in this thesis. First, the working principle and the state-of-the-art of the organic Metal-Insulator- Semiconductor (MIS) diodes. Second, the Biological Field-Effect Transistors (BioFET) as a type of Organic Thin Film Transistor-based (OTFT) sensors, particularly those that detect biomolecules such as DNA hybridization and proteins.

3.3 | INTRODUCTION TO ORGANIC DIODES

As previously introduced, numerous sensors have been presented in the literature. Such sensors are based on electrochemical, or optical approaches. A different type of sensors based on field-effect offers reduced size and weight, and they are compatible with the semiconductor micro-fabrication technology. Among a wide variety of semiconductor-based devices, diodes are two-terminal devices that are simple in terms of architecture. For these reasons, in this thesis we have developed organic sensor diodes based on a polymeric rectifying interface.

Diodes are two terminal devices characterized by an asymmetric Current-Voltage (C-V) behaviour. The terminals are called anode and cathode. Typically, the resistance in forward bias is negligible and in reverse bias condition is high. Diode can be realized using three types of interfaces based on i) p-n junction, ii) the Schottky-Mott barrier formed at the metal-semiconductor (MS) interface, or iii) Metal-Insulator-Semiconductor (MIS) devices. The requirement for a Schottky diode is the use of two different contact metals as anode and cathode. The p-n junctions are not covered in this thesis dissertation due to the low commercial availability and poor air and electrical stability of *n-type* organic semiconductors (OSC). A deeper analysis of MIS structure working principle will be given in Chapter 5, as it is the main device investigated in this thesis for gas sensor applications.

3.3.1 | MIS diodes: state-of-the-art

During the last decade, OSCs have attracted attention as interesting materials for next-generation electronics due to ease in the tuneability of their molecular structure, flexibility, light-weight, and large-area applicability.[29][30][31] In particular, their promising potential low-cost is expected to begin an era of disposable electronics.[32] [33] Organic radio-frequency identification (RFID) tags, which can be used to detect objects automatically in the near-field region (<10 m), are one of the emerging applications in disposable electronics. For this reason, organic RFID tags have been extensively studied over the past few decades.[34][35][36] To realize organic RFID tags, high-frequency (HF) systems and organic rectifiers that convert radio frequency (RF) signal to DC power should be properly designed.

The current density and Rectification Ratio (RR) of the organic diodes can also be designed by controlling the built-in potential formed at the metal/organic or organic/organic interfaces.[37][38][39][40] Because of its importance, studies on interface engineering of organic rectifiers, summarized in Figure 3-4, have been intensively conducted.

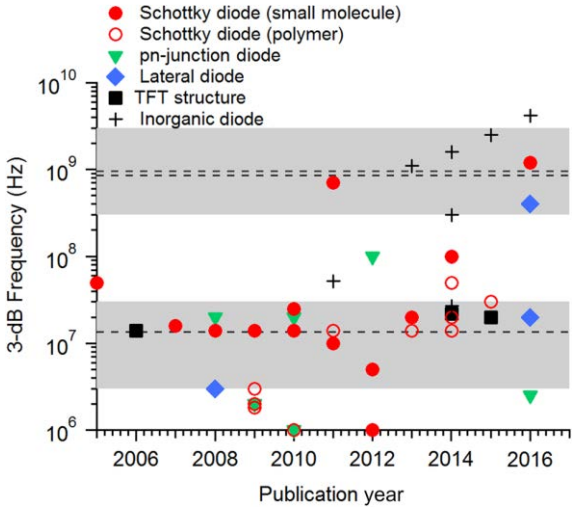

Figure 3-4 Frequency characteristics at -3dB of organic rectifiers published since 2006.The gray line indicated the range of the HF and UHF bands and the dashed lines denote the standard frequencies.[37]

Table 3-1 summarize previously published characteristics of organic rectifiers based on polymers.[37]

Table 3-1 Summary of the most relevant works using polymers for the fabrication of Schottky diodes.[37]

Publication year	Structure	Rectification Ratio	Printed	Ref.
2009	Ag/P3HT/Al	2900	Ag	[41]
2009	Cu/PTAA/Ag	$3.3 \cdot 10^4$	PTAA/Ag	[42]
2009	Au/PEDOT:PSS/P3HT/Al	$3 \cdot 10^4$	-	[43]
2010	Ni/Au/P3HT/Al	393	-	[44]
2014	Cu/PTAA/Ag	100	PTAA/Ag	[45]
2015	Cu/PTAA/Ag	100	PTAA/Ag	[46]

As mentioned before, the interface is one of the most important factors determining their electrical properties. Even if the Work-Function (WF) of a metal electrode is matched with the highest occupied molecular orbital (HOMO) or the lowest unoccupied molecular orbital (LUMO) level of the OSC, an adversely aligned interfacial dipole can shift the vacuum level to an undesirable direction and introduce an additional energy barrier, limiting charge injection.[47][48] To overcome this issue, it is possible to modify the interfacial dipole or to introduce a carrier injection layer.[49][50]

3.3.1.1 | Key factors of organic rectifiers to achieve higher performances

The frequency performance of organic rectifiers depends on the charge transport properties of the organic diodes. There are several key factors that determine and influence these properties. To increase the forward current of an organic diode, high injection efficiency and mobility are required. The rectifying barrier height affects the forward current as well as the reverse current. The thickness of the semiconductor layer is directly related to the transit time of the device, which determines the frequency response of the rectifier. The device area is not directly related to the frequency response, but it is also an important factor. These factors will be discussed in more detail below.

To reduce the injection barrier height for achieving high injection efficiency, several methods have been studied as, for example, energy level alignment using high WF metals or alloys,[51] thermal and electrical annealing,[49] reducing the interface dipole via a self-assembled monolayer (SAM),[52][53], inserting a charge injection layer as a conducting polymer,[50][54][55] a doped organic layer,[56][57] an organic material having an intermediate energy level,[58] or a transition metal oxide.[59] The mobility is principally determined by the intrinsic molecular structure, but it is also much affected by molecular orientation and alignment. The possibility of controlling the surface energy through interface engineering has been largely studied to enhance the molecular orientation and alignment.[52][60]

- **Interface engineering for organic rectifiers**

  As already introduced, the electrical properties of organic rectifiers can be controlled via interface engineering. By controlling the interfacial barrier and the surface energy, the forward and reverse current levels and the molecular orientation can be adjusted.

  Charge injection is one of the primary factors determining the performance of organic rectifiers and improving the efficiency of charge injection can help achieve High Frequency (HF) organic rectifiers. Generally, the surface electronic cloud of metals is rearranged by a repulsion force of the organic electronic cloud that generates a dipole at the metal/organic interface, leading to a negative vacuum level shift.[61] For *p-type* OSC, the injection barrier induced by this adversely aligned dipole limits the charge injection, even if the WF of the metal and the HOMO level of the organic layer are well matched. Inserting a charge injection layer is a commonly used method to improve charge injection efficiency. The dipole at an organic/organic interface is relatively smaller than the dipole at an organic/metal interface and, thus, employing an additional organic layer could be an effective way to reduce the injection barrier at metal/organic interfaces. One of the most widely used conducting polymers exhibiting a high WF and high

conductivity is poly(3,4-ethylenedioxythiophene): poly(styrenesulfonate) (PEDOT:PSS). The high carrier concentration of PEDOT:PSS allows to form a quasi-ohmic contact at the metal/organic interface and its high WF facilitate efficient hole injection from the PEDOT:PSS to the organic layer.[38], [53],[54],[62]

In the same manner, a doped organic layer can be also used as the hole and electron injection layer.[63],[64] These conductive organic layers effectively improve the charge injection. However, they could give rise to a lateral leakage current, resulting in a low RR. Chemical treatments such as ultraviolet ozone or plasma treatments which increase the -OH or $-O_2$ groups at the surface of the electrodes lead to an increment of the effective WF promoting the hole injection.[65] The same result can be obtained by a chemical modification of the electrodes, Copper tetracyanoquinodimethane (CuTCNQ)-modified Cu electrode, for example, presents and increase in the effective WF from 4.6 to 5.2 eV, as shown by Wang H. et. al in [47]. As a result, the forward current density of the pentacene diode with the CuTCNQ-modified Cu electrode was comparable with the one obtained with an Au electrode.[66] The effective WF can also be tuned using SAM treatment thanks to the permanent dipole moment of chemisorbed SAM molecules. Perfluorinated thiol derivatives are commonly used to increase the effective WFs of metals: the thiol groups can easily form a strong bond with the metals and fluorine atoms, exhibiting high electronegativity, can form a negative dipole moment. For example, a 2,3,4,5,6-pentafluorothiopehnol (PFBT) modified Au electrode effectively reduced the injection barrier to 0.1 eV.[67] On the other hand, to improve electron injection, a thin polymer (1–10 nm) surface modifier with aliphatic amine groups such as polyethylenimine ethoxylated (PEIE) and polyethylenimine (PEI) is suitable for the air-stable electron injection layer. Due to the strong molecular and interface dipole of PEIE and PEI, the effective WF of the target material can be lowered by up to 1.5 eV.[68]

- **Modifying the rectifying barrier height**

The Schottky barrier formed at the metal/organic interface imparts rectifying characteristics to the diode. The reverse current of the diode is exponentially suppressed as the Schottky barrier height increases. As already described, a Schottky contact can be formed by the mismatching between the HOMO or LUMO levels of the organic layer and the WF of the metal. For example, the HOMO level of polytriarylamine (PTAA) is known to be 5.1 eV thus forming an ohmic contact with high WF metals such as platinum (5.1–6.3 eV) or printed silver (5.2 eV), which leads to no-rectifying characteristics for the PTAA diode presented in [69]. However, a PTAA/copper electrode interface forms a rectifying contact, thereby reducing the reverse current significantly by 3–5 orders of magnitude (Figure 3-5). Interestingly, the leakage current depends not only on the

metal, but also on its deposition method. Sputtered copper on PTAA generates an additional thin insulating interfacial layer, preventing charge injection from copper to PTAA, which results in a suppression of the leakage current by two orders of magnitude compared with thermally evaporated copper. The leakage current of the diode is an important issue in the rectifier because charge dissipation of the rectifier predominantly arises from the leakage current.[49]

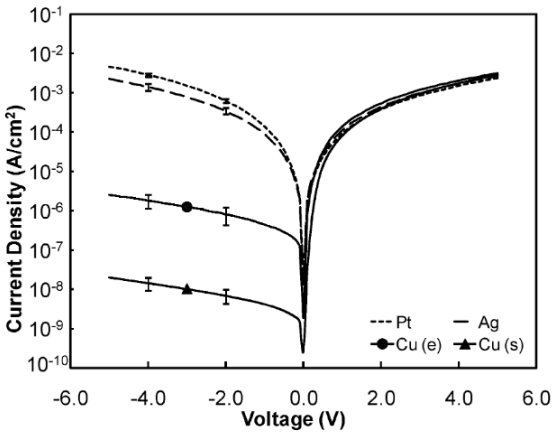

Figure 3-5 J–V characteristics of the PTAA diode with different cathodes.[69]

Figure 3-6A shows the current density–voltage (*J–V*) characteristics of C_{60}/Al diodes with interface layers of WO_3 and WO_3/hexamethyldisilazane(HMDS) for rectifying contacts.[38] Due to the dipole moment of HMDS, the effective WF of WO_3/Al was shifted from 4.3 to 4.6 eV after the HMDS treatment. Compared with the forward current density of the C_{60} diode without the HMDS treatment, the one obtained with the HMDS treatment was significantly improved below the 1V range due to the decrease in barrier height.

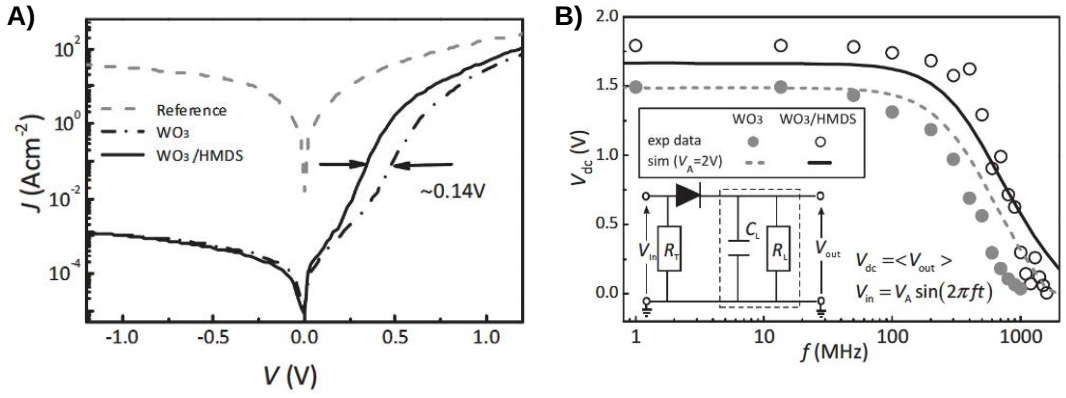

Figure 3-6 A) J–V characteristics of the diodes comprising the Al/C_{60}/ BCP/Al structure, where WO_3 is a dash-dot line, WO_3/HMDS is a solid line, and the absence of a layer is a dash line. B) The average DC component (V_{DC}) of the output voltage (V_{OUT}) obtained for the 2 V sinusoidal incoming RF signal (V_{IN}) with regard to the operating frequency for the C_{60} rectifiers with and without HMDS treatment. The shapes and lines indicate the experimental and the simulation results, respectively.[38]

Moreover, the C_{60} rectifier with HMDS treatment showed only a 0.21 V output voltage drop and an improved 3 dB frequency of 700 MHz (Figure 3-6B). These results indicate that an excessively high barrier height has detrimental effects on the performance of high-speed organic diodes. Therefore, barrier heights should be optimized to maximize the forward current, while the leakage current remains at an acceptable level.

3.3.2 | Gas sensors based on organic diodes: state-of-the-art

The possibility of using organic materials, the need of low power and low-cost processes, and room temperature (RT) operations for electronic sensor devices have led to the development of different implementations and approaches in the fabrication of diodes in terms of architectures and materials. The recent interest in organic materials has opened to the introduction of either i) carbon-based nanomaterials or ii) polymeric materials as components of diodes. Among the former mentioned nanomaterials, graphene represents a material which has been extensively used in the development of sensors due to its special 2D structures that confers high thermal conductivity, high mobility, high surface to volume ratio, and high electrical conductivity. These features have put this material in the center of attention in the development of detection applications including sensors and biosensors.

Recent studies have adopted graphene/semiconductor heterojunction Schottky diodes to develop sensing applications. In 2013, Kim et al. presented a graphene diode sensor for the detection of both liquids and gases, where the material is in contact with *n*- and *p-type* silicon substrates over its entire active area (Figure 3-7A), allowing exposure to liquids and gases from above.[50]

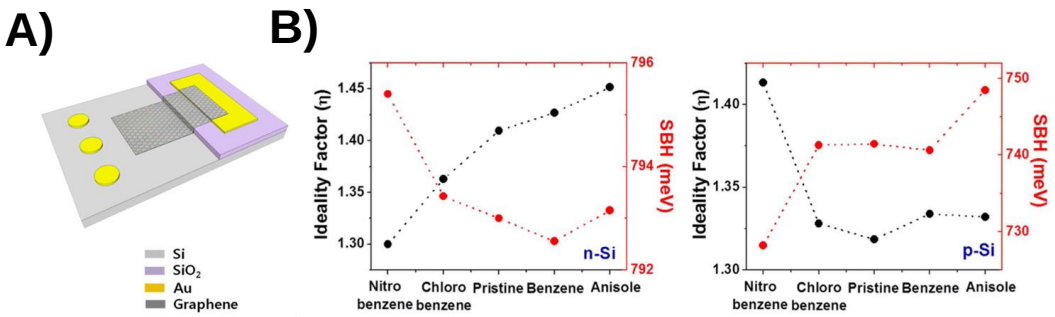

Figure 3-7 A) Scheme of the graphene sensors. B) Variation of the ideality factor and Schottky barrier height for n-type and p-type Silicon in function of different gases.[70]

This diode configuration is used to determine the change in the WF and doping levels of graphene upon exposure to different substances. The diode presented sensitivity towards liquid and gaseous electron donor (E_D) and acceptor (E_A) substances;

such as anisole, benzene, chlorobenzene, nitrobenzene, and gaseous ammonia (Figure 3-7B). The RR obtained for these diodes is 150 with a current density in forward bias of 2-3 $mA \cdot cm^{-2}$. The SBH increases of 0.1 eV in the presence of the stronger E_A, while it decreases of 0.02 eV where the sensor is exposed to the strongest E_D.

Moreover, Uddin et al. proposed a graphene/Si heterojunction Schottky diode as a H_2 sensor with tunable sensitivity and low operational power (Figure 3-8A).[71] Compared to the graphene chemiresistor sensor, the chemi-diode sensor presents more than one order of magnitude higher sensitivity as the molecular adsorption induces Schottky Barrier Height (SBH) changes. Thus, the heterojunction current varies exponentially in reverse bias. The reverse bias operation also enables low power consumption, as well as modulation of the atomically graphene's Fermi level, leading to tunable sensitivity and detection of H_2 down to the sub-ppm range (Figure 3-8B). However, this device is fabricated using Chemical Vapor Deposition (CVD), a conventional and expensive technique onto a rigid inorganic substrate, making it not very suitable for low-cost devices.

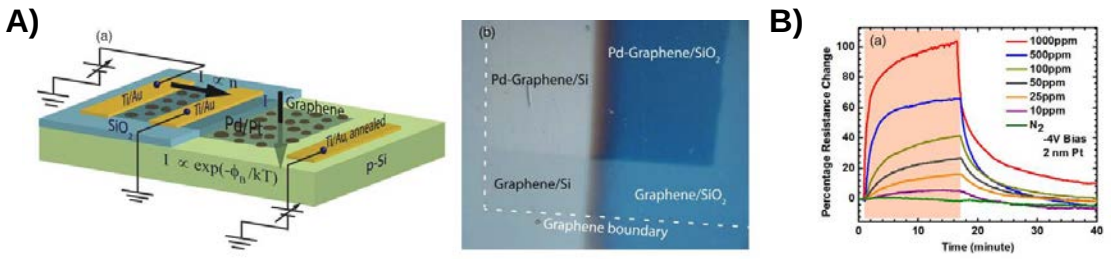

Figure 3-8 A) Device schematic of Pt/Pd-functionalized graphene chemiresistor. (b) Optical image of graphene/p-Si heterojunction Schottky diode. B) Percentage resistance change of Pt-deposited graphene/p-Si device for different H_2 concentration in the range of 1000–10 ppm and in N_2 environment (pink box).[71]

Dai *et al.* proposed an ammonia sensor based on an organic diode with Vertical NanoJunctions (VNJs) to exhibit reliable responses to ammonia breath of rats. The three-dimensional and two-dimensional structures of the proposed solid-state ammonia sensor are shown in Figure 3-9A. A vertical organic diode with a porous top electrode is fabricated. From bottom to top, a simple anode/semiconductor/cathode sandwich structure is formed by using indium tin oxide (ITO)/poly(3-hexylthiophene)(P3HT)/aluminum (Al). Although the devices present highly interesting features, conventional techniques such as thermal evaporation was used to pattern the electrodes. The proposed ammonia sensor has a Limit of Detection (LOD) lower than 20 ppb, a real-time response, a good enough selectivity, a simple structure, a high reproducibility, and a low production cost (Figure 3-9B).[72] Later, the same group achieved even a lower detection limit of 1 ppb by using phenyl-C_{61}-butyric acid methyl ester (PCBM) as the sensing layer, thanks to its nano-porous structure that enlarges the surface to volume ratio.[73]

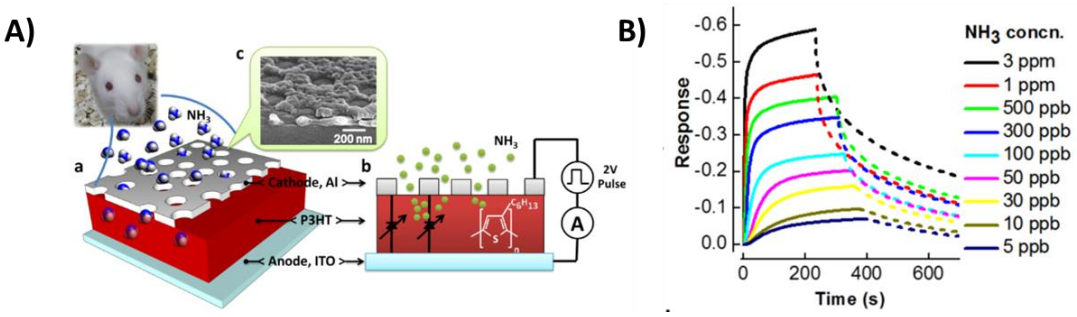

Figure 3-9 A) (a) Three-dimensional and (b) two-dimensional schematic structures of the proposed ammonia sensor, the VNJ-P3HT diode. The molecular structure of P3HT and the equivalent parallel-connected vertical diodes are shown inside panel b. (c) The scanning electron microscope image of the VNJ-P3HT diode. B) Response curve of the sensor with pure nitrogen as the background and with various concentrations of NH_3.[72]

Babaei *et. al* fabricated a H_2O sensor with a ppm-level sensitivity. The H_2O molecules were absorbed on a gold layer deposited on a hydrophobic semiconductor.[74] The sensors consist of two Au/oxidized poly[2-methoxy-5-(2-ethylhexyloxy)-p-phenylenevinylene](MEH-PPV)/Au diodes connected in series with a shared thin film Au electrode exposed to the open atmosphere (Figure 3-10A).

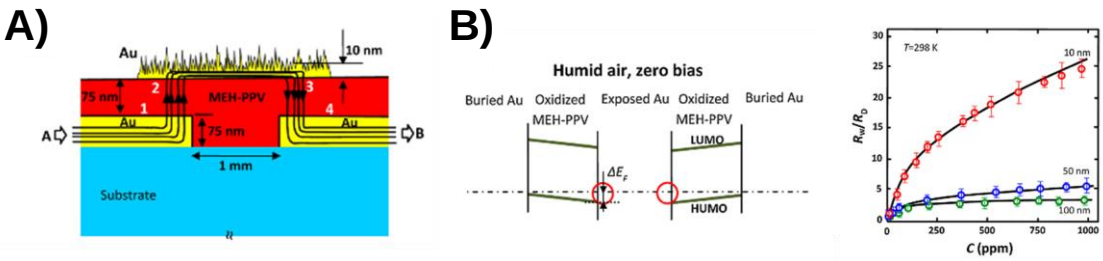

Figure 3-10 A) Schematic diagram of the device structure and the current crowding demonstrated on the device cross-section; the humidity sensitive conduction barrier forms at the interfaces 2 and 3. B) The flat band energy-level diagrams of an Au/oxidized MEH-PPV/Au/oxidized MEH-PPV/Au structure with its central Au electrode exposed to humid atmosphere depicting the H_2O and the change of the resistance due to the adsorption-caused of H_2O molecules.[74]

The charge distribution changes in the gold layers, caused by the surface adsorption of H_2O molecules, alter the *C*-V characteristics of the two gold/semiconductor junction. The fabricated device operates as a resistive humidity sensor whose resistance increases in humid atmospheres (Figure 3-10B). Here, the device is again fabricated using thermal evaporation technique for the electrode patterning.

An interesting attempt presented by Jalil et. al [75] to improve the absorption–desorption process in organic gas sensors at RT is the development of an organic nano-pyramidic structure consisting of vanadyl phthalocyanine (VOPc) sandwiched between a flat Au substrate electrode and a robust smooth Au top contact made by rolled-up

metal nanomembranes. The organic nano-crystal diodes were fabricated on silicon wafers and all the patterning processes were done by conventional photolithography. Moreover, the OSC was deposited by evaporation (Figure 3-11A). In this nanoscale diode, the VOPc crystalline nano-pyramids act as functional units to detect NO_2, and efficient charge transfer from an organic heterojunction is employed to improve the contact resistance between the nanostructures and the electrodes. In this way, both a highly sensitive response to NO_2 molecules and a fast recovery of the sensor are achieved at the same time.

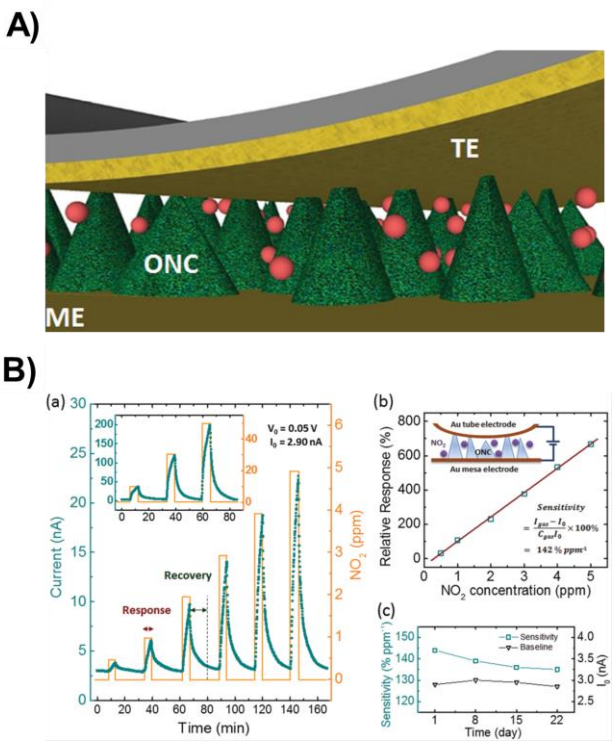

Figure 3-11 A) Conceptual picture of cross section of the VOPc nano-pyramids (green cones). B) Electrical characteristics of the VOPc sensor: a) Response of device to periodic NO_2 exposure. b) Relative response of sensor versus different NO_2 concentrations (from 0.5–5 ppm). c) Stability test in ambient atmosphere: sensitivity (left axis) and baseline (right axis) over time.[75]

When the nanocrystal diode is exposed to the analyte, extra carriers are provided by NO_2 apart from the limited amount of carriers injected from the tube electrode, resulting in an increased current in the output signal. A large area-to-volume ratio leads to a high average sensitivity of 151% ppm^{-1} and a fast recovery time (12 min) (Figure 3-11B).

Finally, another diode approach based on Metal Phtalocyanines (MPcs) was used to develop gas sensors.[76] Metal phthalocyanines are *p-type* OSCs which exhibit high sensitivity to both electron acceptor gases such as O_2 and electron donor gases such as NH_3. The heterodevices of MPcs fabricated using organic–inorganic heterojunction devices with the structure ITO/ZnS/ZnPc/Al are shown in Figure 3-12.

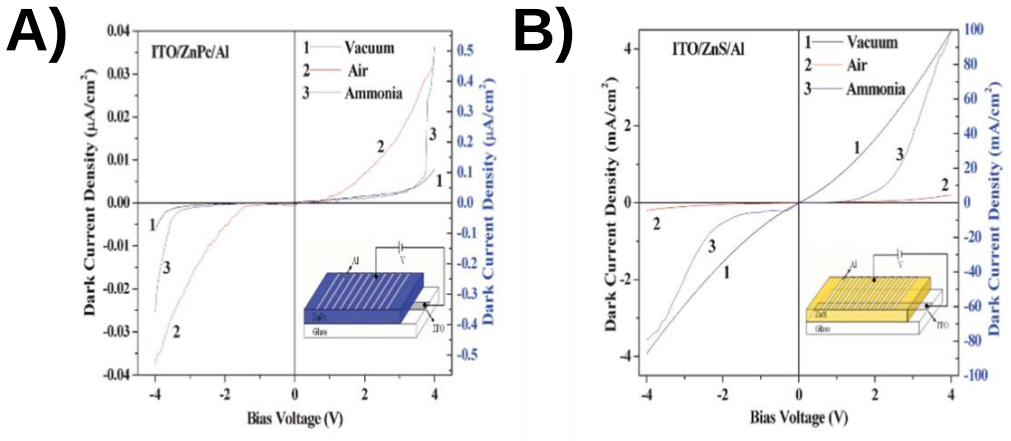

Figure 3-12 Dark current–voltage characteristics under different atmosphere: (1) vacuum, (2) air and (3) ammonia. (1 and 2 correspond to the left scale and 3 correspond to the right scale) for A) ITO/ZnPc/Al and B) ITO/ZnPc/Al device structures.[76]

3.4 | INTRODUCTION TO BIOFET

3.4.1 | Sensors based on organic thin film transistors

Among the electronic devices that can be fabricated using organic technology, a huge interest has been focused on OTFTs, as they represent a fundamental building block for cheap, light-weight, flexible circuits and systems [77], and, as already underlined, a powerful platform for physical, chemical and biological sensing.[78],[79] Most of all, the main advantage of a transistor is that they can easily translate the chemical/biological information into a current, which can be detected with simple electronic instrumentation.

As already underlined, organic molecules can be synthesized in a wide range of structures and morphologies, thus allowing the realization of films especially suitable for sensing applications. In particular, the chemical and physical properties of an OSC can be adjusted in order to enhance a specific sensitivity and selectivity, and also to integrate recognition elements.

OTFTs are three-terminal electronic devices consisting of an OSC layer, an insulating (dielectric) layer, and three electrodes: the source, drain, and gate (Figure 3-13). The active OSC layer can be made of oligomers, polymers, or organic nanostructured materials that are deposited as thin films (few tens of nanometers thick) by, generally, solution casting, spin coating, sublimation, or printing techniques. OTFTs can be fabricated according to different structures and technologies; however, depending on the mechanism used to achieve the current modulation, they are typically categorized into two main categories: Organic Field Effect Devices (OFEDs) and Organic ElectroChemical Transistors (OECTs).

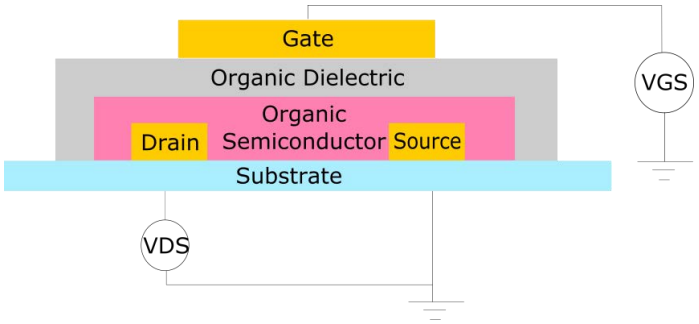

Figure 3-13 Scheme of an Organic Thin Film Transistor under bias. The device is compounded by: metallic gate electrode, organic dielectric and semiconductor, and finally by drain and source electrodes. A potential is applied between drain and source. The current flow is controlled by the gate voltage.

3.4.1.1 | Organic field-effect devices (OFEDs)

In these devices, an electric field is established across a dielectric layer separating the gate electrode from the semiconductor layer. This electric field can manipulate the size and shape of a region of high conductivity and hence, modulate the current flowing through the semiconductor material, creating a relationship between gate voltage (V_g) and drain current (I_d). This category includes Organic Field-Effect Transistors (OFETs), Electrolyte-Gated Organic Field-Effect Transistors (EGOFETs), Ion-Sensitive Organic Field-Effect Transistors (ISOFETs) and Organic Charge-Modulated Field-Effect Transistors (OCMFETs);

As already underlined, OFEDs for biological detection, usually named as Biological Field-Effect Transistor (BioFET), have received a great attention in recent years. In this paragraph, the working principle of OFETs, EGOFETs and ISOFETs will be briefly presented. A deeper analysis of OFET structure and its state-of-the-art as a sensor will be given in Chapter 5, as it is the main device investigated in this thesis for biosensing applications.

The success of OFEDs with respect to other electronic biosensors is mainly related to the peculiar characteristics of FETs as multi-parameter devices, which allow the implementation of a wide range of transduction mechanisms. They can amplify the electrical signals coming from the receptors and, mostly important, they allow the direct detection of biomolecules through their intrinsic properties, such as, for example, electrical charge.

It can be noticed that, also in a very simplified model of the transistor, several elements contribute to the final current: some of them are related to the chosen materials, as charge carrier mobility (μ), insulating capacitance (C_i) and contact resistance (R_C), others to design, as the geometrical channel width (W) and length (L) and others to the operating conditions (the applied voltages, represented by V). The variation of some of these parameters can be correlated with physical, biological or

mechanical signals, so they can be theoretically employed for biochemical transducing, by properly choosing the technology, the materials and the operative condition of the device.

- **Organic Field-Effect Transistors (OFET)**

  The OFET is a three-terminal device, in which a voltage applied to a gate electrode controls the current flow between the source and drain electrodes via an imposed bias. A basic scheme is shown in Figure 3-13 where V_g and V_{ds} are the applied gate and source-drain voltages, respectively.

  Basically, the thin film transistor operates like a capacitor. When a voltage is applied between source and gate, a charge is induced at the insulator-semiconductor interface. This charge forms a conducting channel which conductance is directly related to V_g.

  Different basic mechanisms of BioFETs based on OFETs can be considered [80]:

  - potential changes that are caused by a catalytic reaction product (e.g., between an enzyme and its substrate);
  - potential changes that are caused by surface polarisation effects or the change of dipole moments (e.g., antigen–antibody affinity reactions or DNA (deoxyribonucleic acid) hybridisation), in principle, these devices are able to detect the change of the electric field associated with affinity binding of biomolecules;
  - potential changes that are coming from living biological systems as a result of more sophisticated (bio-)chemical processes (e.g., action potential of nerve cells).

At present, there exist few different BioFETs based on OFET structures and processes for their fabrication, but the principle of using an electric field to create regions of excess charge in a semiconductor substrate in order to enhance or diminish the local conductivity is common to all of them.

- **Electrolyte-Gated Organic Field-Effect Transistors (EGOFET)**

  Electrolyte-gated OFETs are significantly different from classical OFETs: the OSC layer is in contact with an electrolyte instead of a classical dielectric; thus, the conductivity of the semiconducting channel is directly modulated by a solid or a liquid electrolyte put in between the semiconductor and the gate. EGOFETs display a much higher gate capacitance (up to ~1000 higher) than other types of OFETs, which use traditional inorganic or organic non-electrolytic dielectrics; as a consequence, biasing voltages used for EGOFETs are typically much smaller than those necessary for OFETs (<1 V, versus >10 V or even higher). The sensing

capabilities of EGOFETs rely on the possibility of properly functionalizing the gate electrode or OSC by means of specific molecules or functional groups able to interact with the target molecules present inside the electrolyte.[81] The most common architecture is the top-gate, bottom-contact configuration. The gate electrode is immersed in the electrolyte and source and drain electrodes, isolated from the electrolyte, provide electrical contact to the channel (Figure 3-14).[82] Actually, an EGOFET looks more like an OECT than an OFET. However, in an OECT, the on/off switch is produced by electron transfer from the electrolyte and the semiconductor (doping/de-doping), whereas only capacitive processes occur for EGOFETs but no charge transfer.

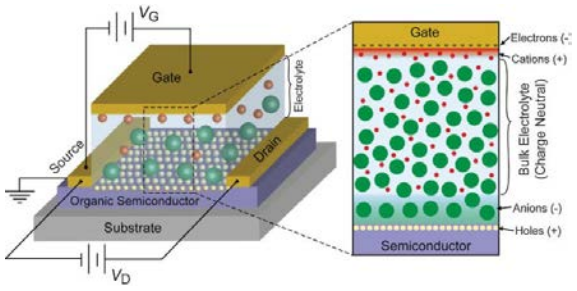

Figure 3-14 Scheme of an electrolyte-gated OFET under bias. For a p-type OSC (as shown here), the application of a negative gate voltage bias causes ion migration within the electrolyte dielectric layer, resulting in the formation of electric double layers at the gate/electrolyte and electrolyte/semiconductor interfaces, which consist of electrons/cations and anions/holes, respectively creating a "gate capacitor". [82]

- **Ion-Sensitive Organic Field-Effect Transistors (ISOFET)**

  ISOFETs are similar to EGOFETs in that they have an electrolyte layer adjacent to the gate electrode (Figure 3-15). However, ISOFETs present a dielectric layer, which it is used for measuring ion concentrations in solution. An ISOFET's threshold voltage depends on the pH of the substance in contact with its ion-sensitive barrier. Moreover, the reference electrode is characterized by a non-polarizable interface; therefore, it guarantees a constant potential drop at interface with the electrolyte. The electric field across the insulating gate dielectric depends on the charge at the electrolyte-insulator interface.[83]

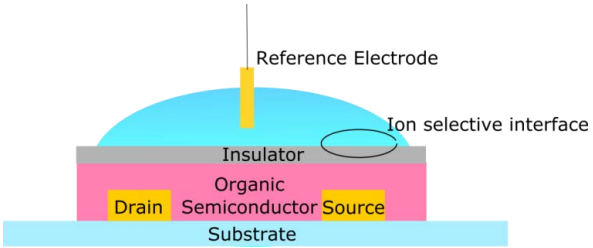

Figure 3-15. Scheme of ISOFET. The device is composed by an OSC, insulator and an ion sensitive membrane/layer.

3.4.1.2 | Organic electrochemical transistors (OECTs)

A very interesting device that has recently attracted large attention for its high sensitivity in bio-analyte detection is the Organic ElectroChemical Transistor (OECT). OECT is a three-terminal device in a transistor configuration (source, gate, and drain). The source and drain are connected by an OSC material in which an electronic current is generated (I_d) in response to a potential difference. A variable potential at the gate controls the magnitude of the drain current by doping and de-doping the channel (Figure 3-16). OECTs presents similarities to the EGOFETs, due to the fact that the electrolyte is an integral part of the device: ions from the electrolyte can penetrate the whole bulk of the polymeric channel.[84]

First examples of OECTs were obtained through electro-polymerization on microelectrodes; typical polymers were polypyrrole, polyaniline, and polythiophene. [85],[86] Nowadays, the most common material used for OECT devices is PEDOT:PSS, which is investigated in various sensing applications.[87]

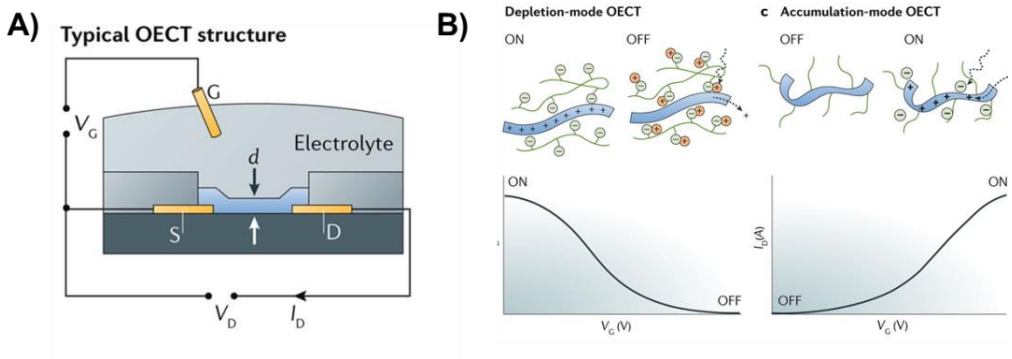

Figure 3-16.A) Scheme of Typical OECT structure B) The device physics of OECT in depletion and accumulation mode.[88]

3.4.2 | BioFET: state-of-the-art

Among a wide variety of examples of BioFETs in the literature, this section is devoted to introduce the most relevant works of these sensors fabricated. In order to compare properly the state-of-the-art, it has been chosen the most relevant BioFET works which use: i) microfabrication techniques and ii) a top sensitive layer. These features have been selected since these are the same features of the BioFET developed in the work of the Chapter 5.

In 2014, W. Huang et al.[89] developed a glial fibrillary acidic protein (GFAP) sensor: they fabricated a *p-type*(pentacene) and *n-type*(a naphthalenetetracarboxylic diimide, NTCDI) OTFT with a receptor–antibody-functionalized top insulator layer based on perfluoropolymer called Cytop. The Cytop layer acts as a second (top) gate dielectric, and any selective binding of the target protein to surface-linked antibody can

be detected. This layer was functionalized by the deposition of hydrocarbon through vapour-deposition technique. Finally, these devices were fabricated onto a rigid Si/SiO_2 substrate. The device structure is shown in Figure 3-17A. Figure 3-17B shows the transfer curve of these devices when a concentration of 400 $ng \cdot mL^{-1}$ of GFAP is introduced. The output V_G curve gradually shifted in the presence of the capture antigen. The sensor performances were also studied by measuring drain current changes on exposure to varying concentrations of GFAP solution, as shown in Figure 3-17C and Figure 3-17D. As expected, the pentacene and 8-3 NTCDI based sensors exhibit opposite current change directions on exposure to GFAP solutions, consistent with the expectation that attached negatively charged species induce lower conductance in *p*-channel transistors and higher conductance in *n*-channel transistors.

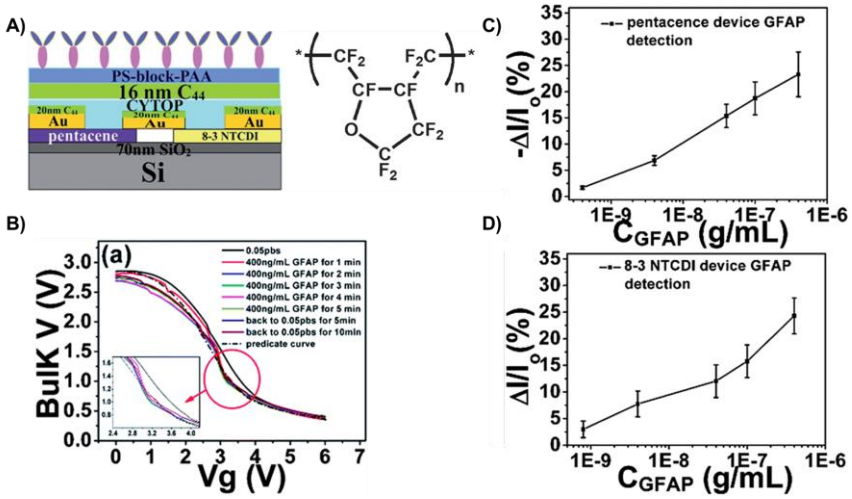

Figure 3-17 A) Device sensor architecture of anti-GFAP modified inverter based on pentacene and 8-3 NTCDI. The CYTOP structure is also shown. B) The sensing behavior of the anti-GFAP modified inverter (using pentacene and 8-3 NTCDI) on exposure to (a) 400 $ng \cdot mL^{-1}$ (8 nM) GFAP and predicted curve (theoretical inverter shift-dotted curve). Drain current changes of anti-GFAP modified pentacene (C) and 8-3 NTCDI (D) devices versus GFAP concentrations; Y bar is the standard deviation of drain current changes.[89]

In 2015, J. Choi et al.[90] developed a study of the effect of an insulator/protein overlayer deposited onto semiconducting active layers in OTFTs with regard to their electrical performance. The active layers used were composed of 6,13-bis(triisopropylsilylethynyl)-pentacene (Tips-Pentacene) blended with poly(amethylstyrene) (PaMS), and the overlayer consisted of a bottom insulating (protecting) layer of an amorphous perfluoropolymer Cytop and a top protein layer of negatively charged bovine serum albumin (BSA) (Figure 3-18A). The active Tips-Pen:PaMS layer was deposited onto the Si wafer substrates from the blended solution using the solution-coating method of H-dip coating. The biomolecules were deposited using a simple solution-coating method which involved a horizontal dip coating process without the need of insulator functionalization. Device surfaces can be fully recovered by rinsing them with pure water which means non stable attachment of the BSA

biomolecule onto the surface (Figure 3-18B).The authors show that the Cytop/BSA overlayer on the Tips-Pen:PaMS active layer improved the electrical performance of the OTFTs; the devices with the Cytop/BSA overlayer exhibited an average effective mobility of 0.25 $cm^2V^{-1}s^{-1}$, which was higher than that of bare devices without any overlayer (0.20 cm^2 $cm^2V^{-1}s^{-1}$). This improved performance of OTFTs is due to the formation of a second current channel in the Tips-Pen:PaMS active layer via the electric field-effect of the negatively charged BSA overlayer (Figure 3-18C). These results demonstrate that OTFTs employing charged protein overlayers show considerable promise for the production of high-performance OTFT based sensors devices.

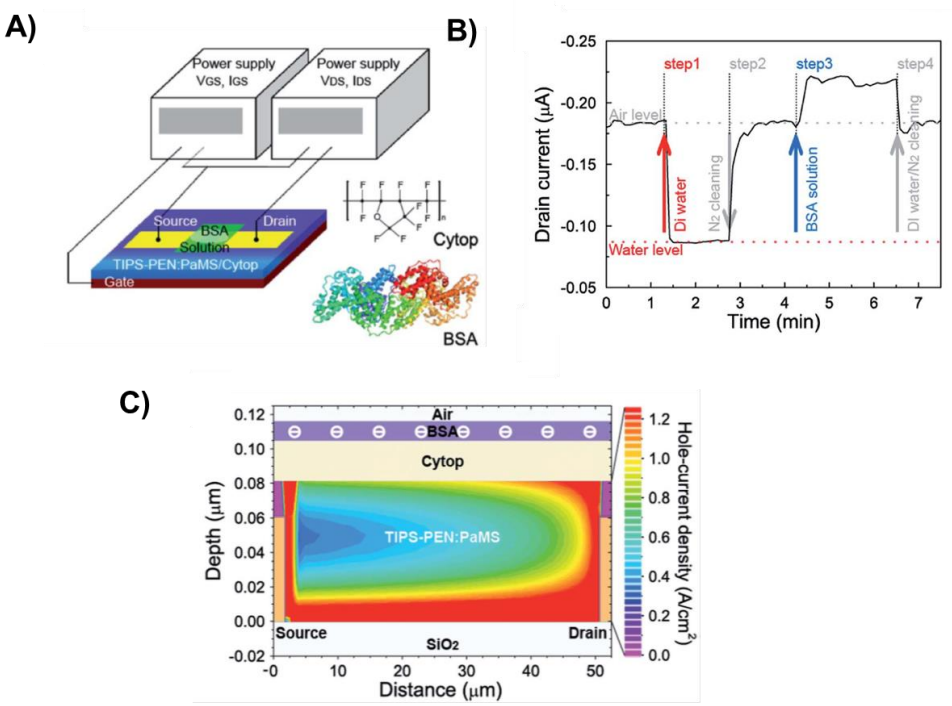

Figure 3-18 A) Schematic of a H-dip-coated OTFT operating in aqueous BSA solutions. B) In situ monitoring of changes in the drain current of the OTFT device for four processing steps, 1–4, with an aqueous BSA solution (50mM, pH 5.7). C) The simulated 2D hole–current density profiles in the Tips-Pen:PaMS layers contacted with Cytop and BSA overlayers according to the ATLAS programme.[90]

Other devices working with aqueous liquid electrolytes were also reported. For example, Kergoat et al. [91] firstly reported a device gated with water. By replacing the gate dielectric by a simple water droplet, they produced a transistor that entirely works in the field-effect mode at voltages lower than 1 V. They called it Water-Gated OFET (WGOFET, Figure 3-19A). In this case, water acts both as the electrolyte and the media responsible for carrying the analytic sample, as they demonstrated in [92] where they developed a DNA sensor. The device, which has a bottom-contact top-gate structure, was built on a silicon wafer with thermally grown oxide. A water droplet was deposited onto the semiconductor to form the gate-dielectric, and a platinum wire was dipped into the droplet to obtain the gate electrode. Figure 3-19B shows the transfer characteristics

showing that probes immobilization entails a current decrease and a shift towards negative voltages of the threshold voltage. Figure 3-19C shows the experimental results obtained after DNA hybridization and for a random target.

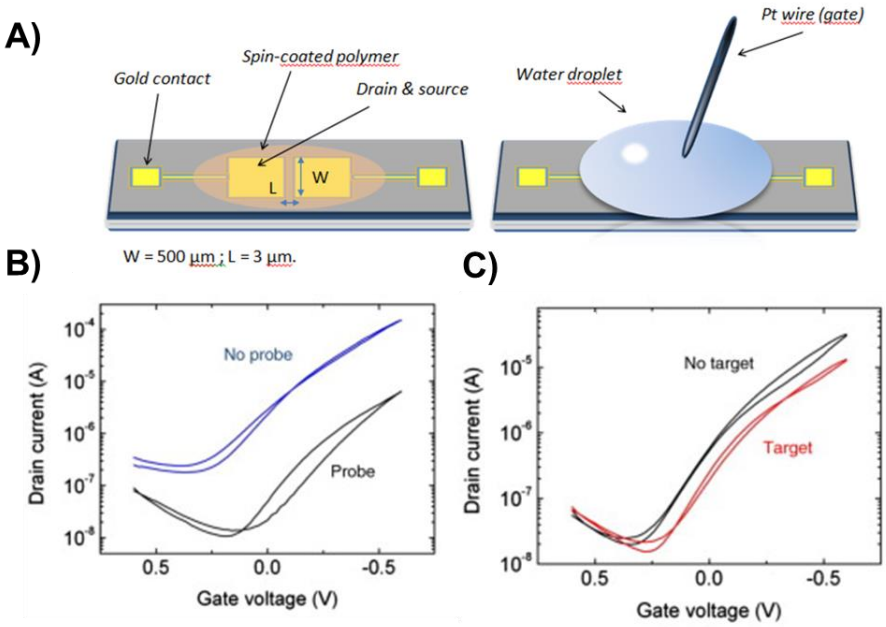

Figure 3-19. A) WGOFET scheme. The device is compound of drain and source gold contacts, an OSC spincoated onto the electrodes and finally the water droplet that acts as a gate. Transfer characteristics of the WGOFET for B) immobilized DNA strain onto the OSC C) the detection of the complementary DNA and random target.[92]

In 2013, Magliulo et al.[93] demonstrated a hydrophilic thin layer (plasma deposited ethylene/acrylic acid (pdEthAA) carrying -COOH groups on P3HT (Figure 3-20A). A comparison between pristine P3HT and pdEthAA/P3HT bilayer is given on Figure 3-20. It is also shown on this figure that the gate current (I_G, red curves and right Y-scale) stay low, which demonstrates the field-effect mode of operation and excludes the electrochemical mode of operation; this shows that the hydrophobic layer fully plays its role by impeding ion penetration in the OSC. In addition, the authors reported that chemical or biological species could be covalently immobilized on such functional hydrophobic/hydrophilic bilayer, such as DNA probes (even if not described in their article).

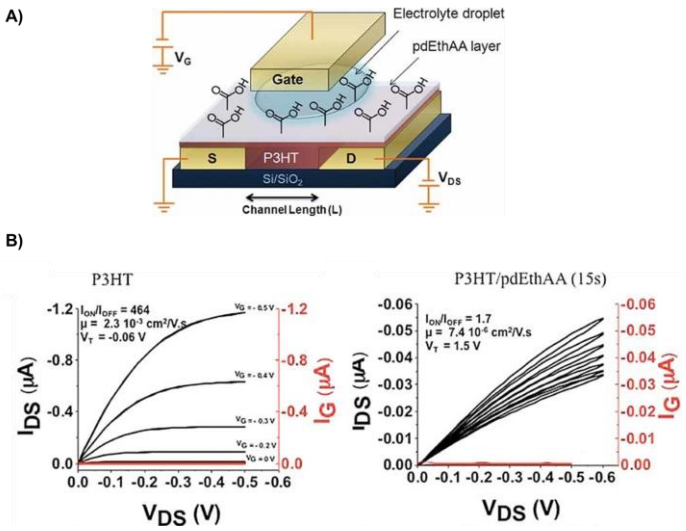

Figure 3-20 A) Scheme of P3HT based transistor with a hydrophilic thin layer. B) Output characteristics of the transistor with and without the pdEthAA layer onto the OSC.[93]

Mulla et al. [94] reported a pBTTT-based EGOFET sensor for streptavidin detection. pBTTT was spin-coated on the device, then a layer of poly(acrylic acid) was spin-coated on the pBTTT layer to have carboxyl functionalities acting as anchoring sites for phospholipid bilayers. The proof-of-concept of the sensor was demonstrated with the streptavidin/biotin couple (Figure 3-21).

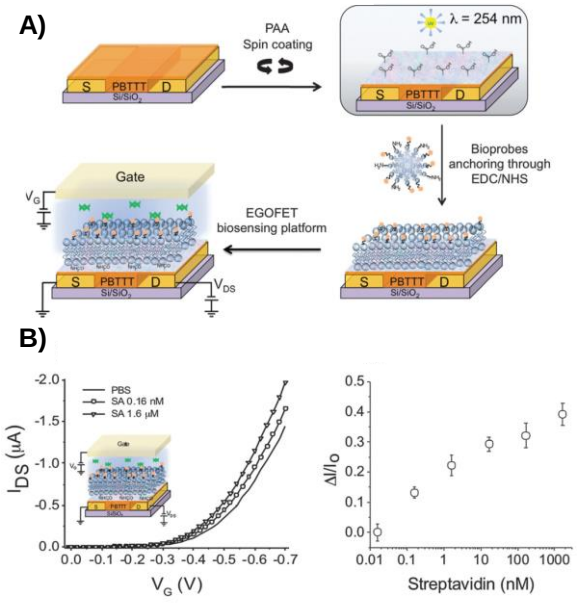

Figure 3-21. A) Schematic illustration of the fabrication process of an EGOFET biosensor: (a) after deposition of pBTTT on the substrate; (b) poly(acrylic acid) coating spin-coated and cross-linked; (c) biotinylated phospholipids anchored on the PAA coating; and (d) EGOFET configuration comprising a gold gate electrode and a droplet of PBS as dielectric. B) (left) I_{DS}–V_G transfer curves in PBS, pH 7.4 (line), and streptavidin solutions at concentrations of 0.16 nM (circles) and 1.6 μM (triangles) in PBS; and (right) relative response of the EGOFET as a function of the streptavidin concentration.[94]

Finally, F. Buth et. al [95] reported a sensor based on solution-gated organic field-effect transistors (SGFETs) which was modified with different surface groups in order to detect pH changes in the electrolyte. To this end, they used the OSC called α -sexithiophene (α6T) and attached onto it with the enzyme penicillinase. The working principle of this sensor is based on the hydrolysis of the amide bond of the β-lactam ring of penicillin (PEN). During this reaction a proton is generated, locally changing the pH of the electrolyte, which in turn is detected by the transistor. Since, however, the pH sensitivity of bare α 6T is rather low, an additional surface treatment is necessary in order to increase the sensitivity towards the pH of the electrolyte. They showed that, after a controlled oxidation of the surface, and with (3-aminopropyl)triethox-ysilane (APTES), which also serves as an anchoring site for the subsequent immobilization of enzymes, the resulting sensors achieve better sensitivity penicillin in the µM range. Figure 3-22A shows the scheme of the SGFET and the modification of the surface wettability thanks to the surface treatments through an angle contact study. Figure 3-22B shows the characteristics of the transistor: upon exposure to the oxidizing environment, APTES- treatment. Figure 3-22C depicts the response of untreated α6T and PEN-modified devices to the subsequent addition of varying amounts of penicillin. As can be clearly seen, only the PEN-modified device shows a clear response to the addition of penicillin, with a sensitivity limit of around 5 µM. A stable current level is reached several seconds after the addition of penicillin. The bare device only shows a small response at higher penicillin concentration, which is due to the pH change in the bulk solution.

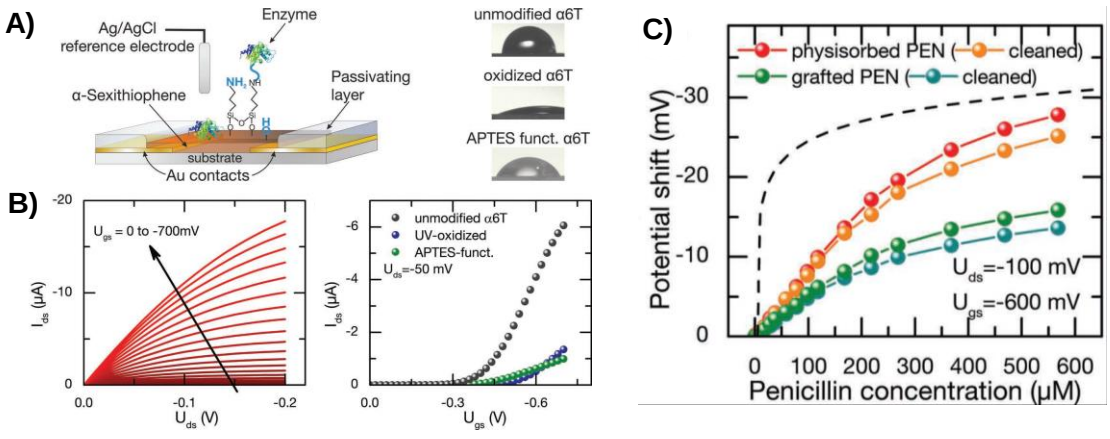

Figure 3-22 A) Schematic drawing of the transistor layout, including the different functionalization steps investigated in this work; and static water contact angle measurements of differently treated α -sexithiophene thin films. B) Typical output characteristic of a transistor with a width-to-length ratio of 4900 recorded, and transfer curves of untreated, oxidized (5 min UV illumination) and APTES-functionalized transistors, measured. C) Plot of the calculated threshold voltage shift due to a change in penicillin concentration of the electrolyte.[95]

3.5 | REFERENCES

[1] White NM, Turner JD. Thick-film sensors: past, present and future. *Meas Sci Technol* 1997; 8: 1–20.

[2] Middelhoek S, Bellekom AA, Dauderstadt U, et al. Silicon sensors. *Meas Sci Technol* 1995; 6: 1641.

[3] Khan S, Lorenzelli L, Dahiya RS. Technologies for Printing Sensors and Electronics Over Large Flexible Substrates: A Review. *IEEE Sens J* 2015; 15: 3164–3185.

[4] Roadmap - my_OEA, http://www.oe-a.org/roadmap (accessed 27 August 2018).

[5] Printed and Flexible Sensors 2017-2027: Technologies, Players, Forecasts. *IDTechEx*, https://www.idtechex.com/research/reports/printed-and-flexible-sensors-2017-2027-technologies-players-forecasts-000504.asp (2016, accessed 28 August 2018).

[6] Göpel W, Heiduschka P. Introduction to bioelectronics: 'interfacing biology with electronics'. *Biosens Bioelectron* 1994; 9: iii–xiii.

[7] Liao C, Zhang M, Yao MY, et al. Flexible Organic Electronics in Biology: Materials and Devices. *Adv Mater Deerfield Beach Fla* 2015; 27: 7493–7527.

[8] Benson DE. Bioelectronics: From Theory to Applications Edited by Itamar Willner and Eugenii Katz (The Hebrew University of Jerusalem). Wiley-VCH Verlag GmbH & Co. KGaA: Weinheim, Germany. 2005. xviii + 476 pp. $255.00. ISBN 3-527-30690-0. *J Am Chem Soc* 2005; 127: 12148–12148.

[9] Iannotta S, D'Angelo P, Romeo A, et al. Scalable and Flexible Bioelectronics and Its Applicationsto Medicine. In: *Large Area and Flexible Electronics*. Wiley-Blackwell, pp. 485–540.

[10] Owens RM, Malliaras GG. Organic Electronics at the Interface with Biology. *MRS Bull* 2010; 35: 449–456.

[11] IUPAC Gold Book, https://goldbook.iupac.org/ (accessed 1 August 2018).

[12] J K, F A. Biosensors in Applications. *J Biosens Bioelectron* 2016; 7: 1–2.

[13] Colomer-Farrarons J, Miribel-Català PL, Rodríguez-Villarreal AI, et al. Portable Bio-Devices: Design of Electrochemical Instruments from Miniaturized to Implantable Devices. *New Perspect Biosens Technol Appl*; 29.

[14] Peixoto AC, Silva AF. 11 - Smart devices: Micro- and nanosensors. In: Rodrigues L, Mota M (eds) *Bioinspired Materials for Medical Applications*. Woodhead Publishing, pp. 297–329.

[15] Chou J. *Hazardous Gas Monitors: A Practical Guide to Selection, Operation and Applications*. McGraw-Hill, 2000.

[16] Fraden J. Physical Principles of Sensing. In: Fraden J (ed) *Handbook of Modern Sensors: Physics, Designs, and Applications*. New York, NY: Springer New York, pp. 53–145.

[17] Guenther M, Gerlach G, Wallmersperger T, et al. Smart Hydrogel-Based Biochemical Microsensor Array for Medical Diagnostics. *Adv Sci Technol* 2012; 85: 47–52.

[18] Patel SV, Mlsna TE, Fruhberger B, et al. Chemicapacitive microsensors for volatile organic compound detection. *Sens Actuators B Chem* 2003; 96: 541–553.

[19] Lazarus N, Fedder GK. Integrated vertical parallel-plate capacitive humidity sensor. *J Micromechanics Microengineering* 2011; 21: 065028.

[20] Salvador J-P, Adrian J, Galve R, et al. Chapter 2.8 Application of bioassays/biosensors for the analysis of pharmaceuticals in environmental samples. In: Petrović M, Barceló D (eds) *Comprehensive Analytical Chemistry*. Elsevier, pp. 279–334.

[21] Organic Nonvolatile Memory Transistors for Flexible Sensor Arrays | Science, http://science.sciencemag.org/content/326/5959/1516 (accessed 1 August 2018).

[22] π-Conjugated Polymers for Organic Electronics and Photovoltaic Cell Applications - Chemistry of Materials (ACS Publications), https://pubs.acs.org/doi/abs/10.1021/cm102419z (accessed 1 August 2018).

[23] Gentili D, Sonar P, Liscio F, et al. Logic-Gate Devices Based on Printed Polymer Semiconducting Nanostripes. *Nano Lett* 2013; 13: 3643–3647.

[24] Sokolov AN, Roberts ME, Bao Z. Fabrication of low-cost electronic biosensors. *Mater Today* 2009; 12: 12–20.

[25] Molino PJ, Wallace GG. Next generation bioelectronics: Advances in fabrication coupled with clever chemistries enable the effective integration of biomaterials and organic conductors. *APL Mater* 2015; 3: 014913.

[26] Hammock ML, Chortos A, Tee BC-K, et al. 25th anniversary article: The evolution of electronic skin (e-skin): a brief history, design considerations, and recent progress. *Adv Mater Deerfield Beach Fla* 2013; 25: 5997–6038.

[27] Sensors | Free Full-Text | Wearable Electronics and Smart Textiles: A Critical Review, http://www.mdpi.com/1424-8220/14/7/11957 (accessed 1 August 2018).

[28] The rise of plastic bioelectronics | Nature, https://www.nature.com/articles/nature21004 (accessed 1 August 2018).

[29] Voss D. Cheap and cheerful circuits. *Nature*. Epub ahead of print 28 September 2000. DOI: 10.1038/35035212.

[30] Berggren M, Nilsson D, Robinson ND. Organic materials for printed electronics. *Nature Materials*. Epub ahead of print 1 January 2007. DOI: 10.1038/nmat1817.

[31] Lee J, Sung WJ, Joo CW, et al. Simplified Bilayer White Phosphorescent Organic Light-Emitting Diodes. *ETRI J* 2016; 38: 260–264.

[32] Organic TFT array on a paper substrate - IEEE Journals & Magazine, https://ieeexplore.ieee.org/document/1336977/ (accessed 3 August 2018).

[33] Forrest SR. The path to ubiquitous and low-cost organic electronic appliances on plastic. *Nature* 2004; 428: 911–918.

[34] Myny K, Rockelé M, Chasin A, et al. Bidirectional communication in an HF hybrid organic/solution-processed metal-oxide RFID tag. *IEEE Trans Electron Devices* 2014; 61: 2387–2393.

[35] Shakiba M, Zavvari A, Aleebrahim N, et al. Evaluating the Academic Trend of RFID Technology Based on SCI and SSCI Publications from 2001 to 2014. *Scientometrics* 2016; 109: 591–614.

[36] Fiore V, Battiato P, Abdinia S, et al. An integrated 13.56-MHz RFID tag in a printed organic complementary TFT technology on flexible substrate. *IEEE Trans Circuits Syst Regul Pap* 2015; 62: 1668–1677.

[37] Kang C, Shin H, Lee C. High-frequency organic rectifiers through interface engineering. *MRS Commun* 2017; 7: 755–769.

[38] Im D, Moon H, Shin M, et al. Towards Gigahertz Operation: Ultrafast Low Turn-on Organic Diodes and Rectifiers Based on C60 and Tungsten Oxide. *Adv Mater* 2011; 23: 644–648.

[39] Ma L, Ouyang J, Yang Y. High-speed and high-current density C60 diodes. *Appl Phys Lett* 2004; 84: 4786–4788.

[40] Lilja KE, Majumdar HS, Pettersson FS, et al. Enhanced Performance of Printed Organic Diodes Using a Thin Interfacial Barrier Layer. *ACS Appl Mater Interfaces* 2011; 3: 7–10.

[41] (12) Effect of Electrode Area on High Speed Characteristics over 1 MHz of Poly(3-hexylthiophene-2,5-diyl) Diode with Inkjet-Printed Ag Electrode, https://www.researchgate.net/publication/233159865_Effect_of_Electrode_Area_on_High_Speed_Characteristics_over_1_MHz_of_Poly3-hexylthiophene-25-diyl_Diode_with_Inkjet-Printed_Ag_Electrode (accessed 3 August 2018).

[42] (12) Gravure printed organic rectifying diodes operating at high frequencies. *ResearchGate*, https://www.researchgate.net/publication/223316784_Gravure_printed_organic_rectifying_diodes_operating_at_high_frequencies (accessed 3 August 2018).

[43] (12) Frequency analysis on poly(3-hexylthiopene) rectifier using impedance spectroscopy. *ResearchGate*, https://www.researchgate.net/publication/248318410_Frequency_analysis_on_poly3-hexylthiopene_rectifier_using_impedance_spectroscopy (accessed 3 August 2018).

[44] Kim KD, Koo JB, Lee JK, et al. Variations in the electric characteristics of an organic Schottky diode with the P3HT thickness. *J Korean Phys Soc* 2010; 57: 124–127.

[45] Heljo P, Lilja KE, Majumdar HS, et al. High rectifier output voltages with printed organic charge pump circuit. *Org Electron* 2014; 15: 306–310.

[46] Heljo PS, Schmidt C, Klengel R, et al. Electrical and thermal analysis of frequency dependent filamentary switching in printed rectifying diodes. *Org Electron* 2015; 20: 69–75.

[47] Diao L, Daniel Frisbie C, Schroepfer DD, et al. Electrical characterization of metal/pentacene contacts. *J Appl Phys* 2007; 101: 014510.

[48] Conjugated organic molecules on metal versus polymer electrodes: Demonstration of a key energy level alignment mechanism: Applied Physics Letters: Vol 82, No 1, https://aip.scitation.org/doi/10.1063/1.1532102 (accessed 3 August 2018).

[49] Kang C, Wade J, Yun S, et al. 1 GHz Pentacene Diode Rectifiers Enabled by Controlled Film Deposition on SAM-Treated Au Anodes. *Adv Electron Mater* 2016; 2: 1500282.

[50] Steudel S, Myny K, Arkhipov V, et al. 50 MHz rectifier based on an organic diode. *Nat Mater* 2005; 4: 597–600.

[51] Chan MY, Lai SL, Fung MK, et al. Efficient CsF/Yb/Ag cathodes for organic light-emitting devices. *Appl Phys Lett* 2003; 82: 1784–1786.

[52] Campbell null, Rubin null, Zawodzinski null, et al. Controlling Schottky energy barriers in organic electronic devices using self-assembled monolayers. *Phys Rev B Condens Matter* 1996; 54: R14321–R14324.

[53] Kwon J, Seol YG, Lee N-E, et al. Study on Ohmic contact improvement of organic Schottky diode utilizing self-assembled monolayer and PEDOT:PSS layers. *J Vac Sci Technol A* 2010; 28: 879–885.

[54] High-frequency polymer diode rectifiers for flexible wireless power-transmission sheets | Articleinformation | J-GLOBAL, http://jglobal.jst.go.jp/en/public/20090422/201102293595463227 (accessed 3 August 2018).

[55] Koch N, Elschner A, Schwartz J, et al. Organic molecular films on gold versus conducting polymer: Influence of injection barrier height and morphology on current–voltage characteristics. *Appl Phys Lett* 2003; 82: 2281–2283.

[56] Kido J, Matsumoto T. Bright organic electroluminescent devices having a metal-doped electron-injecting layer. *Appl Phys Lett* 1998; 73: 2866–2868.

[57] Zhou X, Pfeiffer M, Blochwitz J, et al. Very-low-operating-voltage organic light-emitting diodes using a p-doped amorphous hole injection layer. *Appl Phys Lett* 2001; 78: 410–412.

[58] Chen S-F, Wang C-W. Influence of the hole injection layer on the luminescent performanceof organic light-emitting diodes. *Appl Phys Lett* 2004; 85: 765–767.

[59] Tokito S, Noda K, Taga Y. Metal oxides as a hole-injecting layer for an organic electroluminescent device. *J Phys Appl Phys* 1996; 29: 2750–2753.

[60] Matsuhisa N, Sakamoto H, Yokota T, et al. A Mechanically Durable and Flexible Organic Rectifying Diode with a Polyethylenimine Ethoxylated Cathode. *Adv Electron Mater* 2016; 2: 1600259.

[61] Ishii H, Sugiyama K, Ito E, et al. Energy Level Alignment and Interfacial Electronic Structures at Organic/Metal and Organic/Organic Interfaces. *Adv Mater* 1999; 11: 605–625.

[62] Kang C-M, Cho H, Park M, et al. Effects of insertion of hole injection layers on pentacene rectifying diodes. *J Nanosci Nanotechnol* 2014; 14: 5301–5303.

[63] Kleemann H, Schumann S, Jörges U, et al. Organic pin-diodes approaching ultra-high-frequencies. *Org Electron* 2012; 13: 1114–1120.

[64] Kleemann H, Gutierrez R, Avdoshenko S, et al. Reverse breakdown behavior in organic pin-diodes comprising C60 and pentacene: Experiment and theory. *Org Electron* 2013; 14: 193–199.

[65] Yu HY, Feng XD, Grozea D, et al. Surface electronic structure of plasma-treated indium tin oxides. *Appl Phys Lett* 2001; 78: 2595–2597.

[66] Wang H, Ji Z, Shang L, et al. Interface Effect on the Performance of Rectifier Based on Organic Diode. *IEEE Electron Device Lett* 2010; 31: 506–508.

[67] Jia Z, Lee VW, Kymissis I, et al. In situ study of pentacene interaction with archetypal hybrid contacts: Fluorinated versus alkane thiols on gold. *Phys Rev B* 2010; 82: 125457.

[68] Zhou Y, Fuentes-Hernandez C, Shim J, et al. A Universal Method to Produce Low–Work Function Electrodes for Organic Electronics. *Science* 2012; 336: 327–332.

[69] Enhanced Performance of Printed Organic Diodes Using a Thin Interfacial Barrier Layer - ACS Applied Materials & Interfaces (ACS Publications), https://pubs.acs.org/doi/10.1021/am1009869 (accessed 3 August 2018).

[70] Kim H-Y, Lee K, McEvoy N, et al. Chemically Modulated Graphene Diodes. *Nano Lett* 2013; 13: 2182–2188.

[71] Uddin MA, Singh AK, Sudarshan TS, et al. Functionalized graphene/silicon chemi-diode H_2 sensor with tunable sensitivity. *Nanotechnology* 2014; 25: 125501.

[72] Dai M-Z, Lin Y-L, Lin H-C, et al. Highly Sensitive Ammonia Sensor with Organic Vertical Nanojunctions for Noninvasive Detection of Hepatic Injury. *Anal Chem* 2013; 85: 3110–3117.

[73] Chuang M-Y, Chen J-N, Zan H-W, et al. Modulated gas sensor based on vertical organic diode with blended channel for ppb-regime detection. *Sens Actuators B Chem* 2016; 230: 223–230.

[74] Hossein-Babaei F, Shabani P. A gold/organic semiconductor diode for ppm-level humidity sensing. *Sens Actuators B Chem* 2014; 205: 143–150.

[75] Jalil AR, Chang H, Bandari VK, et al. Fully Integrated Organic Nanocrystal Diode as High Performance Room Temperature NO2 Sensor. *Adv Mater* 2016; 28: 2971–2977.

[76] Chowdhury A, Biswas B, Bera RN, et al. Nanostructured organic–inorganic heterojunction diodes as gas sensors. *RSC Adv* 2012; 2: 10968–10976.

[77] Organic thin-film transistors - Chemical Society Reviews (RSC Publishing), https://pubs.rsc.org/en/content/articlelanding/2010/cs/b909902f#!divAbstract (accessed 1 August 2018).

[78] Kergoat L, Piro B, Berggren M, et al. Advances in organic transistor-based biosensors: from organic electrochemical transistors to electrolyte-gated organic field-effect transistors. *Anal Bioanal Chem* 2012; 402: 1813–1826.

[79] Elkington D, Cooling N, Belcher W, et al. Organic Thin-Film Transistor (OTFT)-Based Sensors. *Electronics* 2014; 3: 234–254.

[80] Schöning MJ, Poghossian A. Recent advances in biologically sensitive field-effect transistors (BioFETs). *Analyst* 2002; 127: 1137–1151.

[81] Electronics | Free Full-Text | Electrolytic Gated Organic Field-Effect Transistors for Application in Biosensors—A Review, http://www.mdpi.com/2079-9292/5/1/9 (accessed 1 August 2018).

[82] Panzer MJ, Frisbie CD. Exploiting Ionic Coupling in Electronic Devices: Electrolyte-Gated Organic Field-Effect Transistors. *Adv Mater* 2008; 20: 3177–3180.

[83] Ritjareonwattu S, Yun Y, Pearson C, et al. An Ion Sensitive Organic Field-Effect Transistor Incorporating the Ionophore Valinomycin. *IEEE Sens J* 2012; 12: 1181–1186.

[84] The organic electrochemical transistor for biological applications - Strakosas - 2015 - Journal of Applied Polymer Science - Wiley Online Library, https://onlinelibrary.wiley.com/doi/10.1002/app.41735 (accessed 1 August 2018).

[85] White HS, Kittlesen GP, Wrighton MS. Chemical derivatization of an array of three gold microelectrodes with polypyrrole: fabrication of a molecule-based transistor. *J Am Chem Soc* 1984; 106: 5375–5377.

[86] Chao S, Wrighton MS. Solid-state microelectrochemistry: electrical characteristics of a solid-state microelectrochemical transistor based on poly(3-methylthiophene). *J Am Chem Soc* 1987; 109: 2197–2199.

[87] Kirchan AE, Kim K, Steward MK, et al. A PEDOT:PSS-based organic electrochemical transistor with a novel double-in-plane gate electrode for pH sensing application. In: *2017 19th International Conference on Solid-State Sensors, Actuators and Microsystems (TRANSDUCERS)*. 2017, pp. 214–217.

[88] Rivnay J, Inal S, Salleo A, et al. Organic electrochemical transistors. *Nat Rev Mater* 2018; 3: 17086.

[89] Label-free brain injury biomarker detection based on highly sensitive large area organic thin film transistor with hybrid coupling layer - Chemical Science (RSC Publishing), https://pubs.rsc.org/en/content/articlelanding/2014/sc/c3sc52638k#!divAbstract (accessed 1 August 2018).

[90] Choi J, Jeon HG, Kwon OE, et al. Improved output characteristics of organic thin film transistors by using an insulator/protein overlayer and their applications. *J Mater Chem C* 2015; 3: 2603–2613.

[91] Kergoat L, Herlogsson L, Braga D, et al. A water-gate organic field-effect transistor. *Adv Mater Deerfield Beach Fla* 2010; 22: 2565–2569.

[92] Kergoat L, Piro B, Berggren M, et al. DNA detection with a water-gated organic field-effect transistor. *Org Electron* 2012; 13: 1–6.

[93] Magliulo M, Pistillo BR, Mulla MY, et al. PE-CVD of Hydrophilic-COOH Functionalized Coatings on Electrolyte Gated Field-Effect Transistor Electronic Layers. *Plasma Process Polym* 2013; 10: 102–109.

[94] Y. Mulla M, Seshadri P, Torsi L, et al. UV crosslinked poly(acrylic acid): a simple method to bio-functionalize electrolyte-gated OFET biosensors. *J Mater Chem B* 2015; 3: 5049–5057.

[95] Buth F, Donner A, Sachsenhauser M, et al. Biofunctional Electrolyte-Gated Organic Field-Effect Transistors. *Adv Mater* 2012; 24: 4511–4517.

4

Inkjet-printed MIS diode-based sensors

In this chapter, the diode working principle is described. Moreover, it will be presented the results obtained in this thesis regarding the development of a polymeric MIS diode. Finally, the MIS diode is used to detect gases.

4.1 | DIODE WORKING PRINCIPLE

4.1.1 | Organic diode based on Schottky interface

The most reported diodes are based on Schottky contact. Figure 4-1 shows the energy diagram of a Schottky junction for an interface based on metal-*n-type* organic semiconductor (OSC) with no traps in the bandgap, i.e. free of interfacial states. When the metal is in contact with the OSC, the Fermi levels (E_F) align and thermodynamic equilibrium is established through the transfer of electrons from the OSC conduction band (E_C) into the metal, since E_C is higher than the energy fermi level of the metal (E_{FM}). These electrons"leave behind" a positively charged zone in the OSC producing a space-charge region corresponding to the zone depleted which is formed in the OSC near the interface with the metal. Charges, equal in magnitude to the depletion charge, appear in the metal at the Metal/Semiconductor (MS) interface.[1]

The existence of potential barrier at the MS contact is the result of the presence of a depletion region leading to a band curvature in the semiconductor equal to Equation 4-1.

$$qV_i = q(\Phi_m - \Phi_{SC}) \qquad \text{Equation 4-1}$$

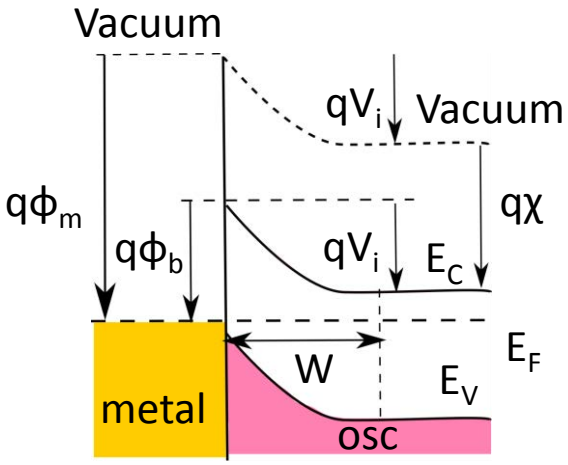

Figure 4-1. Energy band diagram of Schottky contact for n-type semiconductor.

where $q\Phi_m$ is the metal work function and $q\Phi_{SC}$ is the semiconductor work function. This curvature corresponds to a potential barrier V_i which prevents further electrons from migrating into the metal. Electrons in the metal, on the other hand, see a potential barrier, ϕ_b, having an amplitude equal to (Equation 4-2):

$$q\phi_b = q(\Phi_m - \chi) = qV_i + (E_C - E_F) \qquad \text{Equation 4-2}$$

where χ is the electron affinity of the semiconductor. At room temperature the potential barrier is significantly larger than $kT \cdot q^{-1}$ and only a few electrons possess sufficient energy to overcome them.

If forward bias, $V_a>0$, is applied to the diode structure (plus on the metal side, and minus on the OSC side) the potential barrier on the OSC side is decreased from V_i to V_i-V_a (Figure 4-2A). A considerable number of electrons can, therefore, flow from the OSC into the metal. On the other hand, the flow of electrons from the metal into the OSC, remains constant because the potential barrier seen from the metal side, ϕ_b is unchanged. If a reverse bias $V_a<0$ is applied to the structure (minus on the metal side, and plus on the OSC) the potential barrier in the OSC is increased from V_i to V_i+V_a (Figure 4-2B). As a result, the electron flow from the OSC into the metal is reduced while the current from the metal to the OSC remains unchanged leading to small reverse current of electrons.

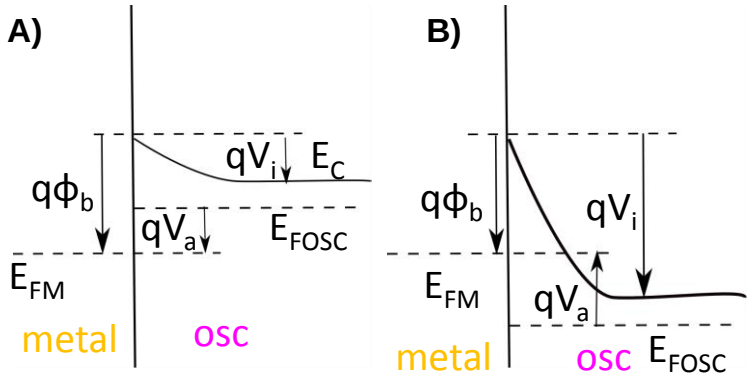

Figure 4-2 Energy band diagram under: A) reverse bias and B) forward bias for a n-type OSC.

4.1.2 | Non-rectifying Schottky interface: ohmic contact

A *priopri* a Schottky barrier is formed due to the contact between a metal and an OSC. However, when the impurity concentration in the OSC is high enough the potential barrier is negligible. The width of the depletion region in the OSC is given by Equation 4-3:

$$W(V_a) = \sqrt{\frac{2\varepsilon_{SC}(V_i - V_a)}{qN_a}} \qquad \text{Equation 4-3}$$

where V_i is the built-in potential barrier height, ε_{sc} is the OSC permittivity, N_a is the acceptor doping concentration and V_a is the applied bias. If the impurity donors concentration is high enough (e.g. $N_D=10^{20}$ cm^{-3}) and $V_a=0$, the thickness of the depletion zone is only 2.5 nm. Therefore, the electrons can easily tunnel such a small potential barrier, which yields to low resistance ohmic contact. An ohmic contact is a non-rectifying contact. The Current-Voltage (*C-V*) characteristics of the contact obeys the Ohm's law *V=I·R*.

Moreover, an ohmic contact can be also observed at MS interfaces when metals with high/low Work Function (WF) are in contact with *p-type*/*n-type* OSC, respectively.

4.1.3 | Influence of interface states

The equations presented previously describe the properties of the Schottky diode with and "ideal" MS interface, which means that the properties of the OSC are not affected by the presence of the metal. However, the intrinsic nature of OSC polymer is disrupted at the interface. This gives rise to a large number of permitted states in the bandgap of the OSC near the interface. These states are called "interface states" or "interface traps". They have energy values between E_V and E_C.

Firstly, it is considered the OSC before contact with the metal (Figure 4-3A). The electrons trapped at the OSC interface form a negative surface charge, which creates a depletion zone in the semiconductor with a magnitude: $q\phi_o= E_F-E_V$. When the metal is contact with the OSC, the alignment of the E_F is achieved by a transfer of electrons from the OSC to the metal, resulting the formation of a depletion zone and a downward curvature of the OSC energy (Figure 4-3B). If it is considered an interface with a large state density, it will lose trapped electrons, and as a consequence the alignment of the E_F will be accomplished by the transfer of electrons from the traps into the metal, instead of from the OSC into the metal. The band curvature variation resulting from the alignment of E_F will form a potential barrier of:

$$q\phi_b = E_g - q\phi_o \qquad \text{Equation 4-4}$$

A large number of interfacial states could result in Fermi-level pinning, such that the energy barrier at the MS interface is pinned irrespective of WF of the metal. The Fermi-level pinning makes the energy barrier at MS interfaces unpredictable, and significantly affects the charge-transport properties of the organic devices. Therefore, proper modification of MS interface properties is inevitable to achieve high performance organic rectifiers.

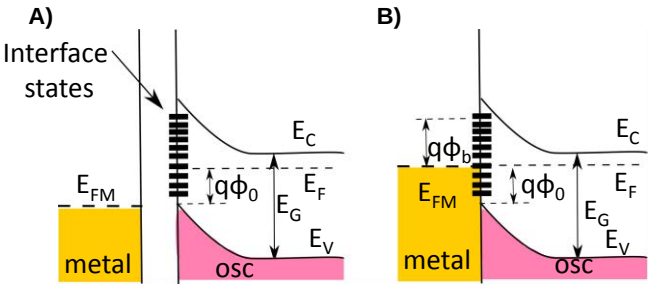

Figure 4-3 Energy bands in the presence of interface states for a n-type OSC: A) before contact with the metal and B) after contact. E_F shifts down relative to E_C at the interface and previously filled traps are emptied.

4.2 | ORGANIC DIODES BASED ON MIS STRUCTURES

The Metal-Insulator-Semiconductor (MIS) diode is the most useful device to study the insulator/OSC interfaces. Since the reliability, the electrical behavior, and the stability of all the OSCs are intimately related to their surface conditions, an understanding of surface physics through the MIS diode is of great importance.[2][3][4][5]

The Barrier Height (BH) is an important parameter that determines the electrical characteristics of MS contact. As explained before, the performance of Schottky contact configuration is drastically determined by the interface quality between the deposited metal and the OSC surface. It is well known that, unless specially fabricated, a Schottky BH (SBH) diode possesses thin interfacial native oxide layer between the metal and the OSC. The existence of such insulating layer converts the MS device into MIS devices and has strong influence on its C-V characteristics.[3],[6]

4.2.1 | Ideal MIS diode

The MIS structure is shown in Figure 4-4 where *d* is the thickness of the insulator and *V* is the applied voltage on the top metal plate. This defines that the voltage, *V*, is positive when the top electrode is positively biased with respect to the bottom electrode, and *V* is negative when the top electrode is negatively biased with respect to the bottom electrode. This convention will be used throughout this chapter.

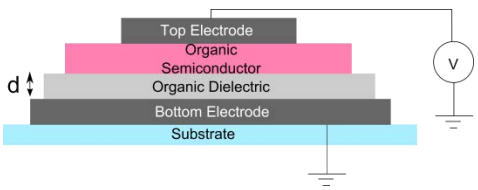

Figure 4-4 Scheme of Metal-Insulator-Semiconductor diode device. The "d" represents the thickness of the organic dielectric.

The energy band diagram of an ideal MIS structure for *V*= 0 is shown in Figure 4-5. An ideal MIS diode is defined as follows: at zero applied bias there is no energy difference between the metal WF and the OSC WF.

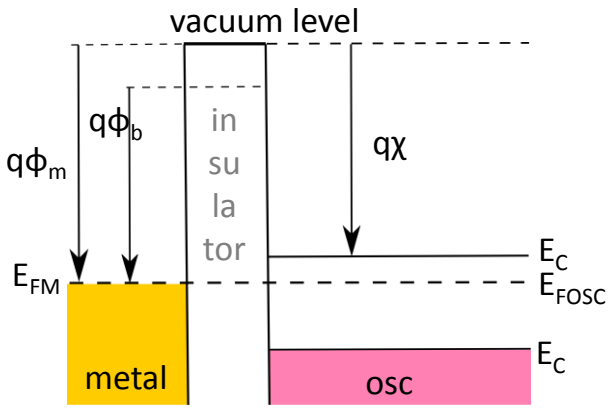

Figure 4-5 Energy band diagrams for ideal MIS structures at V=0 for a n-type OSC.

Electrons overcome the potential barrier between the metal and the OSC through a quantum-mechanical process called Thermionic Emission (TE). This process is activated by the thermal energy of the electrons. Although the potential is clearly larger than $kT \cdot q^{-1}$, at room temperature there exists a non-zero probability that some electrons gather enough energy to overcome the barrier. When a forward bias V_a is applied to the diode, the potential barrier that the electrons need to overcome to flow from the semiconductor into the metal is equal to ϕ_b-V_a. Thus, the application of a bias lowers the potential barrier on the metal side. The origin of this fact is a consequence of electrostatics, an extra charge is attracted by the metal adding an extra field that reduces the potential of the barrier. The TE current that describes the Schottky diode is given by Equation 4-5:

$$I = AA^{*}T^{2}exp\left[\frac{q\phi_b}{kT}\right]\left[\left(\frac{qV_a}{kT}\right) - 1\right] \qquad \text{Equation 4-5}$$

where I_0 is the reverse saturation current, n is the ideal factor, T is the temperature, k is Boltzmann's constant, q is the electron charge, A is the electrode area, Φ_B is the BH and A^{**} is the effective Richardson constant.

4.3 | DEVELOPMENT OF A POLYMERIC MIS DIODE

Organic devices such as capacitors, resistors, thin film transistors and Schottky diodes have been widely studied and optimized in terms of fabrication processes.[7],[8] The development of solution-based electronic components offers the possibility to manufacture flexible and light-weight electronics using cost-effective processes.[9] In recent years, inkjet printing has been receiving growing interest as a method of depositing functional materials, as opposed to more conventional processes. This technique is a versatile approach for the deposition of small amounts of polymer solutions, small molecule dispersions, or nanoparticle suspensions that have specific electrical, optical, chemical, and biological properties onto well-defined locations of various surfaces and substrates.[10],[11] Moreover, inkjet printing is well suited for research, being a mask-less technology oriented to rapid prototyping for production.[12]

Although inkjet printing has been widely used for the fabrication of thin and flexible organic devices,[13] so far, a simple diode still remains a challenge for this technology. One of the most important issues is the requirement to print two different metal electrodes with appropriate WFs to form SBH at the MS interface. The Schottky diode structure requires that one of the electrodes is, for example, Cu or Al. Although copper-based inks are available,[8] these materials need the application of aggressive post-treatments such as intense pulsed light sintering and high curing temperatures, among others,[14],[15] making them incompatible with OSCs and polymeric substrates. Evaporation and sputtering are still the most common fabrication techniques for the patterning of metal electrodes in organic diodes.[16][17][18][19][20] Partially printed organic rectifying diodes are seldom reported.[21] Lilja *et al.* reported a diode with a thin copper oxide-organic material interfacial layer.[22] In this copper-based Schottky diode, one of the electrodes was not inkjet-printed but patterned with gravure technology. Apart from a previous work recently presented in collaboration with the Chemnitz University of Technology,[23] there are no published reports on organic rectifying diodes fully processed by inkjet printing technology and based on silver as high WF metal, for both cathode and anode electrode contacts. Hereby, it is the first work showing that cost-effective processes such as inkjet printing can be used to fabricate rectifying diodes using a MIS structure and ohmic metal contacts.

MIS structures are also a strategy to fabricate rectifying devices. In MIS diodes the rectifying properties originate from the pinning of the Fermi level by interface states. Electronic states at the interface between the insulator and the semiconductor can play a two-fold role: i) they modify the electrostatic potential, which changes the band alignment controlling the carrier flow across the interface, and ii) they act as recombination centers that favor the current across the insulating layer. These features were studied back in the 70's for silicon-based devices by Green and Shewchun.[24] More recently in the organic electronics research area, oxide-based interfacial layers and compounds have been used to adjust energetic barriers to favor, for instance, carrier injection in Organic Light Emitting Diodes (OLEDs),[25] and to establish an ohmic

contact at MS interface in Organic Thin Film Transistors (OTFTs)[26][27][28] and photovoltaic devices.[29]

In this thesis, MIS rectifying diodes were fabricated depositing the insulator by two different methods. Since, it is known that the quality of the polymeric insulator surface depends strongly on its deposition technique, to evaluate the performances of the proposed inkjet-printed layer, the insulator was also deposited using conventional spin-coating method. The effect of the insulating layer processing method on the film morphology and the corresponding electrical properties were analyzed to obtain a very simple fabrication procedure for MIS organic diodes. The main goal of this work is to demonstrate the physical origin of the diode rectifying properties. This mechanism is strongly related to the insulator morphology and to the best of our knowledgement has not been addressed before. Although, the Rectification Ratio (RR) is still lower than state-of-the-art organic based rectifying diodes,[21] this work will potentially motivate the interest of research in polymeric-based diodes produced by ink-jet printing.

4.3.1 | MIS fabrication

MIS diodes were fabricated on 125µm thick Polyethylene-naphthalene (PEN) Teonex Q65FA substrates from Dupont Teijin specially developed for flexible electronics. The silver conductive ink used for the bottom silver(p) electrodes is a 20 wt(%) silver nanoparticle content (Sunchemical Suntronic EMD5603). The top silver(f) electrode is silver conductive paint from Electrolube. The OSC FS0027 is poly(triarylamine) PTAA and it is dissolved in Tetralin at 2wt% from Flexink. Finally, MMAcoMAA is used as insulator layer from MicroChem.

A Fujifilm Dimatix DMP2831 desktop printer was used as the printing setup. The printing was undertaken in a class 10.000 clean-room laboratory environment. The silver(p) nanoparticle ink was previously filtered with a 0.20µm PTFE membrane and deposited by inkjet on the PEN substrate using a Drop Spacing (DS) of 20 µm keeping the printer platen at 40ºC. The patterned layer was sintered at 130ºC for 30 min in a convection oven. The MMAcoMAA layers were deposited using DS 20µm and a platen temperature of 40ºC. After the printing, the layer was cured at 150 ºC for 90 seconds on a hot plate. For the MIS with 3 dielectric layers, MMAcoMAA was printed adopting wet on wet technique using the same curing process. Afterwards, the deposition of the OSC FS 0027 was carried out by drop casting method. Top silver contacts were deposited by drop casting method and dried in air.

The same procedure has been followed for the fabrication of the MIS structures with different dielectrics. A solution of poly(4-vinylphenol) (PVP) using poly(melamine-co-formaldehyde) methylated as crosslinking agent (CL) in propylene glycol methyl ether acetate (PGMEA) (the concentrations of PVP and CL were 90 mg/mL and 45 mg/mL) was inkjet-printed using a DS of 30 µm and keeping the

substrate at room temperature. Cross-linking was performed on a hot plate for 30 minutes at 150°C. The Epoxy ink is the Prielex SU-8 ink from MicroChem. This dielectric was patterned using a DS of 40 µm and keeping the platen temperature at 45 °C and the printhead temperature at 45 °C. The curing process involved a UV treatment for 30 seconds.

The HK-Epoxy insulator is a commercial ink from UTDots, Inc. This ink contains amorphous silica, epoxy resin, and epoxy hardener. It was printed using a DS of 25 µm and heating the platen at 45°C. The curing procedure was carried out on a hot plate at 150°C for 60 minutes.

All the electrical measurements were performed in ambient conditions and ambient light. The MIS structure characterizations were carried out using an Agilent B1500A Semiconductor Analyzer. Capacitive measurements were performed with an Agilent E4980A LCR meter. The images were acquired using a light microscope DM4000 from Leica. The layer thicknesses for the dielectric layers were evaluated using a mechanical surface Dektak profilometer. Atomic Force Microscopy images were carried out using the Nanoscope Veeco Dimension 3100.

4.3.2 | Electrical and morphological characterization of organic inkjet-printed MIS diodes

Recently, the number of conductive inks for inkjet printing has increased.[30] However, silver-based inks are still the gold standard for inkjet-printed conductive contacts due to their high conductivity, high adhesion, relatively low curing temperature, and high printing stability.[31][32][33][34] According to the literature, the work function of inkjet-printed silver electrodes is roughly Φ_M =5 eV due to the presence of oxidized silver on its surface.[35] Therefore, silver is expected to establish an ohmic contact with a typical p-type OSC. To confirm this, a symmetric silver junction with a well-known OSC, the poly(triarylamine) (PTAA) (Figure 4-6A) was fabricated. For all the presented devices, the bottom silver electrodes were inkjet-printed (silver(p)), while the top silver electrodes (silver (f)) were deposited by drop casting using a silver flake ink. The WFs of both the silver(p) and the silver(f) are around Φ_M= -5.2 eV evaluated by Kelvin Probe Force Microscopy (KPFM). Figure 4-6A shows the chemical structure of PTAA and Figure 4-6B shows the current-voltage (C-V) characteristic of the silver/PTAA/silver symmetric junction. The C-V characteristic is perfectly linear up to |30V| confirming the absence of an energetic barrier at the MS interface in agreement with previous studies.[22]

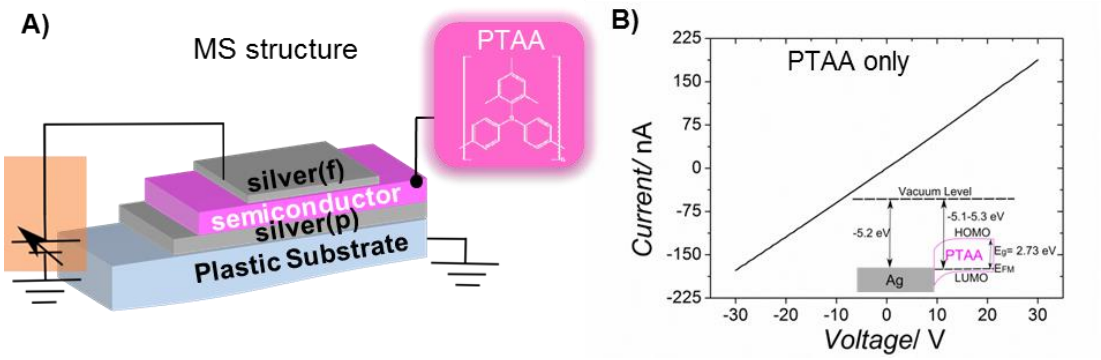

Figure 4-6 A) Schematic illustration of fabricated MS device and the molecular structure of PTAA, B) Current-voltage characteristic of the MS structure. The inset shows the band diagram at the silver electrode interface with the OSC.

In devices referred as MIS(sp) the insulator was deposited by spin coating and in devices referred as MIS(*n*p) the insulator was inkjet-printed. The *n* value indicates the number of inkjet-printed layers. Figure 4-7A depicts the structure and materials employed in the flexible MIS diode structure. In particular, the PTAA semiconductor is deposited onto poly(methylmethacrylate/methacrylic) acid layer referred to here as MMAcoMAA. An optical image of the diode fabricated on a PEN substrate is shown in Figure 4-7B. MIS(sp) structures present a spin coated insulator layer while, MIS(1p) and MIS(3p) were fabricated by inkjet printing one and three MMAcoMAA layers, respectively (see MIS fabrication section).

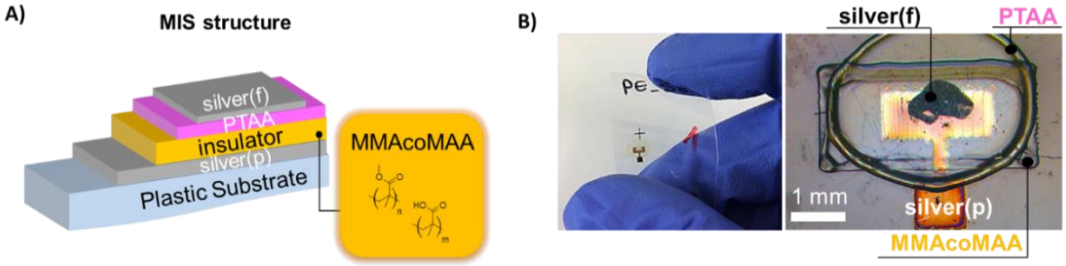

Figure 4-7 Device structure and materials. A) Schematic illustration of the MIS structure and the molecular structure of MMAcoMAA. B) Optical images of a fabricated MIS device.

As already introduced in the section 4.2.1, TE current is one of the most observed conduction mechanism in insulating films. This conduction process is characterized by a linear relationship between the logarithm of current and the square root of the applied electric field.[36]

Through *C-V* characteristics it is possible to determine the eventual presence of a BH using the TE model that can be described by Equation 4-5. Since the Fermi level is not determined by the WF of the metal but rather by the charge present at the insulator

interface, BH is sensitive to the external field producing an image-force barrier that lowers the energy level of the contact. This effect is significant in un-doped polymers or lightly doped OSCs. Therefore, the current used to extract the BH is the one at flat band voltage (V_{FB}) condition.

In order to use the *C-V* response to accurately obtain the BH, it is necessary to know the *A*** parameter. The most compelling reason for an accurate experimental determination of *A*** is that, in practice, the extracted *A*** may vary from the theoretical value.[37] Reliable values of the *A*** can be calculated by employing the modified Richardson plot from the temperature dependence of the *C-V* characteristics, according to Equation 4-6:

$$\ln\left(\frac{I_0}{T^2}\right) = \ln(AA^{**}) - \frac{q\Phi_B}{kT} \qquad \text{Equation 4-6}$$

The fit to the modified Richardson plot should be a straight line, from which the slope and y-axis intercept are the BH and the *A***, respectively. Temperature dependent measurements were carried out for MIS(sp), MIS(1p), and MIS(3p) from 243.15 to 343.15K (Figure 4-8).

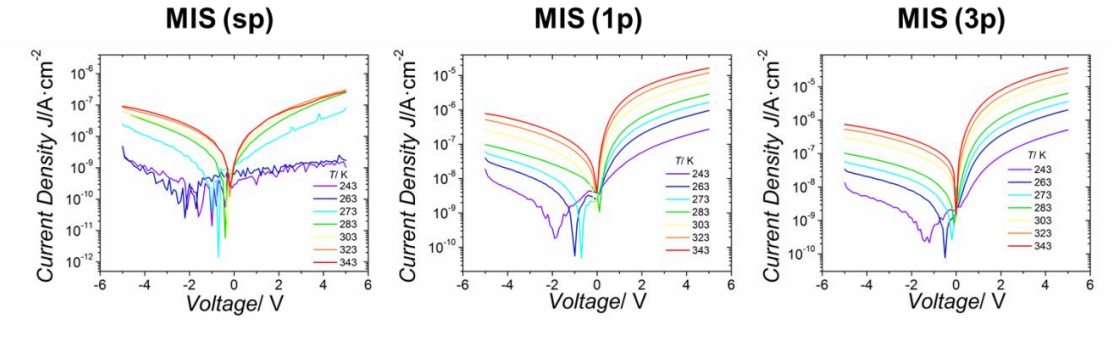

Figure 4-8. Semi-logarithmic plot of the J-V characteristics for spin-coated (MIS(sp)), one (MIS(1p)) and three inkjet-printed layers (MIS(3p)) at different temperatures.

From this plot, the measured *A*** for MIS(sp), MIS(1p) and MIS(3p) are $1.5 \cdot 10^{-5}$ $A \cdot cm^{-2} \cdot K^{-2}$, 0.3 $A \cdot cm^{-2} \cdot K^{-2}$ and 2.7 $A \cdot cm^{-2} \cdot K^{-2}$, respectively as shown in Figure 4-9A. The BH increases of MIS(sp), MIS(1p) and MIS (3p) are determined to be 0.97 eV, 0.36 eV and 0.38eV, respectively as shown in Figure 4-9B and Figure 4-9C.

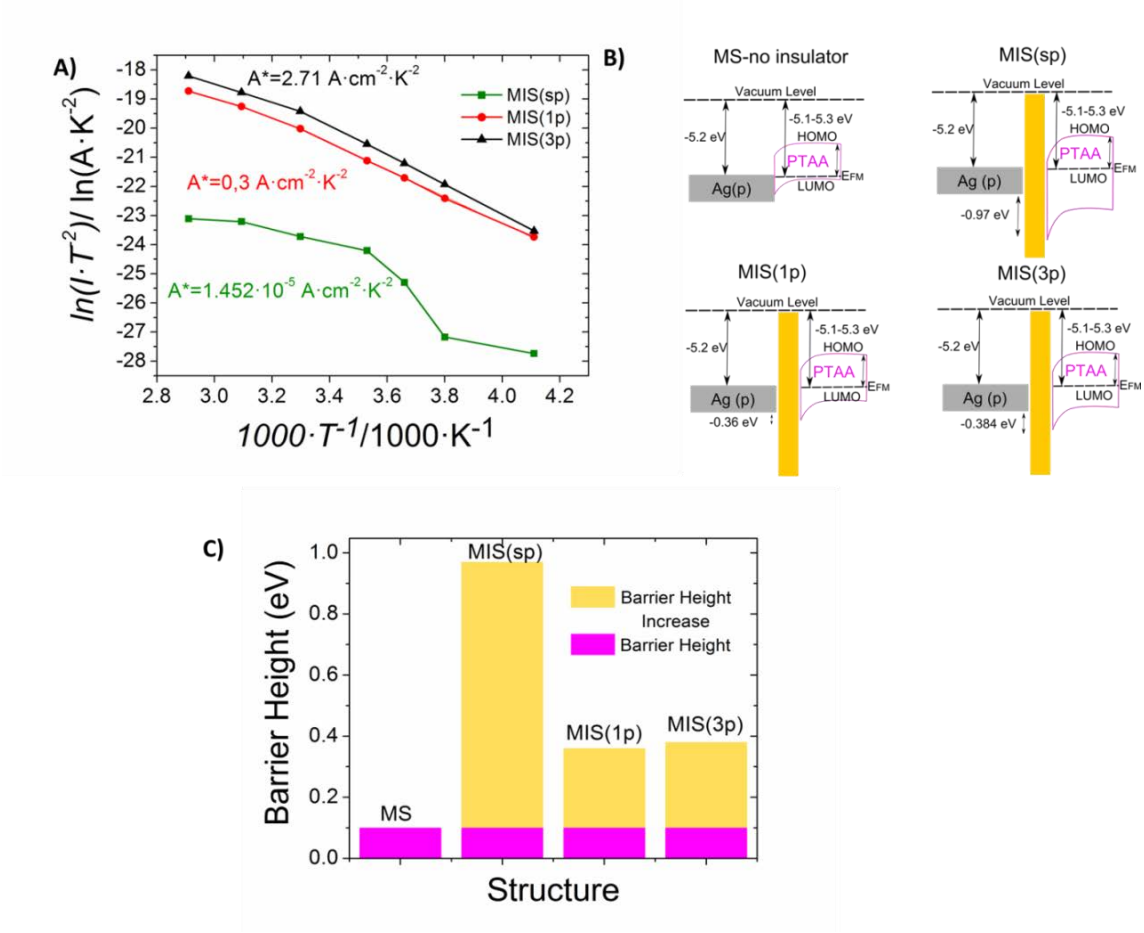

Figure 4-9.A) Richardson plots of $\ln(I \cdot T^{-2})$ versus $1000 \cdot T^{-1}$ for MIS (sp), MIS (1p) and MIS (3p) with its corresponding Richardson constant extracted, B) Schematics of energy band diagram showing the barrier formation for MIS(sp), MIS(1p and MIS(3p) and C) Barrier height increase for each type of MIS diodes compared to MS structure.

Once the presence of a BH is confirmed, the influence of the inserted insulator-semiconductor interface was also evaluated through capacitance-voltage (*C-V*) and *loss-V* measurements. Here $loss = 1 \cdot (\omega R)^{-1}$ where ω is the angular frequency and *R* is the resistance. Being the inverse of the resistance at a particular test frequency, the *loss* parameter can then be interpreted as an AC conductance. The highest BH (MIS(sp)) diode was studied first (Figure 4-10 top). *C-V* and *loss-V* characteristics measured at 1 kHz are shown in Figure 4-10A. Both curves exhibit the two characteristic regimes of accumulation and depletion typical of a functional MIS variable capacitor. The *loss* under accumulation and depletion regimes was $0.5 \cdot 10^{-9}$ F·cm^{-2} and $0.05 \cdot 10^{-9}$ F·cm^{-2}, respectively. These low *loss* values indicate good MMAcoMAA insulating properties. Figure 4-10B shows the corresponding *J-V* characteristic of MIS(sp) diode. The MIS diode has a higher leakage current when driven into accumulation regime (positive voltage on the top silver(f) contact). The *J-V* characteristic exhibits slight rectifying behavior (Figure 4-10B).

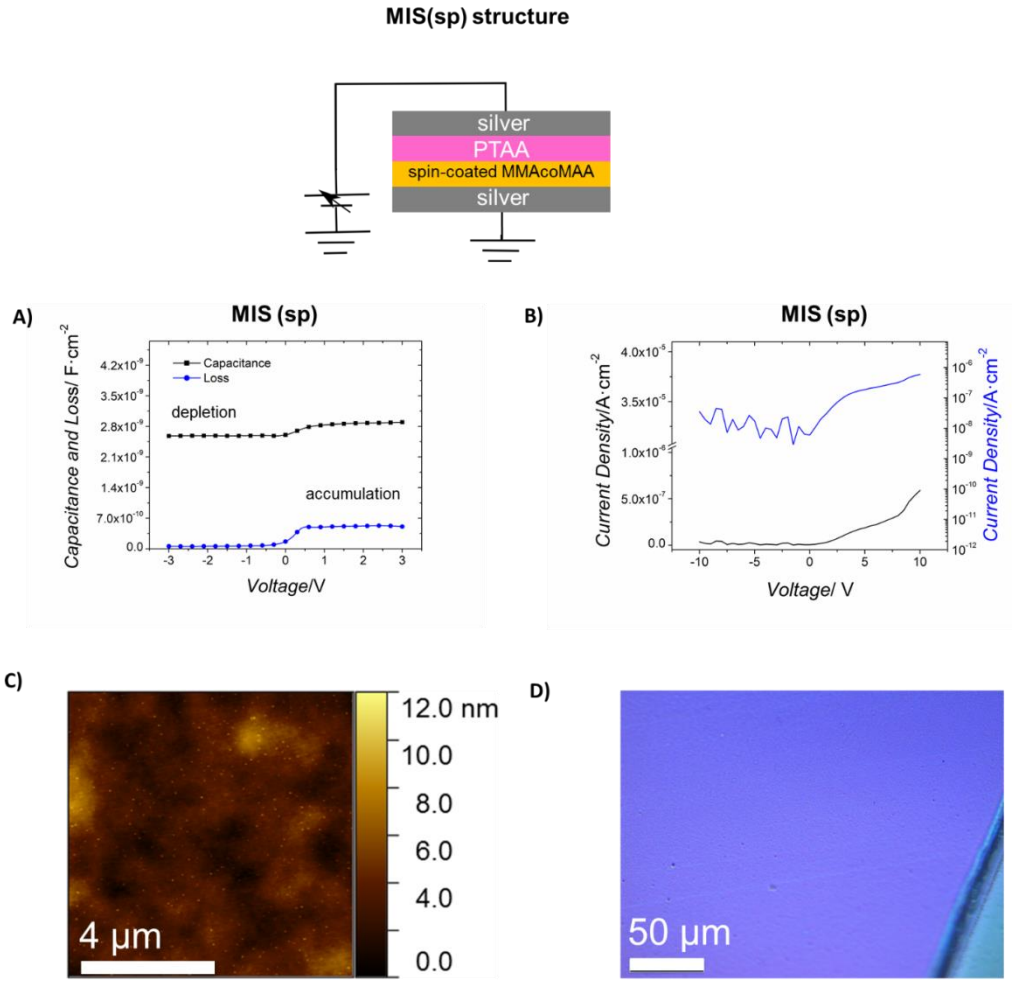

Figure 4-10. Top: Scheme of the spin-coated MIS structure. A) *C-V* and *loss-V* characteristics for spin-coated MIS indicating accumulation and depletion regimes. B) *J-V* characteristics for spin-coated MIS. C) and D) AFM topography and optical image of spin-coated MMAcoMAA layer onto inkjet-printed silver.

At V= |10|V, the RR is approximately 10. In forward and reverse bias, the MIS(sp) reaches values of 0.6 µA·cm^{-2} and 0.04 µA·cm^{-2}, respectively. The *C-V* characteristic at |10V| is almost symmetric. In practical terms, the device with the spin-coated insulating layer reassembles more of a variable capacitor than a rectifying diode. The low leakage current in both polarities is consistent with a high BH at the semiconductor/insulator interface. The high quality of the organic spin-coated insulator film, confirmed by Atomic Force Microscopy (AFM) and optical images (Figure 4-10C and Figure 4-10D), is responsible for the low RR.

Figure 4-11A shows typical *C-V* and *loss-V* characteristics for MIS diode with a single thin insulating layer (MIS(1p)) deposited by inkjet printing. As described above for positive applied voltages, the free holes are injected into the semiconductor and accumulate at the semiconductor/insulator interface causing an increase in capacitance. However, the accumulation capacitance does not saturate. This behavior is attributed to

the high conductance of the insulator. The *loss* value of $3.9 \cdot 10^{-9}$ F·cm^{-2} confirms that the insulator is very leaky. Moreover, a hump in the *C-V* curve appears centered around 0.2 V forward and extending over a small voltage range (see inset Figure 4-11A). These features are often reported for MIS tunneling diodes and are caused by the pinning of the semiconductor Fermi level due to the presence of interfacial states. The underlying physics has been well described in [24].

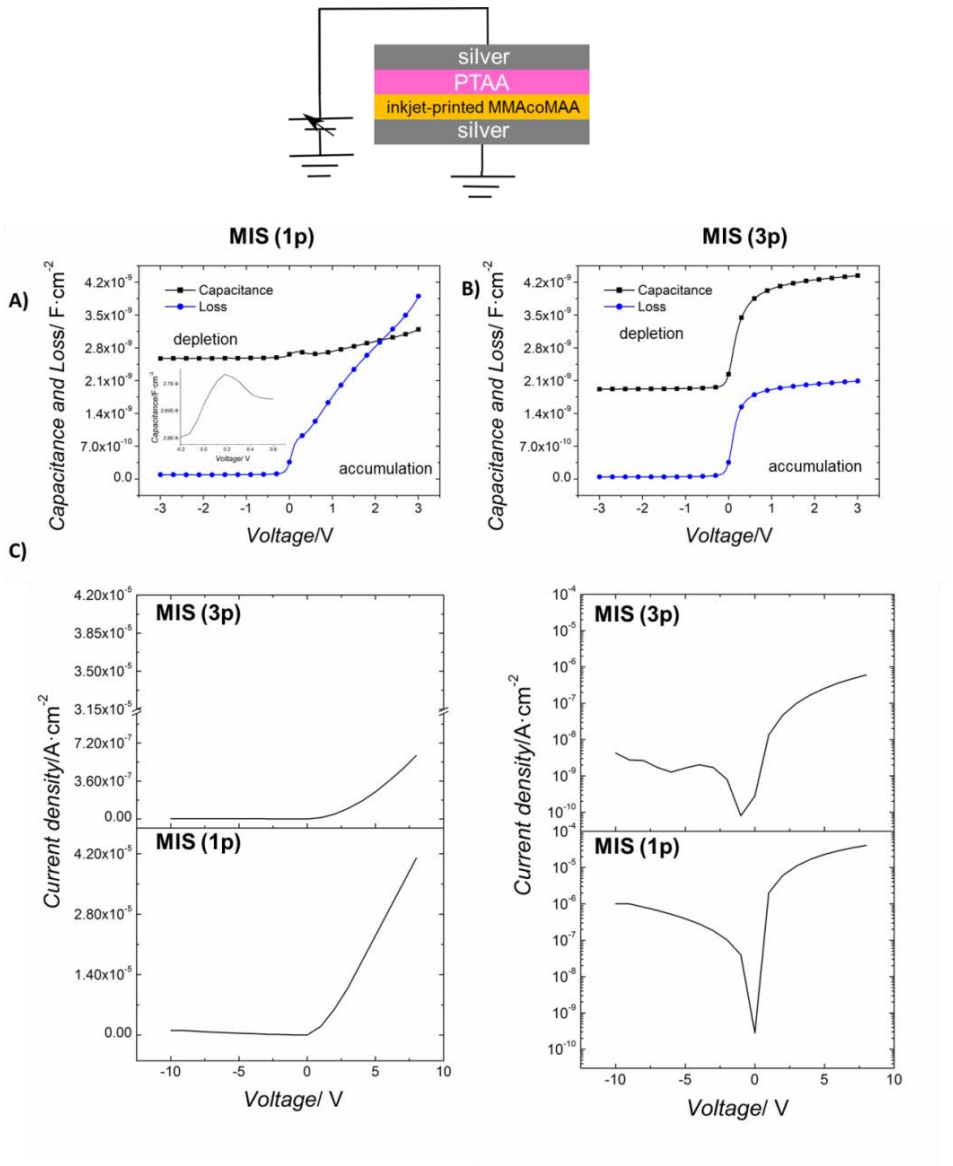

Figure 4-11. Top: Scheme of the MIS device for MIS(1p) and MIS(3p) containing the MMAcoMAA layer inkjet-printed. A) and B) *C-V* and *loss-V* characteristics for MIS(1p) and MIS(3p) indicating accumulation and depletion regimes. The inset in A) shows a zoom of the *C-V* measurement. C) Left: *J-V* characteristics for MIS (1p) and MIS (3p) in a linear plot. Right: Semi-logarithmic plot of the *J-V* characteristics for MIS (1p) and MIS (3p).

When thick insulator layers are fabricated by printing several polymer layers, the electrical behavior of the device becomes similar to an ideal MIS diode. Figure 4-11B

shows the *C-V* and *loss-V* characteristics measured at a frequency of 1 kHz for a MIS diode with 3 printed insulating layers (MIS(3p)). The *C-V* plot shows two well-defined capacitance plateaus. The geometric insulating layer capacitance of $4.2 \cdot 10^{-9}$ F·cm^{-2} is extracted from the plateau in accumulation. The capacitance plateau under reverse bias (depletion) is equal to the series sum of the capacitances of the insulator and of the semiconductor. In comparison with one inkjet-printed MMAcoMMA layer, the three layer thick insulator behaves like a poor leaky insulator and thus, the loss measured is $2 \cdot 10^{-9}$ F·cm^{-2}.

When thick insulator layers are fabricated by printing several polymer layers, the electrical behavior of the device becomes similar to an ideal MIS diode. Figure 4-11B shows the *C-V* and *loss-V* characteristics measured at a frequency of 1 kHz for a MIS diode with 3 printed insulating layers (MIS(3p)). The *C-V* plot shows two well-defined capacitance plateaus. The geometric insulating layer capacitance of $4.2 \cdot 10^{-9}$ F·cm^{-2} is extracted from the plateau in accumulation. The capacitance plateau under reverse bias (depletion) is equal to the series sum of the capacitances of the insulator and of the semiconductor. In comparison with one inkjet-printed MMAcoMMA layer, the three layer thick insulator behaves like a poor leaky insulator and thus, the loss measured is $2 \cdot 10^{-9}$ F·cm^{-2}.

To further investigate the role of the insulating layer on the rectifying properties, a study of its thickness was performed. The MIS(sp), MIS(1p), and MIS(3p) present a thickness of 730 nm, 1 µm, and 1.9-2.1 µm, respectively measured by profilometry. However, from the *C-V* plots the effective insulator layer thicknesses were calculated as 183 nm, 169 nm and 124 nm for MIS(sp), MIS(3p) and MIS(1p), respectively. The disagreement between the measured and extracted MMAcoMAA thicknesses may be explained on the basis of their topographic analysis. The inkjet-printed insulators have a higher surface roughness than the spin-coated ones. Therefore, the semiconductor ink fills the depressions in the MMAcoMAA rough surface underneath creating a partial interpenetrated network of the two materials. This difference in morphology also explains why the MIS(1p) present higher leakage currents than the MIS(3p). The *J-V* curves for MIS(1p) and MIS(3p) are shown in Figure 4-11C. Both *J-V* curves exhibit a pronounced rectifying behavior: at V=|10V|, the RR is 150 for MIS(3p) and 33 for MIS(1p). Decreasing the number of MMAcoMAA layers from three to one, the current of the MIS diode increases 83-fold in accumulation mode. The MIS(1p) structure has forward current two orders of magnitude higher than the MIS(3p) one because the injection of the carriers during accumulation is higher. For thinner insulator layers, the reverse bias current increases and degrades the rectifying properties of the diodes. On the other hand, in the MIS(3p) structure, the presence of a thicker insulator layer lowers the reverse bias current by two orders of magnitude. However, since the dielectric resistance increases, the current injected in forward bias is also lower. These results are in concordance with the respective *loss-V* as well. Table 4-1 summarizes the main parameters of MIS(sp), MIS(1p), and MIS(3p).

Table 4-1 Summary of the deposition techniques, impedance and phase measured by impedance spectroscopy, insulator thicknesses, density current and RR for MIS(sp), MIS(1p) and MIS(3p).

Insulator Layers	Deposition technique	Impedance |Z| [MΩ·cm^{-2}]	Impedance Phase [º]	Insulator Thickness [µm]	Density current at reverse/forward bias [µA·cm^{-2}]	RR	Diode Behavior
1	Spin-coating	12.7·10^{3}	-89.1	0.73	0.04/0.6	15	No
1	Inkjet printing	20.3	-58.7	1	1.5/50	33	Yes
3	Inkjet printing	24.6	-64.8	1.9-2.1	0.004/0.6	150	Yes

This study demonstrates that the rectifying properties of MIS diodes are strongly dependent on the deposition method. For a variety of polymers with similar effective thicknesses, significant rectifying properties are only achieved when the insulator is inkjet-printed. As shown in Figure 4-10 and in Table 4-1 the spin-coated layers have a homogeneous structure, a relative flat surface and good insulating properties. Therefore, spin-coated insulators fail to produce rectifying MIS diodes. The topography of the polymer insulator was evaluated with AFM measurements and optical images taken prior to the semiconductor deposition for MIS(1p) and MIS(3p). From the AFM analysis a porous density of 2.15 holes·µm^{-2} and 0.04 holes·µm^{-2} for one and three printed layers (Figure 4-12.A and Figure 4-12.C) was evaluated. Based on the quantitative analysis of those images, the area of all pinholes corresponds to 7% and 0.8% of the total surface area with an average diameter of 250 nm and 690-930nm for MIS(1p) and MIS(3p), respectively. It is important to mention that the three MMAcoMAA layers were deposited without undertaking a curing process, the so-called wet on wet technique, thus preventing the pinholes from being filled. In addition, optical microscopy images show larger pinholes with diameters in the range of 1.9-2.5 µm and 2.3-3.2 µm with a density of 8000 holes·mm^{-2} and 800 holes·mm^{-2} for MIS(1p) and MIS (3p), respectively (Figure 4-12.B and Figure 4-12.D). The depth of pinholes is shown in Figure 4-13.A and Figure 4-13.B for MIS(1p) and MIS(3p), respectively. For MIS(1p), two kind of pinholes were observed, those with lower diameter present a depth of around 10 nm (Figure 4-13.Ai) while the pinholes with larger diameter have a depth of around 30 nm (Figure 4-13.Aii). For MIS(3p), the lower diameter pinholes present a depth of around 40 nm (Figure 4-13.Bi) while the depth of pinholes with larger diameter is around 80 nm (Figure 4-13.Bii). However, it is worth noting that such pinholes do not result into short-circuits across the MIS structures, as their depth has been established to be much smaller than the actual film thickness. Specifically, the larger pinholes present a depth of 3% and 4% of the total thickness of MIS(1p) and MIS(3p), respectively.

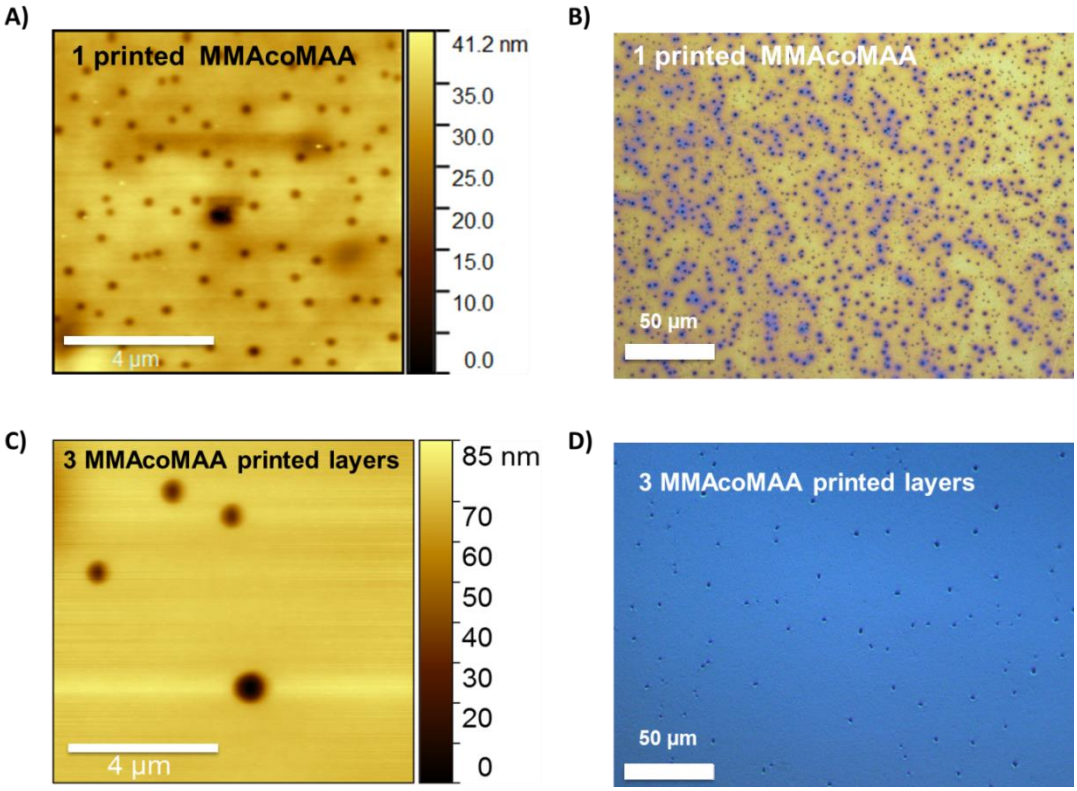

Figure 4-12. Insulating film morphology assessment. A) and B) AFM morphology and optical image for one inkjet-printed MMAcoMAA layer, C) and D) AFM morphology and optical image of three inkjet-printed MMAcoMAA. For all the analysis the MMAcoMAA films were deposited onto inkjet-printed silver(p) electrodes.

The formation of pinholes is a characteristic of solution based polymers.[38],[39] The porosity depends on several factors, such as, among others, the polymer chain length, the type of solvent, and the drying kinetics. The existence of pinholes is already reported to lead to short-circuits between the layers in organic devices.[38],[40] This effect can likely facilitate the PTAA migration through the MMAcoMAA layer and hence cause an increase in the current. In this work, their occurrence is mainly related to the inkjet printing deposition as previously observed in other works.[38] The differences in the layer morphology can thus be related to the different drying kinetics of the film.[11] For fast and homogeneous deposition techniques, such as spin-coating, the creation of pinholes does not occur and the MIS(sp) structure presents low leakage currents and a negligible RR. Instead, as already underlined, in the inkjet-printed diodes, the semiconductor ink creates an interpenetrated network with the MMAcoMAA layer underneath as shown in Figure 4-13.C.

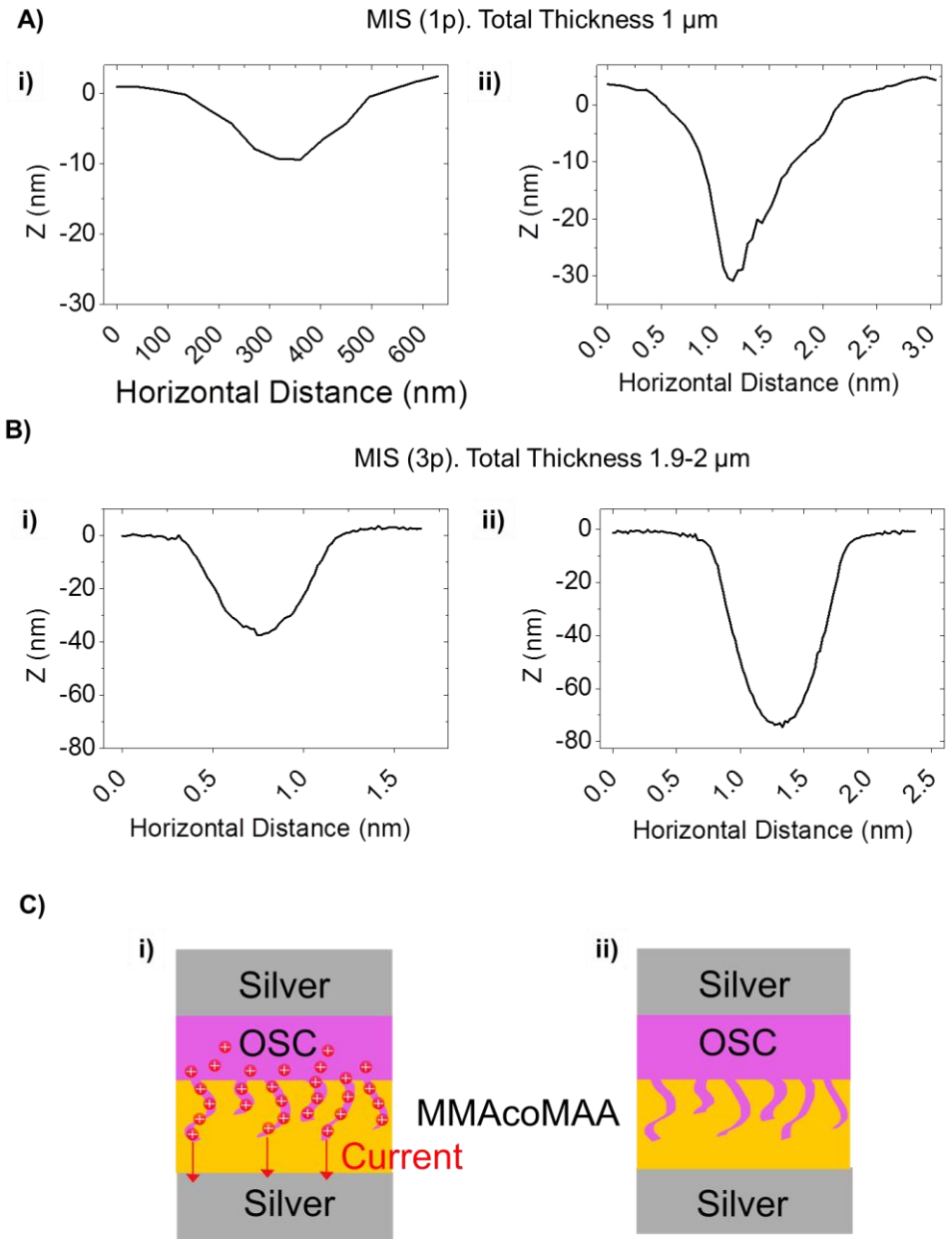

Figure 4-13 A) Profile derived from AFM measurements of MIS(1p) MMAcoMAA film printed over silver electrode for i) low diameter pinhole and ii) high diameter pinhole. B) Profile derived from AFM measurements of MIS(3p) MMAcoMAA film printed over silver electrode for i) low diameter pinhole and ii) high diameter pinhole. C) Schematic view of the MIS structure with pinholes: i) In accumulation mode the thermionic emission across the thinner insulator regions increases the diode current, ii) Under depletion the OSC is depleted of free carriers and the reverse current of the diode is relatively low.

For structures where carriers can easily enter the insulator, the density of free carriers causes a field gradient, which limits the current density. Therefore, a Space-Charge Limited (SCL) current is expected to be observed. Figure 4-14 shows the log(*V*) versus log(*J*) plots for MIS(sp), MIS(3p), and MIS(1p). The MIS (3p), MIS(1p) and MIS(sp) present the power law dependence $J \sim V^n$ with n=1.8, 1.5 and 1.3, respectively, which indicates an SCL conduction with low presence of trapped carriers.[41][42] The extracted slope suggests that the current conduction mechanism of all the presented MIS

diodes is the SCLC mechanism controlled by the presence of traps. The SCLC regime occurs when the equilibrium charge concentration is less than the injected charge concentration. This drive forms a space charge region near the injecting electrode. Therefore, the difference between the diode rectification characteristics of spin-coated and inkjet-printed MMAcoMAA layers is possible due to the film quality related to the deposition technique rather than its thickness.

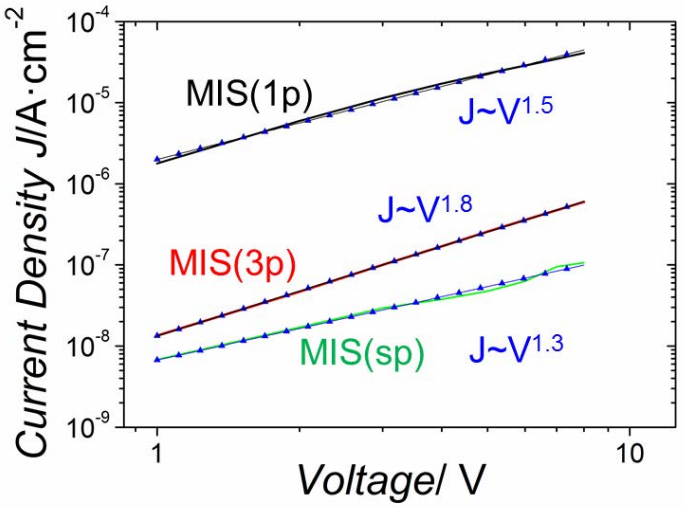

Figure 4-14. Log-log plot of the *J-V* characteristic fitted with straight lines for the different MIS structures characterized. The slope of the fitted SCL currents is shown.

Moreover, a study of the electromechanical behavior of the MIS diodes was performed to complete their electrical characterization and to prove their flexibility. The key advantage of organic MIS diodes compared with traditional silicon based MIS diodes is attributed to their compatibility with flexible substrates. The electromechanical properties of flexible MIS diodes were investigated under tensile strain conditions. For this purpose, the devices were bent using various radii of curvature (R). An electrical characterization of the MIS diodes was performed as a function of the bending radius (Figure 4-15.A). R of 23.5 mm, 15 mm, 10 mm and 6 mm, which corresponds to strains S of 0.26%, 0.41%, 0.62% and 1.04% were used ($S = d \cdot 2 \cdot R^{-1}$, d the thickness of the substrate). The highest S value corresponds to the lowest bending curvature.

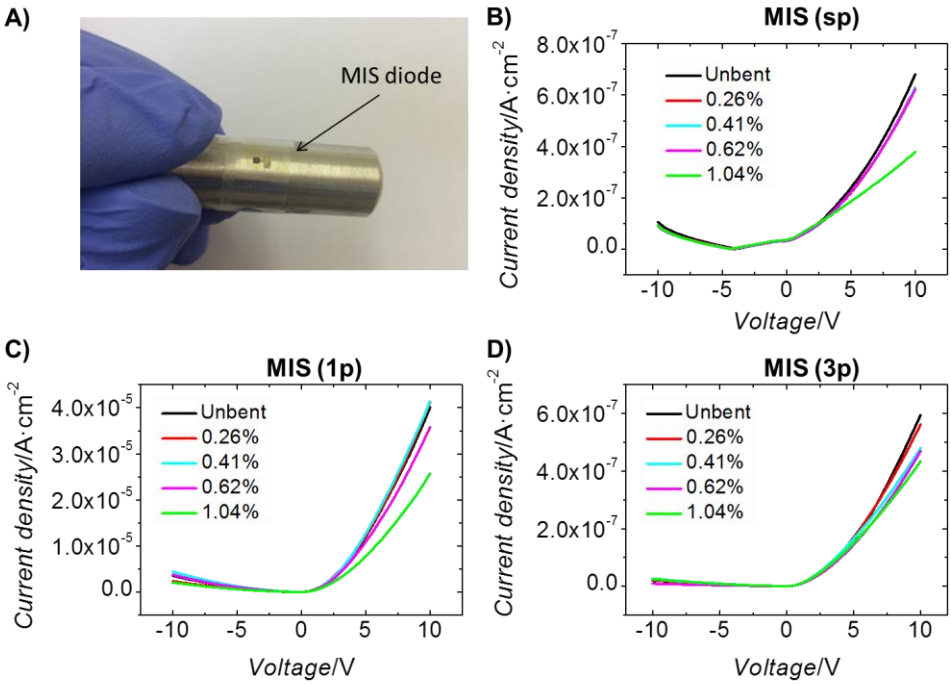

Figure 4-15 A) Photograph of the flexible MIS diode fixed on a metal cylinder for the bending setup. B), C) and D) *J-V* characteristics for MIS(sp), MIS(1p) and MIS(3p) under tensile strains of 0.26%, 0.41%, 0.62% and 1.04%.

Figure 4-15 shows the electrical characteristics as a function of the strain for MIS(sp), MIS(1p) and MIS(3p). For the applied tensile strains of 0.26%, 0.41% and 0.62%, no relevant changes in relative current was observed; however, at the strain of 1.04%, a decrease of the current of 45% and 40% for MIS(sp) and MIS(1p) was obtained, as is shown in Figure 4-15.B and Figure 4-15.C, respectively. For MIS(3p), the current starts to decrease gradually for all the applied strains, for the highest strain of 1.04% the current decreases of about a 27% (see Figure 4-15.D). The decrease of the current is due to a decrease of the semiconductor mobility. This phenomenon is explainable when considering the weak van der Waals forces of the OSC molecules which, under tensile strains, get far apart.[43],[44]

To further demonstrate the working principle of the presented MIS diodes, MIS structures were also fabricated by inkjet printing using other organic insulators: i) cross-linked poly(4-vinylphenol) (cPVP),[38],[45] ii) Epoxy resin (Epoxy), [46],[47] and iii) high-K epoxy resin containing amorphous silica (HK-Epoxy)[48] as shown Figure 4-16.A. Details about the fabrication can be found in the MIS Fabrication section. Figure 4-16.B, C, and D show the *J-V* characteristics for the three MIS structures. All the structures present a rectifying behavior regardless of the insulator thicknesses. As explained before, rectifying properties can be obtained by inserting insulators deposited by inkjet printing technology. Table 4-2 summarizes the respective thicknesses measured by profilometry, density current and RR for the cPVP, Epoxy and HK-Epoxy MIS structures.

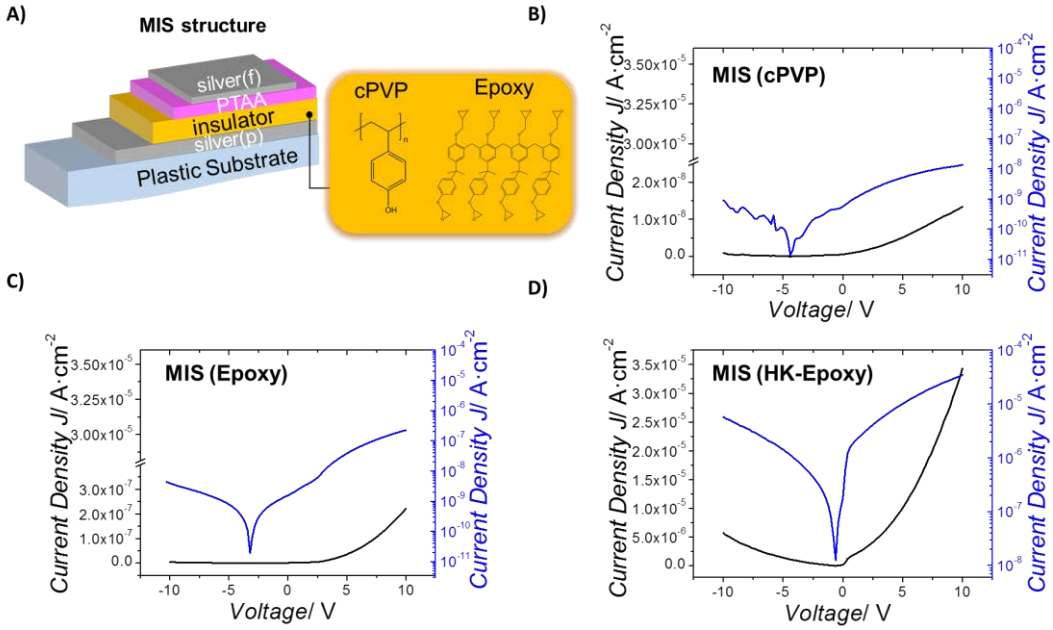

Figure 4-16. A) Schematic illustration of fabricated MIS devices, and the molecular structure of cPVP and epoxy-based inks. B), C) and D) show *J-V* characteristics in linear and semi-logarithmic scale for MIS(cPVP), MIS(Epoxy) and MIS(HK-Epoxy).

As it can be observed in the Table 4-2, the highest RR of 51 was obtained for MIS (Epoxy), whilst MIS(cPVP) and MIS(HK-Epoxy) showed poor electrical performances. This behavior can be explained when considering the permittivity constant of each insulator. The low forward and reverse currents obtained for the MIS(cPVP) structures can be attributed to the insulator low permittivity (ε_r=4).[38] MIS(HK-Epoxy) diodes present a strong reverse leakage current and high forward current because of the high permittivity of the HK insulator (ε_r=10).[49][48] A permittivity constant of 6 allows the MIS(Epoxy) to present the best compromise between the forward and reverse current thanks to an enhanced injection for positive bias.

Table 4-2 Summary of the insulator layers inkjet-printed, impedance and phase measured by impedance spectroscopy, insulator thicknesses, density current and RR for MIS(cPVP), MIS (Epoxy) and MIS(HK-Epoxy).

MIS structure	Insulator Layers	Impedance |Z| [MΩ·cm^{-2}]	Impedance Phase [º]	Insulator Thickness [µm]	Density current at reverse/forward bias [µA·cm^{-2}]	RR	Diode Behavior
cPVP	1	661.5	-78.1	1.5	7.75.10^{-4}/13·10^{-3}	17	Yes
Epoxy	1	8.8·10^{3}	-78	1.9	4.38·10^{-3}/2.2	51	Yes
HK-Epoxy	1	4.8·10^{3}	-77.3	1.7	5.7/34.3	6	Yes

4.4 | OPTIMIZATION OF ORGANIC MIS DIODES USING cPVP AND SP400 MATERIALS FOR NO_2 SENSING

The previous section has explored the working principle of MIS diodes using a polymeric based insulator interface to control the barrier height. One of the most representative figure of merit of MIS diodes is the RR. However, the best achieved RR is 150 using MMAcoMAA as insulator and FS0027 as OSC. The electrical performance can be enhanced by improving these two parameters:

- decreasing the leakage current in reverse bias
- increasing the charge injection in forward bias.

Among the insulators presented in the previous section, cPVP presents the lowest density leakage current in reverse bias; in particular, it is 5 fold lower that the one obtained when MMAcoMAA is used. Based on this result, the optimization of the MIS diode was carried out using cPVP as insulator. Moreover, an improvement of the charge injection was achieved by replacing the FS0027 with a higher mobility amorphous *p-type* OSC, named SP400. Its polymeric nature permits an easy control over its patterning thus reducing its variability because the crystallization does not occur.

In this section, a silver/cPVP/SP400/silver MIS diode is presented. Moreover, *C-V* characteristics and its electrical performance under NO_2 environment as gas sensor will be presented.

4.4.1 | Fabrication recipe

Figure 4-17 shows the scheme and the optical image of the MIS organic diodes fabricated using cPVP as insulator and SP400 as OSC.

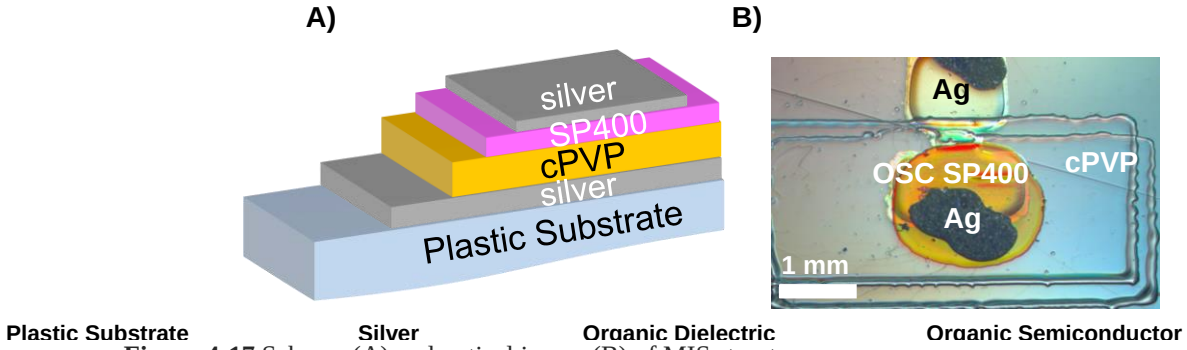

Figure 4-17 Scheme (A) and optical image (B) of MIS structure.

MIS diodes were fabricated on 125µm thick Polyethylene naphthalene (PEN) Teonex® Q65HA substrates from Dupont Teijin specially developed for flexible electronics. Substrates were cleaned with subsequent cycles of acetone, isopropyl

alcohol, and deionized water, and then dried under nitrogen flow. Before printing the devices, a 40W oxygen plasma treatment (Plasma Technology GmbH) was performed for 20 seconds to increase wettability of substrates. A Fujifilm Dimatix DMP2831 desktop printer was used as the printing setup. The silver conductive ink used for the bottom silver(p) electrodes is a 30-35 wt(%) silver nanoparticle content (DGP-40LT-15C from ANP, Korea). A drop spacing (DS) of 20 μm was employed and the printer platen was kept at 40ºC. Finally, the patterned layer was sintered at 120ºC for 30 min in a convection oven. Three different solution of poly(4-vinylphenol) (PVP) using poly(melamine-co-formaldehyde) methylated as crosslinking agent (CL) in propylene glycol methyl ether acetate (PGMEA) were used as insulators layers. The concentrations of PVP and CL are 90 mg/mL and 45 mg/mL, 90 mg/mL and 22.5 mg/mL, and 50 mg/mL and 2.25 mg/mL in solution A, B, and C, respectively. The dielectric layer was inkjet-printed using a DS of 30 μm and keeping the substrate at room temperature. Cross-linking was performed on a convection oven for 30 minutes at 150°C; cross-linking step was performed after each layer deposition. The organic semiconductor is a commercial amorphous p-type semiconductor (Lisicon® SP400, Merck) and it was deposited on the top of the dielectric layer using drop casting, and the curing process was performed on a hot plate for 2 minutes at 100ºC. The top silver(f) electrode is silver conductive paste from Electrolube and it was deposited by means of drop casting technique and dried in air.

The response of the diodes towards nitrogen dioxide was recorded using a homemade stainless steel chamber of 8.6 mL volume connected to a Gometrics MGP2 gas mixer with four Bronkhorst Mass-Flow Controllers. The sensors were exposed up to NO_2 for 15min. The sensors were tested to different NO_2 concentrations at room temperature in dry and dark ambient. To obtain the desired analyte concentration either hydrogen (Praxair, 1000 ppm) or carbon monoxide (Praxair, 1000 ppm) were mixed with pure synthetic air (Carburos Metalicos, 99.99) by means of a mass flow system (Bronkhorst hi-tech 7.03.241). The sensor response was defined as $R=I_A/I_G$, where I_A is the MIS sensor current in air at stationary state and I_G represents the MIS sensor current after 15 min of the analyte exposure.

4.4.2 | Electrical characterization

The analysis of the electrical characteristics of the MIS diodes was performed on the basis of current density-voltage (J-V) curves. The forward bias corresponds to a positive potential applied to silver(f) electrode with respect to bottom silver(p) electrode. As it can be seen in Figure 4-18, all the formulations exhibit non-linear, asymmetric, rectifying behaviors. At V = |10|V, the RRs are approximately 10^3 for the formulation A and B, and 10^2 for the formulation C. In particular, *MIS(A)* presents a maximum forward current density (J_{f_MAX}) of around 0.1 $mAcm^{-2}$ and maximum reverse current (J_{r_MAX}) of around 0.2μAcm^{-2}; *MIS(B)* presents a J_{f_MAX} of around 2.0 μAcm^{-2}

and J_{r_MAX} 1.2 nAcm^{-2}; *MIS(C)* presents a J_{f_MAX} of around 0.7 µAcm^{-2} and J_{r_MAX} of around 1.0 nAcm^{-2}. From these data, it is evident how the electrical characteristics of the presented diodes are strictly related to the different formulation of the insulating layer and to its interaction with OSC. The relation between the electrical behavior and the cross-linker concentration can be explained through impedance analysis.

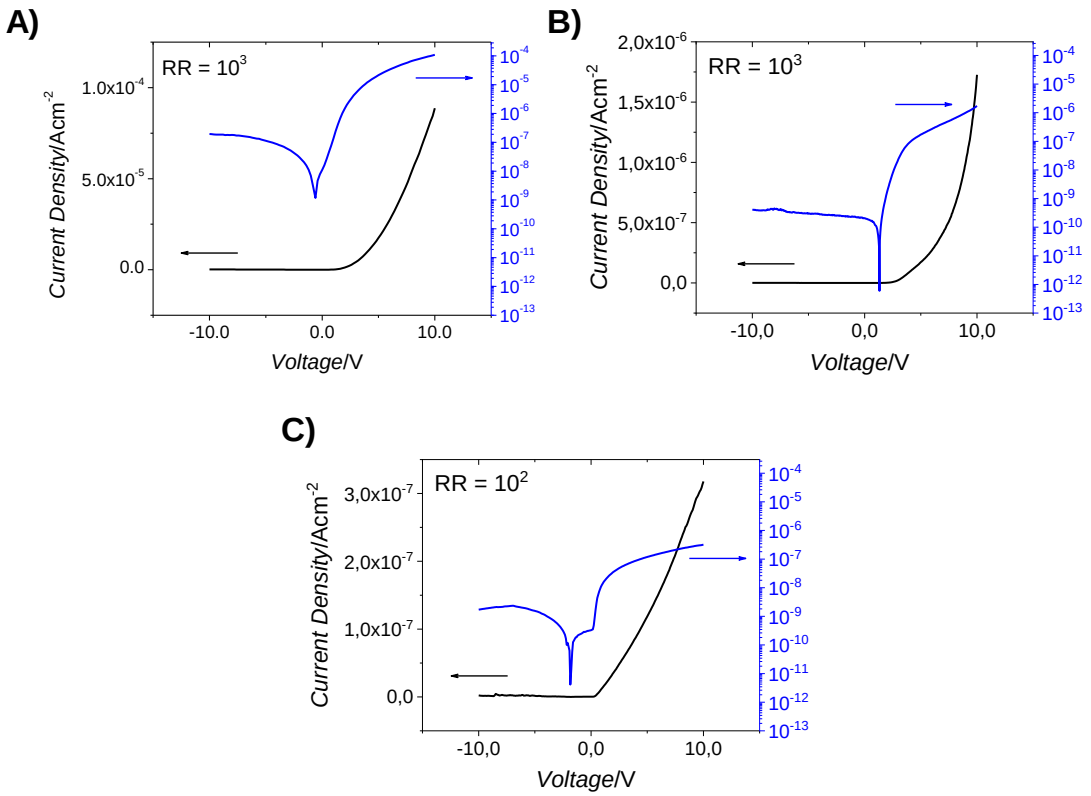

Figure 4-18 J-V characteristics in linear (left) and semilogarithmic (right) scale for MIS(A) (a), MIS(B) (b), and MIS(C) (c) diodes with drop casted organic semiconductor.

Table 4-3 summarizes the electrical parameters obtained for the structures. The impedance and phase angle values were evaluated at a frequency of 1 kHz. For the lowest cross-linker concentration an impedance value of 45 GΩ·cm^{-2} and a phase of around -60º were measured. These values differ from the ones typical of an ideal MIS capacitor and are responsible for the high reverse leakage current obtained for the *MIS(A)* structure. On the other side, the values obtained for the highest cross-linker concentration reassemble more the ones typical of a variable capacitor, giving a relatively high resistance in forward bias and thus, lowering the RR. The best electrical performances were obtained using the formulation B, which presents a good compromise in terms of impedance and output current.

Table 4-3 Electrical parameters of MIS(A), MIS (B) and MIS(C)

MIS structure	Impedance |Z| [MΩ·cm^{-2}]	Impedance Phase [°]	εr	RR	Diode Behavior
A	$45.7 \cdot 10^3$	-63.5	3.8	17	Yes
B	$80.7 \cdot 10^3$	-77.3	4.7	51	Yes
C	$117.7 \cdot 10^3$	-80.5	4.4	6	Yes

As previously explained, several conduction mechanisms have been proposed to describe the conduction through insulating film. Barrier-limited conduction mechanisms include direct tunneling or Fowler-Nordheim (FN) tunneling and Schottky conduction. Bulk-limited conduction mechanisms include SCLC, Poole-Frenkel (PF) conduction, and hopping conduction.[50] Among all, two transport mechanisms mainly occur in this type of structure: the tunneling and the Schottky effect. Depending on the temperature, thickness, and barrier height of the insulating layer, either mechanism predominates.[51] As shown in the *J-V* curves, different slopes were obtained for varied ranges of voltages of the forward voltages, clearly indicating the presence of different transport phenomena in the Ag/cPVP/SP400/Ag structure. The plot in Figure 4-19 is referred to MIS(B) structures; however, the same explication can be applied to MIS(A) and MIS(C) diodes. For low-forward bias region (~0.0-0.5V) is possible to observe a plateau in the J-V curves, which is characteristic of tunneling type conduction. The linear dependence of $\ln(1/V^2)$ with 1/V is characteristic of a Fowler-Nordheim mechanism conduction, which has a transition voltage (V_t) of around 0.32 V. The same value was obtained for the *MIS(C)*, whilst for the *MIS(A)* V_t = 0.80 V. According to the simplest model, the Fowler-Nordheim tunneling current density J is expressed in Equation 4-7.

$$J = AE^2 \exp[-B \cdot E]\,; A = mm^* q^3 8\pi h \Phi_B; \quad B = \sqrt{8\,\pi 32 m^* h^2} q {\Phi_B}^{3/2} \qquad \text{Equation 4-7}$$

where E, m, m*, q, h and Φ_B are respectively the applied field, the electron mass, the effective mass of the electron in the insulator, the electronic charge, the Planck constant, and the barrier height.

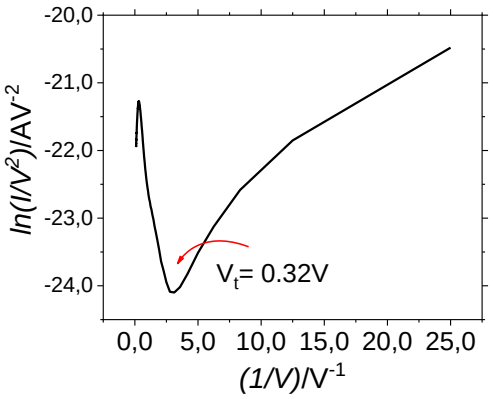

Figure 4-19 Ln(I/V^2) vs 1/V fit of MIS(B) structure.

4.4.3 | MIS diode as NO_2 gas sensor

Considering the obtained results, MIS(B) was chosen to evaluate the possibility of employing the diode structure as a gas sensor.

In recent years, much research efforts have been devoted to gas sensors due to the fact of severe air pollution. Air quality is an important pre-requisite for public health and its pollution for gaseous compounds contributes relevantly to the burden of disease in both industrial and developing countries. Nitrogen dioxide (NO_2), a main pollutant arising from combusted fuel, can cause photochemical smog, acute pulmonary, acid rains, edema, and irritation of eyes and is even suspected to cause cancer.[52] To date, commercial NO_2 sensors are usually bulky, have low selectivity, and high power consumption. Even in the most developed cities spatially resolved urban air quality measurements are currently limited.[53] Therefore, it is highly desirable to develop novel gas sensors that are endowed with efficient manufacturing, high throughput, and good device performance such as high sensitivity/selectivity, light weight and low power consumption.

In the past decade, OSC materials have become promising candidates for gas sensors due to their high sensitivity, low production costs, and multiple function integration.[54] The reversible non covalent bond interaction between OSC and gas molecules causes organic materials to be more suitable than inorganic materials for detecting toxic gas such as NO_2, sulfur dioxide (SO_2), or ammonia (NH_3) at room temperature (RT), which is of great importance for operation in complex and often hazardous gaseous environment.[55] This interaction process leads to a change in the mobile carrier density in the OSC of the devices, resulting in the variation of the output signal. For RT gas sensors, normally a thicker organic active layer provides more sensitive medium and hence a more stable electrical signal. However, disordered surfaces, deep traps, and crystal domain boundaries in organic films render the gas

diffusion and scattering complicated, and substantially decrease the gas absorption–desorption efficiency.

The charge carrier mobility in OSC of MIS diodes is normally determined by the molecular orientation, grain size and grain boundaries especially located at the dielectric/semiconductor interface.[56] Each of them usually plays a vital role in the OSC sensing processes. A change in the current occurs when analyte interact with OSC. The interacted analyte may act as either dopants or traps for charge carrier.

Figure 4-20A shows an optical image of a MIS diode mounted on a To-U package.

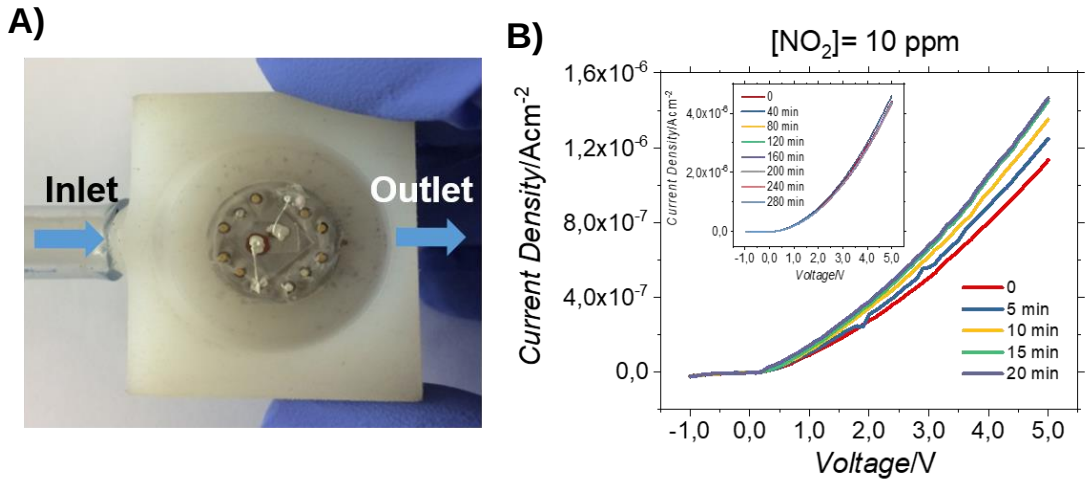

Figure 4-20 Gas sensing setup (A); variation of the current density of the diode in time after the exposure to 10ppm NO_2 concentration (B); stability of the current density signal over 280 minutes (B, inset).

J-V measurements were performed to characterize the electrical response of the MIS diode upon exposure to NO_2 gas. The gas concentration was increased from 1ppm to 100ppm, with an incubation time of 20 minutes before each characterization. As it is shown for 10ppm NO_2 concentration in Figure 4-20B, after this time the current stabilizes. *J-V* curves were recorded at ambient condition, during the same period of time, to exclude any possible current variation due to the device instability (Figure 4-20B, inset). Figure 4-21A shows the J-V characteristics, registered at room temperature, for the different concentrations of NO_2.

The sensitivity response of these devices to NO_2 was evaluated by using the following Equation 4-8:

$$response\ \% = \frac{I_N - I_{N0}}{I_{N0}} \qquad \text{Equation 4-8}$$

where I_{N0} and I_N are the maximum forward currents of the sensor recorded in dry air and in presence of NO_2, respectively.

The sensitivity presents an increase of 7 % by enhancing the on current upon an exposure of a NO_2 concentration of 3 ppm. When the concentration of NO_2 increases to 100 ppm, the response keeps on increasing to around 860 %. Being NO_2 a strong electron acceptor species, it generates holes while interacting with a *p-type* OSC. Therefore, the carrier concentration of the device becomes higher when it is exposed to NO_2 gas. From 2ppm to 100ppm the relationship between the response and the NO_2 concentration is non-linear. However, two different linear regions can be distinguished (Figure 4-21B). From the linear relationship, the slope which denotes the device sensitivity is determined to be 11% ppm^{-1} in the range from 2 to 10 ppm (Figure 4-21C). The value of limit of detection is 0.5 ppm. For the high concentration range (12.5–100 ppm) the sensitivity is 9% ppm^{-1}. The value of limit of detection is 4.37 ppm. The recovery time of about 120 min is extrapolated from the current decreasing process. Compared to previous reports on RT organic NO_2 gas sensors, the recovery time in our work is slower, basically due to the thickness nature of the drop casted OSC.

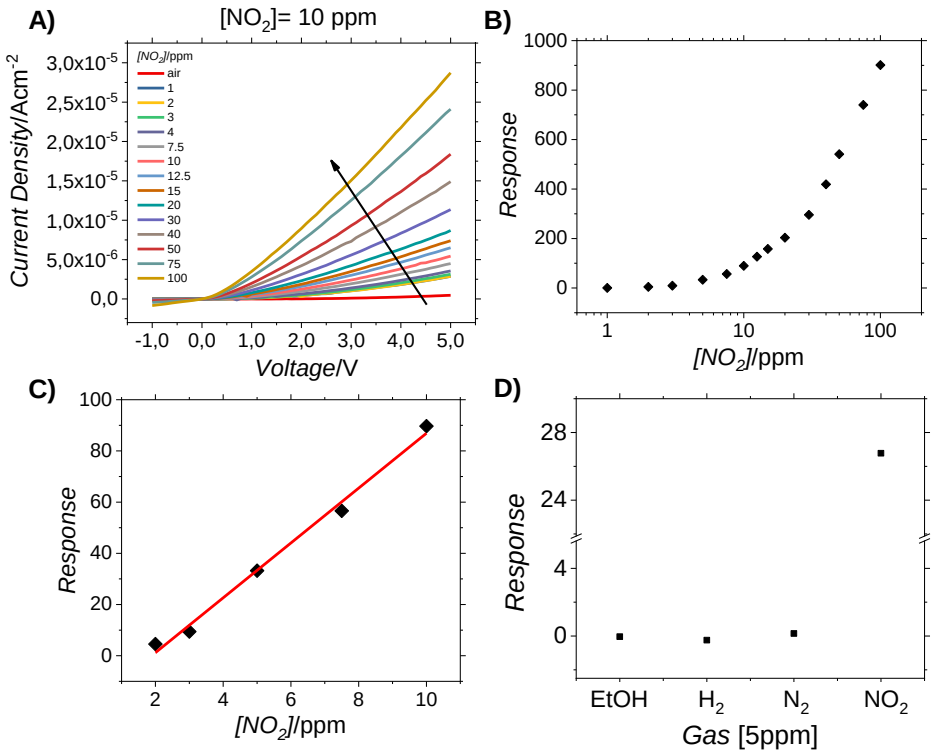

Figure 4-21 (A)J-V characteristics at room temperature for different concentrations of NO_2. (B) and (C); response to different concentrations of NO_2 and; (D) device selectivity.

In gas sensing, the selectivity of the sensor is an important factor as well, Figure 4-21D shows that diodes exhibit a very low sensitivity toward ethanol (EtOH), N_2, and H_2. The investigation and optimization of the device sensing performance in terms of sensitivity (for ultralow concentrations, ppb level) and selectivity will be subject of future studies. However, it is possible to consider this preliminary test as a proof-of-concept of the feasible applications of the presented MIS diodes.

4.5 | CONCLUSIONS

Novel organic inkjet-printed diodes based on MIS structures have been fabricated and characterized. Temperature-dependent measurements are in line with a thermionic emission model for carrier injection into the insulator. The estimated barrier height at semiconductor/insulator interface depends on the thin-film deposition method. MIS diodes based on spin-coated layers exhibit the highest energetic barrier (0.97 eV) for carrier injection, but poor rectifying properties. Despite a low energetic barrier of 0.4 eV, diodes based on inkjet-printed layers have a RR reaching almost two orders of magnitude.

The polymeric MMAcoMAA insulator layer is in principle too thick to allow for a significant carrier transport across it. However, a morphological analysis shows that the semiconductor intermixes with the insulator by filling depressions or micro-pores. This semiconductor-polymer intermixing creates a polymer brush-like morphology that thins the insulating polymer layer. Under forward bias a significant current across the insulator is allowed. Under reverse bias the semiconductor is depleted of free carriers and the current is minimized. This physical model is expected to be only dependent on the insulator morphology and independent of the type of polymer used. This prediction is consistent with the fact that a variety of insulating polymers when deposited by inkjet printing lead to rectifying diodes.

Therefore, inkjet-printed polymer-based interfacial layers could be an ideal approach to develop a new type of rectifying MIS diodes by using low-cost printing technologies.

Finally, an optimization of the electrical performance of the MIS diode were achieve thanks the use of cPVP as insulator and the OSC SP400 allowing the increase of the RR parameter. Moreover, a first example of a NO_2 gas sensor based on the MIS diode is presented as a proof-of-concept for the possible sensing and electronic applications of these structures.

Future work will include the test of higher mobility OSCs and the optimization of their printing parameters in order to achieve higher gas sensor responses.

4.6 | REFERENCES

[1] Physics of Semiconductor Devices, 3rd Edition. *Wiley.com*, https://www.wiley.com/en-es/Physics+of+Semiconductor+Devices%2C+3rd+Edition-p-9780471143239 (accessed 3 August 2018).

[2] Rhoderick EH, Williams RH. *Metal-semiconductor contacts*. Oxford [England]; New York: Clarendon Press ; Oxford University Press, 1988.

[3] (12) Parameter extraction from non-ideal CV characteristics of a Schottky diode with and without interfacial layer. *ResearchGate*, https://www.researchgate.net/publication/243273535_Parameter_extraction_from_non-ideal_CV_characteristics_of_a_Schottky_diode_with_and_without_interfacial_layer (accessed 3 August 2018).

[4] Cowley AM, Sze SM. Surface States and Barrier Height of Metal- Semiconductor Systems. *J Appl Phys* 1965; 36: 3212–3220.

[5] Türüt A, Sağlam M. Determination of the density of Si-metal interface states and excess capacitance caused by them. *Phys B Condens Matter* 1992; 179: 285–294.

[6] Bala S. The Role of Interface State Density in I-V Characteristics of Metal-Semiconductor Contact With Interfacial Layer. 2012; 2: 5.

[7] Hammock ML, Chortos A, Tee BC-K, et al. 25th anniversary article: The evolution of electronic skin (e-skin): a brief history, design considerations, and recent progress. *Adv Mater Deerfield Beach Fla* 2013; 25: 5997–6038.

[8] Chang JS, Facchetti AF, Reuss R. A Circuits and Systems Perspective of Organic/Printed Electronics: Review, Challenges, and Contemporary and Emerging Design Approaches. *IEEE J Emerg Sel Top Circuits Syst* 2017; 7: 7–26.

[9] Someya T, Bauer S, Kaltenbrunner M. Imperceptible organic electronics. *MRS Bull* 2017; 42: 124–130.

[10] Klauk H. *Organic Electronics II: More Materials and Applications*. John Wiley & Sons, 2012.

[11] Teichler A, Perelaer J, Schubert US. Inkjet printing of organic electronics – comparison of deposition techniques and state-of-the-art developments. *J Mater Chem C* 2013; 1: 1910.

[12] Large Area and Flexible Electronics. *Wiley.com*, https://www.wiley.com/en-us/Large+Area+and+Flexible+Electronics-p-9783527336395 (accessed 17 August 2018).

[13] Singh M, Haverinen HM, Dhagat P, et al. Inkjet printing-process and its applications. *Adv Mater Deerfield Beach Fla* 2010; 22: 673–685.

[14] Kim H-S, Dhage SR, Shim D-E, et al. Intense pulsed light sintering of copper nanoink for printed electronics. *Appl Phys A* 2009; 97: 791.

[15] Ko SH, Pan H, Grigoropoulos CP, et al. All-inkjet-printed flexible electronics fabrication on a polymer substrate by low-temperature high-resolution selective laser sintering of metal nanoparticles. *Nanotechnology* 2007; 18: 345202.

[16] Kim S, Cho H, Hong Y, et al. Effect of Electrode Area on High Speed Characteristics over 1 MHz of Poly(3-hexylthiophene-2,5-diyl) Diode with Inkjet-Printed Ag Electrode. *Mol Cryst Liq Cryst* 2009; 513: 256–261.

[17] Lilja KE, Bäcklund TG, Lupo D, et al. Gravure printed organic rectifying diodes operating at high frequencies. *Org Electron* 2009; 10: 1011–1014.

[18] Kang C, Kim S, Hong Y, et al. Frequency analysis on poly(3-hexylthiopene) rectifier using impedance spectroscopy. *Thin Solid Films* 2009; 518: 889–892.

[19] Bose I, Tetzner K, Borner K, et al. Air-stable, high current density, solution-processable, amorphous organic rectifying diodes (ORDs) for low-cost fabrication of flexible passive low frequency RFID tags. *Microelectron Reliab* 2014; 54: 1643–1647.

[20] Gooden K, Laudari A, Knotts G, et al. Printed dielectric-based organic diodes and transistors. *Flex Print Electron* 2016; 1: 015004.

[21] Kang C, Shin H, Lee C. High-frequency organic rectifiers through interface engineering. *MRS Commun* 2017; 7: 755–769.

[22] Lilja KE, Majumdar HS, Pettersson FS, et al. Enhanced Performance of Printed Organic Diodes Using a Thin Interfacial Barrier Layer. *ACS Appl Mater Interfaces* 2011; 3: 7–10.

[23] Mitra KY, Sternkiker C, Martínez-Domingo C, et al. Inkjet printed metal insulator semiconductor (MIS) diodes for organic and flexible electronic application. *Flex Print Electron* 2017; 2: 015003.

[24] Green MA, King FD, Shewchun J. Minority carrier MIS tunnel diodes and their application to electron- and photo-voltaic energy conversion—I. Theory. *Solid-State Electron* 1974; 17: 551–561.

[25] Jha JK, Santos-Ortiz R, Du J, et al. The influence of MoO_x gap states on hole injection from aluminum doped zinc oxide with nanoscale MoO_x surface layer anodes for organic light emitting diodes. *J Appl Phys* 2015; 118: 065304.

[26] Liu Z, Kobayashi M, Paul BC, et al. Contact engineering for organic semiconductor devices via Fermi level depinning at the metal-organic interface. *Phys Rev B*; 82. Epub ahead of print 20 July 2010. DOI: 10.1103/PhysRevB.82.035311.

[27] Liu C, Xu Y, Noh Y-Y. Contact engineering in organic field-effect transistors. *Mater Today* 2015; 18: 79–96.

[28] Azum N, Taib LA, Al Angari YM, et al. π-Conjugated donor-acceptor small molecule thin-films on gold electrodes for reducing the metal work-function. *Thin Solid Films* 2016; 616: 320–327.

[29] Tada A, Geng Y, Wei Q, et al. Tailoring organic heterojunction interfaces in bilayer polymer photovoltaic devices. *Nat Mater* 2011; 10: 450–455.

[30] Raut NC, Al-Shamery K. Inkjet printing metals on flexible materials for plastic and paper electronics. *J Mater Chem C* 2018; 6: 1618–1641.

[31] Highly Conductive Ink Jet Printed Films of Nanosilver Particles for Printable Electronics, http://esl.ecsdl.org/content/8/11/J30.abstract (accessed 22 August 2018).

[32] Perelaer J, de Gans B-J, Schubert US. Ink-jet Printing and Microwave Sintering of Conductive Silver Tracks. *Adv Mater* 2006; 18: 2101–2104.

[33] Titkov AI, Bukhanets OG, Gadirov RM, et al. Conductive inks for inkjet printing based on composition of nanoparticles and organic silver salt. *Inorg Mater Appl Res* 2015; 6: 375–381.

[34] Direct patterning of silver electrodes with 2.4<ce:hsp sp=\"0.25\"/>μm channel length by piezoelectric inkjet printing. DOI: 10.1016/j.jcis.2016.10.016.

[35] Tobjörk D, Kaihovirta NJ, Mäkelä T, et al. All-printed low-voltage organic transistors. *Org Electron* 2008; 9: 931–935.

[36] Sze SM, Ng KK. *Physics of Semiconductor Devices*. John Wiley & Sons, 2006.

[37] Sarpatwari K, Mohney SE, Awadelkarim OO. Effects of barrier height inhomogeneities on the determination of the Richardson constant. *J Appl Phys* 2011; 109: 014510.

[38] Roberts ME, Queraltó N, Mannsfeld SCB, et al. Cross-Linked Polymer Gate Dielectric Films for Low-Voltage Organic Transistors. *Chem Mater* 2009; 21: 2292–2299.

[39] Hawash Z, Ono LK, Raga SR, et al. Air-Exposure Induced Dopant Redistribution and Energy Level Shifts in Spin-Coated Spiro-MeOTAD Films. *Chem Mater* 2015; 27: 562–569.

[40] Calvert P. Inkjet Printing for Materials and Devices. *Chem Mater* 2001; 13: 3299–3305.

[41] Lampert MA. Simplified Theory of Space-Charge-Limited Currents in an Insulator with Traps. *Phys Rev* 1956; 103: 1648–1656.

[42] López Varo P, Jiménez Tejada JA, López Villanueva JA, et al. Space-charge and injection limited current in organic diodes: A unified model. *Org Electron* 2014; 15: 2526–2535.

[43] Nigam A, Fishchuk II, Kadashchuk A, et al. Strain induced anisotropic effect on electron mobility in C60 based organic field effect transistors. *Appl Phys Lett* 2012; 5.

[44] Cosseddu P, Tiddia G, Milita S, et al. Continuous tuning of the mechanical sensitivity of Pentacene OTFTs on flexible substrates: From strain sensors to deformable transistors. *Org Electron* 2013; 14: 206–211.

[45] Conti S, Lai S, Cosseddu P, et al. An Inkjet-Printed, Ultralow Voltage, Flexible Organic Field Effect Transistor. *Adv Mater Technol* 2017; 2: 1600212.

[46] Tetzner K, Bose I, Bock K, et al. Organic Field-Effect Transistors Based on a Liquid-Crystalline Polymeric Semiconductor using SU-8 Gate Dielectrics onFlexible Substrates. *Materials* 2014; 7: 7226–7242.

[47] Robin M, Kuai W, Amela-Cortes M, et al. Epoxy Based Ink as Versatile Material for Inkjet-Printed Devices. *ACS Appl Mater Interfaces* 2015; 7: 21975–21984.

[48] Mitra KY, Polomoshnov M, Martínez- Domingo C, et al. Fully Inkjet-Printed Thin-Film Transistor Array Manufactured on Paper Substrate for Cheap Electronic Applications. *Adv Electron Mater* 2017; 3: 1700275.

[49] Tech_Tip_25_-_Dielectric_Properties_of_Epoxies.pdf, http://www.epotek.com/site/files/Techtips/pdfs/Tech_Tip_25_-_Dielectric_Properties_of_Epoxies.pdf (accessed 22 August 2018).

[50] Hickmott TW. Temperature-dependent Fowler–Nordheim tunneling and a compensation effect in anodized Al-Al2O3-Au diodes. *J Appl Phys* 2005; 97: 104505.

[51] Hemour S, Wu K. Radio-Frequency Rectifier for Electromagnetic Energy Harvesting: Development Path and Future Outlook. *Proc IEEE* 2014; 102: 1667–1691.

[52] Wetchakun K, Samerjai T, Tamaekong N, et al. Semiconducting metal oxides as sensors for environmentally hazardous gases. *Sens Actuators B Chem* 2011; 160: 580–591.

[53] Jalil AR, Chang H, Bandari VK, et al. Fully Integrated Organic Nanocrystal Diode as High Performance Room Temperature NO2 Sensor. *Adv Mater* 2016; 28: 2971–2977.

[54] Polymer Science: A Comprehensive Reference | ScienceDirect, https://www.sciencedirect.com/referencework/9780080878621/polymer-science-a-comprehensive-reference (accessed 22 August 2018).

[55] Zhang C, Chen P, Hu W. Organic field-effect transistor-based gas sensors. *Chem Soc Rev* 2015; 44: 2087–2107.

[56] Lv A, Pan Y, Chi L. Gas Sensors Based on Polymer Field-Effect Transistors. *Sensors* 2017; 17: 213.

5

Organic Inkjet-Printed BioFETs

In this chapter, the Organic Field-Effect Transistors basics and the working principle of Biological Field-Effect Transistors (BioFETs) will be presented. Biosensors based on OFETs have attracted increasing attention due to the possibility of rapid, label-free, and inexpensive detection. However, top-gate BioFETs using a polymer as insulator and an amorphous polymer as organic semiconductor have been seldom reported. In this chapter, the organic field-effect transistor basics will be reported. Then, as experimental results, the development of the BioFET will be presented in two phases. As a first phase a systematic investigation in terms of topographical and electrical characterization has been carried out in order to find the optimal fabrication process for obtaining a reliable polymer insulator. Previous studies have demonstrated that the best electrical performance arises from the use of the perfluoropolymer Cytop^{TM}. Consequently, a simple immobilization protocol was used to ensure the proper attachment of a model biomolecule onto the Cytop's hydrophobic surface whilst keeping its remarkable insulating properties with gate current in the range of dozens of pico Ampers. The top-gate BioFETs used in this study showed durability even when they were exposed to oxygen plasma, wet amine functionalization treatment, and aqueous media. As a second phase, it is presented the inkjet-printed BioFET. Morphological and electrical characterizations were also performed. Finally, as a preliminary result, the both top-gate microfabricated and the inkjet-printed BioFETs demonstrated the capability of detecting the presence of biomolecules through changes in the drain current, which opens the way for further use in the immunosensing field.

5.1 | ORGANIC FIELD-EFFECT TRANSISTORS BASICS

In this chapter various aspects of the characterization and performance of Organic Field-Effect Transistor (OTFT) are considered. The chapter begins by addressing first individual transistors and afterwards addresses on how to perform basic parameter extraction.

This section is organized in the following way. A brief history of the OTFT is presented together with the description of the typical OTFT architectures and the basic operation mechanism. Moreover, the differences between a silicon based Metal-Oxide-Semiconductor Field-Effect Transistor (MOSFET) and an OTFT device are also discussed. Finally, the OTFT electrical parameters are derived.

A Thin Film Transistor (TFT) is a device that uses an electric field to modulate the conduction of a channel located at the interface between a dielectric and a semiconductor. Therefore, it is Field-Effect Transistor (FET) similar to the well-known MOSFET, which is the basic building block of modern integrated circuits. The development histories of TFTs and MOSFETs are parallel in time. The TFT concept was patented in 1925 by Julius Edger Lilienfeld and in 1934 by Osker Heil but at the time no practical applications emerged. In the 1960s several device structures and semiconductor materials like Te, CdSe, Ge and InSb were explored to fabricate TFTs. However, the competition from the MOSFET based on silicon technology forced the TFT to enter in a long period of hibernation. In the early 1970s the need for large area applications in flat panel displays motivates the search for alternatives to the crystalline silicon and the TFT found its niche of application. In 1979, the hydrated amorphous silicon (a-Si:H) becomes a forerunner as a semiconductor to fabricate TFTs. Since the mid-1980s, the silicon-based TFTs have successfully dominate the large area liquid crystal displays (LCD) technology and become the most important devices for active matrix liquid crystal and Organic Light Emitting Diode (OLED) applications. In the meantime, TFTs based on Organic Semiconductor (OSC) channel layers were introduced in the 1990s with electron mobility equivalent to that of a-Si:H. Nowadays, OTFTs are the candidate for incorporation onto flexible substrates. A representative and particularly important example is full-color, video, flexible OLED displays. Small OLED displays on conventional glass substrates for mobile phone and PDA applications are rapidly growing and are displacing LCD screens in the small display sector. OFET technology could be an ideal backplane device for these applications. Nevertheless, the general application niche for OFETs is not entirely defined. Smart cards, disposable electronics, and electronic skins are also currently under intense research.

- **Basic Operation of OTFT**

  An OTFT is formed by placing thin films of the dielectric layer as well as an active semiconductor layer and metallic contacts onto a supporting substrate. Figure 5-1A and Figure 5-1B show a cross-sectional schematic drawing of a MOSFET and an OTFT, respectively. As evident the substrate of an OTFT is an insulating material, whereas the substrate of a MOSFET is a semiconductor material (*p-type*) of different doping as the source and drain diffusions (*n-type*). Source and drain contacts to the semiconducting channel material are injecting contacts to the channel in an OTFT structure and are a *pn* junction in a MOSFET. OTFT and MOSFET operation is similar in that the current from the source to the drain terminal is modulated by the applied gate electric field. Current modulation in an OTFT or in a MISFET can be explained if the Metal-Insulator-Semiconductor (MIS) part of the OTFT is considered as a capacitor. A voltage applied between the metal and semiconductor causes a charge to build up in the semiconductor and the metal gate. The energy-band diagram of an ideal MIS structure is given in Figure 5-1C (for a *p-type* semiconductor). The structure is termed ideal because the bands are flat for zero applied voltage. This is the case when Equation 5-1 is fulfilled.

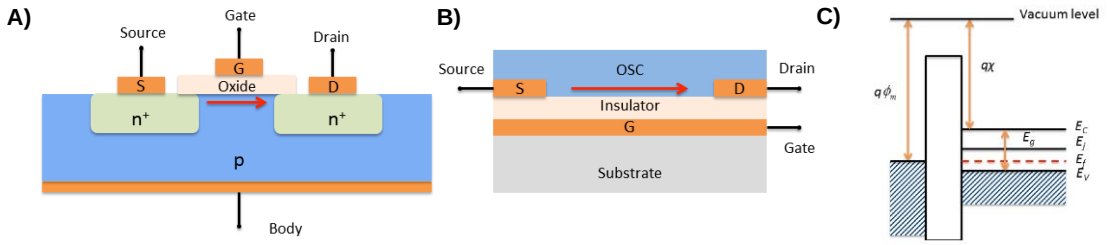

Figure 5-1 Cross-sectional schematic drawing of a MOSFET (A) and an OTFT (B). C) Band diagram of an ideal metal-insulator-semiconductor structure at equilibrium. ϕm is the metal work-function, qχ is the electron affinity measured from the bottom of the conduction band E_C to the vacuum level, E_G thesemiconductor bandgap, E_V the semiconductor valence band, q the absolute electron charge, and E_F the Fermi level and E_I the intrinsic Fermi level.

$$\Phi_M = \chi + \frac{E_G}{2q} + \Phi_B \qquad \text{Equation 5-1}$$

Here, ϕ_M is the metal work-function, qχ is the electron affinity measured from the bottom of the conduction band E_C to the vacuum level, E_G the semiconductor bandgap, q the absolute electron charge, and ϕ_B the potential difference between the Fermi level and the intrinsic Fermi level E_I (which is located very close to midgap) (in the non-ideal case, a small band curvature exists at the insulator-

semiconductor interface, and a small potential V_{FB}, the so-called flat-band voltage, must be applied to the metal to get the flat-band conditions).

When the MIS structure is biased with positive or negative voltages, three different situations may occur at the insulator-semiconductor interface. Considering a p-type semiconductor, for a negative voltage (Figure 5-2A), the bands bend upward and the top of the valence band moves closer to the Fermi level, causing an accumulation of holes near the insulator-semiconductor interface. The interface is thus more conductive than the bulk of the semiconductor. When a small to moderate positive voltage is applied to the gate electrode, majority carrier holes are repelled from the insulator/semiconductor interface so that a depletion layer is formed (Figure 5-2B). When a larger positive voltage is applied to the metal (Figure 5-2C), the bands bend even more downward and the intrinsic level eventually crosses the Fermi level. At this point, the density of electrons exceeds that of the holes, and one enters the inversion regime. The inversion-mode of operation is usually not observed in OFETs. Depending on the gate voltage required to form an accumulation layer, an OTFT can be classified as either an enhancement-mode or a depletion-mode device.

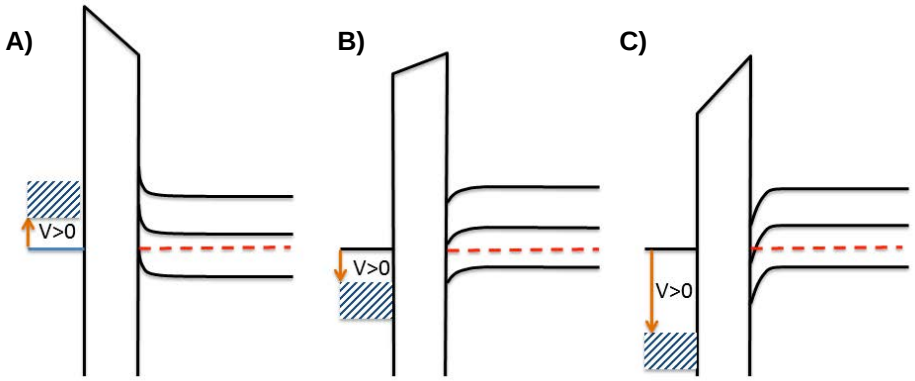

Figure 5-2 Band diagram of an ideal MIS structure under an applied bias. Accumulation (A), depletion (B), and inversion (C) regimes.

In enhancement-mode operation of a *p-channel* OTFT, a negative voltage must be applied to the gate electrode to create an accumulation layer at the insulator/semiconductor interface. For depletion-mode operation, the accumulation layer is already present at zero gate voltage. Thus, for a *p-channel* TFT, a positive gate voltage has to be applied to deplete the accumulation channel and turn the device off. Therefore, an enhancement-mode device is a "normally-off" device, whereas a depletion-mode device is "normally on". In an ideal OTFT model in which traps are neglected, the OTFT would be an accumulation-mode device because of the presence of zero-bias carriers (bulk carriers) available for current conduction. However, the presence of doping or traps, may give rise to

depletion-mode operation of the OTFT. From this description we can appreciate that OTFTs differ from MOSFET in several aspects. Firstly, OTFT works in accumulation layer while MOSFET works under inversion layer. Secondly, thin film layers in TFTs are always grown on top of non lattice matching other materials. The lattice mismatch causes the layer to be amorphous with a high density of defects in particular at the dielectric/semiconductor interface. Thirdly, OTFT is undoped while MOSFET is mostly Si-doped.

- **OTFT architectures**

OTFTs can be fabricated on various types of rigid or flexible substrates, i.e., there is no need for an (expensive) single crystal wafer. There is no limit to the size or material properties of the substrate as long as it can stand the fabrication process environment. In addition, OTFTs can be made from a wide range of semiconductor and dielectric materials. OTFT can be configured into four basic structures on the basis of position of the electrodes as it is shown in Figure 5-3. The patterned source/drain electrodes can be deposited prior to the OSC deposition or after it. The former case is a ‘‘coplanar’’ configuration (popularly called Bottom-Contact, BC) and the latter is ‘‘staggered’’ configuration (also known as Top-Contact, TC). Both the staggered and coplanar configurations are further categorized as Bottom-Gate (BG) and Top-Gate (TG) structures. Different OTFT structures can display quite dissimilar device characteristics while using the exact same materials. In a coplanar configuration, the source drain contacts and the insulator layer are on the same part of the channel whereas, in a staggered configuration, the source drain contacts and the insulator layer are on the opposite part of the channel.

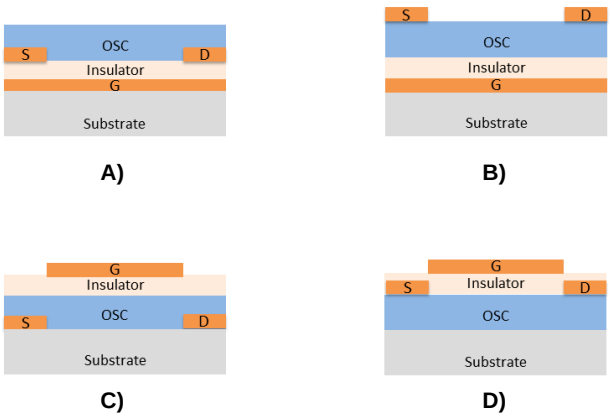

Figure 5-3 Schematic cross-section of common OTFT structures: A) bottom-gate and bottom-contact ; B) bottom-gate and top contact; C) top-gate and bottom contact, and D) top-gate and top contact.

This can be crucial in determining the carrier injection properties of the source/channel interface. In a coplanar structure the metal/semiconductor interface is from a physical point of view a metal/accumulation channel interface (there is an abundance of free carriers in both sides of the interface). Therefore, coplanar devices are expected to be more tolerant to the contact barrier effects. However, the presence of traps may degrade the injection properties of these interfaces. The option for a particular OTFT structure will depend essentially on the fabrication technology available (evaporation, spin coating or printing) and on the best way to achieve clean (trap-free) interfaces.

The Bottom Gate-Bottom Contact (BG-BC) structure is commonly used for fabricating OTFTs since the OSC is deposited at least, without limit prior processing steps. One major disadvantage of this structure is the large contact resistance due to the very small effective area for charge injection into the channel. Moreover, this configuration has the disadvantage that the OSC is deposited on two different materials simultaneously (i.e., the gate dielectric and the source/drain contacts), so that the morphology of the organic thin film can be disrupted by the non-uniformity of the prior profile. Usually, the TC structure exhibits much better performance than the BC structure with source and drain contacts below the semiconductor layer. The advantage of this structure is low contact resistance, due to the large effective area for injecting charge into the semiconductor channel.

In Bottom Gate-Top Contact (BG-TC) structure, the induced channel occurs on the opposite side of the deposited channel material compared to where the source and drain contacts are located. Thus, the main disadvantage of this configuration is that the charges have to transport from the source to the channel through an undoped highly resistive semiconductor layer. Thus, the experimentally obtained mobility and threshold voltage of OTFTs can exhibit thickness dependence.

The Top Gate-Top Contact (TG-TC) is rarely used due to the very small effective area for charge injection into the channel that determines very large contact resistance. In this configuration, since the organic layer should be deposited before other processing steps, the gate insulator could not be compatible with physical deposition methods such as sputtering, due to the damage to the organic material caused by energetic ions during deposition.

Also in the case of Top Gate-Bottom Contact (TG-BC) structure, the gate insulator and gate electrode can act as an encapsulation layer protecting the organic material from moisture or oxygen degradation. Nevertheless, there is a number of process integration challenges associated with this configuration. First, the gate dielectric and gate electrode have to be deposited and structured on top of the OSC layer, and this process must preserve the organic material. Secondly, vertical interconnections and vias between the conductive layers have to be built through the OSC. While this configuration allows that the channel forms

independently from substrate induced interactions, the roughness of the semiconductor-insulator interface in this geometry is determined by the organic thin film, and it is typically much worse than thermal SiO_2. On the other hand, a fundamental advantage of this structure is represented by the low contact resistance, due to the large effective area for injecting charge into the semiconductor channel, which corresponds to the gate/drain and gate source overlap areas.

- **OTFT Working principle**

  In OFETs the current flowing is assured by the direct injection of charges into the source and drain electrodes. The charge injection strongly depends on the matching between the Fermi level of the metal electrodes and HOMO and LUMO of the OSC. In the first models, it was assumed that the vacuum levels of molecular orbitals at the metal-semiconductor interface were aligned according to the Schottky-Mott model, developed for the inorganic semiconductors. As shown in Figure 5-4, the hole injection barrier (Φ_H) was defined through the difference between the ionization energy of the semiconductor (I_E) and the metal work function (Φ_M); the electron injection barrier (Φ_E) was defined through the difference between the electrode work function (φ_M) and the organic electron affinity (E_A).

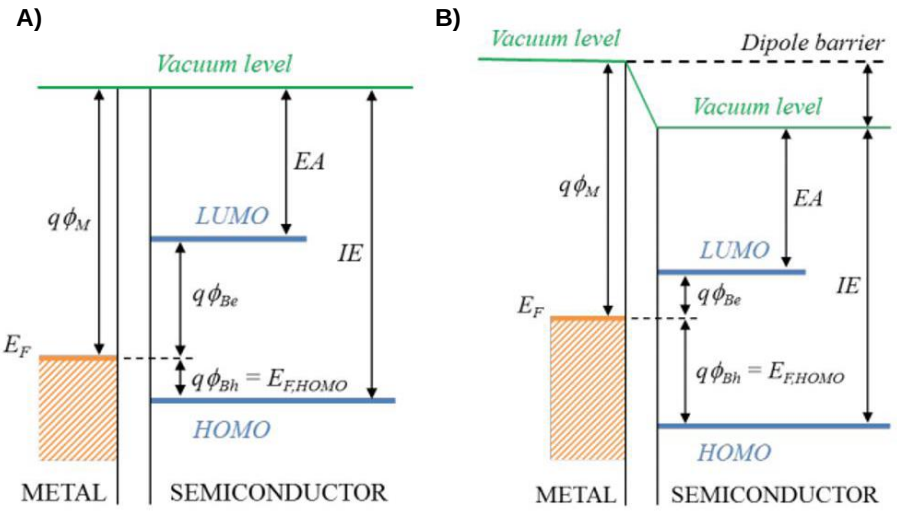

Figure 5-4 Energy diagram of a metal-organic semiconductor interface without (A) and with (B) a dipole barrier.

Afterwards, further studies demonstrated that when atoms and molecules are adsorbed or deposited on the metal surface, there is a breakdown of the vacuum levels alignment. The shift of the metal work function entails the change of the hole and electron injection barriers and, as a consequence, it establishes the type

of charge carriers in the OSC. In a device with the Fermi level of the source and drain electrode close to the HOMO of the semiconductor, holes can be injected/extracted. When the gate is negatively biased with respect to the source (Figure 5-5A), holes are attracted in the channel within few angstroms from the insulator-semiconductor interface and can be driven from source to drain by applying a negative voltage between drain and the source. On the contrary, when the gate voltage is reversed, electrons are induced in the channel. As the Fermi level of the metal is far from the LUMO of the semiconductor, the electron injection/extraction is very unlikely, therefore, no current flows through the semiconductor except for leaks through the insulating layer. In this case, the organic material is named *p-type* as holes are the majority charge carriers, and the device is named *p-channel* as it is activated upon the application of a negative gate potential. OFET with the Fermi level of the source and drain metal close to the LUMO of the semiconductor has a symmetrical behavior. As electrons can be extracted from the source and drain contacts, the current flows when negative charges are induced in the channel, that is, when the gate is positively biased (Figure 5-5B). In this case the semiconductor is called n-type, because electrons are the majority carriers, and the device is named n-channel.

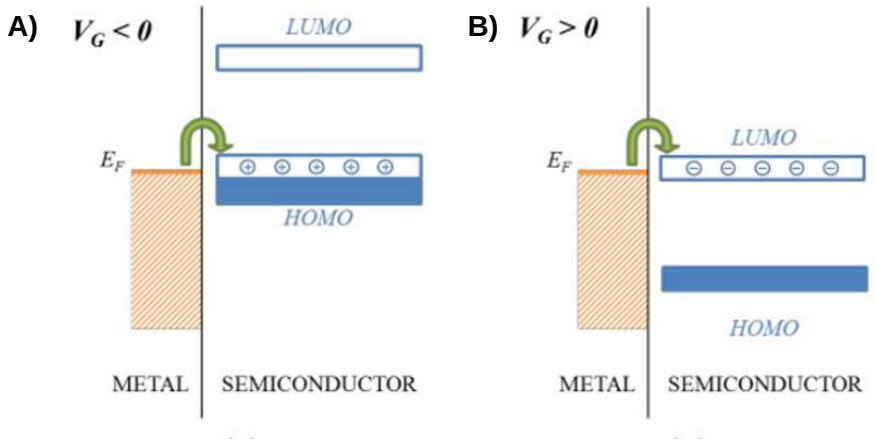

Figure 5-5 Charge injection with respect to the applied voltage in a p-type semiconductor (A) and in a n-type semiconductor (B).

Thus, unlike the classical MOSFETs, which typically work in inversion mode, OFETs always work in accumulation mode. The conduction mainly occurs, in the on-state, due to the layer of charge carriers which forms in the semiconductor within few angstroms from the insulator/semiconductor interface, and after the application of a suitable V_G. Thereby, OTFTs operate through the creation and elimination of a sheet of charge carriers at the gate dielectric/semiconductor interface. These charges are of the same type of the majority charge carriers responsible of the current in the off state. A small fraction of the total drain current is therefore determined by the free carriers in the semiconductor, which

can be thermally generated or produced by unintentional doping. Despite this fundamental difference, the characteristic equations of the inorganic MISFET transistors can be applied, as a first approximation, also to an Organic MISFET, that is:

$$I_{DS} = \mu C_I \left(\frac{W}{L}\right)(V_{GS} - V_T)V_{DS} \qquad \text{Equation 5-2}$$

in the linear zone, where and $V_{DS} < (V_{GS} - V_T)$ and,

$$I_{DS} = \frac{1}{2}\mu C_I \left(\frac{W}{L}\right)(V_{GS} - V_T)^2 V_{DS} \qquad \text{Equation 5-3}$$

in the saturation zone, where $V_{DS} \geq (V_{GS} - V_T)$.

The parameter L is the channel length of the transistor from source to drain in the direction of the current flow, W is the channel width of the transistor, C_I is the capacitance per unit area of the insulating layer, and μ is the field effect mobility. The nature and quality of the OSC is crucial for achieving high OFET performances, which are mainly determined by the charge carrier mobility that represents a measure of the charge carrier drift velocity per unit of electric field. The mobility is also directly related to the switching time of the device. The slope of the $I_{DS}^{1/2}$ versus V_G is related to the mobility for the saturation region due to the square law relation. For the case of the lineal region, the slope I_{DS} versus V_G is related to the mobility. Other important parameters are the Ion/Ioff ratio, which is the ratio between the current in the accumulation mode and the current in the depletion mode. The threshold voltage (V_T) is the V_G corresponding to the opening of the conduction channel. The I_{ON}/I_{OFF} ratio is indicative of the switching performance of OTFTs, ratios of 10^4-10^6 are suitable for most applications and can be reached by state-of-art OTFTs

5.1.1 | BioFET: Working principle

A BioFET contains the following parts: a semiconductor transducer, an insulator layer, a biofunctionalized surface, the analyte, and a reference electrode (the gate in FET terms). The stack of the BioFET is based on the electrolyte–insulator–semiconductor field-effect transistor which ensures the electrical detection of the

biomolecular interactions by their capacitive coupling with the OSC. A scheme of this device with its respective layers is shown in Figure 5-6.

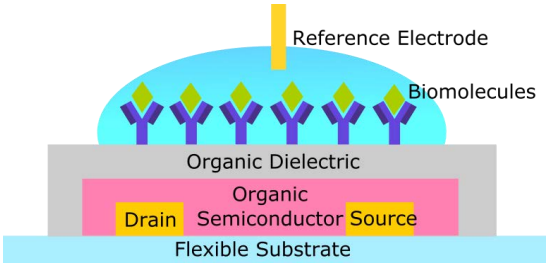

Figure 5-6. Scheme of BioFET. The device is composed by an OSC, insulator which contains onto it the biomolecules. The device is biased through an electrolyte and external reference electrode.

In these devices, the top gate contact is replaced by an electrolytic solution (usually phosphate buffer saline, PBS) and a reference electrode. The insulator layer is biofunctionalized which means that exhibits immobilized biomolecule receptors able to bind the desired molecule. The analyte is an electrolyte solution which contains the dissolved sample molecules. If the target molecules bind to the receptors, a change in the surface charge density occurs. This change alters the potential in the semiconductor and thus the conductivity in the channel of the field-effect transducer. The semiconductor transducer is realized by a conventional field-effect transistor. The insulator layer has two tasks: i) the first is to isolate the channel of the FET from the electrolyte and ii) the second is to electrostatically couple the surface layer charge into the channel.[4]

The amount of accumulated charge on the dielectric insulator gate in the BioFET can result in an increase (or decrease) of the source-drain current. This would create variations in the transistor responses (Current-Voltage curves) that are proportional to the amount of the introduced charge. If the change of the electrical charge is related to the interaction between biological molecules, then it can be used to monitor this process effectively and with very high sensitivity.

In order to understand the basic detection principle of a generalized (bio)chemical sensor, a simplified potential diagram is shown in Figure 5-7.[5]

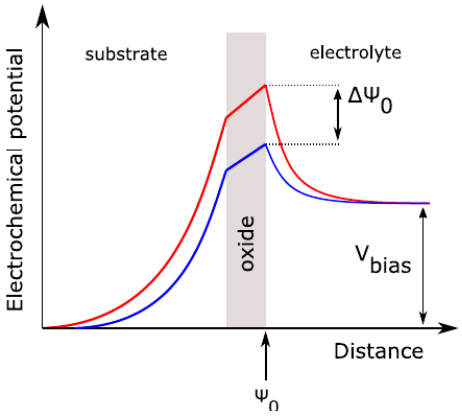

Figure 5-7. Potential over a simplified model of electrochemical cell with an oxide as the interfacial material. The charge binding in the surface creates a potential shift, denoted by $\Delta\psi_0$, at the interface.[4]

The observed responses of a (bio)chemical sensor are originated from the charge σ_0 at the sensing surface. The charge is related to the capacitance of the sensor. The overall sensor capacitance is a parallel combination of the double-layer and sensor (i.e., FET) capacitances, C_{DL} and C_{FET}, respectively, where the latter comprises the insulator gate, C_{INS}, and depletion, C_D, capacitances. The potential change at the sensing surface can be approximated by:

$$\varphi_0 = \frac{\Delta\sigma_0}{C_{DL} + C_{FET}} \qquad \text{Equation 5-4}$$

Depending on the transistor biasing, either of these capacitances can dominate. In weak accumulation, C_D will clearly be smaller and determine the overall sensor capacitance, in contrast to strong accumulation, where C_D is negligible and C_{INS} is relevant.[6] In either case, these capacitances are usually smaller than the double-layer capacitance. Thus, the double layer couples the potentials and, in many cases, it can be omitted from Equation 5-4. Hence, it can be concluded that in these cases the transistor capacitance has a poor effect at the sensing interface.

5.2 | DEVELOPMENT OF ORGANIC BIOFET USING MICROTECHNIQUES

Solution processed OFETs have been extensively studied thanks to their attractive features, such as cost-effectiveness, lightness, mechanical flexibility, and, often, biocompatibility. Currently, the emerging field of organic electronics is driven by the

possibility of achieving mass-scale production by using, for example, roll-to-roll techniques. These characteristics make them ideal candidates for applications, such as sensors,[7][8][9] radio frequency identification,[10],[11] and flat-panel displays,[12],[13] among others. Furthermore, the considerable effort made to optimize OSCs has led to the development of OFETs that can operate in air and humidity for an extended period of time.[14],[15]

Thus, OFETs have the potential to be used as transducers for biological and chemical sensors. Usually, BioFETs represents an OFET that contains a functionalized layer onto which biomolecule receptors, able to bind the analyte, are immobilized. One of the main advantages of BioFETs is their capability of delivering a label-free response, using an electronic read-out set-up.[8]

The most reported BioFETs are based on Organic Electrochemical Transistors (OECTs) and Electrolyte Gated OFETs (EGOFETs).[16][17][18][19] In these structures, detection relies on the functionalization of the OSC layer, which interfaces with an electrolytic solution. For OECTs, the electrolyte is capable of modulating OSC electrical behavior through doping/de-doping mechanisms, while only capacitive processes occur in EGOFETs due to the formation of an Electrical Double Layer (EDL) at the electrolyte/semiconductor interface. However, this characteristic is also one of the main disadvantages of these approaches due to the possible degradation of the OSC caused by its direct exposure to the aqueous medium. On the other hand, in top-gate bottom-contact BioFET geometry, the OSC is not directly exposed to the sensing environment as it is protected by the dielectric, which is in direct contact with the medium to be analyzed. The bio-recognition element is anchored onto the dielectric surface, which acts as the sensing area. This configuration ensures field-effect operation without charge transfer between the electrolyte and the organic semiconductor. This approach has shown good performances thanks to a good operational and environmental stability.[20][21] The working principle is based on a change in the insulator surface potential when the analyte binds to the immobilized biomolecule. The main requirement to operate and to properly transduce this binding event is an effective gate coupling via a field-effect resulting from a good electrical insulator. Thus, it is imperative to study and develop carefully engineered gate dielectrics that can reliably operate at relatively high electric fields.

Polymers are emerging materials in the development of biological opto-electro-mechanical systems thanks to their physical and chemical properties. They can be deposited fairly easily onto thin films by solution-based deposition techniques while their low thermal properties make them highly compatible with polymeric substrates. Numerous works have studied the electrical performance and relative ageing of these polymers when they are used as gate insulators or encapsulation layers.[22][23] [24][25] However, the reliability of bio-functionalized insulating polymers employed in top-gate BioFET structures in relation to the leakage of current across them under relatively high electric fields, is still under-represented in the literature. Moreover, the reliability, stability, and reproducibility of biomolecule immobilization onto sensing areas need to

be assured in top-gate BioFET devices. Recent methods in the attachment of bioactive compounds to polymer surfaces use wet chemical treatments, such as organofunctional silanes,[26] ionized gas treatments, and UV irradiation,[27][28][29] among others. To obtain a stable attachment, and thus a more reliable sensor, the formation of a covalent bond between the biomolecule and the surface is required. These functionalization methods generally require salt-based buffers, organic solvents, and frequently, oxygen plasma treatments that can promote the diffusion of mobile ions inside the polymers causing physical and/or chemical interactions and modification. Moreover, prolonged exposure of polymers to these reagents can also irreversibly damage their insulating properties, producing electrical breakdowns, making it difficult to obtain reliable BioFETs.[30][31][32]

In this context, we present herein a systematic study on a novel, highly-reliable flexible organic top-gate BioFET that uses a perfluoropolymeric material as both a gate insulator and a transducing layer. An electrical characterization of different organic insulators was carried out to obtain a reliable organic insulator which could operate correctly in aqueous media. Amorphous perfluoropolymer dielectric (Cytop^{TM}) was chosen for its favourable insulating properties and used to subsequently develop a reliable functionalized top-gate BioFET. Also advantageous is the fact that immobilization of the receptors onto the insulator by covalent bonding can be achieved using a very simple method involving a model protein. To verify the effectiveness of the immobilization procedure in terms of leakage current, optical (fluorescence) and electrical characterizations over the insulator layer were performed. To the best of our knowledge, this is the first time that such important studies with interest for BioFET development have been reported. The main advantage of the proposed methodology is that it does not require any specialized equipment and thus, can be conducted in most laboratories. Finally, to demonstrate that the developed procedure can be used in immunosensing analysis, the detection of a model antibody was carried out to propel the device into this research field.

5.2.1 | BioFET fabrication

MIE fabrication: MIE devices were fabricated on 125 μm thick Poly/ethylene-2,6-napthalene dicarboxylate (PEN) Teonex Q65HA substrates from Dupont Teijin specially developed for flexible electronics. After cleaning with organic solvents, titanium (Ti) and gold (Au) bottom electrodes (100 nm thick) were thermally evaporated through a shadow mask. Separate depositions of cPVP, SU-8, PMMA and Cytop were carried out as follows. The cPVP was prepared by dissolving PVP in PGMEA at room temperature and the resulting solution was stirred for 30 min. The deposition was carried out by spin coating at 1000 rpm for 30 sec and the resulting layer was then cured at 200 °C for 20 min. The SU-8 was spin-coated at 3000 rpm for 20 sec. and at 5000 rpm for 20 sec and then cured at 95ºC for 30 min and 1 min under UV-source. The PMMA was deposited by spin-coating at 1500 rpm for 30 sec. onto the

metallic electrode, and then cured at 150 °C for 90 sec. on a hot plate. The Cytop solution (CTL-809M with a concentration of 9%, Asahi Glass), without further dilution, was deposited by spin-coating at 1000 rpm for 30 sec. and then cured on a hot plate at 100ºC for 120 min.

Top-gate BioFET fabrication: Flexible bottom-gate BioFETs were fabricated on 125 μm thick Poly/ethylene-2,6-napthalene dicarboxylate (PEN) Teonex Q65HA substrates from Dupont Teijin specially developed for flexible electronics. After cleaning with organic solvents, titanium (Ti) and gold (Au) source and drain electrodes (100 nm thick) were thermally evaporated through a shadow mask having a channel width (W) of 1.5 mm and length (L) of 60 μm. The p-type SP400 OSC from Merck Chemicals were spin-coated at 500 rpm for 15 sec. and after at 1500 rpm for 120 sec. and the solvent was removed by thermal annealing on a hot plate at 100ºC for 120 sec. Finally, the OSC layer was covered with Cytop solution (CTL-809M with a concentration of 9%, Asahi Glass), without further dilution, and was deposited by spin-coating at 1000 rpm for 30 sec. and then cured on a hot plate at 100ºC for 120 min.

Surface functionalization of the Cytop: oxygen plasma was carried out using a microwave plasma generator (Smart Plasma system, Plasma Technology GmH). The condition used was 70W plasma power for 180 sec. Anhydrous 3-aminopropyltriethoxysilane (APTES, 99%) was purchased from Sigma Aldrich and used as received. The hydrolyzed APTES solution was obtained by mixing 95 mL of absolute ethanol and 5 mL of deionized water, and by adding drop by drop 5 mL of APTES under continual stirring. The top-gate BioFETs were immersed in this solution for 120 min. at room temperature, followed by thorough rinsing with ethanol to remove any excess reagent. Finally, the APTES-modified Cytop was heated in a hot plate at 100ºC for 120 min. and then stored in a desiccator under vacuum until further use. Phosphate buffer saline, MES buffer and EDC/NHS were obtained from Sigma Aldrich. Bovine serum albumin (BSA) labeled with Alexa Fluor 555 dissolved in PBS was acquired from Thermofished.

Electrical characterization: A Pt wire immersed in the electrolyte was used to modulate the channel conductivity by a applying a voltage between the electrode and the source contact. All the electrical measurements were carried out using an Agilent B1500A Semiconductor Analyzer. The images were acquired using a light microscope DM4000 from Leica. All the measurements were performed in ambient conditions.

Surface characterization: The layer thicknesses for the dielectric layers were evaluated using a mechanical surface Dektak profilometer. Atomic Force Microscopy images were carried out using a Nanoscope Veeco Dimension 3100. X-ray photoelectron spectroscopy (XPS) analysis was performed in an ultrahigh vacuum apparatus built by SPECS Phoibos 150. The surface wettability was also performed using a contact angle analyzer. Measurements were performed at room temperature under open-air conditions using a DSA 100 contact angle measuring device (Krüss, Germany). Static contact angles were measured using the sessile droplet method.

Antibody immobilization and antigen detection: anti-Human IgG (anti-HIgG, ref. I1886; polyclonal antibody developed in goat), Human IgG (HIgG, ref. I2511) and goat IgG (GIgG, ref. I5256) were purchased from Sigma. The capture antibody was immobilized on the amine-functionalizated Cytop by dropping 20 μL of αHIgG solution at different concentrations prepared in PBS buffer of pH 7.4 and incubating during 90 min at room temperature in a humid ambient chamber. A washing step with PBS solution was then carried out. Subsequently, 20 μL of 0.5% casein (w/v) prepared in PBS buffer of pH7.4 were used to block the possible active binding sites on the BioFET surface. After 60 min incubation at room temperature and further washing with PBS buffer (pH7.4), the immunoreaction was performed by placing 20 μL of a 400 $\mu g \cdot mL^{-1}$ solution of HIgG and leaving for 90 min at room temperature. Finally, the BioFET was rinsed with PBS buffer (pH 7.4) to remove unbounded HIgG prior to the electrical measurements. The same experimental procedure was followed for the control assays, performed with GIgG instead of HIgG.

5.2.2 | Assessment of organic dielectrics for top-gate BioFETs

Perfluoropolymers are the most used insulating polymers as barrier layers in order to protect the OSCs against environmental conditions. These materials present interesting characteristics, such as high electrical breakdown and low water absorption, thanks to the presence of strongly electron-withdrawing groups, making them a good choice for top-gate OFET and BioFET applications.[1],[33] At the same time, because of their hydrophobic nature, the grafting of biomolecules on their surfaces is challenging. Seldom have top-gate BioFETs been reported using perfluoropolymers as the gate insulator. Most of them employ conventional, expensive, and time-consuming techniques, such as Chemical Vapor Deposition (CVD), Plasma Enhanced-CVD (PE-CVD) and high temperatures,[22],[34] to functionalize these materials. Thus, a deep insight into gate dielectric perfluoropolymers-based materials needed to be carried out to ensure a proper functionalization of their surfaces using cost-effective methods without affecting their insulating properties. In particular, the well-known commercial perfluoropolymer Cytop was used in this study.

For comparison purposes, other commonly used organic insulators such as cross-linked poly(4-vinylphenol) (cPVP), [35],[36] epoxy (SU-8), [37],[38] and poly(methyl methacrylate) (PMMA),[39] were evaluated due to their good insulating characteristics and low-temperature processing.

It is known that ions from aqueous solutions and salt-based buffers, typical during working with biological samples, can penetrate into polymer films producing breakdowns through electrolytic processes.[40],[41] The main goal of this work was to engineer a reliable gate polymeric dielectric which can operate in aqueous media. Thus, the performances of the dielectrics under these conditions were investigated at the beginning of the study.

Metal/Insulator/Electrolyte (MIE) capacitors were fabricated for each insulator using a metallic bottom electrode. cPVP, SU-8, PMMA, and Cytop were deposited by the spin-coating technique. Figure 5-8A shows the MIE structure and the molecular structures of each polymer. An electrolytic solution based on Phosphate Buffer Saline (PBS), the most common biological buffer, was placed on top of the insulators. The polarization of the electrolyte was done by immersing a platinum wire into the electrolyte as can be seen in Figure 5-8B. The capacitance and resistance values measured for each dielectric are shown in Figure 5-8C. Impedance Spectroscopy analysis was carried out on these structures to study the resistance of the MIE capacitor. Furthermore, process yield was addressed to ensure a good fabrication methodology over 25 capacitors for each dielectric. The dielectric thicknesses for all the dielectrics were in the range of 800 nm - 1µm. The cPVP structure presented a low resistance and a poor yield and more than 80% were short-circuited. For SU-8, the obtained resistance was from a fairly good insulator but it failed as an endurable dielectric with a yield of 80%. Cytop and PMMA dielectrics presented the highest process yields of almost 100%, thus assuring reliable devices. The PMMA layer had a resistance of 10^9 Ω, while the Cytop layer was one order of magnitude higher at 10^{10} Ω. In view of the electrical performances of the presented insulators, Cytop was chosen as the best candidate for developing the top-gate BioFETs used in this study.

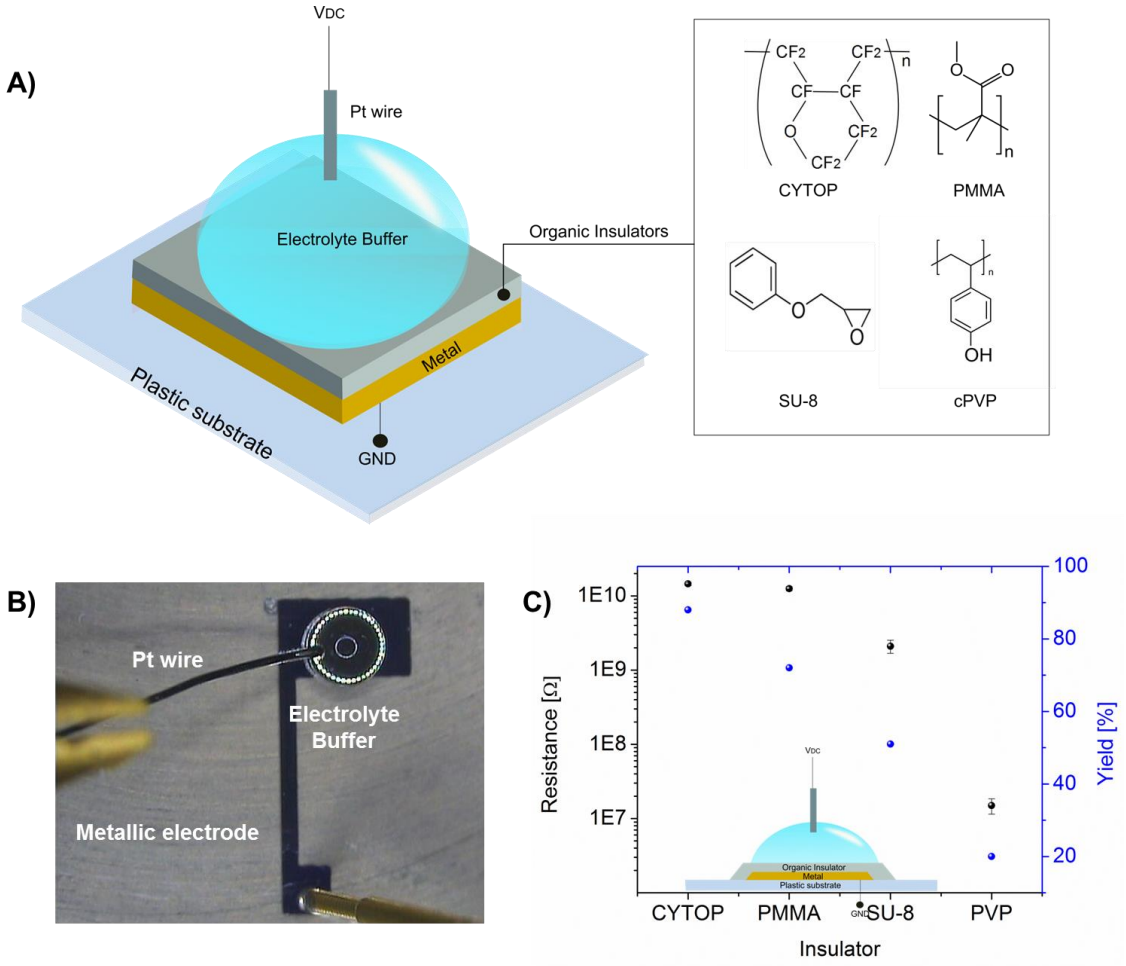

Figure 5-8 A) Scheme of the MIE structure and molecular structures of the organic insulator used. B) Optical image of the MIE electrical characterization and C) Resistance and device yield for each dielectric studied.

5.2.3 | Electrical and morphological study of perfluoropolymer gate dielectric for reliable BioFETs

As already underlined in the introduction, a good transduction of the binding event through an effective capacitive coupling is fundamental for obtaining a good sensor response. The electrical capacitance depends on the geometry of the device (A, area), the dielectric constant of the material (εr), and the film thickness (d), which is interesting because it can be easily controlled during the fabrication process. Thinner dielectric films will result in higher capacitance values and lower operating voltages. In order to find a good compromise between the Cytop thickness and the absence of electrical breakdown, an in-depth study on different thicknesses, surface topography and leakage current was carried out on the MIE structures. The dielectric was spin-coated onto the metallic electrodes at 500 rpm, 1000 rpm, 1500 rpm, and 2000 rpm. These structures were then characterized by performing Current-Voltage (C-V) curves from 0V to 30V. Additionally, in order to study the degradation of the performances under

electrical stress cycles, C-Vs measurements were recorded repeatedly (Figure 5-9.i). The C-V curves provide information about the leakage current across the insulator. Figure 5-9.ii shows the profile cross-sections of the spin-coated insulators over a metallic electrode. Although thinner thicknesses are desired to achieve higher capacitance values, for the Cytop deposition process leakage current is detrimental for the MIE structures fabricated at speeds of 1500rpm and 2500rpm. The current through the insulator reaches values of up to 10^{-4} A. However, at lower speeds, such as 1000rpm and 500rpm, leakage current is greatly improved. The 1000rpm MIE structures presented a current of up to $4.5 \cdot 10^{-11}$ A at 30V, which was maintained over repeated electrical measurements, while the 500rpm structures presented the lowest leakage current of $1.5 \cdot 10^{-11}$ A. From the profilometric analysis (Figure 5-9.iii), it is possible to observe a more regular surface for the 1000rpm, 1500rpm, and 2500rpm layers. The morphology of the layer deposited at 500rpm had the highest roughness because of the low speed process and the relatively high viscosity of the dielectric solution. From the Atomic Force Microscopy (AFM) analysis (Figure 5-9.iii), the evaluated Root Mean Square Roughness (RMSR) of the layers ranged between 0.4nm and 0.5nm. It is important to underline the absence of pinholes through the films.

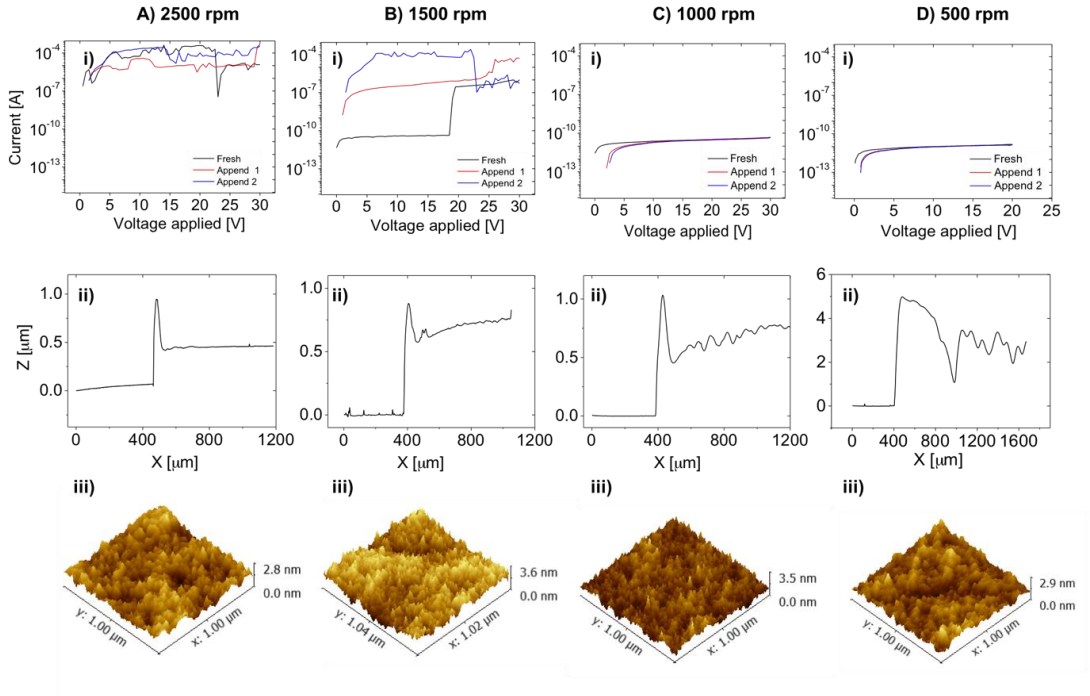

Figure 5-9 A), B), C) and D) show the i) leakage current of the MIE structures for a spin-coated speeds, ii) film thickness of Cytop layers, and iii) AFM topography for 2500, 1500, 1000 and 500 rpm respectively. The current-voltage curves show the current through the Cytop dielectric for a fresh and two append measurements.

Table 5-1 summarizes the main morphological and electrical parameters of the MIE structures. Although the lowest current was obtained for the layer deposited using 500rpm spin coating, its thicknesses varied in the range of microns without ensuring a

good reproducibility of the insulator film. For this reason, 500rpm was not considered for the fabrication of the BioFETs. A good compromise was achieved in terms of excellent electrical insulator performance, insulator thickness, and topography for the 1000rpm layers. This spin coating speed was, thus, chosen for further study of insulator performances.

Table 5-1 Profile thickness, surface roughness, leakage current and device yield for MIE structure for spin-coating speeds of 500, 1000, 1500 and 2000 rpm.

Spin-coating Speed	Profile Thickness [μm]	RMS roughnes [nm]	Leakage current at 20V [pA]	Yield [%]
500 rpm	2.0-3.5	0.38-0.52	12	83
1000 rpm	0.8-0,9	0.35	32	88
1500 rpm	0.7-0.8	0.39	310	58
2500 rpm	0.40-0.45	0.45	2300	20

5.2.4 | Biofunctionalization protocol of the perfluoropolymer for reliable BioFETs

Plenty of immobilization protocols have been developed to attach biomolecules on a wide variety of sensing layers.[27] However, the influence of these functionalization processes on the insulating properties of the organic dielectric materials is not yet well represented in the literature. For the first time, in this work, the optimization of a simple functionalization procedure that permits i) good immobilization of the biomolecule onto the Cytop film, ii) maintaining the insulating properties of the Cytop, and iii) achieving a good process yield, is presented. To this end, different functionalization parameters were considered: pH, type and concentration of the incubation buffers, dry and wet surface treatments, and the protein coupling agent. Bovine Serum Albumin (BSA) labeled with the fluorescent dye Alexa-555 were chosen as the model protein for this study. The efficiency of the immobilization process of the BSA was evaluated using fluorescence microscopy and surface modifications were checked after thorough washing of the modified surfaces. This study has been carried out directly on the MIE structures.

The effect of two of the most common buffer solutions on the devices was first investigated. Like PBS, 2-(N-morpholino)ethanesulfonic acid buffer (MES) is also used in the literature as a buffering agent in biology and biochemistry. It was also chosen because it is the most suitable buffer solution to stabilize the (1-Ethyl-3-(3-dimethylaminopropyl)-carbodiimide)/N-hydroxysuccinimide (EDC/NHS) coupling agent. EDC/NHS chemistry was performed to assist the formation of the amide bond between the amine and carboxylic ends. EDC is a zero-length crosslinking agent commonly used to couple carboxyl or phosphate groups to primary amines and NHS was used to increase the stability of this esterification.[42][43] For both solutions, conventional pHs and concentrations were chosen (see section 5.2.1). As shown in Figure 5-10, a high leakage current and poor device yield was obtained when the 100mM MES buffer was employed (A2). This indicated that this MES buffer provokes irreversible changes to the insulating polymer and should be omitted. For this reason, the same test was performed decreasing the buffer concentration (A3, A4). Considering the obtained results, it was clear that the 10mM PBS (A1) and 10mM MES (A4) buffer solutions lead to the best electrical device characteristics and they were therefore chosen for the subsequent functionalization procedures.

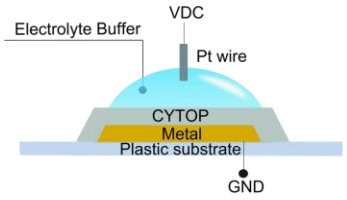

	pH	Electrolyte Buffer	Buffer concentration [mM]
A1	7	PBS	10
A2	5	MES	100
A3	5	MES	50
A4	5	MES	10

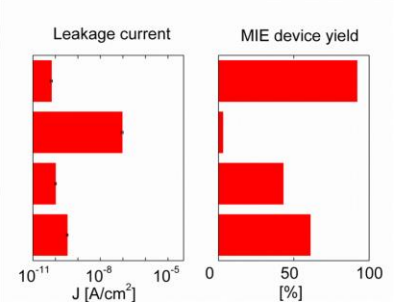

Figure 5-10 Scheme of MIE structure using Cytop as an insulator. The table shows the electrolyte buffer and its concentrations. Leakage current and MIE device yield is shown for each buffer used

The different immobilization procedures used in this paper are shown in Figure 5-11. Initially, a straightforward immobilization procedure based on physical absorption was considered (see Figure 5-11, recipe B1). The absence of a fluorescence signal in Figure 5-11-B1, clearly indicated that the protein could not be attached using weak, electrostatic or van der Waals interactions. This has already been observed in the literature.[44] Taking this result into account, a common oxygen plasma surface treatment was then considered. Oxygen plasma is widely used to activate organic dielectrics.[45],[46] It has been demonstrated that it can be employed to increase the binding strength and the active site available for protein by increasing the surface roughness and the chemical-physical activation of oxygen functional groups on a polymer surface.[47],[48] However, since plasma treatments can etch the polymer and may damage the structural properties of the sensing devices, a soft plasma process with low power for 3 minutes was carried out (see section 5.2.1). The treatment efficiency

was studied using both PBS (pH7.4) and MES (pH 5) buffers. As can be observed in recipe B2 (Figure 5-11), the fluorescence intensity is increased due to the attachment of the BSA onto the Cytop using oxygen plasma treatment and PBS as the buffer. However, the surface coverage is not homogenous as lower efficiency results when the pH 5 buffer is employed (Figure 5-11 recipe B3).

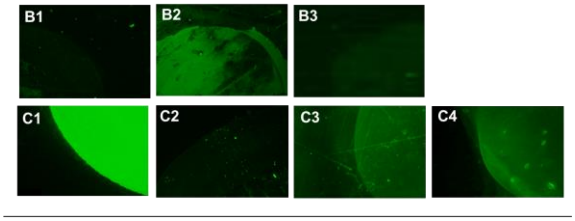

	Incubation Buffer [10mM]	O_2 plasma	BSA coupling agent	APTES
B1	PBS	-	-	-
B2	PBS	applied	-	-
B3	MES	applied	-	-
C1	MES	applied	EDC/ NHS	applied
C2	PBS	applied	EDC/ NHS	applied
C3	PBS	applied	-	applied
C4	MES	applied	-	applied

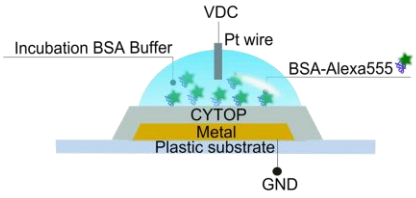

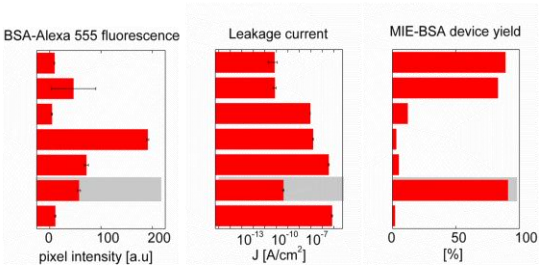

Figure 5-11 Scheme of the MIE structure is shown. The protein used to study the immobilization protocol efficiency was BSA labeled with Alexa555. Fluorescence images (B1-C4) are shown for each recipe. The BSA fluorescence intensity, leakage current and MIE device yields are shown for each recipe (B1 to C4).

Thus, a silanization treatment was introduced to provide an amine-terminated Cytop surface onto which a covalent bonding with the BSA carboxylic ends could be easily formed. The amino-(3-aminopropyl)triethoxysilane (APTES) was coupled to the organic polymer. The surface was previously activated through oxygen plasma treatment to promote the grafting of the APTES onto the insulator film.[42] The amino-functionalization was carried out by immersing the BioFET in an organic solvent-based APTES solution for 2 hours at room temperature (see section 5.2.1). The highest fluorescent intensity was achieved using the protocol based on EDC/NHS, APTES, oxygen plasma, and the MES buffer (Figure 5-11 recipe C1). It is worth mentioning that this recipe is commonly applied to electrochemical sensors to graft biomolecules onto the surface.[42] Nevertheless, this aggressive procedure was detrimental for the Cytop layer as it produced high leakage current leading to low device yield. The same conditions were adopted replacing the MES buffer with the PBS one. This approach substantially decreased the leakage current. However, the BSA immobilization was reduced because the EDC/NHS reaction performs better at pH 5 (Figure 5-11 recipe C2).[49] Less immobilization efficiency was achieved when the EDC/NHS was removed from the protocol, (Figure 5-11 recipe C3 and recipe C4). High leakage current persisted when MES was used as the incubation buffer. The best compromise in terms of BSA immobilization efficiency, leakage current, and device yield was obtained for

the amine-functionalized Cytop surface performed in PBS buffer (Figure 5-11 recipe C3).

As a further demonstration of the effectiveness of the proposed protocol, a quantitative analysis was undertaken. The effect of the oxygen plasma treatment and the attachment of the APTES molecules onto the Cytop surfaces were confirmed by contact angle, AFM, and X-ray Photoemission Spectroscopy (XPS) analysis. Static water contact angle measurement serves as a quick check to confirm the modification of film surfaces. As can be seen in Figure 5-12.A, the contact angle decreases from 110º for untreated Cytop films to 47º upon plasma oxidation of the surface. The decrease in the hydrophobicity of the organic insulator is the consequence of the increase in the density of the oxygen-related moieties on its surface. The expected increase of the contact angle to 107º observed in the APTES treated insulator is in concordance with what is usually observed in amine-terminated surfaces.[19],[50] After the washing step to remove the excess of non-attached APTES, the same contact angle value was measured, indicating a good surface functionalization.

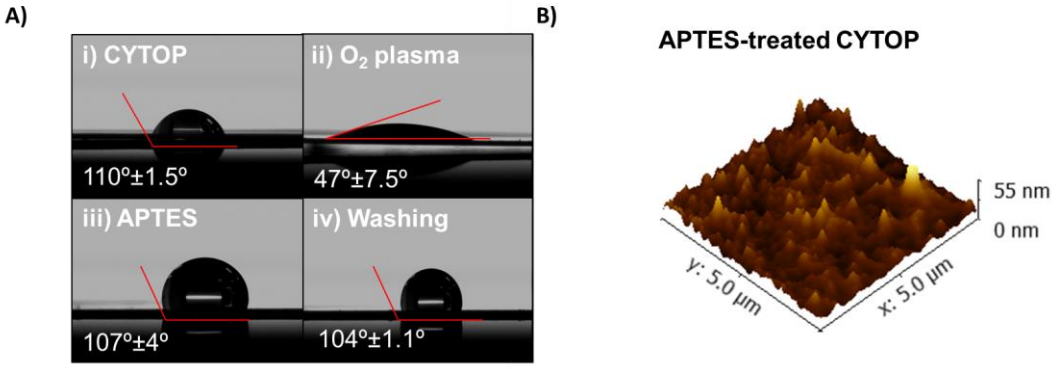

Figure 5-12 A) Contact angle measurement for i) Cytop, ii) oxygen treated Cytop, iii) oxygen and APTES-treated Cytop and iv) oxygen and APTES-treated Cytop after washing, B) 3D topographic AFM image for APTES-treated Cytop.

Additionally, a XPS survey scan was conducted to further confirm the presence of APTES on the Cytop surface. Figure 5-13 depicts the XPS spectra from the Cytop surface before (i) and after (ii) the functionalization procedure. The F 1s peak appears in both spectra at around 689eV, the energy value typical of organic fluorine and already reported for Cytop.[51] Upon APTES functionalization of the Cytop layer, nitrogen and silicon peaks appear on the XPS spectrum (Figure 5-13.ii and upper-left and upper-right insets). These confirm APTES conjugation to the Cytop surface since APTES contains both a terminal amino group and a terminal silicon group which are not present in the bare Cytop, as indicated in Figure 5-13.A and in Figure 5-8. The nitrogen peak at around 400eV can be attributed to the APTES terminal amino group, which at the pH =7.4 utilized in this study, may exist in three different forms (NH_3^+, hydrogen-bonded

NH_2 group (NH_2-H, and free NH_2), as already observed elsewhere.[52] Figure 5-13B shows a broad C 1s peak centered at around 290eV that can be easily attributed to the different C-F bonds of the Cytop molecule [53],[54]; while the C 1s peak at 285eV, shown in the upper central inset in Figure 5-13.B, is typical of the C-C alkyl chain that is present in APTES but not in Cytop.[55]

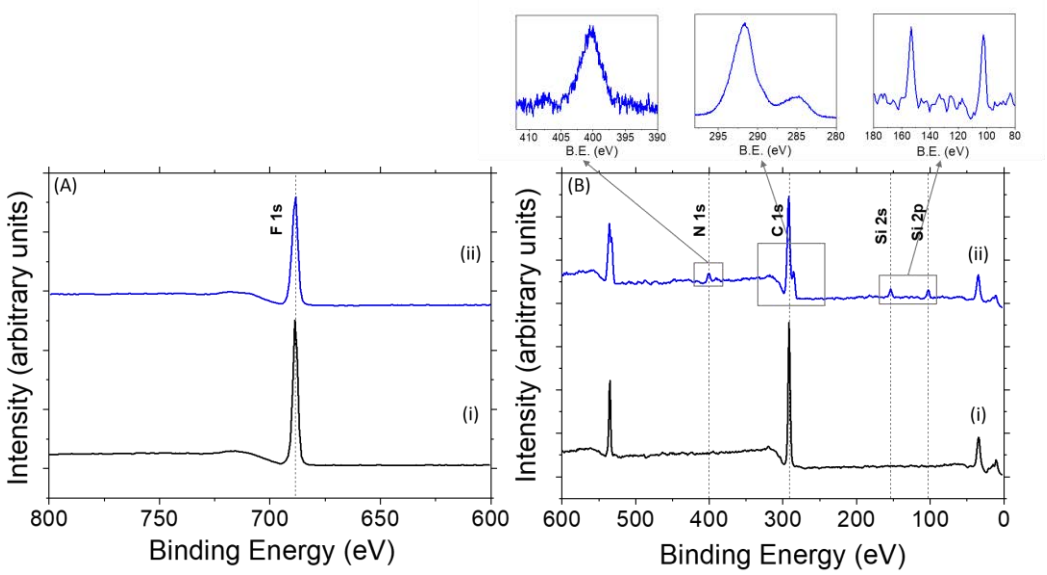

Figure 5-13 XPS spectra of CYTOP surface: before (i) and after APTES functionalization (ii): F 1s (A), N 1s (B), C 1s (B), Si 2s (B), and Si 2p (B). The insets show high-resolution XPS N 1s (left side), C 1s (central), and Si 2s Si 2p (right side) spectra from APTES functionalized CYTOP surface.

5.2.5 | Electrical characterization of top-gate BioFETs in aqueous media

Since the transducing interface of the BioFET structure was Cytop/OSC, the functionalization procedure was initially applied on a bottom-gate OFET with an insulator Cytop layer on the OSC film. This geometry was chosen i) to evaluate the efficiency of the Cytop protecting the OSC from the surface treatments, and ii) to investigate the effect of the immobilization protocol on the Cytop/OSC stack from an electrical point of view. Bottom-gate OFET geometry offers the possibility to separately study the effect of each functionalization step thereby avoiding the degradation of the materials due to the electrical stress induced by the gate voltage when a top-gate configuration is used.

Electrical characterization of the Cytop under immobilization protocol

A bottom-gate bottom-contact OTFT was used to independently measure the effect of the surface treatments and the capability to transduce the presence of the biomolecule when they were located the Cytop. Figure 5-14A and Figure 5-14B show a scheme and an optical image of the fabricated OTFTs, obtained from highly doped Si wafers covered with 300 nm of silicon dioxide (SiO_2) as a gate insulator. After cleaning with organic solvents, titanium(Ti) and gold (Au) source and drain electrodes (100 nm thick) were thermally evaporated through a hard mask having a channel width (W) of 4 mm and length (L) of 20 μm. Merck OSC was spin-coated at 500 rpm for 15 seconds and at 1500 rpm for 120 seconds. The solvent was removed by thermal annealing at 100ºC for 120 seconds. Finally, the OSC layer was covered with a Cytop layer deposited by spin-coating at 1000 rpm for 30 seconds and cured at 100ºC for 120 minutes (Figure 5-14A).

The functionalization developed in this work exposes the Cytop to harsh chemical and physical treatments: i) oxygen plasma and ii) APTES functionalization. Figure 5-14 C-i shows the transfer characteristics of the bottom OTFT for the two surface treatments. The oxygen plasma exposure induces small but nonetheless evident changes in the current. This indicates that the oxygen produces very small but measureable increase of the top Cytop capacitance which has been already observed in other works. [41] The electronegative nature of oxygen molecules can induce the formation of traps states resulting in an increase of the drain current and thus, of the transconductance. After the APTES treatment a decrease of the current was noticed. This behavior can be explained in terms of the presence of charges species. The APTES layer created onto the Cytop contains amino groups which could be in the form of NH_3^+, thus depleting the conduction bulk of the OSC. Finally, to demonstrate the capability of the Cytop/OSC interface to properly couple the biomolecules, a BSA solution was placed onto the Cytop. To discard the effect of the buffer, the BSA was left until dried. Figure 5-14Cii shows that the Cytop/BSA overlayer produced an increase of the drain current. This increase of the current is the result of the creation of new top second-current channel due to the BSA layer acting as a charged layer, as already observed in [44]. This confirms that the device is sensitive to a variation of charge amount on the top of the surface of the Cytop.

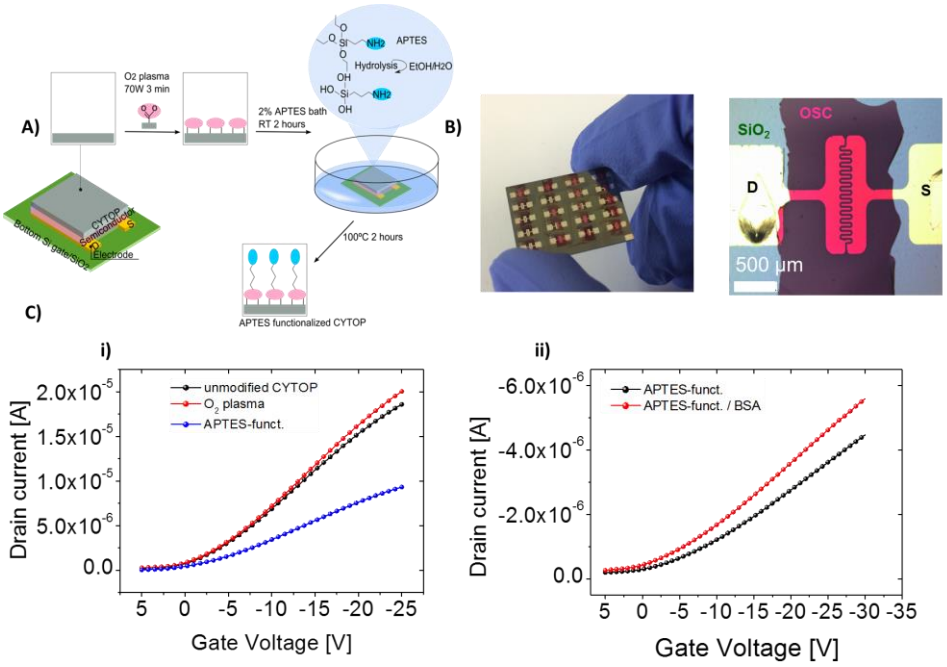

Figure 5-14 A) Scheme of the bottom-gate OTFT and the immobilization protocol applied. B) Optical image of the bottom-gate OTFT and the zoom of the device. C) Transfer characteristics of (i) oxygen plasma and APTES treatment and (ii) containing a BSA overlayer for bottom-gate OTFT.

5.2.6 | Electrical characterization of the top-gate Cytop BioFET

Afterwards, the device performances of top-gate BioFETs were investigated. Figure 5-15A and Figure 5-15B show an optical image and the structure scheme (for the fabrication process see section 5.2.1).

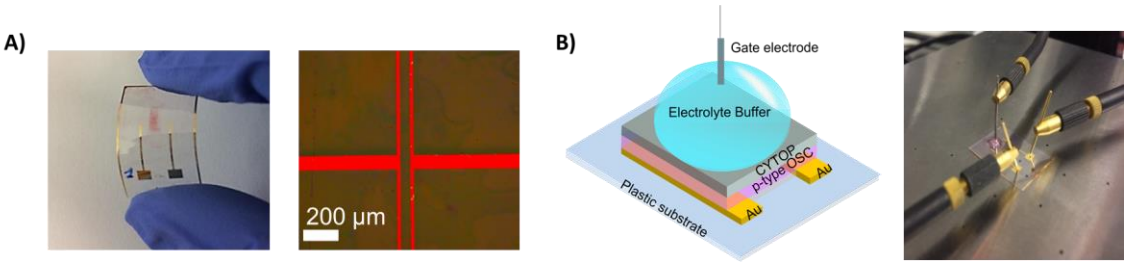

Figure 5-15 A) Optical image of the fabricated top-gate BioFET. The zoom shows the channel of the BioFET. B) Scheme and optical image of the electrical characterization set-up of the top-gate BioFETs.

Figure 5-16A and Figure 5-16B display the transfer and output characteristics of non-functionalized top-gate BioFETs in aqueous media. The transfer characteristics correspond to gate voltage (V_G) sweep while the drain-source voltage (V_{DS}) is kept constant. Output characteristics correspond to simultaneous V_G and V_{DS} sweeps. For all

devices, the mobility and the threshold voltages were estimated from the slope of the square of the drain current versus V_G. It is important to highlight that all the non-functionalized BioFETs presented hysteresis-free electrical behaviors, 15mV at worst, and operated at voltages lower than 10V. Furthermore, as a remarkable achievement in this work, the leakage current of the BioFETs was extremely low, in the range of tens of picoampers. Maximum field-effect mobility and I_{ON}/I_{OFF} ratio were 0.11 $cm^2/V \cdot s$ and 10^3, respectively. All the devices worked in enhancement mode, with threshold voltage values between -1.46V and -2.04V. Table 5-2 summarizes the main top-gate BioFET electrical parameters. The overall performances of the devices reported here are very promising as a good yield process was obtained thereby assuring a proper fabrication procedure that will enable a scalable production. Lower operation voltages could be achieved using crystalline OSCs with higher mobility. However, the occurrence of crystallization phenomenon is not suitable for top-gate configurations

Table 5-2 Electrical parameters of top-gate BioFETs without surface functionalization. All the electrical characteristics were measured under a 10 µL PBS droplet placed over the Cytop.

Vth [V]	µ [$cm^2/V \cdot s$]	I_{ON}/I_{OFF}	|Ig| [A]	Hysteresis [V]
-1.8±0.33	$(7.8\pm1.6)\cdot10^{-2}$	$(8\pm2)\cdot10^{2}$	$(-40\pm7)\cdot10^{-12}$	$(-15\pm0.2)\cdot10^{-3}$

In addition to the static electrical characteristics, operational stability over several cycles was evaluated to confirm the BioFET as a real sensor where several read-outs would be needed. Specifically, this dynamic test was carried out to reveal the time response of the BioFETs and to evaluate its possible degradation over time. It is known that water molecules can create deep traps under continuous bias stress.[41] Figure 5-16C shows a cyclic test where the BioFET was subjected to several on and off gate voltage cycles at constant drain voltage. The gate polarization was varied between -5V (on-state) and 0V (off-state) over 600 cycles, a frequency of 1Hz were employed. As can be seen, the drain current did not deviate, demonstrating the outstanding operational stability of top-gate BioFETs in aqueous media

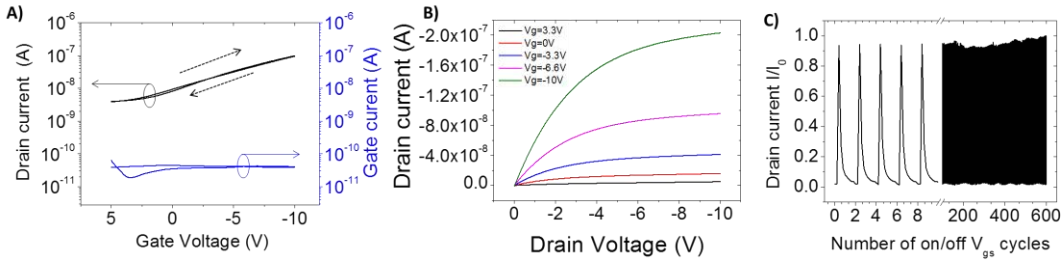

Figure 5-16 A) I_{DS}-V_{GS} and I_{GS}-V_{GS} curves of top-gate BioFET, B) Output characteristic for top-gate BioFET and C) I_{DS} vs V_{GS} (-5V to 0V) at a V_{DS} (-5V) measured up to 600 cycles. All the electrical characteristics were measured under a 10 µL PBS droplet placed over the Cytop layer.

5.2.7 | Antibody immobilization and antigen detection: immunosensing on the BioFET

The immobilization of anti-human IgG (αHIgG) model antibody was first studied to evaluate the potential of the BioFETs as immunosensing platforms. αHIgG protein was immobilized onto the amine-functionalized Cytop insulator through peptide bonds (see section 5.2.1 and Figure 5-17) and its presence on the BioFET was monitored through changes in the drain current. As underlined in the introduction, the decrease/increase in the current is due to the presence of positively/negatively charged molecules that change the surface potential. αHIgG (Isoelectric Point (pI) 6.6-8.5) is negatively charged at the pH of the working buffer (pH 9), so an increase in the current is expected for an increase of the antibody concentration.[56] Figure 5-17B shows the drain current variation as a function of the antibody concentration (in the range between 0 and 500 $\mu g \cdot mL^{-1}$). The percentage change of drain current was evaluated from the transfer curves at the maximum V_{DS} as $\Delta I/I(\%)=[(I_{antibody}-I_0)I_0-1]\cdot 100$ being $I_{antibody}$ and I_0 the drain current with and without the presence of αHIgG. Analysis of the results indicates that the current increases when the antibody is attached onto the amine-functionalized Cytop film, as expected. It is possible to presume that the negative charges of the αHIgG attract the holes to the transistor channel region increasing the overall current.

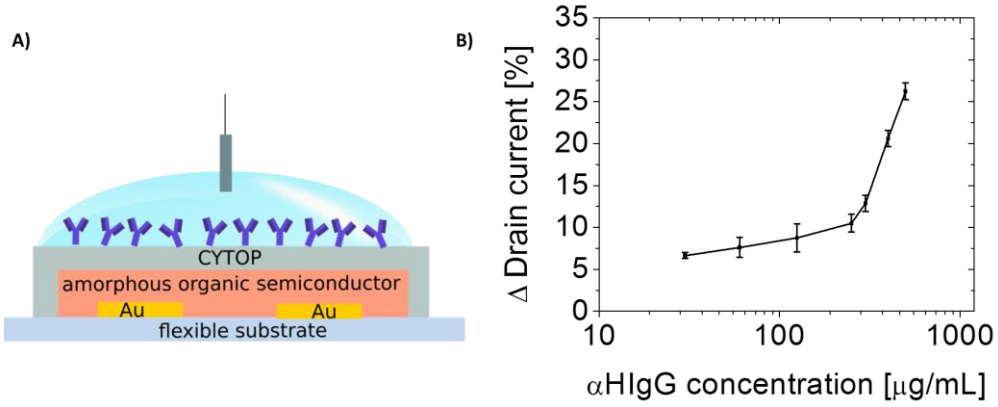

Figure 5-17 A) Schematic of a BioFET modified with αHIgG antibodies onto amine-functionalized Cytop B) Percentage of the change of the drain current (I_{DS}) from functionalized top-gate BioFET as function of αHIgG antibody concentration.

Human IgG (HIgG) antigen was finally evaluated as a model protein to be detected by the immunosensing system. The immunocomplex formation was monitored through drain current measurements. Antibody concentration was fixed at 400 $\mu g \cdot mL^{-1}$ and non-specific absorptions were avoided by the blocking of the BioFET surface with casein before the incubation of the antigen (see the section 5.2.1). Figure 5-18A shows the schematics of the immunosensing system. Blank assays were performed in the absence of antigen (in PBS solution) while control assays correspond to those performed with an unspecific protein (goat IgG (GIgG)). Figure 5-18B shows that an increase of 102% in the drain current was observed in the presence of the antigen due to the immunocomplex formation. A slight increase in the current was recorded for both the blank and the control assays, demonstrating the specificity of the immunosensing system.

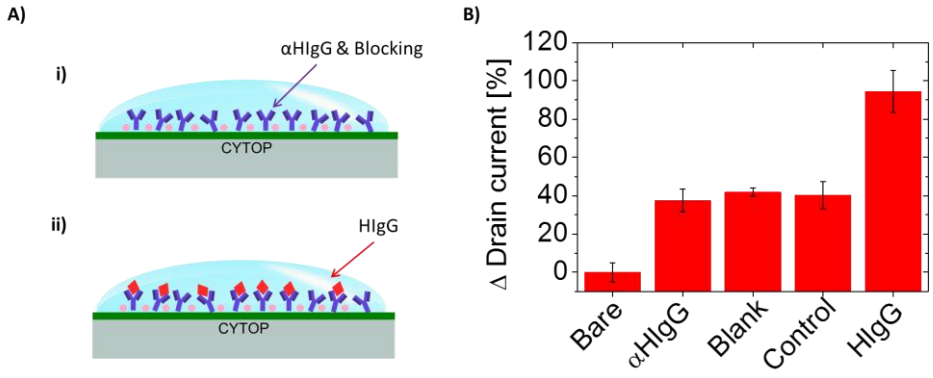

Figure 5-18 A) Schematic of the stepwise functionalization of the BioFET for: i) immobilization of antibodies αHIgG and the casein as the blocking agent to prevent non-specific absorption; and, ii) immunoreaction with HIgG specific antigen. B) Change of the IDS of the BioFETs for bare BioFET and the BioFET modified with antibody, before and after the immunoreaction with HIgG, as well as for the blank and control assays.

5.3 | DEVELOPMENT OF ORGANIC INKJET-PRINTED BIOFET

The development of solution-based materials has opened a new field to manufacture light-weight and flexible electronics using cost-effective processes.[66] Inkjet printing has been used as a method for depositing functional materials since it is a versatile approach for the deposition of small amounts of polymer solutions, small molecule dispersions, or nanoparticle suspensions that have specific electrical, optical, chemical, and biological properties onto well-defined locations of various surfaces and substrates.[67],[68] Moreover, inkjet printing technology is well suited for research, being a mask-less technology oriented to rapid prototyping for production.[69]

However, to the extent of our knowledge just few approaches of partially printed BioFET based on polymers for biomolecules detection have been studied.[70] The first to introduce an all-organic OECT biologically functionalized was proposed by Berthelot.[71] They realized inkjet-printed electrodes based on Poly(3,4-ethylenedioxythiophene):Polystyrene sulfonate (PEDOT:PSS) onto polyethyelene terephthalate (PET) film. The monoclonal murine antibodies (murine mAbs) were deposited by inkjet-printed onto the PEDOT:PSS channel as well. The protein deposition caused a decrease of the transconductance due to the ionic interaction. In the same field of FET biosensors, Fukuda et al. developed a bottom-gate bottom-contact OTFT were the gate, drain and source (D/S) electrodes were inkjet-printed using silver ink. The gate dielectric was deposited by chemical vapor deposition (CVD) and the OSC by a dispenser. An extended gate was used to immobilize the αIgG antibodies and the detection of the antigen IgG produced a change of the current.[72] A different approach was proposed by Liang et al. [73], developing a bottom-gate top-contact FET by printing few layers of MoS_2 flakes onto a Si/SiO_2 substrate as a channel. D/S electrodes were deposited by photolithography; afterwards a layer of SiO_x was sputtered onto them as passivation layer to minimize the leakage current among the D/S contacts and the microfluidic component. Finally, HfO_2 layers were deposited onto the MoS_2 channel as effective layer for biofunctionaliztion. αHuman TNF antibody receptors were attached to the sensing layer producing an increase of the drain current as the concentration of the TNF receptor increase. Moreover, it is worth mentioning that the use of 1D and 2D materials currently are being employed in the mentioned FET based sensors; but, the biggest limitations with using lower dimensional materials are the severe fabrication challenges, impairing their practical applications.

In literature, most studies report on bottom-gate OFETs on flexible substrate wherein the gate electrode and gate dielectric planarize the surface on the channel region or, wherein a planarization layer, typically parylene by CVD, is deposited onto the surface prior to the fabrication of the bottom-gate OFET structure.[22][74][75] Although bottom-gate OFETs can be engineered also to display low-voltage operation, the exposure of the semiconductor layer to the ambient (e.g. air or water) will eventually

lead to changes of the device performance, this feature have been exploited to develop sensors[76], but are less desirable to develop reliable electronic circuits. For this reason, we believe that the use of top-gate OFET geometry is particularly attractive because, in this geometry the OSC layer is protected from the environment while at the same time, the gate dielectric can be engineered to enable top-gate BioFET with biomolecules anchored onto it.

In this section, a fluoropolymer based BioFET has been considered for gate dielectric with the aim to protect the OSC from the surface chemical treatments to anchor the biomolecules. In order to obtain higher layer uniformity and relative thicker layer to avoid gate leakage current, the fluoropolymer was deposited by spin-coating. The D/S electrodes were inkjet-printed using a gold ink which allows i) the good alignment among the Work Functions (WF) of the OSC and the electrode avoiding the use of Self Assembled Monoloyers (SAM) and ii) decrease the cost of the production in comparison with the conventional evaporation technique. Besides, the OSC was also inkjet-printed in a confined area thus avoiding the cross-talking among the devices which is a typical issue from OSC spin coating films over a large area.

Therefore, this work proposes a simple but effective method to achieve inkjet-printed BioFETs for biosensing applications. The device based on top-gate bottom-contact BioFET benefits. In this section, the device developed is based on top-gate bottom-contact BioFET from the section 5.2 which benefits from using polymer based materials which can be produced using low-cost equipments and can be potentially scaled to large-area processes. At the same time, its architecture prevents the OSC to be in direct contact to chemical treatments, and environmental induced degradations.

5.3.1 | BIOFET fabrication

Top-gate inkjet-printed BioFET fabrication: BioFETs were fabricated on 125 μm thick Polyethylene-2,6-napthalene (PEN) Teonex Q65HA substrates from Dupont Teijin specially developed for flexible electronics. After cleaning with organic solvents, and to improve adhesion and the wettability of subsequent printed layers, oxygen plasma was carried out using a microwave plasma generator (Smart Plasma system, Plasma Technology GmH). The condition used was 40W plasma power for 20 sec. The drain and source had been patterned using a Dimatix Materials Printer 2831 (Fujifilm) under ambient conditions. A gold nanoparticle-based ink based on aqueous solution was employed (DryCure JB, Colloidal-ink Company). The ink was deposited using a single drop volume of 10 pL with a cartridge temperature of 35ºC in order to reach high resolution. A drop spacing of 25 μm was used, employing one nozzle and using a temperature of 45ºC. The printed layer was annealed in a hotplate for 45 min at 120ºC in order to remove the solvent and sinter the gold ink. The organic p-type semiconductor SP400-1750 from Merck Chemicals was patterned using inkjet printing technique. The ink was deposited using a single drop volume of 10 pL with a cartridge at room temperature. A drop spacing of 15 μm was used, employing one nozzle in order

to obtain a thin film. During the deposition, the printer platen was kept at room temperature. The printed layer was annealed in a hotplate for 2 min at 100ºC. Finally, the OSC layer was covered with Cytop solution (CTL-809M with a concentration of 9%, Asahi Glass), without further dilution, and was deposited by spin-coating at 1000 rpm for 30 sec. and then cured on a hot plate at 100ºC for 120 min.

Surface functionalization of the Cytop: oxygen plasma was carried out using a microwave plasma generator (Smart Plasma system, Plasma Technology GmH). The condition used was 70W plasma power for 180 sec. Anhydrous 3-aminopropyltriethoxysilane (APTES, 99%) was purchased from Sigma Aldrich and used as received. The hydrolyzed APTES solution was obtained by mixing 95 mL of absolute ethanol and 5 mL of deionized water, and by adding drop by drop 5 mL of APTES under continual stirring. The top-gate BioFETs were immersed in this solution for 120 min. at room temperature, followed by thorough rinsing with ethanol to remove any excess reagent. Finally, the APTES-modified Cytop was heated in a hot plate at 100ºC for 120 min. and then stored in a desiccator under vacuum until further use.

Electrical characterization: A Pt wire immersed in the electrolyte was used to modulate the channel conductivity by a applying a voltage between the electrode and the source contact. All the electrical measurements were carried out using an Agilent B1500A Semiconductor Analyzer. The images were acquired using a light microscope DM4000 from Leica. All the measurements were performed in ambient conditions.

Surface characterization: The layer thicknesses for the dielectric layers were evaluated using a mechanical surface Dektak profilometer. Atomic Force Microscopy images were carried out using a Nanoscope Veeco Dimension 3100.

Antibody immobilization and antigen detection: anti-Human IgG (anti-HIgG, ref. I1886; polyclonal antibody developed in goat) and Human IgG (HIgG, ref. I2511) were purchased from Sigma. The capture antibody was immobilized on the amine-functionalizated Cytop by dropping 20 µL of αHIgG solution at 400 μgmL^{-1} prepared in PBS buffer of pH 7.4 and incubating during 90 min at room temperature in a humid ambient chamber. A washing step with PBS solution was then carried out. Subsequently, 20 µL of 0.5% casein (w/v) prepared in PBS buffer of pH7.4 were used to block the possible active binding sites on the BioFET surface. After 60 min incubation at room temperature and further washing with PBS buffer (pH7.4), the immunoreaction was performed by placing 20 µL of different concentrations solution of HIgG and leaving for 90 min at room temperature. Finally, the BioFET was rinsed with PBS buffer (pH 7.4) to remove unbounded HIgG prior to the electrical measurements

5.3.2 | Morphological study of inkjet-printed BioFET

In order to demonstrate the actual feasibility of inkjet-printed gold electrodes as D/S electrodes, gold ink has been used to print them, because it allows proper energy levels alignment with HOMO level of the OSC, thus forming a good injection at electrode/semiconductor interface. Seldom article have reported the use of gold ink for the fabrication of D/S electrodes. T.Minari et.al patterned the gold electrodes and the OSC by using the surface wettability difference. The gold ink was deposited by an applicator thanks to the previous selective wettability pattern by vacuum ultraviolet (VUV) irradiation.[77] Moreover, another interesting approach done by N.Zhao et al. obtained an inkjet-printed transistor with submicron resolution using lithographically defined hydrophobic patterns to facilitate the channel formation.[78] As can be observed, these works relies on the mechanism by which the channel formation is achieved by controlling the surface tension/wettability. To the best of our knowledge, this is the first work that use gold ink in a plastic substrate to fabricate inkjet-printed transistor-based biosensors, until now PEDOT:PSS and silver ink has been widely used for this purpose.[75][79][80]

When an inkjet-printed ink dries on the surface of a substrate, the solute is generally transported from the center to the edge, and the resulting solute film forms a non-uniform ring-like profile. Deegan et al. studied the so-called coffee-ring effect for colloidal suspension systems.[81] To suppress the coffee-ring effect and to obtain a flat pattern is one of the most important issues to be solved for the devices conformed by stacked layers such as capacitors and thin-film transistors. It is known that electrodes with a trapezoidal-shaped profiles triggers electrical breakdown strength than concave-shaped electrodes.[82]

In order to investigate the microscale features about the thickness and surface morphology of the printed electrodes, contact profilometry, scanning electronic microscope (SEM) and atomic force microscopy (AFM) analysis have been carried out. Contact profilometry was used to study the profile and the thickness of the inkjet-printed layers. AFM and SEM have been employed for evaluating the roughness of the surface. Figure 5-19A shows an optical image of one of the electrodes. From the profile thickness (Figure 5-19B), it is possible to observe that the inkjet-printed electrodes present a thickness ranging from 140 to 167 nm and a flat surface on top. These ultra-thin electrodes are in the range of nanometers of the most reported evaporated electrodes.[83][84][85][86] Although the very thin feature of the electrodes, the resistance measured was 44Ω/square. Wider electrodes were patterned for the D/S pads for a better conductivity while a narrow width was chosen for the channel. Figure 5-19C shows a SEM image where the Au particles were randomly merged together after the curing process, the overall density of Au nanoparticles is good, but a number of boundaries exist between them. AFM image clearly shows that the electrode consists of interconnected Au particles and voids. From AFM analysis (Figure 5-19.D), the root

mean square roughness (RMS) is 30 nm. The printed devices present a channel ranging from 38 to 47 µm.

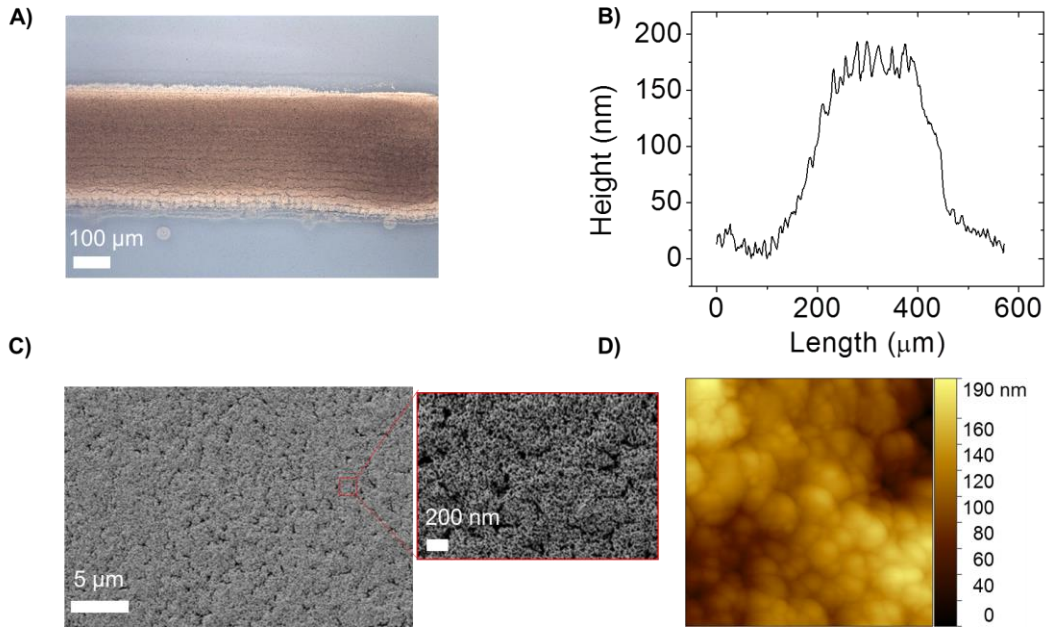

Figure 5-19.A) Optical image of a gold ink-jet printed electrode. Profile measurement B), SEM image C) and AFM image D) of inkjet-printed gold electrode.

Once the printing procedures of thin Au electrodes were assessed, the OSC was patterned into the channel by inkjet printing. Also, in this case, a thin layer is desired. Generally, thicker semiconducting films tend to create unfavorable current paths, which cause larger off-current levels.[36]

Since the BioFET is a stack of thin film layers and its structure is based on TGBC, the morphology of the OSC is paramount in order to achieve a high quality semiconductor/dielectric interface. Furthermore, small molecules based OSCs present larger surface roughness due to grain boundaries typical of polycrystalline materials that can be detrimental for the yield of the dielectric deposited on top.[87] Thus, for a better printability, amorphous OSC was chosen. In order to study the microscale features about the thickness and surface morphology of the inkjet-printed OSC, contract profilometry, SEM and AFM analysis have been carried out. Contact profilometry was used to study the profile and the thickness of the printed OSC layer. AFM and SEM have been employed for evaluating the roughness of its surface. Figure 5-20A shows the profile thickness, it is possible to observe that the inkjet-printed OSC presents a thickness ranging from 90 to 100 nm. This very thin layer is in the range of the spin-coated soluble processable OSC in the state-of-the-art.[88] SEM image shows a good uniformity of the inkjet-printed OSC layer (Figure 5-20B), but from AFM image some agglomeration typical of polymers are visible (Figure 5-20C). The roughness obtained

for the inkjet-printed OSC is 6.95 nm. Finally, the gate dielectric Cytop^{TM} was spin coated using the recipe developed in the section 5.2.1, leading a thickness of 1.2 µm.

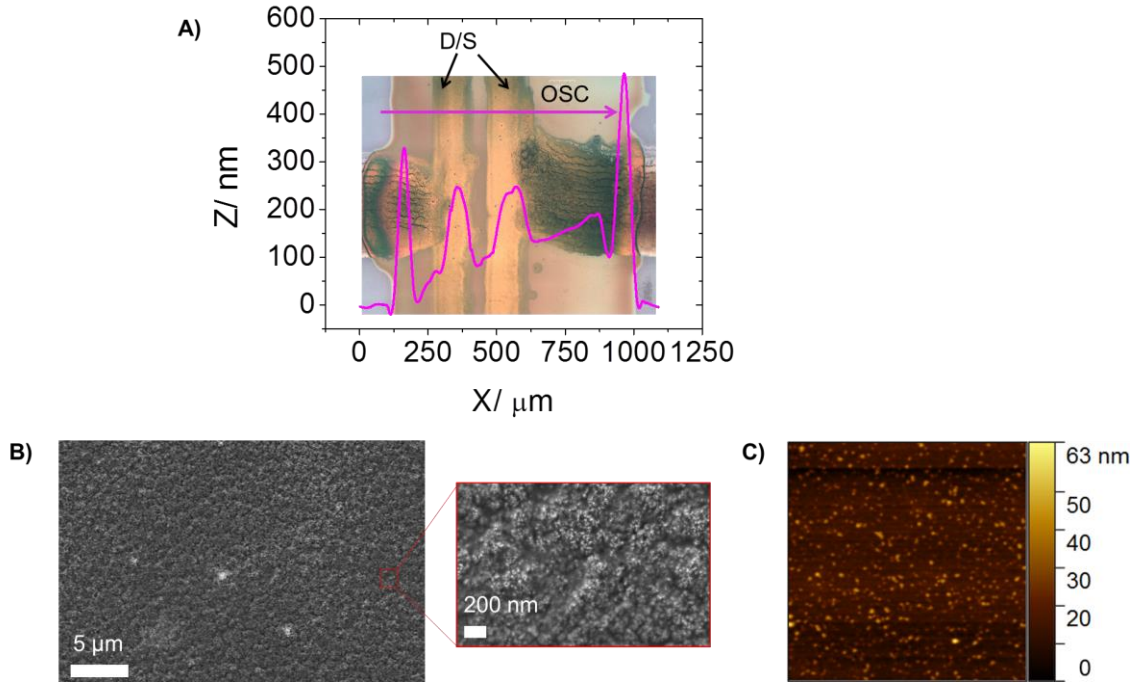

Figure 5-20 A) Profile measurement of the inkjet-printed OSC layer. The inset shows an optical image of the channel of the BioFET, the arrow shows where the profile was measured. B) SEM image C) and AFM image of inkjet-printed SP400 OSC layer.

Figure 5-21A and Figure 5-21B shows an optical image of the inkjet-printed gold electrodes and the BioFET device, respectively.

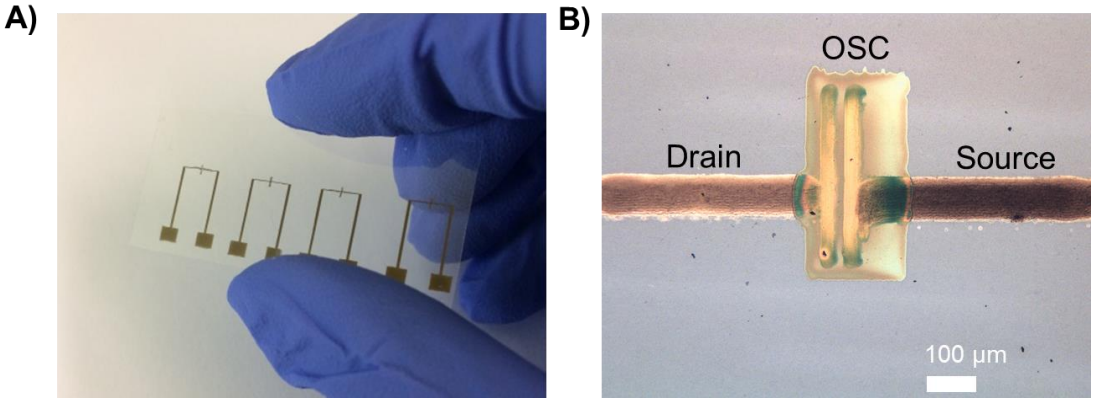

Figure 5-21 Optical image of A) inkjet-printed D/S gold electrodes and B) BioFET device.

5.3.3 | Electrical characteristics of top-gate inkjet-printed BioFETS in aqueous media

Figure 5-22A shows a scheme of the electrical characterization of the BioFET, a droplet of a phosphate buffered saline (PBS) placed onto the Cytop dielectric. Figure 5-22B and Figure 5-22C display the transfer and output characteristics of non-functionalized inkjet-printed top-gate BioFETs in aqueous media. The transfer characteristics correspond to gate voltage (V_G) sweep while the drain-source voltage (V_{DS}) is kept constant. Output characteristics correspond to simultaneous V_G and V_{DS} sweeps. For all devices, the mobility and threshold voltages were estimated from the slope of the square of the drain current versus V_G. It is important to highlight that all the non-functionalized inkjet-printed BioFETs presented near hysteresis-free electrical behaviors, 870mV at worst and 330mV at best case.

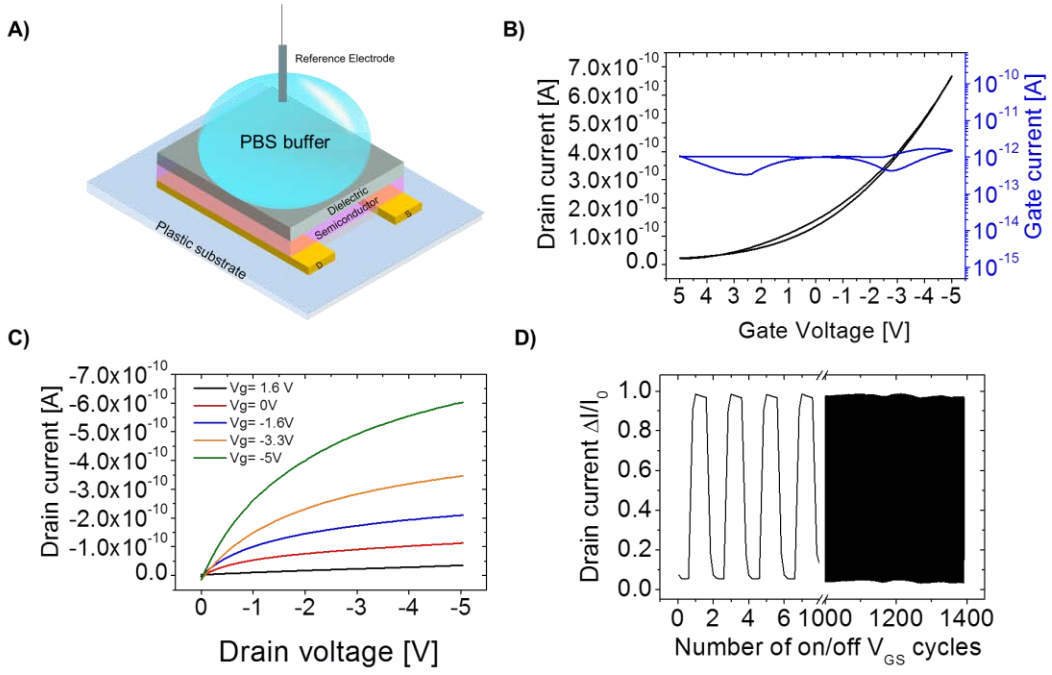

Figure 5-22 A)Scheme of the electrical characterization set-up of the top-gate inkjet-printed BioFETs B) I_{DS}-V_{GS} and I_{GS}-V_{GS} curves of top-gate inkjet-printed BioFET, C) Output characteristic for top-gate inkjet-printed BioFET and D) I_{DS} vs V_{GS} (-5V to 0V) at a V_{DS} (-5V) measured up to 1400 cycles. All the electrical characteristics were measured under a 10 µL PBS droplet placed over the Cytop layer.

From all the devices fabricated, the mobility values and threshold voltages have been estimated from the slope of the $\sqrt{I_{DS}}$ versus V_G. Furthermore, as a remarkable achievement in this work, the leakage current of the BioFETs was extremely low, in the range of tens of picoampers at -5V this means that BioFET can operate correctly at relative high voltage. Particularly, Figure 5-22B and Figure 5-22C shows the transfer curve and output curve until -5V to prove can also operate at significantly lower

voltages. Average field-effect mobility and I_{ON}/I_{OFF} ratio were $1 \cdot 10^{-3}$ $cm^2/V \cdot s$ and 70, respectively. All the devices worked in enhancement mode, with threshold voltage values of -0.5V. Table 5-3 summarizes the main top-gate BioFET electrical parameters.

Table 5-3 Electrical parameters of top-gate inkjet-printed BioFETs without surface functionalization. All the electrical characteristics were measured under a 10 µL PBS droplet placed over the Cytop

Vth [V]	µ [$cm^2/V \cdot s$]	I_{ON}/I_{OFF}	|Ig| [A]	Max. Hysteresis [V]	Min. Hysteresis [V]
-0.5±0.1	$(0.9 \pm 0.05) \cdot 10^{-3}$	69±18	$(-9.6 \pm 0.1) \cdot 10^{-12}$	0.87±0.12	0.33±0.11

In addition to the static electrical characteristics, operational stability of the BioFET over several cycles was evaluated. Figure 5-22D shows a cyclic test where the BioFET was subjected to several on and off gate voltage cycles at constant drain voltage. The applied gate bias was varied between 0V (off-state) and -5V (on-state) over 1400 cycles. As can be observed, the drain current did not deviate, determining the operational stability of top-gate BioFETs in aqueous media.

5.3.4 | Antibody immobilization and antigen detection: immunosensing on the inkjet-printed BioFET

As already studied in the chapter 5.2.4, the functionalization of the Cytop has been carried out using the molecule amino-(3-aminopropyl)triethoxysilane (APTES). More information about the recipe of the functionalization can be found in the section 5.3.1. The effect of the functionalization protocol onto the Cytop was confirmed by the transfer characteristics. Figure 5-23 shows the drain currents of non-functionalized and amine-functionalized BioFET.

As it can be observed, the drain current decreased due to the positive charges of the amine group. In addition, the low measured gate currents of dozens of pA suggests that electrochemical reactions (such as electrolysis) did not occur at the gate insulator of the BioFET during the biofunctionalization process.[89]

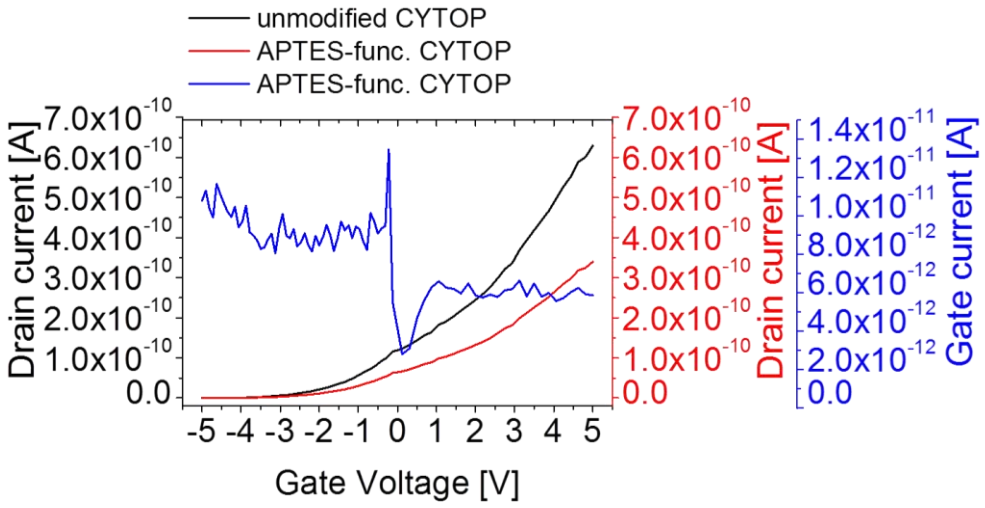

Figure 5-23 Drain and Gate currents for unmodified and APTES-functionalized Cytop. The gate current (blue line) corresponds to the leakage current for an APTES-functionalized BioFET.

Anti-human IgG (αHIgG) model antibody was firstly immobilized onto the amine-functionalized Cytop insulator through peptide bonds (Figure 5-24A). The αHIgG concentration was fixed at 400 $\mu g \cdot mL^{-1}$ and non-specific absorptions were avoided by the blocking of the BioFET surface with casein before the incubation of the antigen. Human IgG (HIgG) antigen was evaluated as a model protein to be detected by the immunosensing system. The immunocomplex formation was monitored through drain current measurements of the transfer characteristics. Figure 5-24B shows the drain current variation as a function of the HIgG concentration (in the range between 0 and 500 $\mu g \cdot mL^{-1}$). The percentage change of drain current was evaluated from the transfer curves at the maximum V_{DS} as $\Delta I/I(\%)=[(I_{antibody}-I_0)I_0-1]\cdot 100$ being $I_{antibody}$ and I_0 the drain current with and without the presence of HIgG. Analysis of the results indicates that the current increases when the antibody is attached onto the amine-functionalized Cytop film, as expected. A linear plot is obtained when relating the percentage change of drain current with analyte HIgG, the fitting function of the curve is $\Delta I/I(\%) = 0.21c$ (where c is the HIgG concentration) with an R^2 of 0.994. Figure 5-24B shows that an increase of 110% in the drain current was observed in the presence of the antigen due to the immunocomplex formation.

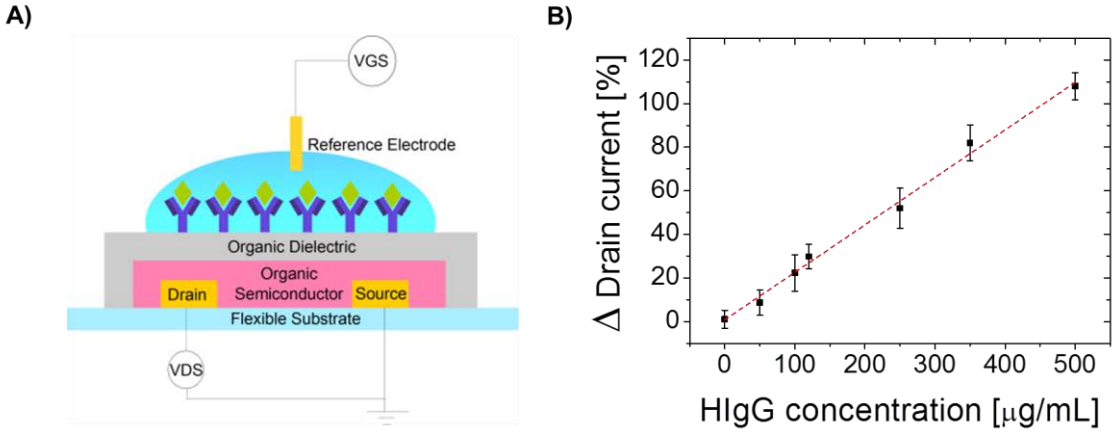

Figure 5-24 A) Schematic of a BioFET modified with αHIgG and HIgG antibodies blocked with casein onto amine-functionalized Cytop and B) Percentage of the change of the drain current (I_{DS}) from functionalized top-gate BioFET as function of HIgG antibody concentration.

As already mentioned, the presence of positively/negatively charged molecules changes the surface potential and therefore, it produces a decrease/increase of the drain current. The Isoelectric Point (pI) of the HIgG is about 6.6-8.5 [56] and it is negatively charged at the pH of the working buffer (pH 9), so an increase in the current is expected for an increase of the antibody concentration. It is possible to presume that the negative charges of the HIgG attract the holes to the transistor channel region increasing the overall current.

Then, the blank experiment is used to calculate the standard deviation (s.d.) for the limit of detection (LOD) value. In our case, the blank means that the experiment was performed the same as the sensing method mentioned above but without analyte. We took three times the value of the s.d. and divided it by the slope of 0.21 from the calibration curve to get a LOD of 5.71 $\mu g \cdot mL^{-1}$. The LOD could be improved theoretically with more controlled and uniform biomolecule attachment. However, this is beyond the scope of this work.

5.4 | CONCLUSIONS

As a first phase, a systematic study on the development of reliable and stable flexible top-gate BioFETs is presented using micro-fabrication techniques such as evaporation and spin-coating. An exhaustive electrical and morphological investigation on different gate insulators was carried out and Cytop was selected for its remarkable insulating properties. The Cytop film was optimized in terms of film thickness and leakage current and an amine-terminated Cytop surface was obtained via a silanization reaction with APTES, on which the immobilization of biomolecules was investigated. Qualitative spectra analysis confirmed the formation of the APTES layer. The protocol used to incubate and attach the antibodies onto the Cytop surface was optimized in order to preserve the insulating properties of the dielectric. It has been observed that MES buffer and the EDC/NHS coupling chemistry produce detrimental effects onto the Cytop. Despite the severe condition of the functionalization process under oxygen plasma and organic solvents and the continuous exposure of the devices to aqueous media, the top-gate BioFET presented remarkable hysteresis-free characteristics with state-of-the-art mobility values. The proposed immobilization protocol is simple and can be reproduced in other laboratory facilities without the use of expensive equipment. In addition, these results demonstrate the feasibility of monitoring the presence of biomolecules through changes in the drain current.

As a second phase, an inkjet-printed BioFET was developed using the same materials and architecture already used previously for the achievement of low-cost devices. The patterning of the D/S electrodes was carried out using a novel Au nanoparticle ink by inkjet printing technology. The low processing temperature (100ºC) on this ink enables use of plastic/paper as a substrate. Moreover, the inkjet-printed electrodes present interesting features such as few hundreds of nanometers of thickness and flat surface as the evaporated electrodes. The OSC was also patterned by inkjet printing technology. The thickness obtained is also in the range obtained by spin-coating technique, in the range of tens nanometers. Finally, the insulator Cytop was deposited by spin-coating following the previously developed recipe in the first phase of this work, thus ensuring a good operability. A deep characterization in terms of morphology has been carried out for the electrodes and the OSC. The electrical characterization of the inkjet-printed BioFET had values for μ of $\sim 1 \cdot 10^{-3}$, and V_T of -0.5V. In comparison with the BioFET fabricated in the first phase, the inkjet-printed BioFET presents an increase of the hysteresis behavior and lower I_{ON}/I_{OFF}. But, the gate leakage currents are comparable for both devices ensuring a good field-effect operation. Therefore, the inkjet-printed BioFET presents minimal lower performances due to the intrinsic limitation of the inkjet printing technology. The electrical performance could be improved by lowering the thickness of the electrodes. Finally, the BioFET was studied as a biosensor which it was functionalized with the already developed recipe in the first phase. The measured drain current as a function of the HIgG analyte has demonstrated the feasibility to use these kinds of devices to detect biomolecules.

Furthermore, thanks to the high operational stability and reliability, it is expected that this novel BioFET device will make an important contribution to the development of new top-gate BioFETs for immunosensing applications. As a future work, the BioFET should be tested under biological matrices such as plasma or urine. Moreover, the sensors should be characterized under dynamic electrical tests.

5.5 | REFERENCES

[1] Kalb WL, Mathis T, Haas S, et al. Organic small molecule field-effect transistors with Cytop^{TM} gate dielectric: Eliminating gate bias stress effects. *Appl Phys Lett* 2007; 90: 092104.

[2] Cheng X, Caironi M, Noh Y-Y, et al. Air Stable Cross-Linked Cytop Ultrathin Gate Dielectric for High Yield Low-Voltage Top-Gate Organic Field-Effect Transistors. *Chem Mater* 2010; 22: 1559–1566.

[3] Walser MP, Kalb WL, Mathis T, et al. Low-voltage organic transistors and inverters with ultrathin fluoropolymer gate dielectric. *Appl Phys Lett* 2009; 95: 233301.

[4] Kaisti M. Detection principles of biological and chemical FET sensors. *Biosens Bioelectron* 2017; 98: 437–448.

[5] Shoorideh K, Chui CO. On the origin of enhanced sensitivity in nanoscale FET-based biosensors. *Proc Natl Acad Sci* 2014; 111: 5111–5116.

[6] Streetman B, Banerjee S. *Solid State Electronic Devices*. Edición: 6. Upper Saddle River, NJ: Prentice Hall, 2005.

[7] Yan F, Mok SM, Yu J, et al. Label-free DNA sensor based on organic thin film transistors. *Biosens Bioelectron* 2009; 24: 1241–1245.

[8] Torsi L, Magliulo M, Manoli K, et al. Organic field-effect transistor sensors: a tutorial review. *Chem Soc Rev* 2013; 42: 8612–8628.

[9] Lai S, Demelas M, Casula G, et al. Ultralow Voltage, OTFT-Based Sensor for Label-Free DNA Detection. *Adv Mater* 2013; 25: 103–107.

[10] Rotzoll R, Mohapatra S, Olariu V, et al. Radio frequency rectifiers based on organic thin-film transistors. *Appl Phys Lett* 2006; 88: 123502.

[11] Myny K, Steudel S, Smout S, et al. Organic RFID transponder chip with data rate compatible with electronic product coding. *Org Electron* 2010; 11: 1176–1179.

[12] Zhou L, Wanga A, Wu S-C, et al. All-organic active matrix flexible display. *Appl Phys Lett* 2006; 88: 083502.

[13] Gelinck G, Heremans P, Nomoto K, et al. Organic Transistors in Optical Displays and Microelectronic Applications. *Adv Mater* 2010; 22: 3778–3798.

[14] Allard S, Forster M, Souharce B, et al. Organic Semiconductors for Solution-Processable Field-Effect Transistors (OFETs). *Angew Chem Int Ed* 2008; 47: 4070–4098.

[15] Zschieschang U, Ante F, Yamamoto T, et al. Flexible Low-Voltage Organic Transistors and Circuits Based on a High-Mobility Organic Semiconductor with Good Air Stability. *Adv Mater* 2010; 22: 982–985.

[16] Cramer T, Chelli B, Murgia M, et al. Organic ultra-thin film transistors with a liquid gate for extracellular stimulation and recording of electric activity of stem cell-derived neuronal networks. *Phys Chem Chem Phys* 2013; 15: 3897.

[17] Khodagholy D, Doublet T, Quilichini P, et al. In vivo recordings of brain activity using organic transistors. *Nat Commun*; 4. Epub ahead of print December 2013. DOI: 10.1038/ncomms2573.

[18] Rivnay J, Inal S, Salleo A, et al. Organic electrochemical transistors. *Nat Rev Mater* 2018; 3: 17086.

[19] Buth F, Donner A, Sachsenhauser M, et al. Biofunctional Electrolyte-Gated Organic Field-Effect Transistors. *Adv Mater* 2012; 24: 4511–4517.

[20] Hwang DK, Fuentes-Hernandez C, Kim J, et al. Top-Gate Organic Field-Effect Transistors with High Environmental and Operational Stability. *Adv Mater* 2011; 23: 1293–1298.

[21] Jung T, Dodabalapur A, Wenz R, et al. Moisture induced surface polarization in a poly(4-vinyl phenol) dielectric in an organic thin-film transistor. *Appl Phys Lett* 2005; 87: 182109.

[22] Khan HU, Jang J, Kim J-J, et al. Effect of passivation on the sensitivity and stability of pentacene transistor sensors in aqueous media. *Biosens Bioelectron* 2011; 26: 4217–4221.

[23] Ha T-J, Kiriya D, Chen K, et al. Highly Stable Hysteresis-Free Carbon Nanotube Thin-Film Transistors by Fluorocarbon Polymer Encapsulation. *ACS Appl Mater Interfaces* 2014; 6: 8441–8446.

[24] Kim W, Javey A, Vermesh O, et al. Hysteresis Caused by Water Molecules in Carbon Nanotube Field-Effect Transistors. *Nano Lett* 2003; 3: 193–198.

[25] Zan H, Hsu T. Stable Encapsulated Organic TFT With a Spin-Coated Poly(4-Vinylphenol-Co-Methyl Methacrylate) Dielectric. *IEEE Electron Device Lett* 2011; 32: 1131–1133.

[26] Joshi M, Pinto R, Rao VR, et al. Silanization and antibody immobilization on SU-8. *Appl Surf Sci* 2007; 253: 3127–3132.

[27] Kim D, Herr AE. Protein immobilization techniques for microfluidic assays. *Biomicrofluidics* 2013; 7: 041501.

[28] Laib S, MacCraith BD. Immobilization of Biomolecules on Cycloolefin Polymer Supports. *Anal Chem* 2007; 79: 6264–6270.

[29] Goddard JM, Hotchkiss JH. Polymer surface modification for the attachment of bioactive compounds. *Prog Polym Sci* 2007; 32: 698–725.

[30] Klauk H. *Organic Electronics II: More Materials and Applications*. John Wiley & Sons, 2012.

[31] Reliability of Organic Field-Effect Transistors - Sirringhaus - 2009 - Advanced Materials - Wiley Online Library, https://onlinelibrary.wiley.com/doi/epdf/10.1002/adma.200901136 (accessed 22 August 2018).

[32] Han SH, Kim JH, Jang J, et al. Lifetime of organic thin-film transistors with organic passivation layers. *Appl Phys Lett* 2006; 88: 073519.

[33] CYTOP™ Technical Information. *AGC Chemicals Europe*, https://www.agcce.com/cytop-technical-information/ (accessed 22 August 2018).

[34] Huang W, Besar K, LeCover R, et al. Label-free brain injury biomarker detection based on highly sensitive large area organic thin film transistor with hybrid coupling layer. *Chem Sci* 2014; 5: 416–426.

[35] Roberts ME, Queraltó N, Mannsfeld SCB, et al. Cross-Linked Polymer Gate Dielectric Films for Low-Voltage Organic Transistors. *Chem Mater* 2009; 21: 2292–2299.

[36] Fukuda K, Takeda Y, Mizukami M, et al. Fully Solution-Processed Flexible Organic Thin Film Transistor Arrays with High Mobility and Exceptional Uniformity. *Sci Rep* 2014; 4: 3947.

[37] Kim CH, Tondelier D, Geffroy B, et al. Characterization of the pentacene thin-film transistors with an epoxy resin-based polymeric gate insulator. *Eur Phys J Appl Phys* 2012; 57: 20201.

[38] Tetzner K, Bose I, Bock K, et al. Organic Field-Effect Transistors Based on a Liquid-Crystalline Polymeric Semiconductor using SU-8 Gate Dielectrics onFlexible Substrates. *Materials* 2014; 7: 7226–7242.

[39] Huang T-S, Su Y-K, Wang P-C. Poly(methyl methacrylate) Dielectric Material Applied in Organic Thin Film Transistors. *Jpn J Appl Phys* 2008; 47: 3185–3188.

[40] Ieda M. Dielectric Breakdown Process of Polymers. *IEEE Trans Electr Insul* 1980; EI-15: 206–224.

[41] Hwang DK, Fuentes-Hernandez C, Fenoll M, et al. Systematic Reliability Study of Top-Gate p- and n-Channel Organic Field-Effect Transistors. *ACS Appl Mater Interfaces* 2014; 6: 3378–3386.

[42] Vashist SK, Lam E, Hrapovic S, et al. Immobilization of Antibodies and Enzymes on 3-Aminopropyltriethoxysilane-Functionalized Bioanalytical Platforms for Biosensors and Diagnostics. *Chem Rev* 2014; 114: 11083–11130.

[43] Dixit CK, Vashist SK, MacCraith BD, et al. Multisubstrate-compatible ELISA procedures for rapid and high-sensitivity immunoassays. *Nat Protoc* 2011; 6: 439–445.

[44] Choi J, Jeon HG, Kwon OE, et al. Improved output characteristics of organic thin film transistors by using an insulator/protein overlayer and their applications. *J Mater Chem C* 2015; 3: 2603–2613.

[45] Grimaldi IA, Testa G, Persichetti G, et al. Plasma functionalization procedure for antibody immobilization for SU-8 based sensor. *Biosens Bioelectron* 2016; 86: 827–833.

[46] Landgraf R, Kaiser M-K, Posseckardt J, et al. Functionalization of Polymer Sensor Surfaces by Oxygen Plasma Treatment. *Procedia Chem* 2009; 1: 1015–1018.

[47] Yuan Y, He H, Lee LJ. Protein A-based antibody immobilization onto polymeric microdevices for enhanced sensitivity of enzyme-linked immunosorbent assay. *Biotechnol Bioeng* 2009; 102: 891–901.

[48] Bilek MM, McKenzie DR. Plasma modified surfaces for covalent immobilization of functional biomolecules in the absence of chemical linkers: towards better biosensors and a new generation of medical implants. *Biophys Rev* 2010; 2: 55–65.

[49] Nakajima N, Ikada Y. Mechanism of Amide Formation by Carbodiimide for Bioconjugation in Aqueous Media. *Bioconjug Chem* 1995; 6: 123–130.

[50] Tang L, Lee NY. A facile route for irreversible bonding of plastic-PDMS hybrid microdevices at room temperature. *Lab Chip* 2010; 10: 1274.

[51] Zheng Y, Shi W, Kong J, et al. A Cytop Insulating Tunneling Layer for Efficient Perovskite Solar Cells. *Small Methods* 2017; 1: 1700244.

[52] Williams EH, Schreifels JA, Rao MV, et al. Selective streptavidin bioconjugation on silicon and silicon carbide nanowires for biosensor applications. *J Mater Res* 2013; 28: 68–77.

[53] Hanada Y, Sugioka K, Midorikawa K. UV waveguides light fabricated in fluoropolymer CYTOP by femtosecond laser direct writing. *Opt Express* 2010; 18: 446–450.

[54] Yamada T, Fukuhara K, Matsuoka K, et al. Nanoparticle chemisorption printing technique for conductive silver patterning with submicron resolution. *Nat Commun* 2016; 7: 11402.

[55] Acres RG, Ellis AV, Alvino J, et al. Molecular Structure of 3-Aminopropyltriethoxysilane Layers Formed on Silanol-Terminated Silicon Surfaces. *J Phys Chem C* 2012; 116: 6289–6297.

[56] Determination of isoelectric points and relative charge variants of 23 therapeutic monoclonal antibodies. DOI: 10.1016/j.jchromb.2017.09.033.

[57] Sajid M, Osman A, Siddiqui GU, et al. All-printed highly sensitive 2D MoS2 based multi-reagent immunosensor for smartphone based point-of-care diagnosis. *Sci Rep*; 7. Epub ahead of print 19 July 2017. DOI: 10.1038/s41598-017-06265-1.

[58] Sirringhaus H, Brown PJ, Friend RH, et al. Two-dimensional charge transport in self-organized, high-mobility conjugated polymers. 1999; 401: 4.

[59] Huitema HEA, Gelinck GH, Putten JBPH van der, et al. Plastic transistors in active-matrix displays. *Nature* 2001; 414: 599.

[60] Baude PF, Ender DA, Haase MA, et al. Pentacene-based radio-frequency identification circuitry. *Appl Phys Lett* 2003; 82: 3964–3966.

[61] Torsi L, Dodabalapur A, Sabbatini L, et al. Multi-parameter gas sensors based on organic thin-film-transistors. *Sens Actuators B Chem* 2000; 67: 312–316.

[62] Kergoat L, Piro B, Berggren M, et al. Advances in organic transistor-based biosensors: from organic electrochemical transistors to electrolyte-gated organic field-effect transistors. *Anal Bioanal Chem* 2012; 402: 1813–1826.

[63] Sugano R, Tashiro T, Sekine T, et al. Enhanced memory characteristics in organic ferroelectric field-effect transistors through thermal annealing. *AIP Adv* 2015; 5: 117106.

[64] Minami T, Minamiki T, Hashima Y, et al. An extended-gate type organic field effect transistor functionalised by phenylboronic acid for saccharide detection in water. *Chem Commun* 2014; 50: 15613–15615.

[65] Huang W, Diallo AK, Dailey JL, et al. Electrochemical processes and mechanistic aspects of field-effect sensors for biomolecules. *J Mater Chem C* 2015; 3: 6445–6470.

[66] Someya T, Bauer S, Kaltenbrunner M. Imperceptible organic electronics. *MRS Bull* 2017; 42: 124–130.

[67] Organic Electronics II: More Materials and Applications. *Wiley.com*, https://www.wiley.com/en-es/Organic+Electronics+II%3A+More+Materials+and+Applications-p-9783527326471 (accessed 8 August 2018).

[68] Teichler A, Perelaer J, Schubert US. Inkjet printing of organic electronics – comparison of deposition techniques and state-of-the-art developments. *J Mater Chem C* 2013; 1: 1910.

[69] Sekitani T, Yokota T, Someya T. Large-Area, Printed Organic Circuits for Ambient Electronics. In: *Large Area and Flexible Electronics*. Wiley-Blackwell, pp. 365–380.

[70] Sarkar D, Liu W, Xie X, et al. MoS_2 Field-Effect Transistor for Next-Generation Label-Free Biosensors. *ACS Nano* 2014; 8: 3992–4003.

[71] Faddoul R, Coppard R, Berthelot T. Inkjet printing of organic electrochemical immunosensors. In: *2014 IEEE SENSORS*. 2014, pp. 1088–1091.

[72] Fukuda K, Minamiki T, Minami T, et al. Printed Organic Transistors with Uniform Electrical Performance and Their Application to Amplifiers in Biosensors. *Adv Electron Mater* 2015; 1: 1400052.

[73] Nam H, Oh B-R, Chen P, et al. Multiple MoS_2 Transistors for Sensing Molecule Interaction Kinetics. *Sci Rep* 2015; 5: 10546.

[74] Top-gate organic field-effect transistors fabricated on paper with high operational stability. DOI: 10.1016/j.orgel.2016.11.026.

[75] Conti S, Lai S, Cosseddu P, et al. An Inkjet-Printed, Ultralow Voltage, Flexible Organic Field Effect Transistor. *Adv Mater Technol* 2017; 2: 1600212.

[76] Zhang C, Chen P, Hu W. Organic field-effect transistor-based gas sensors. *Chem Soc Rev* 2015; 44: 2087–2107.

[77] Minari T, Kanehara Y, Liu C, et al. Room-Temperature Printing of Organic Thin-Film Transistors with π-Junction Gold Nanoparticles. *Adv Funct Mater* 2014; 24: 4886–4892.

[78] Zhao N, Chiesa M, Sirringhaus H, et al. Self-aligned inkjet printing of highly conducting gold electrodes with submicron resolution. *J Appl Phys* 2007; 101: 064513.

[79] Shiju K, Praveen T, Aneesh J, et al. Organic field effect transistor with conductivity enhanced PEDOT: PSS composite electrodes. Bikaner, Rajasthan, India, pp. 1139–1140.

[80] Sanyoto B, Kim S, Park W-T, et al. Solution processable PEDOT:PSS based hybrid electrodes for organic field effect transistors. *Org Electron* 2016; 37: 352–357.

[81] Deegan RD, Bakajin O, Dupont TF, et al. Capillary flow as the cause of ring stains from dried liquid drops. *undefined*, /paper/Capillary-flow-as-the-cause-of-ring-stains-from-Deegan-Bakajin/58a3d6931999d59bd35dbea5b288601ea0557e60 (1997, accessed 6 August 2018).

[82] Fukuda K, Sekine T, Kumaki D, et al. Profile Control of Inkjet Printed Silver Electrodes and Their Application to Organic Transistors. *ACS Appl Mater Interfaces* 2013; 5: 3916–3920.

[83] Janneck R, Heremans P, Genoe J, et al. Influence of the Surface Treatment on the Solution Coating of Single-Crystalline Organic Thin-Films. *Adv Mater Interfaces* 2018; 5: 1800147.

[84] A plastic electronic circuit based on low voltage, organic thin-film transistors for monitoring the X-Ray checking history of luggage in airports. DOI: 10.1016/j.orgel.2018.04.029.

[85] Ohyama A, Miyazawa J, Yokota Y, et al. Printing technology based on isotropic liquid phase of naphthalene diimide derivatives for n-type organic transistors. *Org Electron* 2018; 58: 231–237.

[86] Yang T, S. Mehta J, M. Haruk A, et al. Targeted deposition of organic semiconductor stripes onto rigid, flexible, and three-dimensional substrates. *J Mater Chem C* 2018; 6: 2970–2977.

[87] Don Park Y, Lim JA, Lee HS, et al. Interface engineering in organic transistors. *Mater Today* 2007; 10: 46–54.

[88] Zhang F, Di C, Berdunov N, et al. Ultrathin Film Organic Transistors: Precise Control of Semiconductor Thickness via Spin-Coating. *Adv Mater* 2013; 25: 1401–1407.

[89] Minamiki T, Minami T, Sasaki Y, et al. An Organic Field-effect Transistor with an Extended-gate Electrode Capable of Detecting Human Immunoglobulin A. *Anal Sci* 2015; 31: 725–728.

6

Conclusions and future work

This chapter describes the general conclusions of this thesis dissertation in relation with the initial objectives, and, afterwards, it lists open issues and potential future research goals.

As already stated, a new technology for low-cost and large area applications is emerging to cover the cost and technological gaps associated with conventional microelectronic processing techniques. The research, as well as the industry community, is working to lead the next electronic revolution at low-cost: Flexible, Organic and Large Area Electronics (FOLAE).

The main goal of this thesis has been to provide new approaches on the development of organic electronic devices with a particular attention devoted to gas sensing and biosensing applications. Specifically, the developed devices have the common objective to overcome the drawbacks derived from the current use of rigid and inorganic materials. Moreover, the use of printing techniques allows the fabrication of low-cost devices. Therefore, the focus of this research is the fabrication of new device configurations by controlling the morphology and the electrical parameters of the inkjet-printed materials on flexible substrates. The methodology for optimizing the technological parameters is presented for each fabricated device since each functional layer requires different manufacturing steps in order to obtain the best performances. The right combination of these parameters has allowed the achievement of new devices which can operate properly for the final sensing application.

In this thesis two different approaches for chemical and biological sensing platforms have been proposed.

The first approach is based on the use of inkjet-printed MIS diodes to detect NO_2 gas. Since the fabrication of MIS diodes is one of the most challenging research areas in Printed Electronics (PE) and represents a key future for the development of more complex circuits, a thorough investigation on the electrical properties of a polymeric rectifying interface has been successfully performed. The novel use of polymeric interfaces to obtain electrical rectifying behaviours opens a new research field for the fabrication of full inkjet rectifying circuits without the use of different metal electrodes. The deep study of the printing parameters of the MMAcoMAA dielectric has permitted the optimization of its deposition process and the subsequent development of diodes. The analysis of the dielectric surfaces pointed out that the chemico-physical properties of this layer have a key role on its electrical behaviour. Furthermore, it has been demonstrated the robustness and the versatility of the proposed structure since it can be fabricated using different dielectrics. These first results demonstrate an outstanding achievement that can be important from an industrial scale-up point of view. For the realization of the inkjet-printed sensor devices, an organic dielectric (cPVP) and high-mobility OSC (Merck SP400) has been used to obtain rectification ratios up to 3000 at |10V|. The MIS based sensors shows good electrical response to NO_2 against other gases such as EtOH, H_2 and, N_2. The interaction of the NO_2 molecules and the OSC produce an increase of the current proportional to the concentration of the gas that can be easily read. Figure 6-1 shows a table of contents with the most representative results for the chapter "*Inkjet-Printed MIS diode-based sensors*".

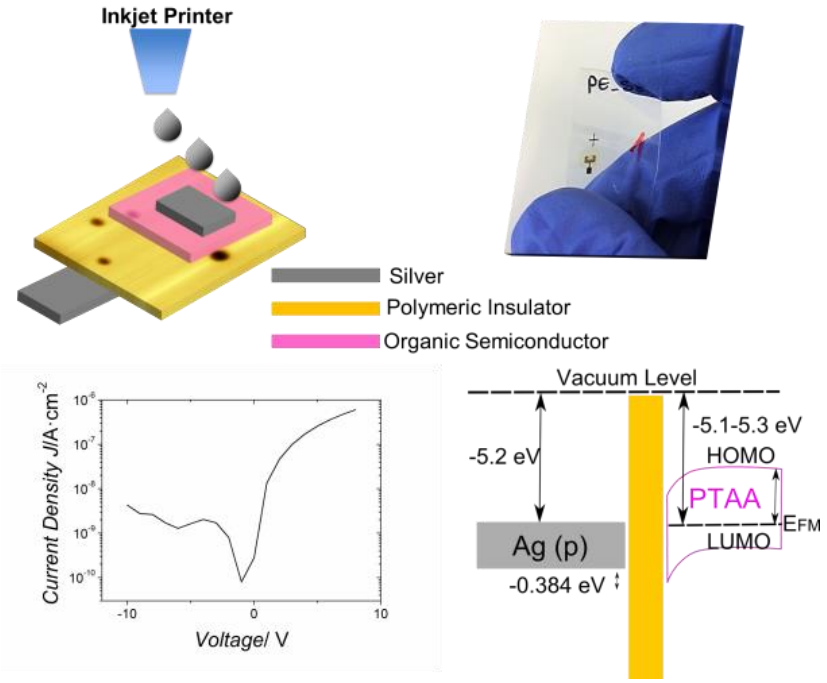

Figure 6-1 Inkjet-printed MIS diode fabricated with organic materials.

The second approach is based on the use of organic BioFETs to detect biomolecules. In order to achieve functional devices, the development of these sensors have been carried out using two different methodologies: during a first phase, conventional microfabrication techniques were employed while, in the second phase of the research, inkjet printing technique was used to deposit the thinnest components of the devices, i.e. the OSC and the drain-source electrodes. This procedure was chosen to initially study and optimize the materials using a mature technology. Different aspects of the BioFET have been addressed:

- A thorough study of the leakage current through the Cytop™ insulator as a function of its thickness has been performed allowing the achievement of very good insulating properties when operated under aqueous media (leakage currents down to dozens of 10^{-12}A).
- A simple and effective functionalization method has been proposed to attach biomolecules onto the hydrophobic Cytop™ surface. Different techniques such as AFM, XPS, and fluorescence have been used in order to demonstrate the successful functionalization.
- The developed BioFET has been electrically characterized showing good electrical performance at relatively low voltages (|10| V).
- The BioFET sensors have been validated as an immunosensor. The antibody HIgG has been used as a proof-of-concept biomolecule analyte.

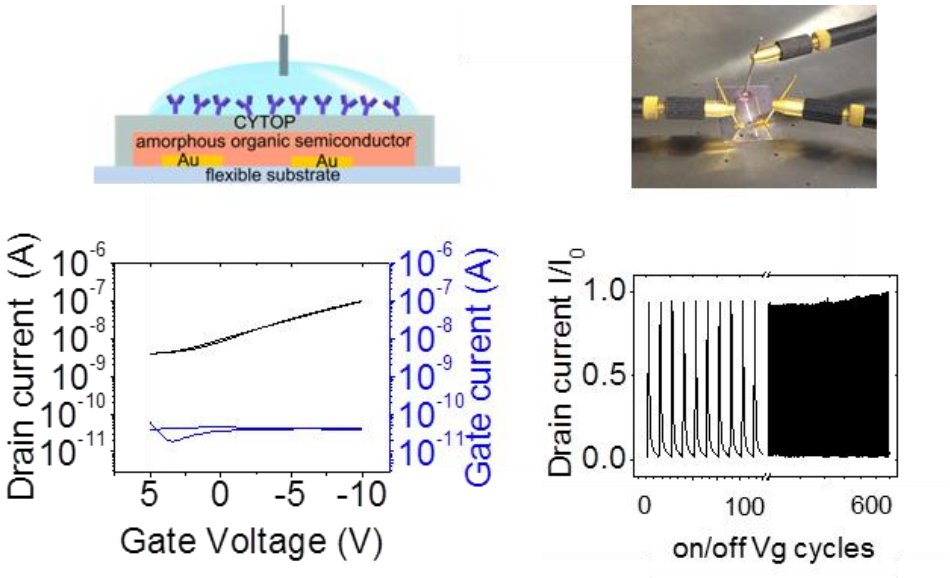

Figure 6-2 Micro-fabricated organic BioFET and its electrical characteristics.

Finally, the development of the BioFET by inkjet printing technique has been successfully addressed. The results of the work are summarized as:

- Inkjet printing parameters has been tuned in order to achieve thin layers in the range of hundreds of nanometres. This achievement has permitted the migration of the BioFET fabrication from conventional techniques to inkjet printing. The devices, in fact, show similar electrical characteristics.
- A new colloidal gold ink has been used for the fabrication of the drain and source electrodes. This novel approach, not already explored in the literature, offers interesting advantages to the devices: low oxidation rate, biocompatibility, and a better carrier injection due its high work function.
- The developed functionalization of the Cytop^{TM} has been applied to this structure to attach biomolecules.
- The developed BioFET has been electrically characterized and has shown good performances.
- The inkjet-printed BioFET sensors have been validated as immunosensors. The antibodies HIgG has been used as a proof-of-concept analyte opening a new research field in the inkjet-printed sensors.

Figure 6-2 and Figure 6-3 show a table of contents with the most representative results for the chapter ”*Organic Inkjet-Printed BioFETs* ”.

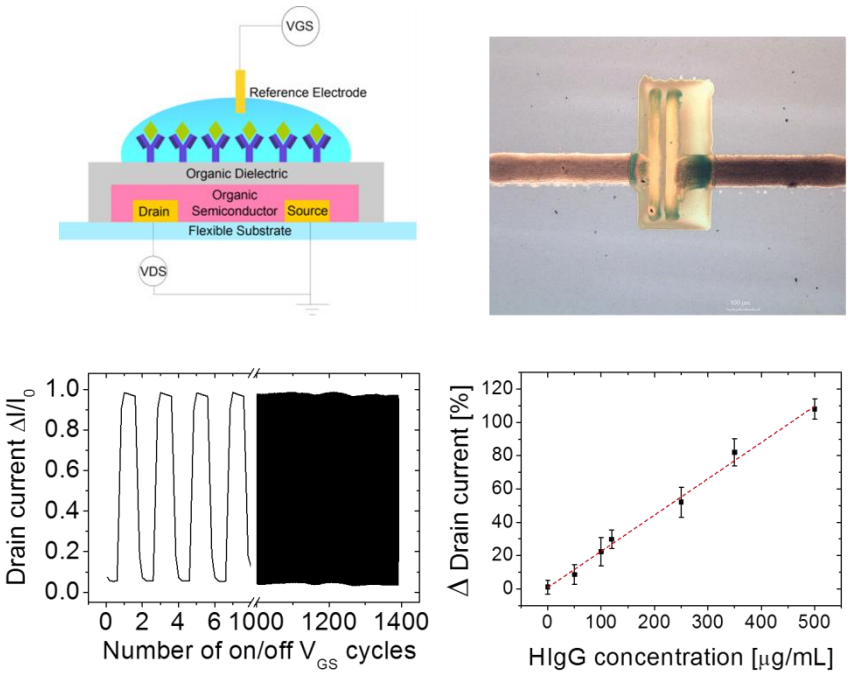

Figure 6-3 Inkjet-printed BioFET and its electrical performance

As a future work, some specific issues should be further considered for each presented device.

Regarding the MIS structures, the main open issue is the improvement of the frequency response of the diodes. Several routes can be used to enhance this aspect such as the use of thin OSC layers and high-mobility OSC materials. Moreover, higher rectification ratios can be achieved using other organic dielectrics. Thus, a wide variety of formulations of organic dielectrics and OSC could be evaluated in order to optimize the electrical behaviours. However, this was not the goal of this thesis since it represents an optimization in terms of rheological-chemical properties of the materials which differs from our background.

For the BioFETs, the main target is to use new high-mobility OSC materials in order to reduce the operation voltages and to increase the sensitivity. However, considering the top gate archiceture, this step is not straightforward since the device electrical performances could be easily affected by the crystallization process typical of small-molecules. Moreover, the sensing evaluation performed in this thesis has to be considered as a proof-of-concept. Since the electrical performances of the structures have been already optimized, the devices should be further characterized as biosensors using other specific antibodies e.g. for detection of biomarkers. Finally, complex matrixes can be tested to study the specificity under real samples.

Annex A: List of Publications

The list of publications shall be considered for the evaluation of this PhD Dissertation. Moreover it is included the congress assisted during the thesis:

1. **Articles**

   Paper I (accepted and published):

   Martínez-Domingo C, Conti S, Terés L, Gomes H.L, Ramon E. Novel flexible inkjet-printed Metal-Insulator-Semiconductor organic diode employing silver electrodes. Org Electron 2018; 62: 335–341. DOI:10.1016/j.orgel.2018.08.011 [7]

   Paper II (submitted, 2018):

   Carme Martínez-Domingo, Silvia Conti, A. de la Escosura-Muñiz, Ll. Terés, E. Ramon and A. Merkoçi, "Systematic Study of Fluoropolymer Insulator for Flexible Top-Gate BioFETs"

   Paper III (submitted, 2018):

   Carme Martínez-Domingo, Silvia Conti, A. de la Escosura-Muñiz, Ll. Terés, E. Ramon and A. Merkoçi, "Development of Inkjet-Printed Flexible Top-Gate BioFETs for biosensing applications"

2. **Conferences**

   -Poster at "International Thin-Film Transistor Conference", Delft, Holland, 2014.

   -Poster at "Large Organic and Printed Electronics Conference (LOPE-C), Munich, Germany, 2014.

   -Poster at "Biosensors Congress", Gothenburg, Sweden, 2016.

Moreover, the PhD candidate also has participated in the following articles but whose results are related but not included in this thesis Dissertation:

1. Gomes HL, Medeiros MCR, Villani F, Canudo J, Loffredo F, Miscioscia, **Martínez-Domingo C**, et al. All-inkjet printed organic transistors: Dielectric surface passivation techniques for improved operational stability and lifetime. Microelectron. Reliab 2015; 55:1192–1195.DOI: 10.1016/j.microrel.2015.05.006.[8]

2. Sowade E, Ramon E, Mitra KY, **Martínez-Domingo C**, et al. All-inkjet-printed thin-film transistors: manufacturing process reliability by root cause analysis. Sci Rep 2016; 6: 33490. DOI: 10.1038/srep33490.[9]

3. Sowade E, Mitra KY, Ramon E, **Martínez-Domingo C**, et al. Up-scaling of the manufacturing of all-inkjet-printed organic thin-film transistors: Device performance and manufacturing yield of transistor arrays. *Org Electron* 2016; 30: 237–246.DOI: 10.1016/j.orgel.2015.12.018.[10]

4. Mitra KY, Polomoshnov M, **Martínez-Domingo C**, et al. Fully Inkjet-Printed Thin-Film Transistor Array Manufactured on Paper Substrate for Cheap Electronic Applications. Adv Electron Mater 2017; 3: 1700275.DOI: 10.1002/aelm.201700275.[11]

5. Mitra KY, Sternkiker C, **Martínez-Domingo C**, et al. Inkjet printed metal insulator semiconductor (MIS) diodes for organic and flexible electronic application. Flex Print Electron 2017; 2: 015003.DOI: 10.1088/2058-8585/2/1/015003.[12]

6. Ramon E, **Martinez-Domingo C**, Alcalde-Aragones A, et al. Development of a Simple Manufacturing Process for All-Inkjet Printed Organic Thin Film Transistors and Circuits. IEEE J Emerg Sel Top Circuits Syst 2017; 7: 161–170.DOI: 10.1109/JETCAS.2016.2617205[13]

Other articles and projects that the PhD candidate has participated not directly related to this thesis dissertation can be found in the Annex B: Scientific Curriculum Vitae.

Annex B: Scientific Curriculum Vitae

Carme Martinez Domingo

Born: 25th December 1987 in Barcelona

carme.martinez@imb-cnm.csic.es, carme.martinez@icn2.cat

Current Position: PhD student at the Institute of Microelectronics of Barcelona (IMB-CNM) and the Catalan Institute of Nanotechnology (ICN2) developing inkjet printing biosensors and electronic devices based on nanotechnology for low cost and disposable point-of-care devices.

Studies

- Universitat Autònoma de Barcelona 2014-Present

PhD student in Electronic Engineering. Title of the thesis: "Inkjet printed devices for chemical and biosensing applications" Expected thesis submission date: First semester 2018

In this thesis, a lab on a chip (LOC) platform will be developed by using printing technologies onto flexible substrates yielding to the development of an all-integrated, portable and low cost sensor system, compatible with the "single-use sensor" concept.

- Universitat Autònoma de Barcelona 2012-2011

Master of Micro and Nanoelectronic Engineering

Final Degree Project in "Characterization of Inkjet-Printed Organic Thin-Film Transistors". Advisor: Eloi Ramon, Henrique Leonel-Gomes and Jordi Carrabina. Final mark: 9.5/10.

- Universitat Autònoma de Barcelona 2011-2009

M.S. Degree in Electronic Engineering

·Final Degree Project in "Breakdown and switching in high-K dielectrics". Advisor: Jordi Suñé. Final mark: 9.5/10

- Universitat Autònoma de Barcelona 2009-2005

B.S Degree in Telecommunications Engineering, Electronic System specialty

·Final Degree Project in "Analysis and signal processing for forecast maps generation". Advisor: Jose Salcedo. Final mark: 8.5/10

Work Experiences

• Institute of Microelectronics of Barcelona and Catalan Institute of Nanotechnology 2014-Present

The current thesis will be developed in the framework of national project called "New solutions based on Printed Electronics for the detection of physical variables and liberation of organic compounds" as collaboration between Catalan Institute of Nanotechnology, Institute of Microelectronics of Barcelona and CARINSA company, S.A. (Barcelona). In this project, the goal is to develop a set of sensors to detect chemical and biological compounds in food packaging. In addition Near Field Communication (NFC) technology is used as sensor reading system.

• Catalan Institute of Nanotechnology 2016-2017

The current thesis will be developed in the framework of national project called "Smart Printed Paper: Printed Electronics para nuevas funcionalidades en papel" as collaboration between Catalan Institute of Nanotechnology and JUSMER company, S.A. (Barcelona). In this project, the goal is to develop a set of sensors to detect microorganisms in clinical paper. In addition Chipless tags (RFID) technology is used as sensor reading system.

• Centre for research in Ambient Intelligence and Accessibility in Catalonia

Universitat Autònoma de Barcelona 2011- 2014

R&D Engineer in the Printed Microelectronics Group

The research interests of our group have been directed towards the Flexible Organic and Large Area Electronics (FOLAE)- Printed Electronic research. My research task is focused on electrical characterization of both active and passive printed devices such as transistors, resistors, capacitors and diodes by inkjet printing technology. Furthermore, I collaborate with the group of Nanobioelectronics and Biosensors group at ICN (Catalan Institute of Nanotechnology) developing Biosensors by inkjet technology.

Research projects

• "Network of Excellence for building up Knowledge for improved Systems Integration for Flexible Organic and Large Area Electronics (FOLAE) and its exploitation (FlexNet)", EU FP7 (contract 247745), 1/1/2010-31/12/2012.

• "Technology & Design Kits for Printed-Electronics (TDK4PE)", EU FP7 (contract 287682), 1/10/2011-30/9/2014

• "NANOCARDIOFLEX - Desarrollo de biosensores sobre tecnología flexible y rígida para la detección de marcadores cardíacos", Ministerio de Economía y Competitividad (RTC-2015-4184-1), 25/2/2015-31/12/2017. Funding: 175.584 €.Partners: BRIP Apps AlphaSIP SL, Universidad Complutense de Madrid, IDIBAPS, IMB-CNM.

• "SMART PRINTED PAPER: Printed Electronics para nuevas funcionalidades en papel", Ministerio de Economía y Competitividad (RTC-2014-2619-7), 1/2/2014-31/12/2016. Funding: 155.284 €.Partners: Jusmer SL, ICN, IMB-CNM.

• "Nuevas Soluciones basadas en PRINTED ELECTRONICS para la detección de variables físicas y la liberación de compuestos orgánicos", Ministerio de Industria, Energía y Turismo (TSI-100101-2013-94), Technology transfer contract with CARINSA, S.A. 1/1/2013-31/12/2015. Funding: 62.125 €.

Scientific Publications

➢ *Inkjet Printed Electronics Field*

• Martínez-Domingo C., Conti S., Terés L. Gomes, H.L., Ramon E., "Novel flexible inkjet-printed Metal-Insulator-Semiconductor organic diode empolying silver electrodes". Organic Electronics 2016, 62, 335-341. DOI: 10.1016/j.orgel.2018.08.011 (IF= 3.68 @2017)

• Mitra, K. Y., Polomoshnov, M., Martínez-Domingo, C., Mitra, D., Ramon, E., & Baumann, R. R. "Fully Inkjet-Printed Thin-Film Transistor Array Manufactured on Paper Substrate for Cheap Electronic Applications". Advanced Electronic Materials 2017, 3, 1700275. DOI: 10.1002/aelm.201700275, (IF = 4.193 @2016, Q1 - 24/147-UB).

• Ramon, E., Martínez-Domingo, C., Alcalde-Aragonés, A., & Carrabina, J., "Development of a Simple Manufacturing Process for All-Inkjet Printed Organic Thin Film Transistors and Circuits", IEEE Journal on Emerging and Selected Topics in Circuits and Systems, Pages 161-170, Volume 7, Issue 1, March 2017, DOI: 10.1109/JETCAS.2016.2617205, (IF = 2.542 @2016, Q2 - 79/260-IQ).

• Mitra, K. Y., Sternkiker, C., Martínez-Domingo, C., Sowade, E., Ramon, E., Carrabina, J., Gomes, H.L. & Baumann, R. R., "Inkjet printed metal insulator semiconductor (MIS) diodes for organic and flexible electronic application", Flexible and Printed Electronics, 2017, 2(1), 015003, DOI:/10.1088/2058-8585/2/1/015003, (No IF available yet: new IOP journal since 2016)

• Sowade, E., Ramon, E., Mitra, K. Y., Martínez-Domingo, C., Pedró, M., Pallarès, J., Loffredo, F., Villani, F., Gomes, H.L., Terés, Ll., Baumann, R. R., "All-inkjet-printed thin-film transistors: manufacturing process reliability by root cause analysis", Nature Scientific Reports, 6, 33490, September 2016, DOI: /10.1038/srep33490, (IF = 5.228 @2015, Q1 - 7/63-RO).

• Silvia Conti, Carme Martinez-Domingo, Stefano Lai, Piero Cosseddu, Eloi Ramon, Annalisa Bonfiglio, "Towards low-voltage inkjet printed Organic Field Effect Transistors for biosensing applications", Poster at E-MRS 2016 Fall Meeting, September 19 to 22, 2016

• Carme Martínez-Domingo, Eloi Ramon and Arben Merkoçi, "Capacitive based paper biosensor", Poster at Biosensors Conference, 25–27 May 2016, Gothenburg, Sweden.

• Kalyan Y. Mitra, Enrico Sowade, Eloi Ramon, Carme Martinez-Domingo, Fulvia Villani, Fausta Loffredo, Henrique L. Gomes, Reinhard R. Baumann, "Performance and reliability mapping for all Inkjet-printed thin-film-transistor arrays using industrial inkjet accessories", Poster at LOPE-C, 8th International Conference and Exhibition for the Organic and Printed Electronics Industry 2016, Munchen (Germany), April 2016.

• Enrico Sowade, Kalyan Y. Mitra , Eloi Ramon, Carme Martínez-Domingo, Fulvia Villani, Fausta Loffredo, Henrique L. Gomes, Reinhard R. Baumann, "Up-scaling of the manufacturing of all-inkjet-printed organic thin-film transistors: Device performance and manufacturing yield of transistors arrays", Journal of Organic Electronics Vol. 30 (2016) pp 237-246, doi: 10.1016/j.orgel.2015.12.018.

• Henrique L. Gomes, Maria C Raposo de Medeiros, Fulvia Villani, Joana Canudo, Fausta Loffredo, Ricardo Miscioscia, Carme Martinez-Domingo, Eloi Ramon, Enrico Sowade, Reinhard R Baumann, Ian McCulloch, Jordi Carrabina, "All-inkjet printed organic transistors: dielectric surface passivation techniques for improved operational stability and lifetime", Journal Microelectronics Reliability (accepted, publication pending).

• Mohammad Mashayekhi, Adria Conde, Tse Nga Ng, Ping Mei, Eloi Ramon, Carme Martinez-Domingo, Ana Alcalde, Lluís Terés, Jordi Carrabina, "Inkjet Printing Design Rules Formalization and Improvement", Journal of Display Technology, Volume:PP , Issue: 99 (2015), doi 10.1109/JDT.2015.2405135.

• Kalyan Yoti Mitra, Enrico Sowade, Carme Martínez-Domingo, Eloi Ramon, Jordi Carrabina, Henrique Leonel Gomes and Reinhard R. Baumann, "Potential up-scaling of inkjet-printed devices for logical circuits in flexible electronics", AIP Conference Proceedings 1646, 106 (2015); doi: 10.1063/1.4908590.

• Kalyan Y. Mitra, Enrico Sowade, Christoph Sternkiker, Carme Martínez-Domingo, Eloi Ramon, Jordi Carrabina, Reinhard R. Baumann, "Investigation on electrical stress over metal-insulator-metal (MIM) structures based on compound

dielectrics for the inkjet-printed OTFT stability", Journal of Applied Mechanics and Materials Vol. 748 (2015) pp 129-133, doi:10.4028/www.scientific.net/AMM.748.129

• Mariana Medina-Sánchez, Carme Martínez-Domingo, E. Ramon and A. Merkoçi , "An Inkjet-Printed Field-Effect Transistor for Label-Free Biosensing", Advanced Functional Materials Journal, 2014, 24, 6291-6302.

• Carme Martínez-Domingo, Mariana Medina-Sánchez, Sandrine Miserere, Henrique L. Gomes, Eloi Ramon and Arben Merkoçi, "Ink-jet printed FET for biosensing applications", Poster at Biosensors Congress 2014, Melbourne (Australia).

• Henrique L.Gomes, M.C.R Medeiros, F. Villani, A.T. Negrier, F. Loffredo, R. Miscioscia, C. Martínez-Domingo, E. Ramon, E. Sowade, Kalyan Y. Mitra, R.R. Baumann, I. Mc-Culloch and Jordi Carrabina, "All-inkjet printed organic transistors: dielectric surface passivation techniques for improved operational stability and lifetime", Journal of Display Technology (accepted, press pending), September 2014.

• Francesc Vila, Adrià Conde, Jofre Pallarès, Lluís Terés, Carme Martínez-Domingo, Eloi Ramon, Jordi Carrabina, "Semi-automatic PE Technology & Device Library Characterization for PDK Development", Oral presentation at LOPE-C, 6th International Conference and Exhibition for the Organic and Printed Electronics Industry 2014, Munchen (Germany), May 2014.

• Carme Martínez-Domingo, Mariana Medina-Sánchez, Sandrine Miserere, Henrique L.Gomes, Arben Merkoçi and Eloi Ramon, "Inkjet-based OFET biosensor on flexible substrate platform", Poster at LOPE-C Conference, Munich, March 2014.

• Mitra, K. Y., Martínez-Domingo, C., Sowade, E., Ramon, E., Gomes, H. L., & Baumann, R. R. "Inkjet-printed rectifying metal-insulator-semiconductor (MIS) diodes for flexible electronic applications", MRS Proceedings (Vol. 1628, pp. 13-1628). Cambridge University Press, DOI: http://dx.doi.org/10.1557/opl.2014.389, January 2014.

• Medeiros, M. C., Martinez-Domingo, C., Ramon, E., Negrier, A. T., Sowade, E., Mitra, K. Y.,Baumann, R. R., McCulloch, I., Carrabina, J., & Gomes, H. L. "Inkjet-Printed Organic Electronics: Operational Stability and Reliability Issues". ECS Transactions, 53(26), 1-10. ISSN 1938-5862.

• M. C. R. Medeiros, F. Villani, A. T. Negrier, F. Loffredo, R. Miscioscia, C. Martinez-Domingo, E. Ramon, E. Sowade, K. Y. Mitra, R. R. Baumann, I. McCulloch, J. Carrabina and H. L. Gomes, "All-inkjet printed electronic circuits: Dielectrics and surface passivation techniques for improved operational stability and lifetime", 10th International Thin-Film Transistor Conference, Delft, January 2014.

• Ramon, E., Martínez-Domingo, C., Alcalde-Aragonés, A., Carrabina, J., Conde, A., Pallarès, J., & Terés, L., "Large-Scale Fabrication of All-Inkjet Printed Organic Thin Film Transistors: a Quantitative Study", Oral presentation at NIP & Digital

Fabrication Conference (Vol. 2014, No. 1, pp. 455-460). Society for Imaging Science and Technology, Philadelphia (USA).

• Carme Martínez-Domingo, Mariana Medina-Sánchez, Sandrine Miserere, Henrique L. Gomes, Eloi Ramon, Arben Merkoçi, "Fabrication and characterization of inkjet printed biosensor platform", Poster at Biosensors 2013, Melbourne (Australia).

• Henrique Gomes, Maria Medeiros, Enrico Sowade, Kalyan Mitra, Carme Martinez-Domingo, Eloi Ramon, Iain McCulloch, Reinhard Baumann, "Assessment of dielectrics for all-ink-jet printed organic thin film transistors", Oral presentation at 12th European Conference on Molecular Electronics, London, 3 – 7 September 2013.

• Carme Martinez-Domingo, Mariana Medina-Sánchez, Eloi Ramon, Ana Alcalde-Aragonés, Sandrine Miserere, Jordi Carrabina, Arben Merkoçi, Henrique L. Gomes, "Material characterization and electrochemical performance for all-inkjet organic ISFET-based biosensor", Oral presentation at 223rd ECS Meeting (May 12-17, 2013). Toronto (Canada).

• J. Carrabina, E. Ramon, F. Vila, C. Martinez, J. Pallarés, Ll. Terés, "Design Rules Checking for Printing Electronic Devices: Concept, generation and usage", Proceedings of 40th International Research Conference Advances in Printing and Media Technology. Oral presentation at IARIGAI 2013, Chemnitz (Germany).

• Adrià Conde, Jofre Pallarès, Lluís Terés, Carme Martinez-Domingo, Eloi Ramon, Jordi Carrabina, "PCell based devices & structures for Printed Electronics and related semiautomatic characterization loop", Proceedings of the XVIII Conference on the Design of Circuits and Integrated Systems, 2013. Oral presentation.

• Eloi Ramon, Carme Martínez-Domingo and Jordi Carrabina, "Geometric Design & Compensation Rules Generation and Characterization for all-Inkjet Printed Organic Thin Film Transistors", Journal of Imaging Science and Technology (accepted, press pending), December 2012.

• M. Medina-Sánchez, C. Martínez-Domingo, E. Ramon, S. Miserere, A. Alcalde-Aragonés, J. Carrabina & A. Merkoçi , "Ink-jet printed FET for biosensing applications", Proceedings of microTAS 2012, Okinawa (Japan).

• Carme Martínez-Domingo, Eloi Ramon, Ana Alcalde-Aragonés, Jordi Carrabina, "Inkjet Geometric Design Rules Generation and Characterization", Proceedings of International Conference on Digital Printing technologies & Digital Fabrication (NIP28-DF), Quebec (Canada), September 2012; ISBN / ISSN: 978-89208-302-2, p. 308-311.

• E.Díaz, E.Ramon, C.Martínez-Domingo, A.Alcalde-Aragonés, J.Carrabina, "Inkjet Resistor Design and Characterization", Proceedings of 8th International Conference on Organic Electronics (ICOE), Tarragona, June 2012.

• Ana Alcalde-Aragonés, Eloi Ramon, Mariana Medina-Sánchez, Carme Martínez-Domingo, Sandrine Miserere, Arben Merkoçi and Jordi Carrabina , "New materials for biosensing", Poster at ISFOE 2012, Tessaloniki (Greece).

• Carme Martínez-Domingo, Eloi Ramon, Ana Alcalde-Aragonés, Jordi Carrabina, "Inkjet Geometric Design Rules Generation and Characterization", Proceedings of LOPE-C, 5th International Conference and Exhibition for the Organic and Printed Electronics Industry 2012, ISBN: 978-3-00-038122-5, pp. 293-297 Munchen (Germany).

• E.Díaz, E.Ramon, C.Martínez-Domingo, A.Alcalde-Aragonés, J.Carrabina, "Inkjet Resistor Design and Characterization", Proceedings of 8th International Conference on Organic Electronics (ICOE), Tarragona, June 2012. Oral presentation.

• Mariana Medina-Sánchez, Eloi Ramon, Ana Alcalde-Aragonés, Sandrine Miserere, Carme Martínez-Domingo, Jordi Carrabina, Arben Merkoçi, "Ink-jet printed FET for biosensing applications", Poster at Biosensors 2012, Cancun (Mexico).

• Francesc Vila, Carme Martínez-Domingo, Eloi Ramon, Lluís Terés, Jordi Carrabina, "Layout to Bitmap: A layout design compensator and converter for Printed Electronics", Poster at Swiss e-Print, Basel (Switzerland), November 2011.

➢ *Reliability in High-k dielectrics Field*

• Conde A., Martinez C., Jimenez D., Miranda E. , Rafi J. M. , Campabadal F. , Sune J. " Modeling the breakdown statistics of Al2O3/HfO2 nanolaminates grown by Atomic-Layer-Deposition", Solid State Electronics Volume 71, May 2012, Pages 48–52. Selected Papers from the ULIS 2011 Conference. Impact Factor: 1.39

• C. Martínez-Domingo, X. Saura, A. Conde, D. Jiménez, E. Miranda, J.M. Rafí, F. Campabadal, J. Suñé " Initial leakage current related to extrinsic breakdown in HfO2/Al2O3 nanolaminate ALD dielectrics" Proceedings of the 17th Biennial International Insulating Films on Semiconductor Conference (Grenoble). Microelectronic Engineering 88 (2011) 1380–1383.

• X. Saura, J. Suñé, E. Miranda, D. Jiménez, C. Martínez-Domingo, S. Long, M. Liu, J.M. Rafí and F. Campabadal," Threshold switching in MOS structures with HfO2" Proceedings of 17th Conference on "Insulating Films on Semiconductors" (Grenoble, 2011).

Awards

2014 Charles E. Ives Journal Award. Society for Imaging Science and Technology. Received at Philadephia (USA), September 2014.

Course invited

Lecture "Printed device characterization" given at the Engineering School (UAB) on April 29th 2015.

Others activities

- *Courses and Congress assisted*

"Biosensors 2016 Congress", 25th-27th Gothenburg 2016, Sweden.

"LOPE-C Congress 2012", 19th-21th June 2012, Munich, Germany.

"Emerging Technologies for Biomedical Diagnostics", 6th-13th May 2016, Università degli Studi di Cagliari, Sardegna, Italia.

"LabVIEW Core 1 course", official course given by National Instruments, 26th-28th January 2016, Universitat Autònoma de Barcelona, Spain.

"SCOPUS", 9th June 2015, Universitat Autònoma de Barcelona, Spain.

"OTFT Circuit Design Course", COLAE, June 30-July 3th 2014, Barcelona, Spain.

"Scanning Electron Microscope training course" 17th-21th June 2013, Servei de Microscòpia, Universitat Autònoma de Barcelona, Spain.

"7th International Summer School "Nanosciences & Nanotechnologies, Organic Electronics & Nanomedicine" (ISSON13) 6-13 July 2012, Thessaloniki, Greece.

- *Stay abroad*

• Practical-stage period in the field of Printed and Organic Electronic, 25th April-25th July 2016,

Università degli Studi di Cagliari, Sardegna, Italia.

- *Grants*

• ICREA 2009-10-SU, ICREA Grant for the development of the research project "Breakdown and resistive switching in high-K dielectrics", 15th June 2010-30 July 2011, Department of Electronic Engineering, Universitat Autònoma de Barcelona.

Skills

- *Electronics*

EDA: Mixed-signal VLSI design flow using Cadence tools (Virtuoso, Composer, Spectre) for design, layout and post-layout analysis, PSPICE, Quartus (Altera).

Physical characterization techniques: SEM, mechanical profilometry and confocal.

Electrical characterization: LCR meters, Semiconductor Analyzer (Agilent B1500A, Keithley 4200, HP 4155) and Automatic Probe Station.

- *Micro-Fabrication*

Micro-Fabrication: Inkjet printer Fujifilm Dimatix DMP2831, Spincoater, Oxygen plasma cleaner, PDMS molding, Lateral Flow strips and Organic Light-Emission Diodes. Characterization: Spectrophotometer SpectraMax M2e and Contact Angle equipment.

- *Chemistry-Biology*

Synthesis of nanoparticles and polymers, Biofunctionalization of surfaces and Preparation of buffers. I have been working also with nanomaterials such as magnetic nanoparticles, graphene,etc and biomolecules such as antibodies, bacteria, etc.

- *Computer*

Simulation: Matlab

Programming: C++

Test: LabView, GPIB, experience testing chips using oscilloscopes and logic analysis systems.

OS: Windows (advanced user), Mac OSC (domestic user)

- *Communication*

Writing: Experience in writing technical reports and technical papers/journals.

- *Languages*

Catalan: Mother tongue

Spanish: Mother tongue

English: Fluent in reading, listening, writing and speaking.

Italian: Fluent in reading, listening, writing and speaking

List of Abbreviations

AFM	Atomic Force Microscopy
APTES	Amino-(3-aminopropyl)triethoxysilane
BCTG	Bottom Contact Top Gate
BioFET	Biological Field-Effect Transistor
BSA	Bovine Serum Albumin
C-V	Current-Voltage
DOD	Drop-on-Demand
DS	Drop Spacing
EDC/NHS	(1-Ethyl-3-(3-dimethylaminopropyl)-carbodiimide)/N-hydroxysuccinimide
EGOFET	Electrolyte-Gated Organic Field-Effect Transistor
GIgG	Goat IgG
HIgG	Human IgG
HOMO	Highest Occupied Molecular Orbital
ISOFET	Ion Sensitive Organic Field-Effect Transistor
LUMO	Lowest Occupied Molecular Orbital
MES	2-(N-morpholino)ethanesulfonic acid buffer
MIE	Metal-Insulator-Electrolyte
MIS	Metal-Insulator-Semiconductor
MMAcoMAA	poly(methylmethacrylate/methacrylic) acid
OE	Organic Electronics
OECT	Organic Electrochemical Transistor
OFET	Organic Field-Effect Transistor
OSC	Organic Semiconductor
OTFT	Organic Thin Film Transistor
PBS	Phosphate Buffer Saline
PE	Printed Electronics
PEN	polyethylene naphthalate
PET	polyethylene terephthalate
PTAA	poly(triarylamine)
R2R	Roll-to-Roll
RFID	Radio Frequency Idenification
RR	Rectification Ratio
RT	Room Temperature
SBH	Schottky Barrier Height
SCLC	Space Charge Limited current
SEM	Scanning Electronic Microscope
TE	Thermionic Emission
TFT	Thin Film Transistor
UV	Ultraviolet

WF	Work Function
XPS	X-ray Photoemission Spectroscopy